

UNIVERSITY OF NOTTINGHAM  
SCHOOL OF CIVIL ENGINEERING  
NOTTINGHAM GEOSPATIAL INSTITUTE

PhD ENGINEERING SURVEYING AND SPACE GEODESY

Title:

**IONOSPHERIC SCINTILLATION EFFECTS ON GNSS:  
MONITORING AND DATA TREATMENT DEVELOPMENT**

Student: Vincenzo Romano

Student ID: 4071605

Course of Study: Part-time

Supervisors: Dr. Marcio Aquino, Prof. Alan Dodson, Dr. Giorgiana De Franceschi

Outside Organization: Istituto Nazionale di Geofisica e Vulcanologia (Rome, Italy)

*Thesis submitted to the University of Nottingham for the degree of Doctor of Philosophy, June 2016*

## PREFACE

This thesis is submitted in fulfilment of the requirements for a degree of Doctor of Philosophy at Nottingham Geospatial Institute (NGI), University of Nottingham, UK. The research has been conducted at the outside organization Istituto Nazionale di Geofisica e Vulcanologia (INGV), located in Rome, Italy. It was supervised by Dr. Marcio Aquino (main supervisor), Prof. Alan Dodson at NGI and Dr. Giorgiana De Franceschi at INGV.

This thesis should be cited as:

Romano, V. (2016), *Ionospheric scintillation effects on GNSS: monitoring and data treatment development*, Ph.D. dissertation, Nottingham Geospatial Institute, The University of Nottingham, Nottingham, UK.

## **ABSTRACT**

The increasing importance of satellite navigation technologies in modern society implies that a deeper knowledge and a reliable monitoring of the scintillation phenomena are essential to warn and forecast information to the end users and system designers. In fact, warnings, alerts and forecasting of ionospheric conditions may wisely tune the development of GNSS-based services to obtain the necessary levels of accuracy, integrity, and immediacy for reliable life-critical applications. The PhD research project is within the framework of the longstanding NGI-INGV collaboration, increasingly consolidated in the framework of many international projects. NGI pioneered GPS ionospheric scintillation monitoring in Northern Europe with GISTM (GPS ionospheric scintillation and TEC monitor, Van Dierendonck et al., 1993; Van Dierendonck, 2001) receivers. Between June 2001 and December 2003, four units were installed in the UK and Norway mainland, covering the geographic latitudes from 53° N to 70° N. Data was stored and analysed, focusing on statistical analyses and impact for GNSS users (Rodrigues et al., 2004, Aquino et al., 2005a, Aquino et al., 2005b). These units were decommissioned in 2004 and, then, re-deployed together with additional new receivers, in UK, Norway, Italy and Cyprus. An additional station was deployed by the NGI in Dourbes, Belgium (in collaboration with the Royal Meteorological Institute of Belgium) between 2006 and 2011. INGV leads the ISACCO (Ionospheric Scintillation Arctic Campaign Coordinated Observations) project in the Arctic, started in 2003, in which frame the management of three GISTM receivers in Svalbard (De Franceschi et al., 2006) and another two at European mid-latitudes, Chania (Greece) and Lampedusa (Italy), is currently undertaken. The PhD research project contributed to the reinforcement of the NGI-INGV GISTM network developing monitoring, data management and quality tools. Such activities have supported the continuity and the control of the receiving stations, as well as the access and the preservation of the both real-time and historical data acquired. In fact, a robust, continuous data acquisition and a wise management of the GISTM network are of paramount importance for Space Weather applications, as they are the basis on which reliable forecasting and now-casting of possible effects on technological systems lean. Moreover, the possibility to use the data for scientific and applicative purposes depends upon well-established data quality procedures and upon a detailed knowledge of the sites in which each receiver comprising the network are deployed. Starting from these considerations, and in the framework of the aforementioned collaborative context, the PhD work aimed at improving the monitoring techniques and developing novel data processing to improve the data quality.

Scintillation measurements are contaminated by multiple scattering encountered by the GNSS signal due to buildings, trees, etc. Such multipath sources need to be identified to keep the quality of the scintillation and TEC data as higher as possible. This can be achieved by removing these sources of errors or mitigating their effects by filtering the data. A novel station characterization technique has been introduced, developed and discussed in this thesis. The results demonstrated that this is a promising method to improve the quality of data (Romano et. al 2013). The results obtained so far motivated the development of the data filtering procedures. The filtering was aimed at filtering-out spurious, noisy data based on general

assumptions about statistical data analysis (outlier analysis), thus efficiently removing multipath affected measurements and reducing the data loss with respect to applying a fixed elevation angle cut-off threshold. This is particularly important in case of not well covered regions (e.g. forests, deserts, oceans, etc.), as the field of view spanned by each antenna is optimized. During the PhD activities, the filtering technique has been also tested and validated against real and simulated data. To show how the development of the filtering method is able to efficiently clean multipath and signal degradation from GNSS data, it was applied in two different cases:

- First, it was applied to the data published in a climatological study (Alfonsi et al. 2011), carried out with the NGI-INGV GISTM network at high-latitudes. Each station was characterized using the station characterization method, and then the data were filtered using the filtering method. Then, the new climatological maps were generated and compared to the original ones. The percentage of the filtered-out data obtained by applying the standard threshold of  $20^\circ$  on the elevation angle and the filtering technique for each station demonstrated how the latter is able to meaningfully reduce the data loss. The filtering extends the field of view of the network and, then, improves the capability of investigating the dynamics of the ionosphere over larger areas.
- Second, the data used in this application were acquired by the CIGALA/CALIBRA network of PolaRxS receivers during the whole year of 2012. The elevation angle cut-off significantly reduced the capability of the network to depict the ionosphere northward of the geomagnetic equator and above the Atlantic Ocean, east of Brazil. This approach limited the data loss to 10-20%, while the traditional cut off of  $15^\circ$ - $30^\circ$  on the elevation angle led to losses of 35-45%. This method not only optimized the capability of GNSS networks, but also helped in planning the installation of additional new receivers aiming to enlarge network coverage in the framework of the CALIBRA project. The enlarged field of view made it possible to identify the increased occurrence of scintillation along the northern crest of the Equatorial Ionospheric Anomaly (EIA).

To summarize and to introduce the reader into this thesis, specific issues here addressed are:

- Development of software procedures and hardware designs to optimize the station configurations of the existing measurement network of GISTM (GPS Ionospheric Scintillation and TEC Monitor).
- Development of techniques for remote, automatic instrument control and setting.
- Development of data management tools to achieve quasi real-time data accessibility.
- Development of data analysis methods to assess station characterization.
- Development of techniques to perform data quality filtering.
- Perform acquisition of experimental and simulation data.
- Support scientific investigations through the high quality of the NGI-INGV network data.

## LIST OF JCR PAPERS

The list includes the papers where part of the PhD research work is included. Only papers published on JCR journals are listed.

- **Romano V**, S. Pau, M. Pezzopane, L. Spogli, E. Zuccheretti, M. Aquino, C. M. Hancock, eSWua: a tool to manage and access GNSS ionospheric data from mid-to-high latitudes, *ANNALS OF GEOPHYSICS*, 56, 2, 2013, R0223, doi: 10.4401/ag-6244.
- **Romano, V.**, Spogli, L., Aquino, M., Dodson, A., Hancock, C., Forte, B., GNSS station characterisation for ionospheric scintillation applications, *Advances in Space Research* (2013), doi: <http://dx.doi.org/10.1016/j.asr.2013.06.028>.
- Spogli L., L. Alfonsi, **V. Romano**, G. De Franceschi, Galera Monico Joao Francisco, Milton Hirokazu Shimabukuro, Bruno Bougard, Marcio Aquino, Assessing the GNSS scintillation climate over Brazil under increasing solar activity, *Journal of Atmospheric and Solar-Terrestrial Physics*, Volumes 105–106 (2013), Pages 199–206, ISSN 1364-6826, <http://dx.doi.org/10.1016/j.jastp.2013.10.003>.
- Alfonsi, Lu., Spogli L, De Franceschi G, **Romano V**, Aquino M, Dodson A, Mitchell CN (2011). Bipolar climatology of GPS ionospheric scintillation at solar minimum. *RADIO SCIENCE*, vol. 46, ISSN: 0048-6604, doi: 10.1029/2010RS004571.
- Alfonsi L, Spogli L, Tong JR, De Franceschi G, **Romano V**, Bourdillon A, Huy ML, Mitchell CN (2011). GPS scintillation and TEC gradients at equatorial latitudes in April 2006. *ADVANCES IN SPACE RESEARCH*, vol. 47, p. 1750-1757, ISSN: 0273-1177, doi: 10.1016/j.asr.2010.04.020.
- Spogli, L., L. Alfonsi, G. De Franceschi, **V. Romano**, M. H. O. Aquino and A. Dodson (2010), Climatology of GNSS ionospheric scintillation at high and mid latitudes under different solar activity conditions, *Il Nuovo Cimento B*, DOI 10.1393/ncb/i2010-10857-7.
- Spogli L., L. Alfonsi, G. De Franceschi, **V. Romano**, M. H. O. Aquino and A. Dodson (2009), Climatology of GPS ionospheric scintillations over high and mid-latitude European regions, *Ann. Geophys.*, 27, 3429-3437.
- Aquino M., J.F.G. Monico, A.H. Dodson, H. Marques, G. De Franceschi, L. Alfonsi, **V. Romano**, M. Andreotti (2009), Improving the GNSS Positioning Stochastic Model in the Presence of Ionospheric Scintillation, *Journal of Geodesy*, DOI 10.1007/s00190-009-0313-6.
- Beniguel Y., **V. Romano**, L. Alfonsi, M. Aquino, A. Bourdillon, P. Cannon, G. De Franceschi, S. Dubey, B. Forte, V.E. Gherm, N. Jakowski, M. Materassi, T. Noack, M. Pozoga, N.C. Rogers, P. Spalla, H.J. Strangeways, M. Warrington, A. Wernik, V. Wilken, N.N. Zernov (2009), Ionospheric scintillation monitoring and modelling, *Annals of Geophysics*, 52, 3/4.

## ACKNOWLEDGEMENTS

I would like to sincerely thank my main supervisor Dr. Marcio Aquino for his support and continuous suggestion, making the PhD course full of questions and answers, ideas and discovers. I would also like to thank Prof. Alan Dodson and Dr. Giorgiana De Franceschi for their precious feedback and inspiring supervision. I am indebted to NGI, INGV, EPSRC and Royal Society for having supported my research activity in the framework of this PhD.

Heartfelt thanks to my colleagues at INGV Luca Spogli, Lucilla Alfonsi, Claudio Cesaroni and Enrico Zuccheretti for their friendship and support as well as to the friends at NGI, Craig Hancock and Melania Susi.

This thesis would not be possible without the encouraging of my various and extraordinary family. A special thought goes to my daughter Matilde and son Francesco wishing them the most coloured and musical discovers.

*Time is very slow for those who wait  
very fast for those who are scared  
very long for those who lament  
very short for those who celebrate  
but for those who love time is eternal.*

Henry van Dyke

## LIST OF CONTENTS

PREFACE .....	1
ABSTRACT .....	3
LIST OF JCR PAPERS.....	5
ACKNOWLEDGEMENTS.....	6
LIST OF CONTENTS.....	7
LIST OF FIGURES.....	8
LIST OF TABLES.....	11
LIST OF ACRONYMS.....	12
<b>1 CHAPTER 1 – INTRODUCTION .....</b>	<b>14</b>
1.1 MOTIVATION AND PURPOSE OF THE RESEARCH .....	14
1.2 SCIENTIFIC BACKGROUND AND REVIEW OF LITERATURE .....	16
1.3 THESIS STRUCTURE.....	20
<b>2 CHAPTER 2 – IONOSPHERIC MONITORING AND DATA MANAGEMENT .....</b>	<b>21</b>
2.1 MONITORING .....	21
2.2 THE ESWUA SYSTEM.....	25
2.3 APPLICATIONS OF DATA MONITORING AND MANAGEMENT .....	34
<b>3 CHAPTER 3 – METHODOLOGY, DATA ANALYSIS AND RESULTS.....</b>	<b>44</b>
3.1 STATION CHARACTERIZATION .....	44
3.1.1 <i>Method</i> .....	44
3.1.2 <i>Nottingham data analysis</i> .....	47
3.1.3 <i>Antenna survey</i> .....	51
3.1.4 <i>Trondheim data analysis</i> .....	52
3.1.5 <i>Nottingham station behaviour during the “Halloween Storm”</i> .....	55
3.2 FILTERING TECHNIQUE .....	60
3.2.1 <i>Method</i> .....	61
3.2.2 <i>Test of the filtering technique</i> .....	62
<b>4 CHAPTER 4 - APPLICATIONS USING REAL AND SIMULATED DATA .....</b>	<b>68</b>
4.1 APPLICATION IN SCINTILLATION CLIMATOLOGY .....	68
4.2 APPLICATION ON THE CIGALA/CALIBRA NETWORK.....	75
4.3 TECHNIQUE VALIDATION THROUGH APPLICATION WITH SIMULATED DATA.....	82
<b>5 CHAPTER 5 – CONCLUSIONS AND RECOMMENDATIONS FOR FUTURE WORKS .....</b>	<b>95</b>
<b>6 REFERENCES.....</b>	<b>103</b>
<b>7 APPENDICES.....</b>	<b>108</b>
7.1 ACQUISITION SCRIPT FOR NOTTINGHAM STATION.....	108
7.2 PHP CODE FOR NOTTINGHAM STATION .....	113
7.3 FORTRAN CODE FOR THE CONVERTER.....	125
7.4 WATCHDOG SCRIPT IMPLEMENTED ON THE NOTTINGHAM GISTM STATION.....	127
7.5 SCRIPT TO SEND THE DATA IN REAL TIME TO ESWUA SYSTEM. IT IS IMPLEMENTED ON THE NOTTINGHAM GISTM STATION. ....	128
7.6 SCRIPT TO ACQUIRE 1 S RINEX DATA TO BE IMPLEMENTED IF NEED BE. ....	130
7.7 PHP PROGRAM TO SEND A DAILY EMAIL REPORTING THE STRUCTURED DATA FOR EACH STATION. IT IS IMPLEMENTED AT ESWUA SYSTEM. ....	133
7.8 SUBROUTINE READMEANDATA.C OF THE GBSC TO INCLUDE CCSTDDEV AND C/N INTO THE MAPS. ....	136
7.9 EXAMPLES OF GBSC INPUT DATACARDS: MEANMAP.DATACARD AND OCCUMAP.DATACARD .....	141
7.10 DATA_ROOT_FILTER.C ROUTINE TO PREPARE ROOT FILES WITH FILTERED DATA .....	144
7.11 DATA_PREP ROUTINE TO PREPARE GISTM OUTPUT FILES .....	148

## LIST OF FIGURES

Figure 2.1.1. The GISTM receiver station located at Longyearbyen (Svalbard, Norway, 78.2 N, 16.0 E).	23
Figure 2.2.1. eSWua home page ( <a href="http://www.eswua.ingv.it">www.eswua.ingv.it</a> ).	26
Figure 2.2.2. Location of the NGI-INGV GISTM network integrated in eSWua. Maps are from Google MAP TM.	27
Figure 2.2.3. eSWua system architecture	28
Figure 2.2.4. The IESSG GISTM initial web page at eSWua ( <a href="http://www.eswua.ingv.it/nottingham">www.eswua.ingv.it/nottingham</a> ).	30
Figure 2.2.5. Snapshot of polar plot recorded at Ny-Ålesund on October, 4th 2012.	30
Figure 2.2.6. The “Linear Plot” tool developed to access data from the Nottingham GISTM station.	31
Figure 2.2.7. The download interface sub-page.	32
Figure 2.3.1. Corrected S4 for satellites observed at station LYBO with elevation >30° (top); height error from pseudorange-only solution without mitigation (middle); Height error from pseudorange-only solution with mitigation (bottom), from Aquino et al. (2009).	34
Figure 2.3.2. Equivalent vertical TEC, phase and amplitude scintillation for GPS satellite ‘PRN 31’ recorded at the Svalbard receiver between 20:00 and 24:00 UT on October 30, 2003 and plotted as a function of the geographic latitude of the subionospheric point calculated for the assumed ionospheric altitude of 350 km.	36
Figure 2.3.3. Data flow of the statistical study (Romano, 2009).	37
Figure 2.3.4. Correlation plot between S4 and $\sigma_\phi$ for all stations during October 2003. Dependence on elevation angle is shown with different colours. This plot shows the different impact of the multipath on the two scintillation indices: S4 is much more affected.	38
Figure 2.3.5. Block diagram of the data preparation chain	39
Figure 2.3.6. Maps of the percentages of occurrence of phase scintillation in magnetic latitude and magnetic local time, separating the IMF Bz positive and negative conditions. (left) Northern Hemisphere and (right) Southern Hemisphere (black and red curves reproduce the Feldstein auroral ovals for IQ = 0.3, respectively). Extracted from Alfonsi et al., 2011.	40
Figure 2.3.7. Map of Sigma Phi percentage of occurrence above the weak scintillation threshold (0.1 radians). The black curve is the modelled Feldstein oval for IQ = 0, while the black boxes identify the ionospheric hot spots. Extracted from Spogli et al., 2013	41
Figure 2.3.8. Map of the percentages of occurrence of S4 above 0.1 rad for SCINTMON (Jan–Oct 2009, top plot) and PolaRxS (Feb–Oct 2011, bottom plot) in Geographic Latitude vs. Universal Time.	42
Figure 3.1.1. Azimuth–elevation map of the Code-Carrier divergence standard	47
Figure 3.1.2. Azimuth–elevation map of the standard deviation of the L1 C/N	47
Figure 3.1.3. Latitude–longitude map of the percentage of occurrence of	48
Figure 3.1.4. Top plot: azimuth–elevation map of the percentage of occurrence	49
Figure 3.1.5. Azimuth–elevation map of the percentage of occurrence of phase	50
Figure 3.1.6. First Fresnel zone radius as a function of distance.	51
Figure 3.1.7. Map of the campus.	52
Figure 3.1.8. Maps of the standard deviation of L1C/N in geographic coordinates for the considered period of 2008 (top) and 2009 (bottom).	53
Figure 3.1.9. Maps of Code Carrier Divergence Standard Deviation in geographic coordinates for the periods considered in 2008 (top) and 2009 (bottom).	54
Figure 3.1.10. Maps of the standard deviation of the Code Carrier Divergence Standard Deviation in geographic coordinates for the periods considered in 2008 (top) and 2009 (bottom).	55
Figure 3.1.11. Time profiles of S4 (top) and $\sigma_\phi$ (bottom) for all satellites in view as measured by NSF06 on 30 October 2003.	56
Figure 3.1.12. Time profiles of S4 (top) and $\sigma_\phi$ (bottom) for all satellites in view as measured by NSF06 on 31 October 2003.	57

Figure 3.1.13. Time profiles of vTEC (top) and ROT (bottom) for all satellites in view as measured by NSF06 on 30 October 2003. ....	58
Figure 3.1.14. Time profiles of vTEC (top) and ROT (bottom) time profiles for all satellites in view as measured by NSF06 on 30 October 2003. ....	58
Figure 3.1.15. Azimuth–elevation map of the standard deviation of L1 C/N for.....	59
Figure 3.1.16 Azimuth–elevation map of the Code Carrier Divergence Standard Deviation.....	60
Figure 3.1.17. Azimuth–elevation maps of the $\sigma_\phi$ standard deviation (left) and percentage of occurrence above 0.1 radians (right) for the period 27 October to 3 .....	60
Figure 3.2.1 Logic diagram of the Filtering method .....	62
Figure 3.2.2. Map of the $\sigma_{CCSTDDEV}$ in azimuth vs. elevation for Rome GISTM station on L1 frequency for 2012. ....	63
Figure 3.2.3. Distribution of the $\sigma_{CCSTDDEV}$ corresponding to Rome GISTM data in 2012. The red lines indicate 5 different values of $k$ to determine the cut-off thresholds ( $k=1, k=2, k=3, k=4$ and $k=5$ ). The two histograms (top and bottom) report same quantities but with two different x-axis scales. ....	64
Figure 3.2.4. $\sigma_{CCSTDDEV}$ cut-off values (blue line) and number of filtered out bins (red line) for different values of $k$ from 1 to 5. ....	64
Figure 3.2.5 On the left the Azimuth vs. Elevation maps of Mean (top) and Standard Deviation of CCSTDDEV (bottom) and on the right the corresponding maps filtered with $k= 1$ . Data processing is related to the data acquired by the GISTM station of Rome in 2012. ....	65
Figure 3.2.6. On the left the Azimuth vs. Elevation maps of Mean (top) and Standard Deviation of CCSTDDEV (bottom) and on the right the corresponding maps filtered with $k= 2$ . Data processing is related to the data acquired by the GISTM station of Rome in 2012. ....	66
Figure 3.2.7. On the left the Azimuth vs. Elevation maps of Mean (top) and Standard Deviation of CCSTDDEV (bottom) and on the right the corresponding maps filtered with $k= 3$ . Data processing is related to the data acquired by the GISTM station of Rome in 2012. ....	66
Figure 3.2.8 On the left the Azimuth vs. Elevation maps of Mean (top) and Standard Deviation of CCSTDDEV (bottom) and on the right the corresponding maps filtered with $k= 4$ . Data processing is related to the data acquired by the GISTM station of Rome in 2012. ....	67
Figure 3.2.9 On the left the Azimuth vs. Elevation maps of Mean (top) and Standard Deviation of CCSTDDEV (bottom) and on the right the corresponding maps filtered with $k= 5$ . Data processing is related to the data acquired by the GISTM station of Rome in 2012. ....	67
Figure 4.1.1. (top to bottom) Maps of: percentage occurrence of $\sigma_\phi$ , percentage occurrence of the S4, ROT and ROT RMS, in geomagnetic coordinates. Northern Hemisphere (left) and Southern Hemisphere (right). Black and red curves reproduce the Feldstein auroral ovals for $IQ=0$ and $IQ=3$ , respectively. ....	69
Figure 4.1.2. a) Map of the $\sigma_{CCSTDDEV}$ in azimuth vs. elevation for the BTNO GISTM station on L1 frequency for 2008; b) corresponding map of the $\sigma_{CCSTDDEV}$ filtered with $k= 1.5$ ; c) Distribution of the $\sigma_{CCSTDDEV}$ of BTNO GISTM data for 2008, the red line indicates the value of the cut-off threshold for $k=1.5$ . ....	70
Figure 4.1.3. a) Map of the $\sigma_{CCSTDDEV}$ in azimuth vs. elevation for the DMCO GISTM station on L1 frequency for 2008; b) corresponding map of the $\sigma_{CCSTDDEV}$ filtered with $k= 1.5$ ; c) Distribution of the $\sigma_{CCSTDDEV}$ of DMCO GISTM data for 2008, the red line indicates the value of the cut-off threshold for $k=1.5$ . ....	70
Figure 4.1.4. a) Map of the $\sigma_{CCSTDDEV}$ in azimuth vs. elevation for the LYBO GISTM station on L1 frequency for 2008; b) corresponding map of the $\sigma_{CCSTDDEV}$ filtered with $k= 1.5$ ; c) Distribution of the $\sigma_{CCSTDDEV}$ of LYBO GISTM data for 2008, the red line indicates the value of the cut-off threshold for $k=1.5$ . ....	71
Figure 4.1.5. a) Map of the $\sigma_{CCSTDDEV}$ in azimuth vs. elevation for the NSF01 GISTM station on L1 frequency for 2008; b) corresponding map of the $\sigma_{CCSTDDEV}$ filtered with $k= 1.5$ ; c) Distribution of the $\sigma_{CCSTDDEV}$ of NSF01 GISTM data for 2008, the red line indicates the value of the cut-off threshold for $k=1.5$ . ....	71
Figure 4.1.6. a) Map of the $\sigma_{CCSTDDEV}$ in azimuth vs. elevation for the NYAO GISTM station on L1 frequency for 2008; b) corresponding map of the $\sigma_{CCSTDDEV}$ filtered with $k= 1.5$ ; c) Distribution of the	

<i><math>\sigma_{CCSTDDEV}</math> of NYAO GISTM data for 2008, the red line indicates the value of the cut-off threshold for <math>k=1.5</math>.</i>	72
Figure 4.1.7. a) Map of the $\sigma_{CCSTDDEV}$ in azimuth vs. elevation for the NYA1 GISTM station on L1 frequency for 2008; b) corresponding map of the $\sigma_{CCSTDDEV}$ filtered with $k= 1.5$ ; c) Distribution of the $\sigma_{CCSTDDEV}$ of NYA1 GISTM data for 2008, the red line indicates the value of the cut-off threshold for $k=1.5$ .	72
Figure 4.1.8. $\sigma_{CCSTDDEV}$ cut-off values (blue line) for $k=1.5$ ; the percentage of filtered out bins (red line) relative to the total number of filled bins for each station.	73
Figure 4.1.9. Percentage of discarded data applying the standard threshold of $20^\circ$ on the elevation angle (red line); percentage of discarded data applying the filtering technique (blue line) for each station.	73
Figure 4.1.10. (top to bottom) Filtered maps of: percentage occurrence of $\sigma_\phi$ , percentage occurrence of the S4, ROT and ROT standard deviation, in geomagnetic coordinates. Northern Hemisphere (left) and Southern Hemisphere (right). Black and red curves reproduce the Feldstein auroral ovals for $IQ=0$ and $IQ=3$ , respectively.	74
Figure 4.2.1. Percentage of data coverage of the CIGALA/CALIBRA network considering the full dataset for 2012, obtained respectively applying no threshold on the elevation angle (a) and with a threshold of $20^\circ$ (b). Both maps and the geomagnetic equator (red line) are projected to a height of 350 km.	77
Figure 4.2.2. (a) Map of the $\sigma_{CCSTDDEV}$ in azimuth vs. elevation for MANA (GPS+GLONASS data on L1 frequency) for 2012. (b) Corresponding distribution of the $\sigma_{CCSTDDEV}$ . The red line indicates the cut-off for mild outliers.	78
Figure 4.2.3. Filtered data map of the $\sigma_{CCSTDDEV}$ in azimuth vs. elevation for MANA (GPS+GLONASS data on L1 frequency) for 2012.	79
Figure 4.2.4. $\sigma_{CCSTDDEV}$ Cut-off values (blue line) for $k=1.5$ ; the percentage of filtered out bins (red line) relative to the total number of filled bins for each station in the CIGALA/CALIBRA network.	79
Figure 4.2.5. Percentage of filtered out data applying a cut-off elevation angle of $20^\circ$ (red line) and percentage of filtered out data applying the filtering technique (blue line) for each station in the CIGALA/CALIBRA network.	80
Figure 4.2.6. Percentage of data coverage of the CIGALA network receivers considering the full dataset for 2012 after the filtering procedure. The map and the geomagnetic equator (red line) are projected to a height of 350 km.	81
Figure 4.2.7. Map of percentage of occurrence of S4 above 0.25, in geographic coordinates (GPS + GLONASS, L1 frequency) in the UT range 22-04 UT.	81
Figure 4.3.1. Logic flow diagram followed in simulation to apply the station characterization and filtering methods to simulated data.	83
Figure 4.3.3. Spirent multipath tool user interface set up for the simulation of the Scenario A.	85
Figure 4.3.4. Time profiles of S4 for all satellites during the first day of acquisition. The simulated configuration is set up without scintillation and multipath effects. Each colour corresponds to a different satellite.	86
Figure 4.3.5. Time profile of S4 for all satellites during the second day of acquisition. The simulated configuration comprises multipath effects.	87
Figure 4.3.6. Time profile of S4 for all satellites during the third day of acquisition. The simulated configuration comprises the scintillation effects on PRN 17 (light grey trace).	87
Figure 4.3.7. Azimuth–elevation map of the percentage of occurrence	88
Figure 4.3.8 Time profiles of S4 for all satellites during the fourth day of acquisition. The simulated configuration comprises scintillation and multipath effects.	88
Figure 4.3.9. Azimuth–elevation map of the percentage of occurrence	89
Figure 4.3.10. Map of the $\sigma_{CCSTDDEV}$ in azimuth vs. elevation for the simulation of Scenario A for the Nottingham station on L1 frequency for the fourth day of simulation. Simulation comprises scintillation on PRN 17 and multipath effects.	89
Figure 4.3.11. Distribution of the $\sigma_{CCSTDDEV}$ corresponding to the fourth day of data acquisition simulation. The red line indicates the cut-off threshold for $k=1.5$ .	90

Figure 4.3.12. Filtered data map of the $\sigma_{CCSTDDEV}$ in azimuth vs. elevation for the simulation of Scenario A. ....	91
Figure 4.3.13. Filtered time profiles of S4 for all satellites during the fourth day of acquisition of Scenario A. ....	91
Figure 4.3.14 Filtered time profiles of S4 for all satellites. ....	92
Figure 4.3.15. Time profiles of $\sigma_{\phi}$ for all satellites during the fourth day of acquisition of Scenario A. The simulated configuration comprises scintillation and multipath effects. ....	93
Figure 4.3.2. Extract of the User Commands File arranged for implementing scintillation effects in the simulation of Scenario A. ....	84

## LIST OF TABLES

Table 1.1.1. Schematic for the thesis structure. ....	20
Table 2.1.1. Main features of the NGI-INGV GISTM network in the European Northern Hemisphere. ....	22
Table 2.1.2. Parameters logged for every satellite in view and recorded in the S60 15-minute file. ....	24
Table 2.2.1. Main features of the GISTM receivers in eSWua. ....	26
Table 2.2.2. GNSS ionospheric data systems". ....	33
Table 2.2.3. Feature comparison between five of the main GNSS data management systems. ....	33
Table 2.3.5. Summary of monitoring and data management tools developed during the PhD course ..	43
Table 3.1.1 Summary of the data analysed from 2008 and 2009. ....	52
Table 3.2.1. Cut-off values for different k values and the corresponding number of bins filtered out ....	63
Table 4.1.1. Receiver ID, location and geographic coordinates of the network (adapted from Alfonsi et al., 2011). ....	68
Table 4.2.1. List of the CIGALA/CALIBRA network receivers used in the analysis. ....	76
Table 4.3.1. Simulation features of Scenario A. ....	85

## LIST OF ACRONYMS

AACGM	Altitude Adjusted Geomagnetic Coordinates
ADR	Accumulated Doppler Range
AIS	Advanced Ionospheric Sounder
ASCII	American Standard Code for Information Interchange
C/N	Carrier to Noise Ratio
CALIBRA	Countering GNSS high Accuracy applications Limitations due to ionospheric disturbances in BRAzil – FP7 Project
CCDIV	L1 Code/Carrier divergence
CCSTDDEV	Standard Deviation of L1 Code/Carrier divergence
CHAIN	Canadian High Arctic Ionospheric Network.
CIGALA	Concept for Ionospheric-Scintillation Mitigation for Professional GNSS in Latin America – FP7 Project
CALIBRA	Countering GNSS high Accuracy applications Limitation due to ionospheric disturbance in BRAzil, FP7 project
DB	Database
DGPS	Differential GPS
DLL	Delay Locked Loop
EIA	Equatorial Ionospheric Anomaly
EPSRC	Engineering and Physical Sciences Research Council
eSWua	electronic Space Weather upper atmosphere
EU	European Union
FP7	Seventh Framework Programme for Research
GBSC	Ground Based Scintillation Climatology
GISTM	GPS Ionospheric Scintillation and TEC Monitor
GLONASS	GLObal NAVigation Satellite System
GNSS	Global Navigation Satellite Systems
GPIB	General Purpose Interface Bus
GPS	Global Positioning System
IESSG	Institute of Engineering Surveying and Space Geodesy
IMF	Interplanetary Magnetic Field
INGV	Istituto Nazionale di Geofisica e Vulcanologia
IPDM	Ionospheric Perturbation and Detection Monitoring
IPP	Ionospheric Pierce Point
IQ	Magnetic Activity Level
ISACCO	Ionospheric Scintillation Arctic Campaign Coordinated Observations
ISMR	Ionospheric Scintillation Monitoring Records
ITN	Initial Training Network
JCR	Journal of Controlled Release
MIDAS	Multi-Instrument Data Analysis System
NGI	Nottingham Geospatial Institute
OEXO	ovenized crystal oscillator
PhD	Doctor of Philosophy
PHP	Personal Home Page
PLL	Phase Lock Loop
PRN	Pseudo-Random Number
RF	Radio Frequency
RINEX	Receiver Independent Exchange Format

RMS	Root Mean Square
ROT	Rate of TEC change
SAMA	South Atlantic Magnetic Anomaly
SBAS	Satellite Based Augmentation Systems
SCINTMON	Cornell Scintillation Monitor
SLOG	Scriptable Logger
SME	Small Medium Enterprise
SNR	signal-to-noise-ratio
sTEC	slant Total Electron Content
SV	Satellite Vehicle
SWACI	Space Weather Application Center - Ionosphere
TEC	Total Electron Content
TECu	TEC unit
TOI	Tongue of Ionization
TOW	Time of Week
TRANSMIT	Training Research and Applications Network to Support the Mitigation of Ionospheric Threats – EU project
UDP	User Datagram Protocol
URL	Uniform Resource Locator
vTEC	Vertical TEC
WAAS	Wide Area Augmentation System

# 1 CHAPTER 1 – INTRODUCTION

---

## 1.1 MOTIVATION AND PURPOSE OF THE RESEARCH

The increasing importance of satellite navigation technologies for modern society means that knowledge and monitoring of scintillation events are essential so that warnings and forecast information can be made available to end users and system designers. Users and designers of GNSS systems (such as the GPS, GLONASS, and the forthcoming Galileo) need warnings (now-cast and forecast) of ionospheric conditions in order to guarantee the necessary levels of accuracy, integrity, and immediacy for reliable life-critical applications. This is especially important in the face of severe geospatial perturbations, when mitigation tools are required to minimize the degrading effects on satellite signals (loss of lock, lower accuracy, and reduced satellite availability). Ionospheric Scintillation can affect GNSS receivers in several ways:

- When scintillation activity is low to moderate, the signals exhibit increased noise levels which may limit positioning accuracy. This is more obvious in applications like surveying, geodesy, construction, etc.
- When scintillation activity is moderate to high the signals exhibit major disturbances and receivers may have considerable difficulty maintaining signal track.

The research project is dedicated to developing new methods of data analysis, and the enlargement, management, and development of the first Northern European network of GPS receivers suitably modified to monitor the upper atmosphere. This network was carefully realised for the recent solar maximum when this kind of knowledge and expertise was greatly in demand by a large number of bodies, both in the government and private sectors. High solar activity poses a serious threat to satellite based navigation and telecommunications systems because the artificial satellite signals propagate through the Earth's ionosphere, which is very strongly influenced by magnetic and solar activity. Under external perturbed conditions, the ionosphere can become extremely irregular and the disruptive effects on these technological systems are critically amplified. Despite great advances over the past 40 years, scientific knowledge of the complex Sun-Earth system is far from complete, with some fundamental questions remaining unanswered. The description of the conditions in space that affect Earth and its technological systems, i.e. Space Weather, remains far from satisfactory. In this context, ionospheric effects at equatorial, auroral, and mid latitude regions represent a major set of space weather effects that still need to be better characterized and understood. Improvements can be achieved with coordinated continuous observations through time and space, of adequate resolution and easily accessible data. This is a fundamental contribution towards establishing a global set of observations, of particular value for driving, validating, or assimilating into global models of the geospace environment.

The research project is within the framework of a longstanding NGI-INGV collaboration, consolidated in the framework of two ended projects:

- Royal Society International Joint Project "Original and Novel Solutions to Counter GNSS Ionospheric Scintillation Effects"<sup>1</sup>;

---

<sup>1</sup> <https://www.nottingham.ac.uk/ngi/research/propagation-effects-on-gnss/projects/project-listing.aspx>

- COST296 action “Mitigation of Ionospheric Effects on Radio Systems” (Bourdillon et al., 2009).

As a consequence of scientific results obtained in the WP3.3 “Ionospheric scintillation monitoring and modelling” of the COST296 action (Beniguel et al., 2009), the formation of a consortium to establish an ‘Ionospheric Perturbation and Detection Monitoring (IPDM)’ network in Europe was proposed. This formed the foundation for a research initiative, and potentially for a service by means of the TRANSMIT project<sup>2</sup>. The TRANSMIT project is a Marie Curie Initial Training Network (ITN), funded under the EU FP7 framework. The project has ended in February 2015 and it’s vision is to act as the enabler of the Ionospheric Perturbation Detection and Monitoring (IPDM) network, i.e. “...an operational European-wide information service, capable of detecting and monitoring the whole spectrum of ionospheric perturbations and related scintillations (via geo-plasma warnings, now-casts, and forecasts) for the wider European user community, including SME's, government offices, commercial and public users...”<sup>3</sup>. TRANSMIT’s primary mission is to provide Europe with the next generation of researchers, equipping them with skills through a comprehensive and coordinated multi-disciplinary, inter-sectorial, industry-led training programme. The training is intended to equip the new researchers with an in-depth understanding of the threats posed by the ionosphere to modern technological systems, and in particular the GNSS value chain, and respond to the needs of various stakeholders for robust counter-measures to deal with these threats. The secondary aim of the TRANSMIT project is to develop real-time integrated state-of-the-art tools to mitigate ionospheric threats, making these tool available and accessible to the various stakeholders via the “Transmit Prototype” system (Sato et al., 2014 and [www.transmit-prototype.net](http://www.transmit-prototype.net)).

In this collaborative context, this PhD work aims to improve monitoring techniques and develop novel data processing in the field of ionospheric scintillations. The research contributes towards the realization of a modern international upper atmosphere network in Europe, advancing the understanding of the physical processes causing the ionospheric effects that are potentially disruptive for positioning and navigation systems. This knowledge is crucial for Space Weather applications aiming to forecast and now-cast possible effects on technological systems, and is of particular interest for the design of receivers for the forthcoming Galileo system.

Specific aims of the research were:

- Development of software procedures and hardware designs in order to optimize the station configurations of the existing GISTM (GPS Ionospheric Scintillation and TEC Monitor) network.
- Development of techniques for remote, automatic instrument control and setting.
- Development of data management tools to achieve quasi real-time data accessibility.
- Data analysis to assess station characterization and data quality filtering techniques.
- Perform acquisition of experimental and simulation data
- Apply data analysis to case studies.

The environmental conditions at each receiver location that contaminate scintillation measurements, such as buildings, trees and other interfering features, need to be identified in order to improve the quality of the scintillation and TEC data. This is

---

<sup>2</sup> [www.transmit-ionsphere.net](http://www.transmit-ionsphere.net)

<sup>3</sup> <http://ipdm.nottingham.ac.uk>

achieved by removing these local sources of errors or mitigating their effects by data filtering. The identification of the directions in which a signal is systematically affected by such sources is the first step towards a new data filtering method, which is one of the aims of this research project and which has not been attempted before, according to current literature. This procedure involves identification of ray-paths affected by error sources that could mimic scintillation and lead to signal degradation. This research work introduces a novel method to characterize GISTM data and then to filter out spurious data, which is able to efficiently remove multipath affected measurements and in most of the cases reducing the data loss with respect to applying a fixed elevation angle cut-off threshold.

## **1.2 SCIENTIFIC BACKGROUND AND REVIEW OF LITERATURE**

The ionosphere is a dispersive medium in which RF signals are refracted by an amount dependent on the given signal frequency and ionospheric electron density. The ionosphere is made up of ionized plasma and can be classified into four regions, D, E, F1, and F2. The D region typically extends from 50 to 90 km and has a negligible effect on GPS frequencies. The E region typically extends from 90 to 140 km and is produced by solar soft X-rays and also has a negligible effect on GNSS frequencies. The F1 region typically extends from 140 to 210 km and has a significant influence on GNSS frequencies. The heights of these regions are not fixed and they fluctuate a great deal. The F1 region is estimated to account for 10% of daytime ionospheric induced errors affecting GNSS signals. The D, E, and F1 regions are associated with daytime UV (ultra violet) ionization and hence are not present at night. The F2 region typically extends from 210 to 1000 km. It is the most active region and its influence on GPS frequencies is fundamental. The F2 region is present at night unlike the D, E, and F1 regions. Most of the day-to-day (diurnal) effects can be reasonably well modelled, however the ionosphere exhibits levels that can lead to non-deterministic effects such as scintillation effects. The ionosphere has the following main effects (among others) on GPS signals: 1) group delay of the modulated signal, 2) carrier phase advance, 3) scintillation, and 4) Faraday rotation (Klobuchar, 1996).

The ionosphere is a turbulent medium, characterized by a large variability of spatial and temporal scales.

In regions of small spatial scale irregularities, i.e. electron density fluctuations, rapid random phase variations can be produced by phase irregularities in the emerging wavefront (Hargreaves, 1992). These are referred to as phase scintillations. Diffraction of a signal (interference across the wavefront) also leads to variations in signal amplitude, referred to as amplitude scintillation (or amplitude fading, for reductions in signal strength) (Skone and de Jong, 2000). Small-scale electron density irregularities are usually embedded into larger scale plasma structures, which develop at altitudes ranging from 200 to 1000 km. Sometimes, irregularities in the E layer between 90 and 100 km can produce radio wave scintillations, particularly in the presence of sporadic-E and auroral E (Aarons, 1982).

Moreover, the strength of the ionospheric turbulence has been found to increase the rapidity of the fades of trans-ionospheric signals, resulting in sudden phase transitions that could further lead to overbearing impacts on the phase lock loop (PLL) of the receiver (Strangeways, 2009; Strangeways et al., 2011).

Scintillation effects are significant in equatorial regions ( $\pm 30^\circ$  geomagnetic latitude) with the largest effects in the region of  $\pm 10^\circ$  and in auroral and polar latitudes (Kintner et al., 2009). Equatorial scintillation most commonly occurs from 19:00 to 24:00 hours local time (Klobuchar, 1996). Amplitude fading can be larger than 20 dB in this region during high solar activity (Basu et al., 1988).

Fading may lead to loss of lock with the satellites, and in general GPS receiver loses lock on L2 signal more often than on L1 for the same satellite traversing ionospheric irregularities (El-Arini et al., 2009; Strangeways, 2009).

Scintillation is also frequent in the auroral and polar cap regions ( $65^\circ$  to  $90^\circ$  geomagnetic latitude). Scintillation phenomenology in such regions is different from that in the equatorial and the two are not really correlated. In fact, while scintillation at low latitudes is due to the Equatorial Ionospheric Anomaly formation (see, e.g. Jin et al, 2008), scintillation at high latitude is due to patches of plasma density and density troughs, the steep edges of which are unstable, so that smaller scale density structures develop along these edges leading to scintillation (De Franceschi et al., 2008). Moreover, within the auroral oval and cusp, energetic particles precipitating from the outer space can produce increases of the ambient electron density, creating irregular structures and turbulence.

In addition, while at equatorial latitudes scintillation shows a roughly constant diurnal variation, due to the regular behaviour of the geomagnetic field, scintillation at high latitude is not restricted to any local time period and can last for many hours, even days (Skone and Cannon, 1998). Scintillation at high latitude increases during magnetic storms.

In general, auroral zone scintillation effects are less severe than equatorial ones and can induce amplitude fading of no more than 10 dB (Cannon et al., 1997).

Scintillation also has a seasonal dependence. It is less common in the American, African, and Indian latitudes during the months of April to August, when conversely it occurs most frequently in the Pacific region. These effects are reversed during the rest of the year (Klobuchar, 1996). Basu et al. (1988) determined a strong correlation between ionospheric scintillation and sunspot number. Scintillation effects are therefore expected to be stronger and more frequent during a solar maximum.

The occurrence, spatial distribution, characteristics, and dynamics of ionospheric irregularities are among the most widely studied, but nevertheless unresolved, issues in ionospheric phenomenology. The mitigation of the effect of ionospheric irregularities on GNSS propagation remains an enduring problem because of their spatially patchy occurrence regions, their high velocities and their temporal variability. In spite of much progress, the physics of ionospheric irregularities is far from being understood. Their behaviour is still unpredictable within current ionospheric models and their negative effects on radio communications can be quite significant. It is reasonable to say that an effective description of the appearance and behaviour of the ionospheric irregularities that cause signal scintillations is the last great unsolved problem in ionospheric science applied to communications and navigation.

The signal distortions caused by scintillation can affect GNSS receiver performance from degradation of accuracy (through range errors) to a complete loss of signal tracking. They can degrade the performance of navigation systems and generate errors in received messages. Since ionospheric scintillation originates from random electron density irregularities acting as wave scatterers, research into the formation and

evolution of irregularities is closely related to scintillation studies. Over the past four decades there has been a lively interest in this field. Many excellent reviews of scintillation theory and observations (e.g. Aarons, 1982, 1993; Yeh and Liu, 1982; Basu and Basu, 1985, 1993; Bhattacharyya et al., 1992) have been published. Comprehensive reviews of the physics of ionospheric irregularities can be found in a book by Kelley (1989) and in various articles (e.g. Keskinen and Ossakow, 1983; Kintner and Seyler, 1985; Tsunoda, 1988; Huba, 1989; Heppner et al., 1993; Fejer, 1996).

The required levels of accuracy, functional consistency, and availability of GNSS signals are sometimes not satisfied, compromising commercial operations like offshore navigation and station keeping, including safety-critical applications. In order to better investigate the physics of the upper atmosphere and provide useful tools for radio communications and satellite navigation, several kinds of experimental data must be collected, realistic models developed, and most importantly useful real-time indices and alerts must be made available. Over the next few years, the first operative stages of Galileo will require concrete support regarding the monitoring, nowcasting, and forecasting of the ionized atmosphere. Only a well established infrastructure providing reliable real-time data can fit this need. A robust data bank would provide the necessary experimental foundations to investigate ionospheric plasma dynamics and develop a wide variety of modern tools: a database for space weather purposes, ionospheric tomographic imaging, scintillation modelling for scientific aims and for mitigation techniques, and so on. The eSWua (electronic Space Weather upper atmosphere, Romano et al., 2008) aims to achieve this, motivated by the awareness that geosciences need structured digital data and appropriate scientific procedures developed ad hoc by experts, unrestricted and shared among the international community.

The investigation of the small-scale rapidly evolving irregularities that cause radio scintillation is conducted with systems of special GPS receivers sampling the ionosphere at the high rate of 50 Hz (see, e.g., De Franceschi et al., 2006; Van Dierendonck, 2001). Combining the measurements from these instruments with a large geodetic GPS network provides a reasonably detailed description of ionospheric disturbances in terms of both ionospheric background perturbation and irregularity appearance (Mitchell et al., 2005), indicating the importance of a multi-instrument approach in this kind of research. High latitude irregularities result from precipitation of energetic electrons along terrestrial magnetic field lines into the high latitude ionosphere. This phenomenon characterizes geomagnetic or magnetospheric substorms, when associated irregularities in electron density (at altitudes of 100 to 500 km) generate scintillation effects (cf. Aarons, 1982). Auroral intensifications during a substorm event have time scales on the order of 15 minutes, and in intense events multiple intensifications can occur over a period of hours (Rostoker, 1991). The auroral oval can expand several degrees towards the equator during such events (i.e. over Northern Europe, Northern United States), and the magnitude and frequency of substorms are functions of the solar cycle.

GNSS receiver tracking performance can be degraded in the presence of scintillation effects. Rapid phase variations cause a Doppler shift in the GNSS signal, which may exceed the bandwidth of the phase locked loop (PLL), resulting in a loss of phase lock (Leick, 1995). Additionally, amplitude fades can cause the signal-to-noise-ratio (SNR) to drop below the receiver threshold, resulting in loss of code lock. These effects have

a larger impact on tracking loops that employ codeless and semicodeless technologies compared with full code correlation systems. Codeless and semicodeless tracking loops experience losses of 27 to 30 dB, and 14 to 17 (Leick, 1995) respectively, compared with full code correlation, and are therefore more susceptible to the effects of amplitude fading. The L2 PLL also employs a narrower bandwidth ( $\approx 1$  Hz, compared with  $\approx 15$  Hz for L1) to eliminate excess noise, and is more susceptible to phase scintillations. These effects are therefore a significant concern for users who require dual frequency data (i.e. for estimation of ionospheric effects, or resolution of wide-lane ambiguities). The results of such studies depend not only on the magnitude of the observed scintillation activity, but also on the receiver tracking capabilities, which can vary widely between manufacturers and models. Therefore, in order to fully assess the impact of ionospheric activity on GPS signal availability, it is important to establish the range of performance between various receiver models.

There are also ongoing studies on the mitigation of polar and auroral scintillation effects on GNSS applications, which consider the variance of the output error of both the receiver PLL and DLL (Delay Locked Loop), under the premise that these variances better express the quality of, respectively, the phase and code range measurements used to calculate position (Aquino et al., 2009). The capability of incorporating phase and amplitude scintillation effects into the variance of these tracking errors, via the models of Conker et al. (2003), allows the application of relative weights (based on the inverse of these variances) to measurements from different satellites. This proposed mitigation technique gives the least squares stochastic model used by the receiver for position computation a more realistic representation, in particular in a scintillation scenario, when the ionospheric irregularities affect each satellite differently. A mitigated solution based on pseudorange and carrier phase measurements was implemented and compared with the non-mitigated solution, for a baseline of  $\sim 125$  km between the INGV stations in Longyearbyen ( $\sim 78^\circ\text{N}; \sim 16^\circ\text{E}$ ) and Ny-Ålesund ( $\sim 79^\circ\text{N}; 12^\circ\text{E}$ ). During a period of occurrence of high phase scintillation it was observed that problems related to carrier phase ambiguity resolution affecting positioning accuracy (height in particular) were reduced by the use of the proposed mitigated solution (Aquino et al., 2009).

The above literature review covers scintillation effects and their mitigation as the background of the PhD work. The literature review about the subjects presented and discussed in chapters 2, 3 and 4 is inserted in the relevant sections of these chapters. In particular: Chapter 2 presents the development of techniques for remote, automatic instrument control and setting as well as development of data management tools to achieve quasi real-time data accessibility; Chapter 3 is related to the development of methods and data analysis tools to assess the station characterization and the data quality by filtering techniques; and Chapter 4 is focused on the application to the previous results to specific case studies.

### 1.3 THESIS STRUCTURE

This thesis is composed of five chapters and two sections as shown in Table 1.1.1.

Chapter 1	Introduction: <ul style="list-style-type: none"><li>- Motivation and purpose of the research</li><li>- Scientific background and review of literature</li><li>- Thesis structure</li></ul>
Chapter 2	Monitoring and data management: <ul style="list-style-type: none"><li>- Monitoring</li><li>- eSwua</li><li>- Applications</li></ul>
Chapter 3	Methodology, data analysis and results: <ul style="list-style-type: none"><li>- Station characterization</li><li>- Filtering technique</li></ul>
Chapter 4	Applications: <ul style="list-style-type: none"><li>- Application in scintillation climatology</li><li>- Application on the CIGALA/CALIBRA network</li><li>- Validation with simulated data</li></ul>
Chapter 5	Conclusions
Section 6	References
Section 7	Appendices

*Table 1.1.1. Schematic for the thesis structure.*

Chapter 1 is the introduction chapter of the thesis including the motivation and purpose of the research as well as a scientific overview of the literature about the ionospheric scintillation and its effects on GNSS. Chapter 2 gives the report on the work carried out related to the monitoring and data management applications; it has been done mostly in the first part of the PhD Course. Chapter 3 concentrates on the methodology considered in the investigations of this thesis and the related data analysis results, presented both for station characterization method and the data filtering technique. Chapter 4 presents the application of the results in different cases: scintillation climatology, CALIBRA project and simulated data. Chapter 5 focus on the conclusion for the thesis and puts forward recommendations for the future work. Section 6 contains a list of the references and Section 7 provides the appendices.

## 2 CHAPTER 2 – IONOSPHERIC MONITORING AND DATA MANAGEMENT

### 2.1 MONITORING

The Nottingham Geospatial Institute (NGI), formerly the Institute of Engineering Surveying and Space Geodesy (IESSG) of the University of Nottingham, pioneered GPS ionospheric scintillation monitoring in Northern Europe with GISTM (GPS ionospheric scintillation and TEC monitor, Van Dierendonck et al., 1993; Van Dierendonck, 2001) receivers. Between June 2001 and December 2003 four units were installed at stations in the UK and Norway, covering the geographic latitudes from 53° N to 70° N, approximately. Due to operational limitations no high rate data was stored and analyses were based solely on the ionospheric scintillation indices, focusing on statistical analyses and impact for GNSS users (Rodrigues et al., 2004, Aquino et al., 2005a, Aquino et al., 2005b). These units were decommissioned in 2004 and then, with the support of the Engineering and Physical Sciences Research Council (EPSRC) and within the framework of the Polaris project (grant no. EP/H003479/1), they were re-deployed, together with additional new receivers, at Bronnoysund (Norway), Trondheim (Norway), Lerwick (UK), Newcastle (UK), Nottingham (UK), Rome (Italy), and Nicosia (Cyprus, in collaboration with the Frederick Institute of Technology), where high rate (50 Hz) data as well as scintillation parameters are being recorded. An additional station was deployed by the NGI in Dourbes, Belgium (in collaboration with the Royal Meteorological Institute of Belgium) between 2006 and 2011. The Istituto Nazionale di Geofisica e Vulcanologia (INGV) is in charge of the ISACCO (Ionospheric Scintillation Arctic Campaign Coordinated Observations) project in the Arctic, which started in 2003, and currently runs three GISTM receivers in Svalbard (De Franceschi et al., 2006) and another two at European mid latitudes: Chania (Greece) and Lampedusa (Italy). The stations are listed in Table 2.1.1.

The use of the same kind of GPS receivers allows INGV and NGI to exploit baselines of different lengths for the estimation of positioning errors due to scintillation, and to investigate their mitigation by developing correction algorithms (Aquino et al., 2009). The network covers a wide range of latitudes in the northern European sector with a chain of permanent stations. The chain offers a unique opportunity to analyse long-term data across the entire network and establish an ionospheric climatology for Northern Europe (Spogli et al., 2009).

ID	Station	Owner	Latitude (°N)	Longitude (°E)	Status
NYA1	Ny-Ålesund (Svalbard, Norway)	INGV	78.93	11.86	In operation
NYA0	Ny-Ålesund (Svalbard, Norway)	INGV	78.92	11.93	In operation
LYB0	Longyearbyen(Svalbard, Norway)	INGV	78.17	15.99	In operation
BRON	Bronnoysund (Norway)	NGI	65.46	12.21	In operation
NSF02	Trondheim (Norway)	NGI	63.41	10.40	In operation
LERW	Lerwick (Scotland, UK)	NGI	60.15	-1.13	In operation
NYM17	Newcastle (England, UK)	NGI	54.98	-1.61	In operation

NSF06	Nottingham (England, UK)	NGI	52.94	1.19	In operation
NSF01	Rome (Italy)	NGI	41.83	12.51	In operation
NSF05	Dourbes (Belgium)	NGI	50.09	4.60	Stopped in 2011
LAM0	Lampedusa (Italy)	INGV	35.52	12.62	In operation
CHA1	Chania (Crete, Greece)	INGV	35.51	24.02	In operation
CYPR	Nicosia (Cyprus)	NGI	35.14 N	33.48	In operation

*Table 2.1.1. Main features of the NGI-INGV GISTM network in the European Northern Hemisphere.*

The GISTM system consists of a NovAtel OEM4 dual-frequency receiver with special firmware and a stable ovenized crystal oscillator. These form the main components of the GPS signal monitors, which are specifically configured to measure amplitude and phase scintillation from the L1 frequency GPS signals, and ionospheric TEC (Total Electron Content) from the L1 and L2 frequency GPS signals. The principal features of the GISTM are the following (Van Dierendonck, 2005):

- Tracks and reports scintillation and TEC measurements from up to 11 GPS satellites in view.
- A 25 Hz raw signal intensity noise bandwidth and a 15 Hz phase noise bandwidth to insure that all the spectral components of both amplitude and phase scintillations are measured. Phase data and amplitude data are sampled at a rate of 50 Hz.
- Single frequency (L1) satellite carrier phase is compared against a stable ovenized crystal oscillator to insure that all phase scintillation effects are recorded.
- Software is included in the GISTM to automatically compute and log the amplitude scintillation index,  $S_4$ , and phase scintillation index,  $\sigma_\phi$ , the latter computed over 1, 3, 10, 30, and 60 seconds. In addition, TEC and TEC rate are each logged every 15 seconds. Phase and amplitude data, either in raw form or detrended (to remove systematic variations), can also be logged at 50-Hz.

All scintillation and TEC data are stored locally and transmitted to a data server (isacco.ingv.it) in quasi-real time. The 50 Hz raw data are transmitted to the data server where they remain readily available for post-processing analysis. Amplitude scintillation is traditionally monitored with the  $S_4$  index, which is the standard deviation of the received power normalized by its mean value derived from the detrended received signal intensity. A high-pass filter is used for detrending the raw amplitude measurements. A fixed choice of a 0.1 Hz 3-dB cut-off frequency for phase filtering is used. The GISTM can also log carrier and code phase range data from both the L1 and L2 signal frequencies, so that these can be converted to the RINEX (Receiver Independent Exchange) format using a NovAtel proprietary software, therefore allowing manipulation and processing using different positioning techniques. A typical configuration of a GISTM station is shown in Figure 2.1.1.



Figure 2.1.1. The GISTM receiver station located at Longyearbyen (Svalbard, Norway, 78.2 N, 16.0 E).

Range data was also recorded for all the collected data, and can be converted to the RINEX format.

The Nottingham and Trondheim receivers are configured and set up using two specifically developed scripts. The script code for Nottingham is reported in Appendix 7.1. The program used for acquisition is “slog”, a proprietary software of NovAtel Inc.<sup>4</sup> Slog is a Win32 console application that uses a script to control GPS receivers and equipment in order to log data in a repeatable, controlled manner. It is particularly useful in long-term data collection and monitoring installations when stability and organised archiving are important, as in the present study. Some of the Slog features are (more details can be found at “SLOG – Scriptable Logger - Users Guide”, Novatel Inc. D00993 v.60, 2008 ):

- Slog is a single executable, SLOG.EXE. No DLLs are required.
- The scripts can be created with a simple editor such as Microsoft Notepad. A two-pass read of the script gives notification of most format errors on the first pass.
- Ports can be RS232/RS422 serial, instrumentation GPIB or Internet UDP.
- All data received is immediately recorded in its unmodified form. Device name masking allows concurrent string transmission on two or more ports. Data can be copied (by log id if desired) from one port to another, or to a file.
- It controls the GNSS/GPS simulator.
- It checks for error responses from a card, time shifts in the PC clock, overruns on the serial line, and many other glitches to assist in debugging.
- Loops, if, and jump statements provide script flow control.
- Prototyped subroutines and include files allow compact scripts.
- Parameters used within the script can be defined from the command line.
- Equations can be generated to step equipment, or to control script execution.
- Incoming data can be scanned for use in the script or writing out to a file.
- Re-connection at the same baud rate can be achieved without loss of data.

Several scripts were developed within the framework of the PhD research project to optimize the acquisition procedure step by step, especially as concerns the reliability

<sup>4</sup> <http://www.novatel.com>

of the receiver-PC connection and data transmission. The script reported in Appendix 7.1 (referred to the Nottingham receiver, but similar to the Trondheim script) is the version currently running.

The script developed is able to simultaneously produce two different kinds of files. The first, known as “S60”, is used for acquiring the parameters: one minute information related to navigational and observational data with files generated every 15 minutes, stored locally, and sent by ftp to the eSWua system. The second type, called “RWD”, contains the 50 Hz L1 signal sampling amplitude and phase data, generated every hour and stored locally.

The parameters logged for every satellite in view are reported in Table 2.1.2.

Parameter	Description	Sampling
Versiona	Receiver version information	once
Rxconfiga	Log the receiver configuration	once
Rxstatureventa	Receiver status events	on change
WAAS 18B	Sbas iono grid	on change
WAAS 26B	Sbas iono delays	on change
Gpsephemb	New ephemeris	on change
Rangeb	The range data	5 seconds
WN	Week number	1 minute
TOW	Time of week	1 minute
PRN	PRN	1 minute
Az	SV Azimuth angle degrees	1 minute
Elev	SV Elevation angle degrees	1 minute
C/No	Carrier / Noise (dB-Hz)	1 minute
S4	Total S4 (dimensionless)	1 minute
S4Corr	Correction to total S4 (dimensionless)	1 minute
SIG1	1-second phase sigma (radians)	1 minute
SIG3	3-second phase sigma (radians)	1 minute
SIG10	10-second phase sigma (radians)	1 minute
SIG30	30-second phase sigma (radians)	1 minute
SIG60	60-second phase sigma (radians)	1 minute
DIV	Average of Code/Carrier divergence (metres)	1 minute
CCSTDDEV	Standard Deviation of Code/Carrier Divergence (metres)	1 minute
TEC45	TEC at TOW - 45 (TECU)	1 minute
$\Delta$ TEC45	Relative TEC from TOW - 60 to TOW - 45 (TECU)	1 minute
TEC30	TEC at TOW - 30 (TECU)	1 minute
$\Delta$ TEC30	Relative TEC from TOW - 45 to TOW - 30 (TECU)	1 minute
TEC15	TEC at TOW - 15 (TECU)	1 minute
$\Delta$ TEC15	Relative TEC from TOW - 30 to TOW - 15 (TECU)	1 minute
TEC0	TEC at TOW (TECU)	1 minute
$\Delta$ TEC0	Relative TEC from TOW - 15 to TOW (TECU)	1 minute
L1Lck	L1 Lock time (seconds)	1 minute
L2Lck	L2 Lock Time (seconds)	1 minute
L2 C/NO	L2 Carrier / Noise (dB-Hz)	1 minute

Table 2.1.2. Parameters logged for every satellite in view and recorded in the S60 15-minute file.

The RWD file collects raw phase measurements and raw amplitude measurements at a rate of 50 Hz-. Each log contains data blocks for all the satellites being tracked, with each data block containing 50 data sets. The first set is for the time specified in Time of Week (TOW), the second set at TOW+0.02 seconds, and so on. The ADR (phase) of the tracking model is applied in this log, including frequencies up to the tracking loop bandwidth (default at 10 Hz). This log also includes raw 1-second TEC and  $\Delta$ TEC data. The scale factor of the raw power measurements is meaningless because the actual receiver and antenna gains are unknown. Ultimately, this does not matter because the measurements are subsequently normalized by detrending and S4 forming. The raw phase measurements include satellite motion, the rate of change of the ionosphere, and satellite and receiver oscillator drift. Thus, observation of scintillation in the measurements is impossible without detrending, although the use of FFT programs with windowing may be applied without detrending (Van Dierendonck, 2007). The data acquisition and transfer problems identified for the Nottingham and Trondheim stations were resolved during the research period. Two external programs were developed to automatically guarantee data transmission to the eSWua system<sup>5</sup> (Appendix 7.5) and to restart the acquisition procedure in cases of interruptions due to TCP/IP issues (Scripts in Appendix 7.4). These programs are currently running successfully and have improved the continuity of acquisitions. In March 2012 the monitoring activity of the PhD Course has included the installation of a GISTM station in Rome Italy. The work has included the development of the acquisition script and the data management tools. The station owner is NGI and it is hosted at the headquarters of INGV.

## **2.2 THE ESWUA SYSTEM**

Within the framework of the research project, some of the data from the NGI GISTM stations were integrated into the data management system called eSWua (electronic Space weather upper atmosphere, Romano et al., 2008) in order to develop specific tools for these stations. eSWua is installed at INGV, the outside organization supporting the PhD course.

The need to standardize historical and real-time observations for a number of stations made it necessary to develop a well designed database. eSWua is a hardware-software system based on measurements from instruments installed by the upper atmosphere physics group of the Istituto Nazionale di Geofisica e Vulcanologia, now also including the GISTM stations operated by the NGI (Romano et al., 2013). The eSWua website<sup>6</sup> provides access to the database designed to organize and manage the large volume of acquired information (Figure 2.2.1). The locations of the GISTM stations included in eSWua are shown in Figure 2.2.2 and schematically listed in Table 2.2.1.

---

<sup>5</sup> [www.eswua.ingv.it](http://www.eswua.ingv.it)

<sup>6</sup> [www.eswua.ingv.it](http://www.eswua.ingv.it)



Figure 2.2.1. eSWua home page (www.eswua.ingv.it).

ID	Station	Owner	Latitude (°N)	Longitude (°E)
BTNO	Mario Zucchelli Station	INGV	-74.70	164.11
DMC0	Concordia Station - Dome C	INGV	-75.10	123.33
DMC1	Concordia Station - Dome C	INGV	-75.11	123.31
NYA0	Ny-Ålesund (Dirgibile Italia Station)	INGV	78.92	11.93
NYA1	Ny-Ålesund (Kartverk)	INGV	78.93	11.86
LYB0	Longyearbyen	INGV	78.17	15.99
NSF01	Trondheim	University of Nottingham	63.44	10.40
NSF05	Dourbes	University of Nottingham	50.09	4.60
NSF06	Nottingham	University of Nottingham	52.94	1.19

Table 2.2.1. Main features of the GISTM receivers in eSWua.

The schematic architecture of eSWua is based on three high performing servers, as illustrated in Figure 2.2.3. These servers can store database tables, process user requests, and deliver various services. The first server, eSWua, hosts the system website and is devoted to user interface management, achieved using PHP and Java

applications. eSWua server applications are also designed to guarantee protected access to the database tables and data files.

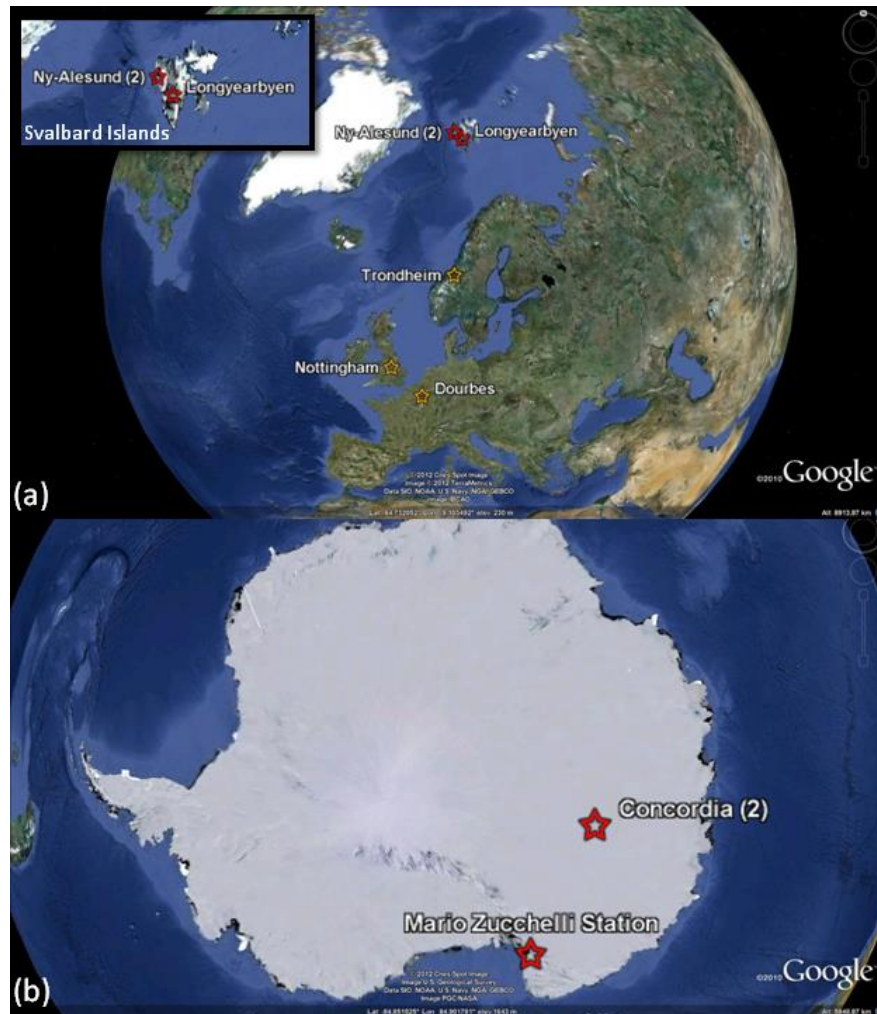


Figure 2.2.2. Location of the NGI-INGV GISTM network integrated in eSWua. Maps are from Google MAP TM.

The other two servers, ISACCO and ESKIMO2, are dedicated to collecting and storing all the data from the instruments, received over the internet or on dedicated lines, and tabulating them in various databases. The ISACCO server receives data from high latitude instruments, while the ESKIMO2 server handles data from all middle and low latitude instruments. Both servers populate the databases and manage queries from the eSWua server for the processing of user requests and to provide various outputs. The servers are supported with backup and storage units to complete the system hardware. The backup process continuously updates duplicate copies of all the databases through an incremental procedure with no need to interrupt database acquisition. The storage processes are instead designed to record a copy of the original raw data from the different instruments in order to maintain the possibility of rebuilding the databases at any time.

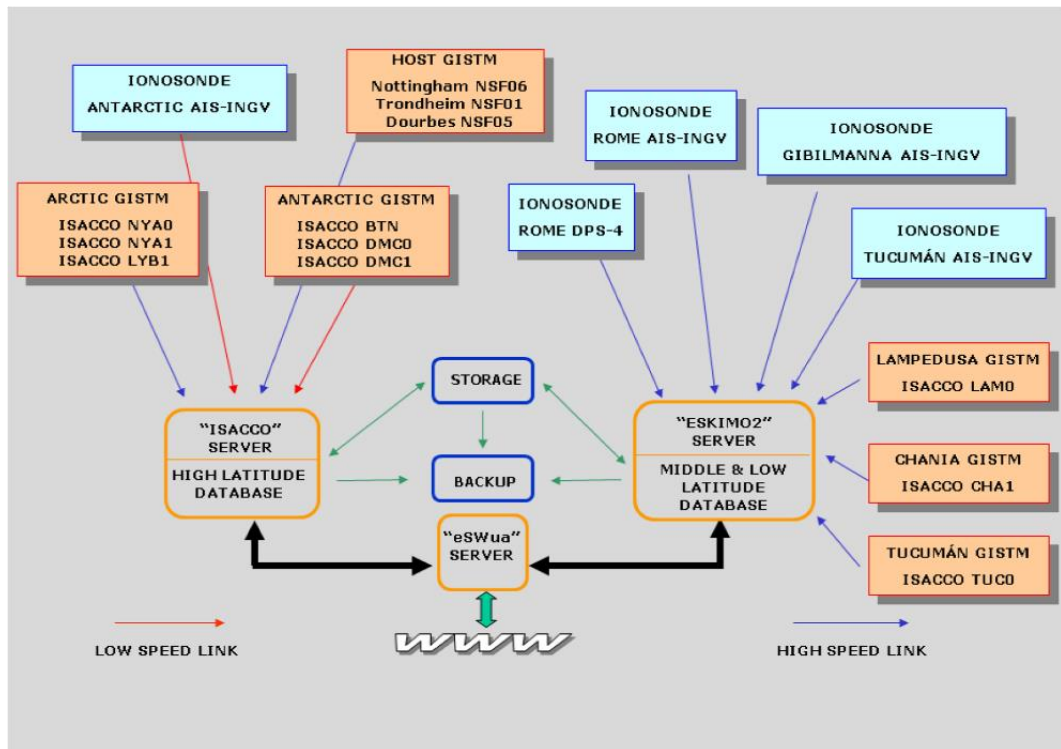


Figure 2.2.3. eSWua system architecture

In Figure 2.2.3 the different colours represent different instrument types: orange rectangles represent GISTMs, cyan rectangles indicate ionosondes, blue arrows are real-time fast connections, and red arrows represent once a day "on demand" connections. The green single and double ended arrows are internal connections used for backup and mass storage purposes. The thick black arrows indicate connections between servers and databases.

Every 15 minutes a binary file is produced by each GISTM instrument and sent to the ISACCO server. Measurements are made for every visible GPS satellite at a one-minute sampling rate. The database tables are populated with a total of 35 navigational and observational parameters, structured in real-time in the database for each station. Among the observational parameters, the most relevant are:

- the phase scintillation index ( $\sigma_\phi$ ) calculated over different time intervals (1, 3, 10, 30, 60 seconds);
- the amplitude scintillation index ( $S_4$ ) calculated every minute;
- the slant Total Electron Content (sTEC) and the vertical Total Electron Content (vTEC) every 15 seconds;
- the 15 seconds delta TEC;
- the Code Carrier divergence and its Standard Deviation (every 60 seconds) of L1 frequency;
- the average Carrier to Noise ratio (every 60 seconds) of L1 (L1 C/N) and L2 (L2 C/N).

Among the navigational parameters, the most useful are:

- locktime (every 60 seconds) of L1 and L2, L1locktime and L2locktime respectively;
- Azimuth and Elevation of each satellite in view;
- latitude and longitude of the ionospheric piercing point at 350 km along the ray path, Lat(350km) and Long(350km) respectively;
- Pseudo random number to identify the satellites (PRN).

The GISTM station performs 50 Hz sampling, producing corresponding binary raw data files. In order to allow fast data access, the raw data files are stored in the eSWua storage device and only referenced in the database.

Considering the volumes of data collected by the 9 GISTM instruments, only a well organized database allows extrapolation and comparison of the more interesting events. This also enables correlation between data from different instruments. An extraction procedure automatically runs and converts the binary file into ASCII format. A PHP batch procedure reads this file and populates the database. Data for each GISTM receiver are organized in monthly tables. These tables list all the measured values along with some calculated parameters useful for the spatial localization of the measurement. Each record includes all the parameters at a certain time for a specific satellite. The data are structured in tables containing 29 measured parameters and 6 calculated values. All the instrument specific data and station constants are stored in a further table. Each instrument has its own automatic procedure for the population of the database (the PHP script realised to populate the DB with the data of Nottingham GISTM station is reported in Appendix 7.2).

The website (Figure 2.2.1) is organized into four main sections titled "Ionospheric monitoring", "Scintillation monitoring", "Riometer monitoring", and "Educational". In the "Scintillation monitoring" section users can access the "Arctic", "Antarctic", "Mediterranean", or "Equatorial" regions. There is an additional icon button labelled "Host" which allows users to access the GISTM receiver data managed by the University of Nottingham. The section of the DB designated to the TEC and scintillation data was designed to address the needs of space weather as well as scientific users. The web tools make it possible to display, plot, extract, and download the data for each station. This interactive website, supported by the well organized database, is a powerful tool for the scientific and technological community in the fields of telecommunications and space weather.

The data transmission procedure, DB population algorithm, linear plot and polar plot visualization tools, statistics page, and users' management system are all fully implemented. Web access to data and tools is established for hosting the data from the Nottingham, Trondheim, and Dourbes sites. The data and tools can be accessed at [www.eswua.ingv.it/nottingham](http://www.eswua.ingv.it/nottingham) or following the path: home -> host-> University of Nottingham (the PHP script realised to generate and visualise the linear plots of Nottingham station is reported in Appendix 7.2). The initial page shows a panorama of the three stations with a display of the last data processed by the system (Figure 2.2.4).

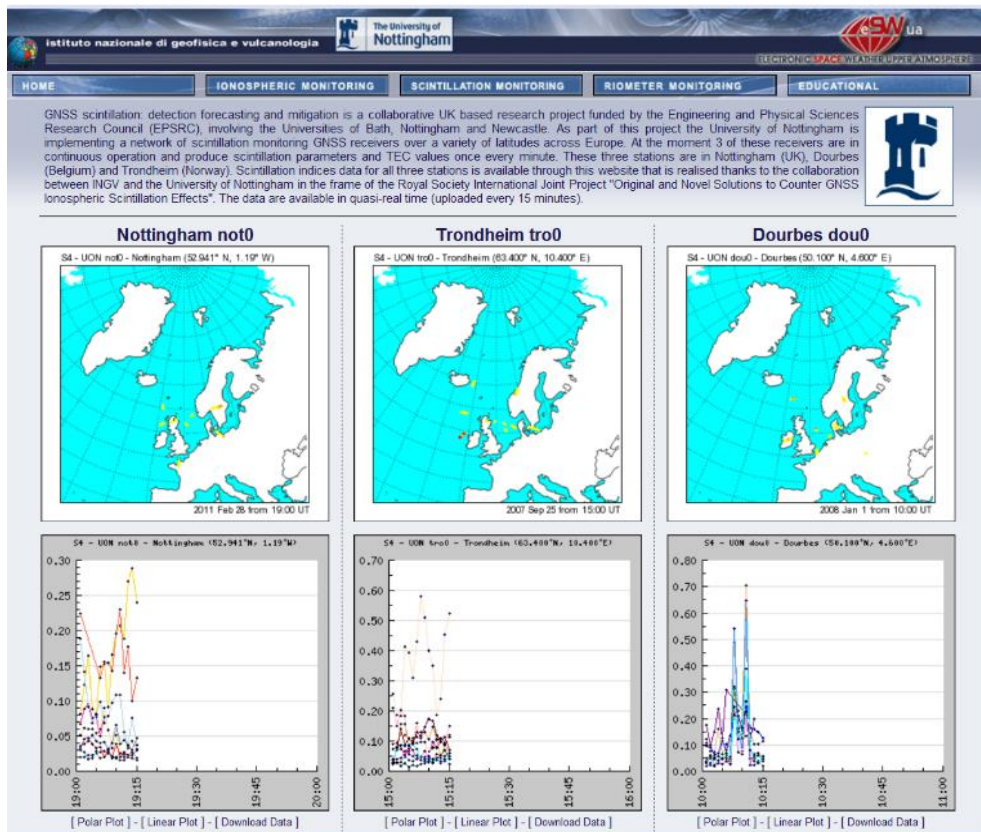


Figure 2.2.4. The IESSG GISTM initial web page at eSWua ([www.eswua.ingv.it/nottingham](http://www.eswua.ingv.it/nottingham)).

Users can click on the links to specific station sites to open a page containing the latest hourly polar and linear plots. From this page, they can click one of the following links: “Polar Plot”, “Linear Plot”, or “Download Data”. The “Polar Plot” link, allows polar plots to be surveyed (Figure 2.2.5). In this subsection, users can set the reference station, date, starting hour, and time interval for the plot (from among 1, 2, 4, 6, 12, and 24 hours), the satellites to be plotted, and the relevant parameter (from among S4,  $\sigma_{\phi}$ , vTEC, and Track). Users can also select a threshold for both the elevation angle and locktime of the L1 frequency. The numbered squares listed on the right indicate the IDs of the satellites that contributed data for the plot.

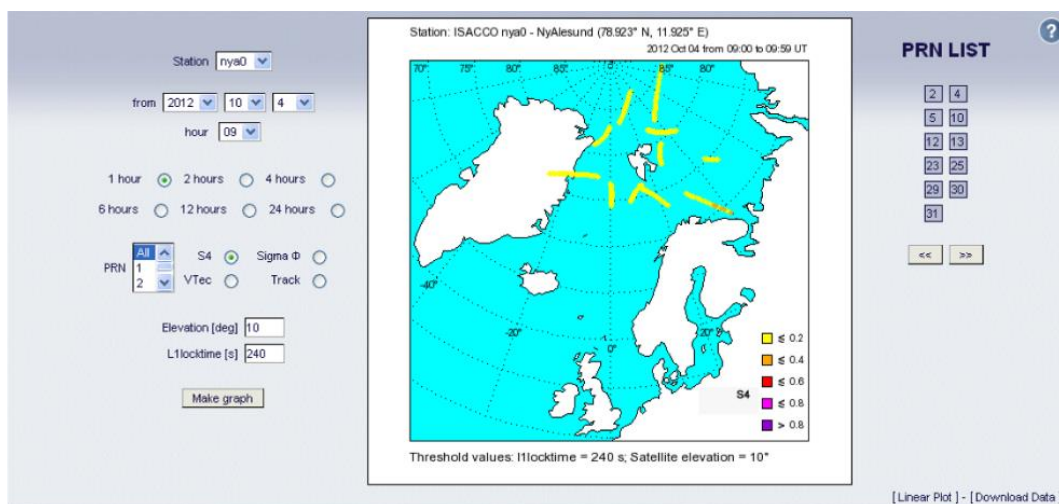


Figure 2.2.5. Snapshot of polar plot recorded at Ny-Ålesund on October, 4th 2012.

The “Linear Plot” link provides linear plots of the selected measured parameters. Figure 2.2.6 shows an example of use of the “linear plot” tool, representing the behaviour of scintillation indices for the Nottingham station on the 25<sup>th</sup> of February 2011 from 18:00 to 19:00 UT. Again, users can set the station, date, starting hour, and time interval for the plot (between 1 and 6 hours), the satellites contributing data, and the relevant parameter from among S4,  $\sigma_{\phi}$  60s,  $\sigma_{\phi}$  1s, vTEC, sTEC, L1 C/N, L2 C/N, L1Locktime, L2Locktime, Code carrier, Standard dev, Lat(350km), Long(350km), Relative TEC, PRN, Azimuth, and Elevation. As for the Polar Plot function, users can select a threshold for both elevation angle and L1locktime. Unlike the previous subsections, in this case users have the option of plotting data from all PRNs, both GPS and geostationary satellites (SBAS).

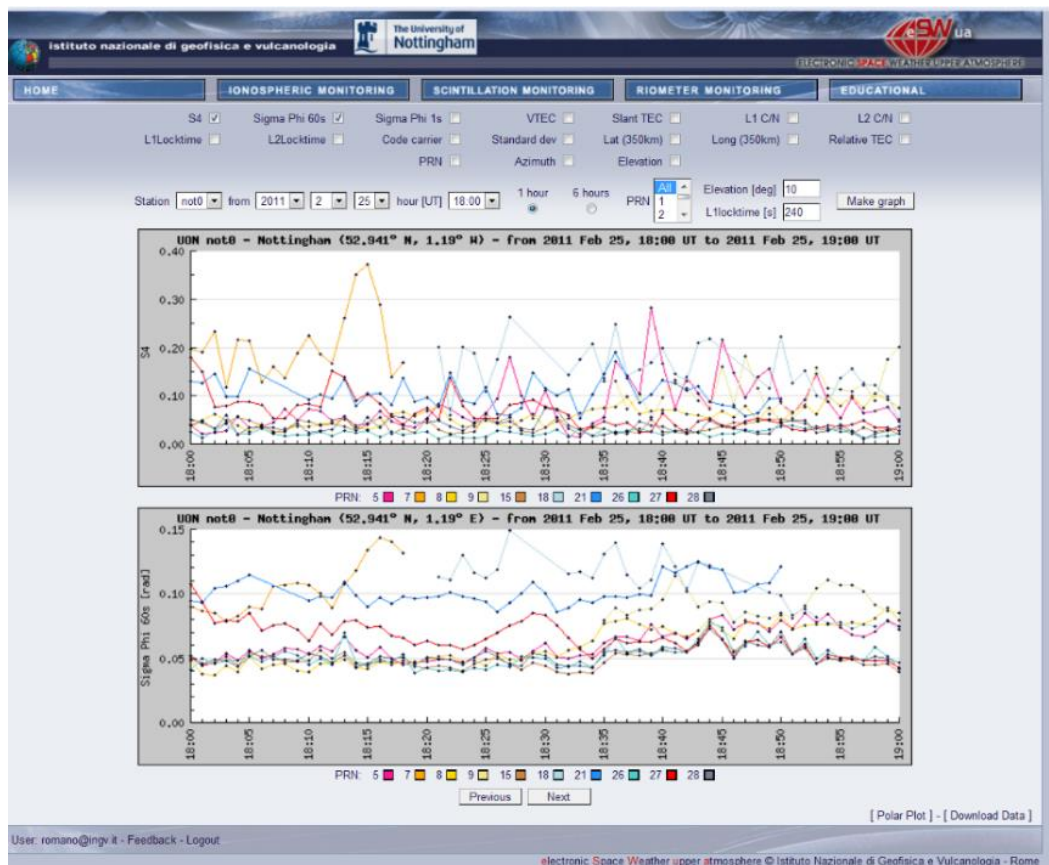


Figure 2.2.6. The “Linear Plot” tool developed to access data from the Nottingham GISTM station.

The “Download Data” link enables data to be downloaded in various file formats: binary (BIN), converted from BIN to standard ASCII (EST), and RAW (Figure 2.2.7). Users can set the station, date, time, and corresponding parameters. Users also have the possibility of selecting elevation angle and L1locktime, as well as the PRN to which the data refer.

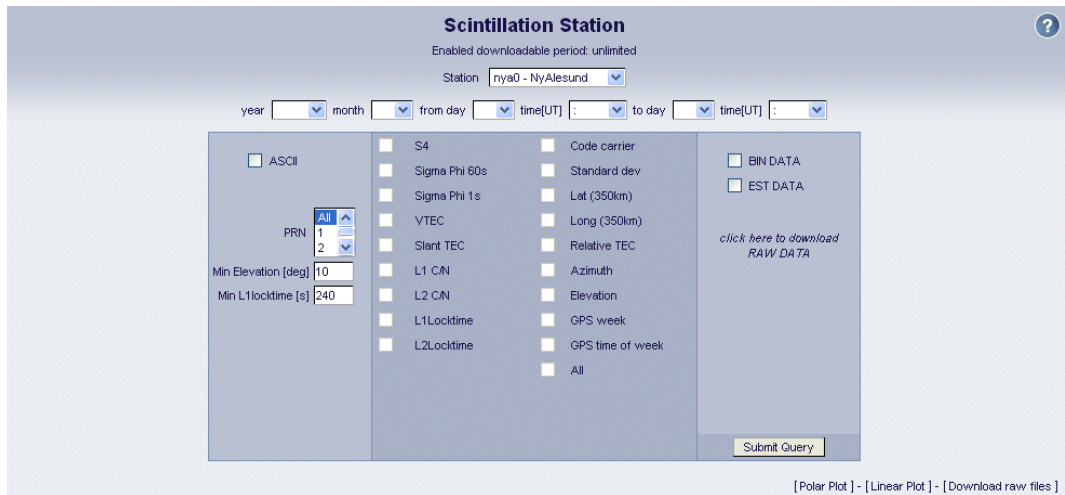


Figure 2.2.7. The download interface sub-page.

A tool is provided to monitor the access statistics, located on the bottom right corner of the eSWua home page. Since its implementation, the eSWua system has been accessed on average about 5000 times per year. eSWua administrators also have another statistical tool available for monitoring more detailed data (individual access, statistics for single pages, and so on).

Access by external users to the Nottingham eSWua site can be authorized by the accredited administrator. On the eSWua "Manage User" page the administrator alone can enable access of registered users to selected data and tools regarding the NGI GISTM data. The administrator also has access to the statistical tool providing detailed statistics of access and tools used, updated in real time. A daily report on the data received and processed is sent automatically to a mailing list of the personnel involved in network management. This automatic email is also useful for checking the status of remote stations on a daily basis (script in Appendix 7.7).

In conclusion, eSWua was designed to provide access to data and other outputs, like the plots and maps mentioned above, not only for scintillation indices but also for the main output parameters of the receivers and TEC related data. A comparison is presented of the technical solutions adopted to develop eSWua and four of the other best known databases devoted to GNSS ionospheric data, summarized in Table 2.2.2 in terms of system name, access URL, owner, and data access policy. Table 2.2.3 compares the five different ionospheric GNSS data management systems in terms of the features listed below.

- Scintillation indices: the presence of scintillation indices is reported both for amplitude (S4) and phase ( $\sigma_\phi$ ) with "A" and "P" respectively.
- TEC data: availability of GNSS TEC data is reported.
- GNSS parameter data: availability of other GNSS parameters such as carrier to noise ratio, lock time, coordinates of ionospheric piercing point, etc.
- GNSS data plots: availability of visualization tools such as linear plots, maps, etc.
- Data downloading tool: accessibility to data by downloading from the site.
- Scintillation raw data: accessibility to high rate sampling data. The sampling rate is indicated when available.
- Refresh time data (min): indication of the refresh time in minutes between the availability of two consecutive data updates on the site.

- Data availability statistics: indication of the presence of tools for data availability visualization and statistics.
- GNSS data geographic coverage: indication of the geographic area spanned by the GNSS receiver data included on the site.
- Other Ionospheric data: indication of the presence of complementary ionospheric data acquired by ionospheric radar systems, riometers, etc.

This comparison demonstrates that eSWua can be considered as the state-of-the-art system for GNSS ionospheric data.

System	URL	Owner	Access policy
CHAIN	<a href="http://chain.physics.unb.ca/chain/">http://chain.physics.unb.ca/chain/</a>	Consortium of Canadian institutions	Full access upon registration
eSWua	<a href="http://www.eswua.ingv.it">www.eswua.ingv.it</a>	Istituto Nazionale di Geofisica e Vulcanologia (INGV)	Restricted anonymous access  Registration required for full access  Free full access for scientific purposes
IPS	<a href="http://www.ips.gov.au/">http://www.ips.gov.au/</a>	Australian Government - Bureau of Meteorology, Radio and Space Weather Services	Free full access
Madrigal	<a href="http://madrigal.haystack.edu/madrigal/">http://madrigal.haystack.edu/madrigal/</a>	Massachusetts Institute Technology (MIT - Haystack Observatory)	Registration required for full access
SWACI	<a href="http://swaciweb.dlr.de">http://swaciweb.dlr.de</a>	German Aerospace Centre e. V. (DLR)	Restricted anonymous access

Table 2.2.2. GNSS ionospheric data systems<sup>7,8,9,10,11</sup>.

System	Scintillation indices	TEC data	GNSS parameter data	GNSS data plots	Data downloading tool	Scintillation raw data	Refreshing time data (min)	Data availability statistics	GNSS data geographic coverage	Other Ionospheric data
	Amplitude Phase	Yes No	Yes No	Yes No	Yes No	Yes (Hz) No		Yes No	Arctic Antarctic Low Latitude Mid Latitude	Yes No
CHAIN	A, P	Y	Y	Y	Y	Y (50)	5	Y	Ar	Y
eSWua	A, P	Y	Y	Y	Y	Y (50)	15	N	Ar, An, L, M	Y
IPS	A, P	Y	N		N	N	10	N	An, L, M	Y
Madrigal	planned to be included	Y	N		Y	N	N	Y		Y
SWACI	A, P	Y	N	N	N	N	1	N	Ar, L, M	N

Table 2.2.3. Feature comparison between five of the main GNSS data management systems.

<sup>7</sup><http://chain.physics.unb.ca/chain/>

<sup>8</sup> [www.eswua.ingv.it](http://www.eswua.ingv.it)

<sup>9</sup> [www.ips.gov.au/](http://www.ips.gov.au/)

<sup>10</sup> <http://madrigal.haystack.edu/madrigal/>

<sup>11</sup> <http://swaciweb.dlr.de>

### 2.3 APPLICATIONS OF DATA MONITORING AND MANAGEMENT

The data monitoring, handling and structuring included in the research project also supported attempts to apply new techniques for mitigating scintillation effects on the GNSS signal data acquired at Ny-Ålesund and Longyearbyen (Aquino et al., 2009).

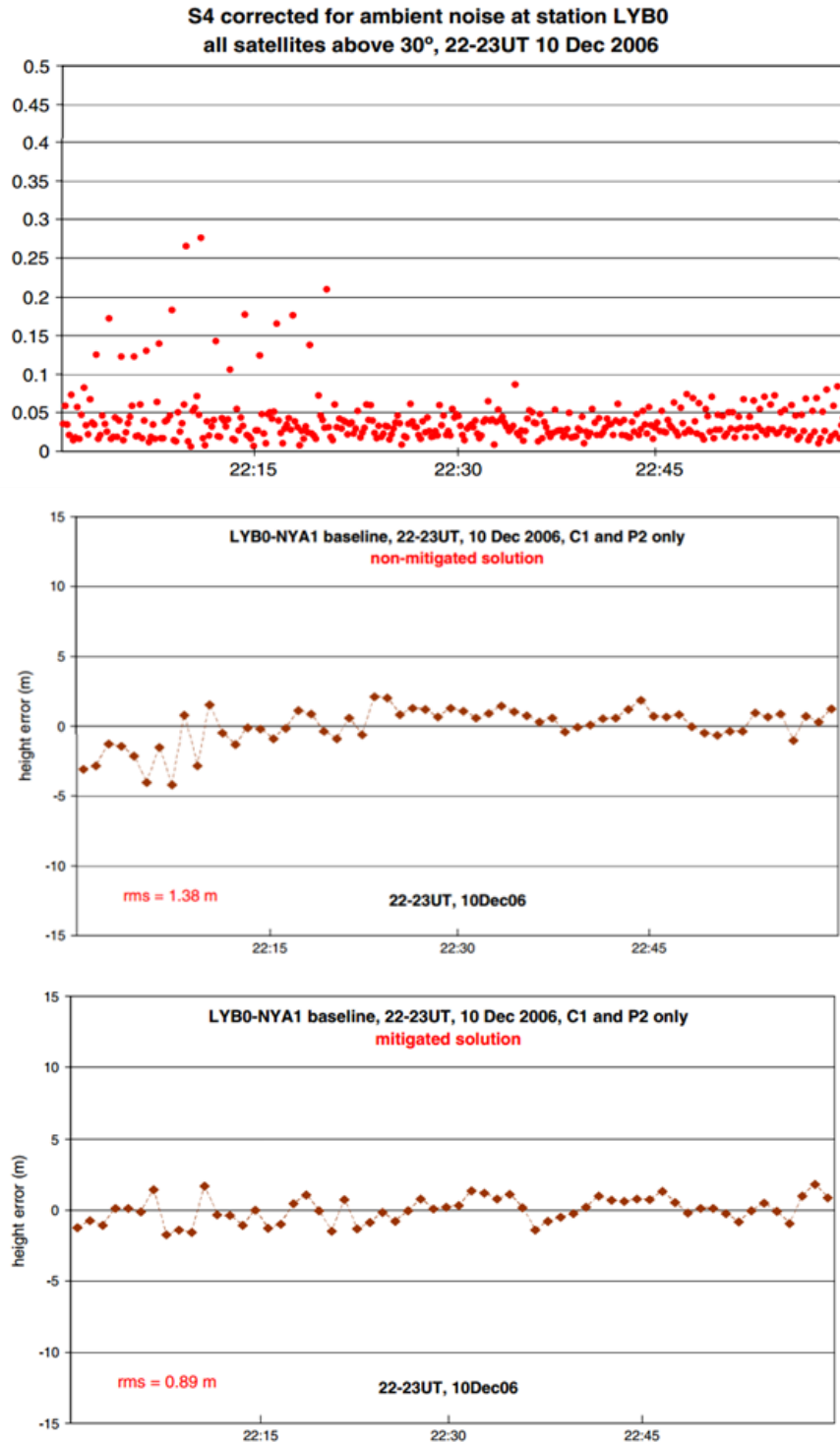


Figure 2.3.1. Corrected S4 for satellites observed at station LYB0 with elevation >30° (top); height error from pseudorange-only solution without mitigation (middle); Height error from pseudorange-only solution with mitigation (bottom), from Aquino et al. (2009).

Figure 2.3.1 shows the improvement in height error from the DGPS solution when applying the mitigation technique (bottom panel) compared to the non-mitigated solution (middle panel) in a scintillating environment (top panel). In particular, in this paper a data set of 1 hour session (22:00 to 23:00 UT on 10/12/2006) has been selected from the stations of LYBO and NYA1. Top panel shows the S4 for all satellites observed at LYBO, during the considered period, with elevation greater than 30°. An enhancement against the overall background is visible early in the session. Middle panel shows the height error from pseudorange-only solution without applying the proposed mitigation technique. The baseline is LYBO-NYA1; larger errors roughly correspond with higher S4 values. Bottom panel shows the results applying the mitigation technique. Improvement is clear at the start of the session with the RMS height error dropping from 1.38 to 0.89 m. More details on the technique can be found in Aquino et al., 2009.

The quality and volume of data collected by INGV and NGI has encouraged original investigations into the formation of the ionospheric irregularities that cause scintillations, the dynamics of high latitude plasma under disturbed conditions, and the development of countermeasures, i.e. mitigation techniques. International collaborations with groups that manage similar experimental observations, and experts in irregularity and scintillation modelling, gave rise to several opportunities to exchange expertise and data (Mitchell et al., 2005; De Franceschi et al., 2008; Aquino et al., 2009, Alfonsi et al., 2011, Spogli et al., 2013, Romano et al., 2013). Observations from GISTM receivers in Northern Europe were used, for example, to investigate the dynamics of ionospheric plasma during the storm events of October 30 and November 20, 2003. The total electron content (TEC) and scintillation data combined with ionospheric tomography produced by MIDAS (Multi-Instrument Data Analysis System) revealed strong enhancements and steep gradients in TEC during night-time under a prevailing negative Bz component of the Interplanetary Magnetic Field (IMF). Amplitude and phase scintillation maxima were often co-located with the TEC gradients at the edge of plasma patches, revealing the presence of small scale irregularities and suggesting association with the Tongue of Ionization (TOI) convecting in an anti-sunward direction from the American sector across the polar cap (Mitchell et al., 2005; De Franceschi et al., 2008). In these storms, the physical mechanism responsible for the majority of scintillation events appears to be gradient drift instability, as indicated by the coincidence of enhancement of S4 and  $\sigma_\phi$  with the edges of steep TEC gradients (Figure 2.3.2, Mitchell et al., 2005). These findings encourage further investigations while at the same time underlining the need also to perform statistical studies that investigate which ionospheric conditions most favour scintillations. Both these approaches require reliable continuous monitoring of the ionosphere to investigate the formation and evolution of ionospheric irregularities. The present PhD contributes significantly to these needs since it guarantees correct operation of the monitoring stations, while at the same time offering the possibility of changing instrument settings in the case, for example, of special measurement campaigns. Moreover, a section of the research project involved the realization of tools for structuring the data in a suitable way for analysis on a statistical basis, as well as for investigating individual case studies. These tools have been continuously enhanced

to match the needs of specific investigations, further supporting research into the ionospheric plasma conditions that produce scintillation effects in GNSS signals.

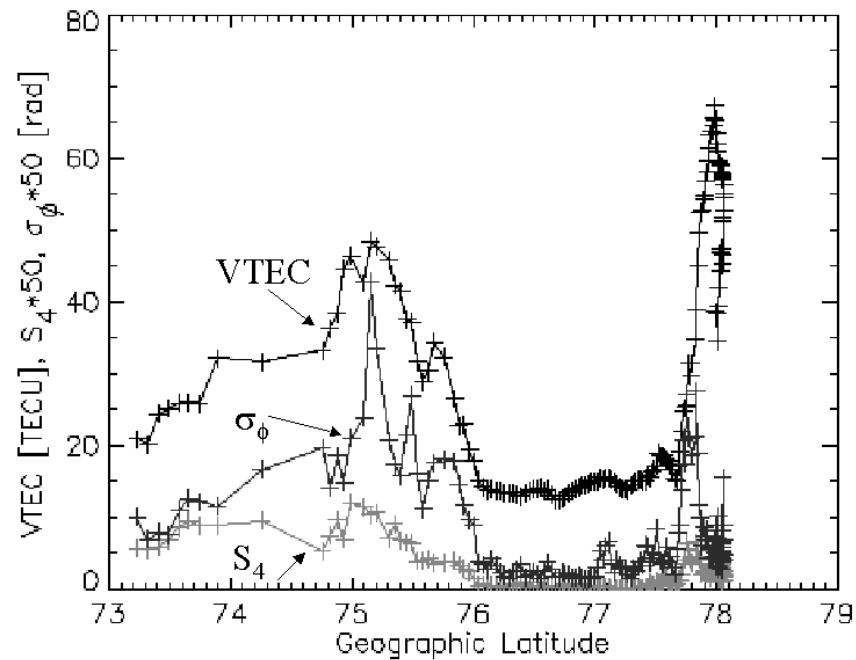


Figure 2.3.2. Equivalent vertical TEC, phase and amplitude scintillation for GPS satellite 'PRN 31' recorded at the Svalbard receiver between 20:00 and 24:00 UT on October 30, 2003 and plotted as a function of the geographic latitude of the subionospheric point calculated for the assumed ionospheric altitude of 350 km.

As part of the PhD course, data preparation algorithms for statistical studies were developed. The work focused on harmonizing and merging data acquired by different receivers owned by INGV and NGI. The first algorithms were developed to analyse two major magnetic storms and relative marked scintillation events occurring on the 30 to 31 October and 20 to 21 November 2003. In order to ensure a statistically meaningful analysis, data acquired from October to December 2003 were pre-processed. The stations considered were Hammerfest (HAM), Bronnoysund (BRO) and Ny-Ålesund (NYA0). Merging data from various stations permits a more detailed investigation of the dynamics of the ionospheric irregularities that cause scintillation, since it is possible to sound different ionospheric sectors, in this case auroral to cusp latitudes. The data from the NYA0 station are available from the eSWua database, while the data from the BRO and HAM stations are available by ftp from the INGV server (*eskimo.ingv.it*). The code developed for this analysis has to be very robust since the total volume of data is very large, of the order of 1 million data points per station. Consequently, all the code routines had to be debugged to avoid crashes and possible memory overflows.

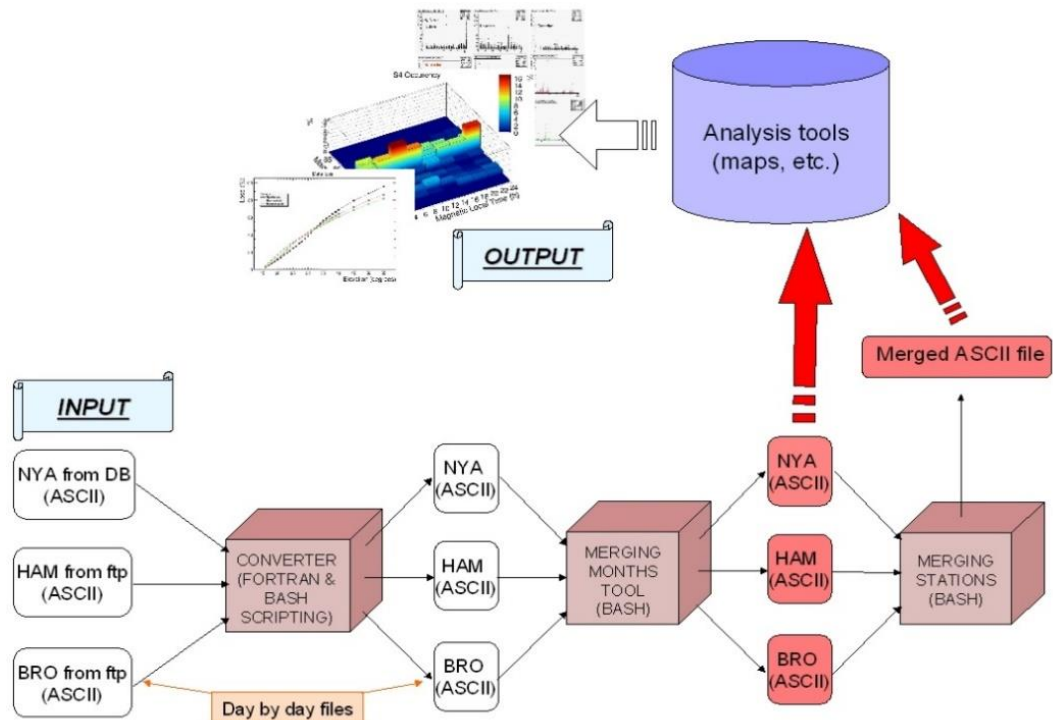


Figure 2.3.3. Data flow of the statistical study (Romano, 2009).

Figure 2.3.3 illustrates the data flow, with the first analytical step being the selection of parameters of interest from the complete list of available data. Next, a converter is developed to structure the data from the three stations in the same way. The converter is programmed in FORTRAN and rewrites a data file for a given day and station into a new standard format output file. The NYA conversion program is somewhat different from the BRO and HAM converter due to the diverse data structure of the original files. Appendix 7.3 provides the code for the HAM and BRO converter. The conversion process is iterated for the total number of days of the period of interest, and for the three stations, using a script written in bash. The chosen structure, in which the parameters of interest are stored, is the following: Year – Month – Day – Hour – Minute – GPSweek – PRN - S4 - SigmaPhi(60sec.) – vTEC - L1C/N - L2C/N - Lat(350km) - Long(350km) – Elevation. The daily data files are sent to the Merging Months Tool, which is a shell script written in bash that merges the data from the same month for each station. In order to allow incidental use of the daily data in further analyses, this script is separated from the previous one. At this point the monthly data can be sent directly to the final stage of the data flow, the Analysis Tools, or it can be redirected to another tool, called the Merging Station Tool, which is another shell script written in bash that builds a unique file containing data from the three stations separately for each month. The data preparation described above enables interfacing with the Analysis Tools package, which produces the plots. The Analysis Tools were developed in collaboration with INGV colleagues in a C++/C-like language that is interpreted by the ROOT system<sup>12</sup> for analysis and plotting in physics. The statistical study is a collaboration between NGI and INGV, and the results are presented in the paper Spogli et al., 2009. Figure 2.3.4 shows an example statistical study of the correlation plot

<sup>12</sup> <http://root.cern.ch/>

between  $S4$  and  $\sigma_\phi$  for the three stations during October 2003. Black dots are for an elevation threshold of  $15^\circ$ , while red dots refer to a threshold of  $30^\circ$ . This data preparation algorithm was further developed and tuned to also include data acquired by the PolRxS<sup>13</sup>, Javad, and SCINTMON (Cornell Scintillation Monitor, Beach & Kintner 2001) receivers into the preparation chain.

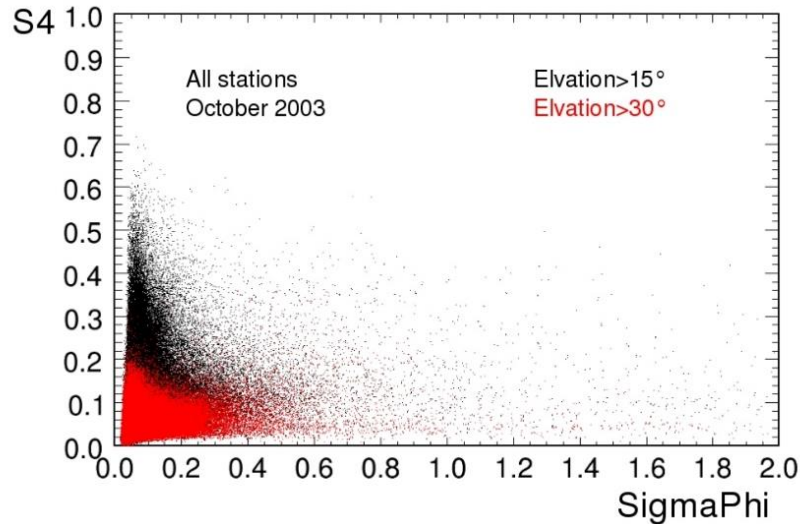


Figure 2.3.4. Correlation plot between  $S4$  and  $\sigma_\phi$  for all stations during October 2003. Dependence on elevation angle is shown with different colours. This plot shows the different impact of the multipath on the two scintillation indices:  $S4$  is much more affected.

The data preparation chain for scintillation parameter data currently includes 3 stages:

1. Data\_prep: input from the receiver output (ISMR or ASCII format), producing daily files in ASCII format by merging the input data (Appendix 7.11).
2. Data\_magcoord: input from the previous stage, calculating Altitude Adjusted Geomagnetic Coordinates (AACGM, Baker and Wing, 1989) and Magnetic Local Time. Output is the same as input, but with an extra column listing the coordinates and time of the calculated quantities. This stage is only for middle and high latitude receivers, since AACGM coordinates cannot be defined for low latitude receivers.
3. Data\_root: input from the previous stage, transforming the data into the native ROOT format. Output is daily data files in .root format.

The data in .root are then processed, producing maps, plots, etc. Figure 2.3.5 presents a schematic block diagram of the procedure.

<sup>13</sup> <http://www.septentrio.com/products/receivers/polarxs>

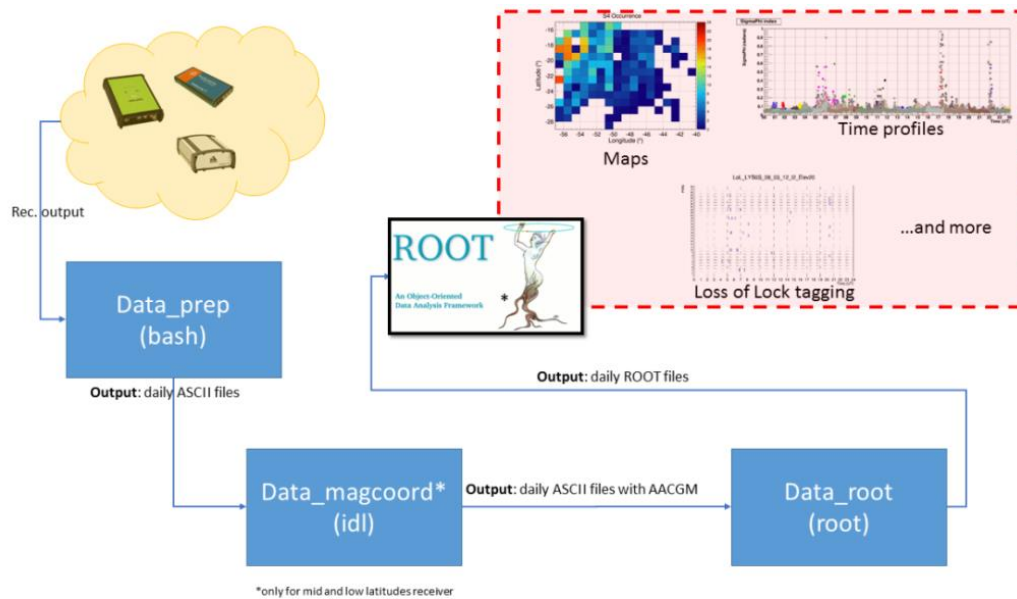


Figure 2.3.5. Block diagram of the data preparation chain

The data preparation chain provides a robust procedure to feed ad hoc analysis tools developed to study the ionospheric impact on GNSS. In addition, the data harmonisation achieved by the preparation chain is vital when applying climatological and statistical techniques, which utilize data not only from single stations, but also entire networks of receivers.

Rigorous and astute data preparation has formed the basis for various climatological studies published in peer reviewed journals. These include the paper authored by Alfonsi and co-authors (2011), presenting a bipolar climatology of GPS scintillation data under heliogeophysical conditions (year 2008). The network considered includes 4 receivers in the Northern Hemisphere and two in the Southern. The northern array allows the observation of subauroral, auroral, cusp, and cap sectors, while the southern array essentially covers the cusp and cap regions. The study discusses how the IMF orientation influences scintillation distribution in magnetic local time, highlighting the important role of plasma inflow and outflow from and to the magnetosphere at noon and midnight (Figure 2.3.6).

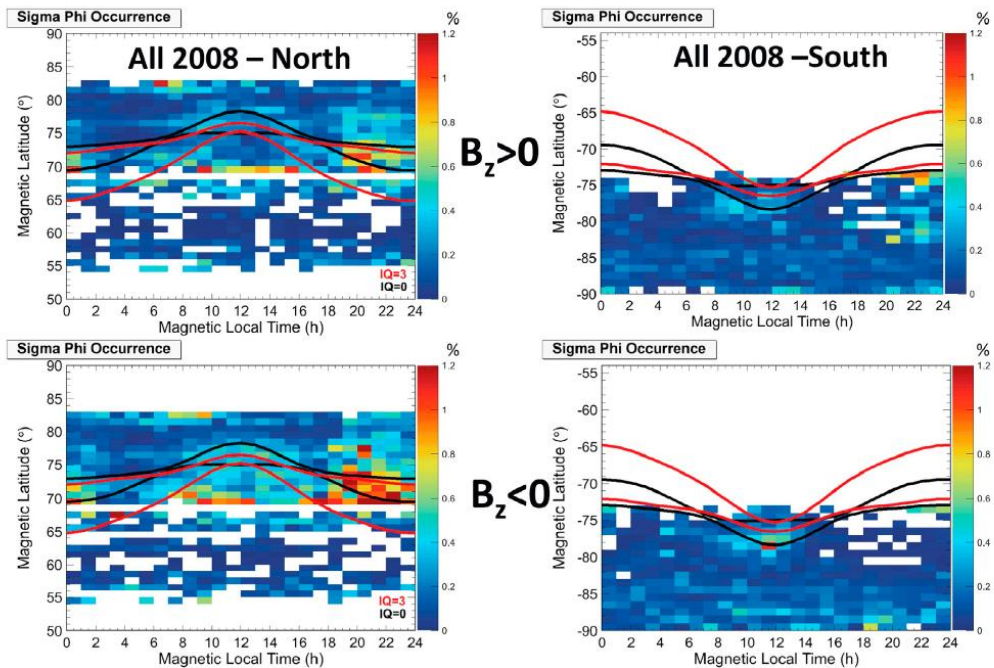


Figure 2.3.6 Maps of the percentages of occurrence of phase scintillation in magnetic latitude and magnetic local time, separating the IMF  $B_z$  positive and negative conditions. (left) Northern Hemisphere and (right) Southern Hemisphere (black and red curves reproduce the Feldstein auroral ovals for  $IQ = 0.3$ , respectively). Extracted from Alfonsi et al., 2011.

The data analysis technique is discussed in greater detail below, in Chapter 3. Other meaningful results following appropriate data preparation are those presented in the paper by Spogli and co-authors (2013), in which the network consists of nine GISTM receivers covering a very large area of the Southern Hemisphere, from sub-equatorial Latin America to the South Pole, across the South Atlantic Ocean. The paper defined a climatological picture that provided a general and simultaneous overview of the crucial areas of the ionosphere and hours of the (magnetic) day in which scintillation was more likely to occur during the rising phase of the last solar maximum. Ionospheric 'hot spots' were defined, including:

- POST, in which scintillation is assumed to be mainly due to the evolution of post-sunset irregularities.
- SAMA, in which scintillation is assumed to be mainly due to irregularities induced by particle precipitation in the South Atlantic Magnetic Anomaly.
- CUSP, in which scintillation is assumed to be mainly due to irregularities induced by direct particle precipitation at the cusp.
- TAIL, in which scintillation is assumed to be mainly due to irregularities induced by reconnection with the magnetotail at around magnetic noon.
- PATC, in which scintillation is assumed to be mainly due to electron density patches moving across the polar cap.

Figure 2.3.7 presents a map of phase scintillation occurrence, with the hot spots identified and further analysed.

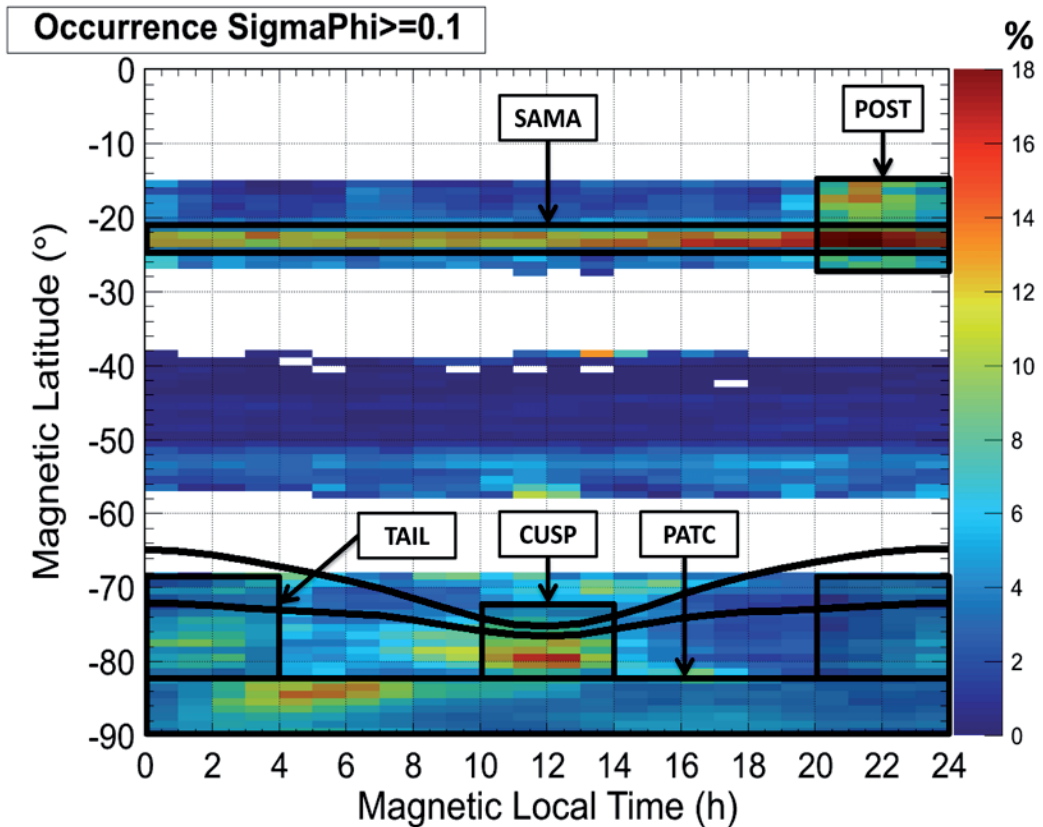


Figure 2.3.7. Map of Sigma Phi percentage of occurrence above the weak scintillation threshold (0.1 radians). The black curve is the modelled Feldstein oval for  $IQ = 0$ , while the black boxes identify the ionospheric hot spots. Extracted from Spogli et al., 2013.

The decision to tune the data preparation algorithms to ingest data from other receivers was motivated by an interest in characterizing the low latitude ionosphere within the framework of the CIGALA project<sup>14</sup>, in which INGV and NGI were consortium members. Some of the work completed within the framework of CIGALA led to the publication of a paper in which the ionosphere over Brazil, and in particular over São Paulo state, was characterized using the PolarXS and SCINTMON receivers. Figure 2.3.8 presents a comparison between the 2 kinds of receivers in terms of occurrence of moderate/strong amplitude scintillation. The comparative study shows agreement between the two datasets, which define similar climatological pictures of

<sup>14</sup> <http://www.gsa.europa.eu/concept-ionospheric-scintillation-mitigation-professional-gnss-latin-america>

the scintillation phenomena, albeit with differences due to the contrasting heliogeophysical conditions of the two periods, i.e. 2009 (SCINTMON) and 2011 (PolaRxS).

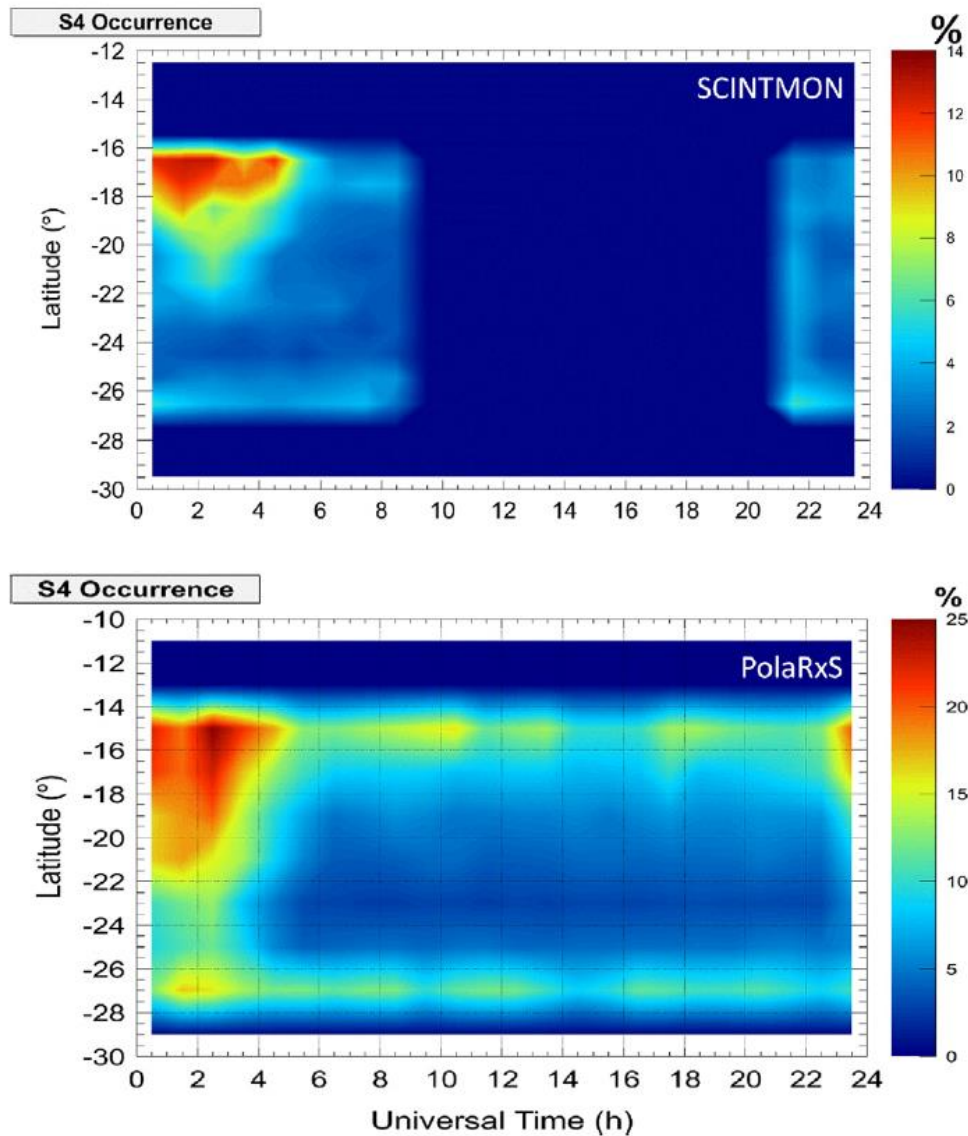


Figure 2.3.8. Map of the percentages of occurrence of S4 above 0.1 rad for SCINTMON (Jan–Oct 2009, top plot) and PolaRxS (Feb–Oct 2011, bottom plot) in Geographic Latitude vs. Universal Time.

The experience gathered during the development of the acquisition programs enabled the realization of a specific script to acquire RINEX format data at a 1s sampling rate. RINEX files are typically produced every hour, but this time interval can be adjusted by the user according to specific needs. This acquisition procedure uses the second serial communication port of the receiver and can operate without affecting the regular acquisition of raw and processed scintillation data (script in Appendix 7.6). Continuous acquisition of RINEX was assessed, in collaboration with the thesis supervisors, not to be currently of scientific interest, and so this script has not yet been put into operation. However, it has been fully tested and is ready for easy implementation in response to specific needs. It was used, for example, again within the CIGALA project<sup>15</sup>, to produce

<sup>15</sup> [www.fp7cigala.eu](http://www.fp7cigala.eu)

a data set of 1s RINEX to support the development of a scintillation receiver as one of the aims of this project.

Table 2.3.5 summarises the main data management and monitoring tools developed in the framework of the research project.

Developed TOOL	Description	Year (1-6)	Parag.
Acquisition script for Nottingham GISTM station	The script manages the GISTM acquisition of the Nottingham station (Appendix 7.1)	1	2.1
Acquisition script for Trondheim GISTM station	The script manages the GISTM acquisition of the Trondheim station	1	2.1
Program to send automatically Nottingham GISTM data to eSWua	Program to automatically send "S60" data to eSWua data management system by ftp (Appendix 7.5)	2	2.2
Data Base population	PHP program to populate the eSWua DB with the NGI GISTM data (Appendix 7.2)	2	2.2
Data converter	FORTRAN program to convert the data from NYA, BRO and HAM in the same format (Appendix 7.3)	2	2.3
Watchdog program for Nottingham GISTM station	External program to automatically guarantee the continuity of the acquisition of the Nottingham station, restarting the acquisition procedure in cases of interruptions ( Appendix 7.4)	3	2.1
Watchdog program for Trondheim GISTM station	External program to automatically guarantee the continuity of the acquisition of the Trondheim station, restarting the acquisition procedure in cases of interruptions ( Appendix 7.4)	3	2.1
1s RINEX script acquisition program	SLOG script to acquire RINEX format data at a 1s sampling rate by GISTM (Appendix 7.6)	3	2.3
Data visualization tool, PHP code	PHP program to generate and visualise the linear plots of NGI stations on eSWua (Appendix 7.2)	3	2.2
Data downloading tool, PHP code	PHP program to download data of the NGI stations on eSWua (Appendix 7.2)	3	2.2
User management tool, PHP code	PHP program to manage by a friendly-user interface the users registered on the NGI data management section of eSWua	4	2.2
Automatic email procedure	PHP script to send by email a daily report on the data received and processed.	4	2.2
Data_prep	ROOT subroutine to produce daily files in ASCII format by merging the input data (Appendix 7.11 )	4	2.3
Readmeandata.C	ROOT subroutine to calculate mean and standard deviation of CCSTDDEV and C/N (Appendix 7.8)	4	3.1.1
Acquisition script for Rome GISTM station	The script manages the GISTM acquisition of the Rome station	5	2.1
Data_root_filt.C	ROOT subroutine to prepare data filtered in a suitable format to be ingested by the data analysis tool (Appendix 7.10)	5	3.2.1

*Table 2.3.5. Summary of monitoring and data management tools developed during the PhD course. Course-year corresponding when the tool has been developed and the related paragraph of the thesis are also reported.*

## 3 CHAPTER 3 – METHODOLOGY, DATA ANALYSIS AND RESULTS

---

### 3.1 STATION CHARACTERIZATION

The NGI-INGV GISTM network covers a wide range of latitudes in the northern European sector with a chain of permanent stations. Each receiver has a unique location which needs to be characterised in order to ensure the quality of the scintillation and TEC data, and remove environmental site related errors. This analysis started with an assessment of a data set collected during quiet ionospheric conditions as defined by mid-latitude and sub-auroral stations, and was then followed by a case study of a severe geomagnetic storm (see paragraph 3.1.5).

The features in the environment at each receiver location that contaminate scintillation measurements need to be identified in order to improve the quality of the scintillation and TEC data. This is achieved by removing the local sources of errors or mitigating their effects by data filtering. This procedure involves identification of ray-paths affected by error sources that could mimic scintillation and lead to signal degradation. Any features in the environment (trees, buildings, etc.) that cause multipath and degradation are identified and, when feasible, physically removed. The identification of the directions in which a signal is systematically affected by such sources is the first step towards a new data filtering method, which will be discussed in section 3.2. The following paragraphs describe the method developed to characterize station environment, and then the results of the application of this method to GISTM data from the monitoring stations in Nottingham and Trondheim are illustrated. Finally, some analyses of Nottingham GISTM data acquired during the so-called Halloween Storm of October 2003, the strongest of the last solar cycle, are shown and the results discussed whilst considering the previously established station characterisation. The results presented in this section are partially extracted from Romano et al., 2013.

#### 3.1.1 Method

Each station is characterized by investigating signal quality parameters such as L1 Carrier to Noise Ratio (L1 C/N), L2 Carrier to Noise Ratio (L2 C/N), L1 Code/Carrier divergence (CCDIV), Standard Deviation of L1 Code/Carrier divergence (CCSTDDEV), and their impact on scintillation measurements for each selected station in the network. The L1 C/N and L2 C/N parameters indicate the quality of reception, while the CCSTDDEV gives an indication of the multipath activity on the L1 frequency (Van Dierendonck et al., 1993, Romano et al., 2013). This allows determination of possible sources of signal distortions affecting scintillation and TEC measurements for each single station included in the network. In particular, latitude-longitude maps and azimuth-elevation maps of the mean and standard deviation values of L1 C/N and CCSTDDEV, and of the percentage of occurrence of the scintillation indices above selected thresholds, are shown to indicate the areas of the environment and ray path directions most affected by signal degradation. The maps of mean and standard deviation are produced by evaluating the distribution of all the values of the investigated quantity for each bin defining the map. This analysis was achieved by modifying and adding new features to the Ground Based Scintillation Climatology

(GBSC) technique developed at INGV in collaboration with NGI (Spogli et al., 2009 and 2010, Alfonsi et al., 2011).

The GBSC was originally developed to identify the areas of the ionosphere in which ionospheric scintillation is more likely to occur. GBSC relied on the internationally adopted phase and amplitude scintillation, TEC and Rate of TEC change (ROT) parameters. GBSC outputs maps of the mean values, standard deviations and percentages of occurrence above arbitrary threshold of the above mentioned quantities. The coordinates system can be selected in terms of pairs of the following: geographic coordinates (latitude and longitude), altitude adjusted geomagnetic coordinates (magnetic latitude and magnetic longitude), universal time, magnetic local time, azimuth and elevation. Such coordinates refers to the ionospheric piercing point, assumed to be located at 350 km.

The percentage of occurrence  $O$  is evaluated in each bin of the map according to the following definition:

$$O = \frac{N_{thr}}{N_{tot}} \quad 3.1$$

where  $N_{thr}$  is the number of data points corresponding to the considered parameter above a given threshold and  $N_{tot}$  is the total number of data points in the bin. If the parameter can assume both negative and positive values (for example, ROT), its absolute value is considered.

Scintillation indices and TEC can be projected to the vertical, in order to account for varying geometrical effects on the measurements made at different elevation angles. According to Mannucci et al (1993), Alfonsi et al. (2011) and Spogli et al. (2013), to avoid the geometry ambiguity the scintillation indexes and TEC have been verticalised using the following formulas:

$$\sigma_{\Phi}^{vert} = \frac{\sigma_{\Phi}^{slant}}{(F(\alpha_{elev}))^{0.5}} \quad 3.2$$

$$S_4^{vert} = \frac{S_4^{slant}}{(F(\alpha_{elev}))^{\frac{p+1}{4}}} \quad 3.3$$

$$vTEC = \frac{sTEC}{F(\alpha_{elev})} \quad 3.4$$

where  $\sigma_{\Phi}^{slant}$  and  $S_4^{slant}$  are the indices directly measured at a given elevation angle along the slant path, sTEC is the slant TEC. In the three formulas above,  $F(\alpha_{elev})$  is the obliquity factor, that is defined as (Mannucci et al., 1993):

$$F(\alpha_{elev}) = \frac{1}{\sqrt{1 - \left(\frac{R_E \cos \alpha_{elev}}{R_E + H_{IPP}}\right)^2}} \quad 3.5$$

where  $R_E$  is the Earth radius and  $H_{IPP}$  is the height of the Ionospheric Piercing Point, assumed to be 350 km, and  $p$  is the phase spectral slope.

According to formula (19) of Rino (1979), which describes the signal phase variance as a function of the zenith angle, and as described in Spogli et. al (2013) the exponent of formula 3.2 is 0.5, while the exponent of formula 3.3, according to formula (31) of Rino (1979), depends on the spectral index of the phase scintillation spectrum, and on the anisotropy of the irregularity. The power spectrum slope (*log vs log*), as described in Spogli et al. (2013), is assumed to be  $p=2.6$ , from which  $\frac{p+1}{4} = 0.9$ . However, slight

differences on this assumption do not have a meaningful impact on a statistical representation of large datasets. An analytic description of the angular dependence of the scintillation indices, as in the above formulas 3.2 and 3.3, is possible only under the conditions of weak scattering and when the single phase screen approximation is suitable. This is not the case when strong scintillation occurs.

These formulae are for isotropic irregularities as they include no properties of the ionospheric irregularities nor any consideration of the relative directions of the propagating wave and the alignment of the major (long) axis of the irregularities. The ionospheric irregularities are generally considered to be field aligned and for this case the scintillation can be significantly enhanced for waves travelling near the geomagnetic field direction and for sheets of ionisation, propagating at any elevation through the L-shell of the ionisation (Rino et al. 1979, Strangeways et al., 2014).

Being aware of such limitations, the GBSC is a statistical technique aiming at representing the scintillation environment in a way as much as possible independent on the location(s) of the receiver(s). In this sense, the verticalisation process addresses the need to avoid geometrical effects on the results. The corresponding bins of the mean and standard deviation maps are filled with the distribution mean value and standard deviation, respectively. The binning of the GBSC maps can be selected according to the available statistics and to obtain a meaningful fragmentation of the map.

GBSC runs under the ROOT environment<sup>16</sup> and is written in the ROOT native language, which inherit from C/C++. GBSC is composed by two main routines: one dedicated to the occurrence calculation (occumap.C) and one to the mean and standard deviation maps (meanmap.C) The GBSC maps are output in:

- Main image formats (gif, png, ps, eps, etc.);
- ASCII files
- ROOT Objects, i.e. histograms in ROOT native format

The modification of the GBSC has been done, in the framework of the PhD, to include signal parameters measured by the GISTM receiver, such as:

- The standard deviation of the Code-Carrier Divergence (CCSTDDEV), calculated on the L1 over 60 seconds;
- Carrier to noise ratio (C/N) on L1 and L2, every 60 seconds.

In particular, the GBSC code has been made more general, by extending the possibility to output the occurrence, mean values and standard deviation maps of the CCSTDDEV and the C/N. Such implementation is then used to develop the station characterization and data filtering techniques. In Appendix 7.8 is listed the subroutine readmeandata.C, which is the core of the GBSC-meanmap, as it loops on the map bins to calculate mean and standard deviation of the investigated quantity. In readmeandata.C is possible to see part of the implementation to include the CCSTDDEV and the C/N, as original part of the research project. The new features of the GBSC maps can be selected through two dedicated datacards (occumap.datacard and meanma.datacard), of which two examples are given in Appendix 7.9.

Techniques to assess multipath features in acquired data can also be found in Van Dierendonck (2001) and Benton and Mitchell (2011). The present work focuses on identifying bins where the probability of detecting a deteriorated signal is high.

---

<sup>16</sup> <http://root.cern.ch>

The characterisation of the environment of the Nottingham station (receiver ID: NSF06) was carried out using the data acquired during 2008, which was a very quiet year from a geomagnetic and solar point of view, allowing the impact of ionospheric turbulence to be ignored. The number of days used in the analyses cover 96.2% of the whole year, with only a small data gap from 3 to 15 April 2008. The field of view of the station covers the range (40; 65)°N in latitude, and (-25; 25)°E in longitude.

### 3.1.2 Nottingham data analysis

Figure 3.1.1 shows the Code-Carrier divergence standard deviation, averaged over the whole of 2008 on an azimuth-elevation map. Larger values below an elevation angle of 20 degrees are indicative of multipath activity in the regions around the azimuths 45°, 145°, and 240° roughly corresponding to the NE, S-SE, and SW directions respectively.

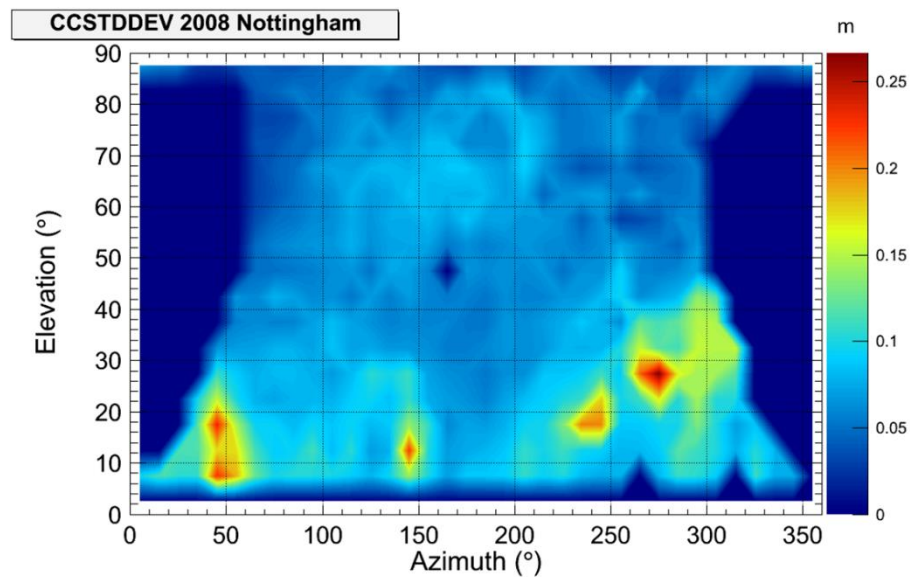


Figure 3.1.1. Azimuth–elevation map of the Code-Carrier divergence standard deviation averaged over the whole of 2008, recorded by the Nottingham receiver.

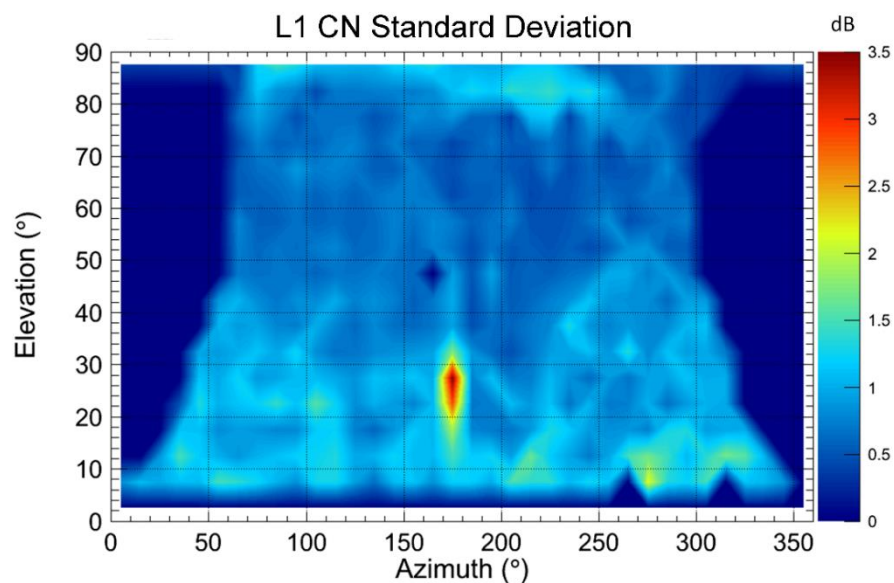


Figure 3.1.2. Azimuth–elevation map of the standard deviation of the L1 C/N ratio over the whole of 2008, recorded by the Nottingham receiver.

Figure 3.1.2 shows the L1 C/N standard deviation for the whole of 2008 on an azimuth-elevation map, indicating significant signal quality degradation in the region around azimuth  $170^\circ$  and at elevation angles between  $20^\circ$  and  $30^\circ$ . This degradation is caused by a very tall chimney in proximity to the station, as will be discussed in more detail below.

Figure 3.1.3 presents the percentage of occurrence of amplitude scintillation index  $S_4$  above 0.1 for the whole of 2008, on a latitude-longitude map in geographic coordinates for an assumed sub-ionospheric point at 350 km. The threshold of 0.1 was chosen because it characterises weak scintillation activity. It immediately appears in Figure 3.1.3 that some regions of the ionosphere viewed by the Nottingham receiver exhibit a high likelihood of observing amplitude scintillation, in particular the region between  $(-10; -8)^\circ\text{E}$  in longitude and  $(47; 50)^\circ\text{N}$  in latitude, where the percentage of occurrence is almost 100%, indicating an almost omnipresent degradation of the GPS signal amplitude.

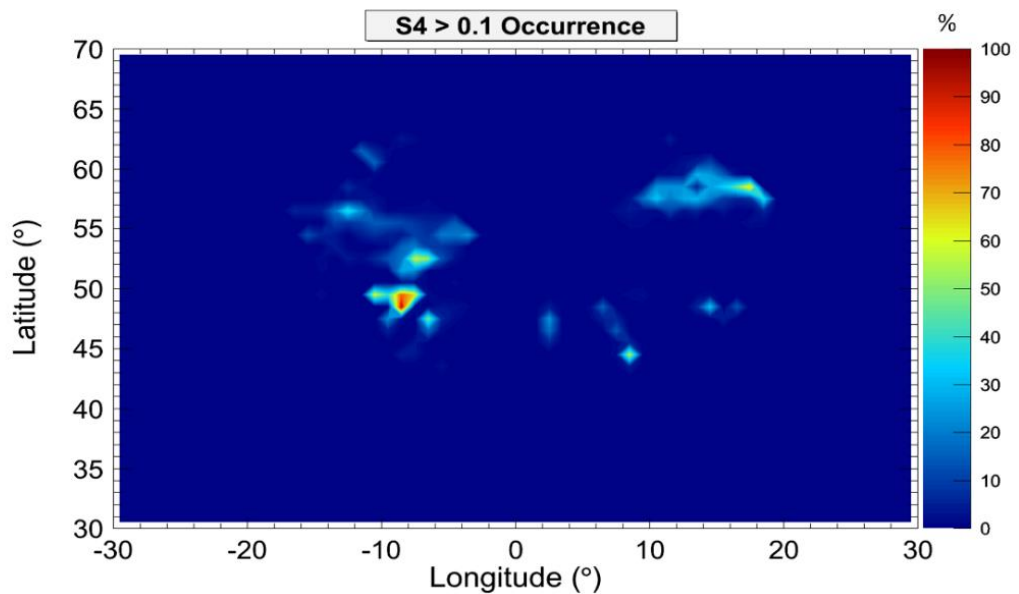


Figure 3.1.3. Latitude-longitude map of the percentage of occurrence of amplitude scintillation index  $S_4$  above 0.1 for the whole of 2008, recorded by the Nottingham GISTM receiver.

Figure 3.1.4 (top panel) shows the same percentage of occurrence of amplitude scintillation above 0.1 as in Figure 3.1.3, but on an azimuth-elevation map, while the bottom panel is the same, but with the intensity scale maximum adjusted to 10%. This allows easier comparison of the amplitude scintillation index with the percentage of occurrence of the phase scintillation index above 0.1 radians, as shown in Figure 3.1.5.

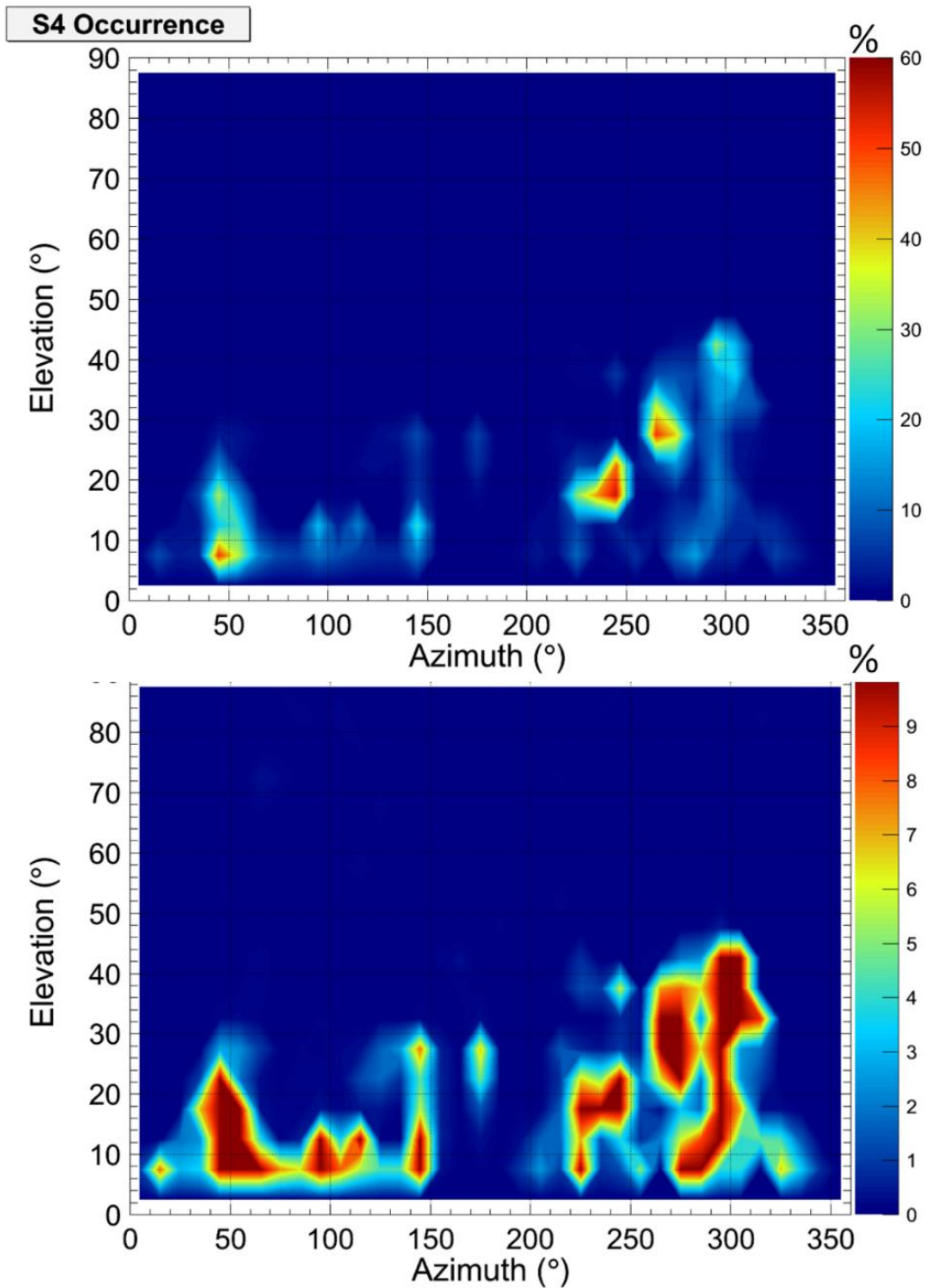


Figure 3.1.4. Top plot: azimuth–elevation map of the percentage of occurrence of amplitude scintillation index  $S_4$  above 0.1 for the whole of 2008, recorded by the Nottingham receiver. Bottom plot: same as top plot, but obtained by constraining the scale maximum to 10%.

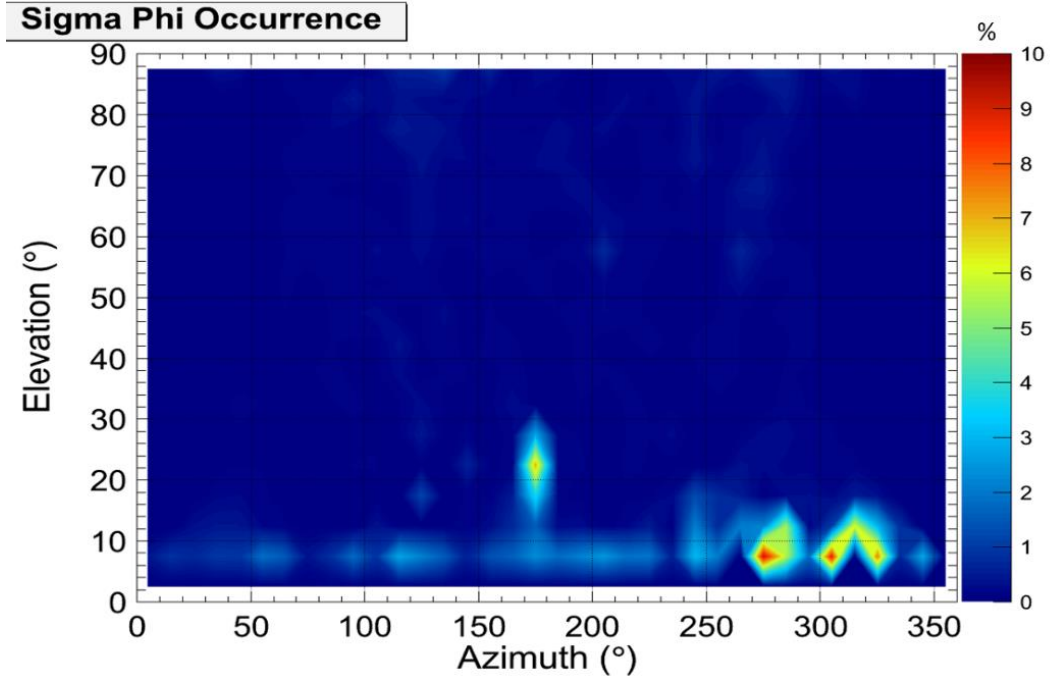


Figure 3.1.5. Azimuth–elevation map of the percentage of occurrence of phase scintillation index  $\sigma_\phi$  above 0.1 radians over the whole of 2008, recorded by the Nottingham receiver.

Figures 3.1.4 and 3.1.5 show that amplitude scintillation, evident in Figure 3.1.3, and phase scintillation both occur at low elevations. It is also interesting to note that the area indicated above as in line of sight of the chimney presents very similar values for the percentage of occurrence (about 10%). The amplitude and phase response of an electromagnetic wave to structures is determined by Fresnel filtering, which strongly suppresses the contribution on scales larger than the radius of the first Fresnel zone  $R_f$ , which can be easily calculated from the relation:

$$R_f = \sqrt{\lambda D}, \quad (1)$$

where  $\lambda$  is the wave length (about 19 cm for L1) and  $D$  is the distance to the screen producing diffraction effects. Considering that the chimney is about 90 m away from the receiver antenna, about 80 m high and that the antenna is on the roof of the former IESSG building, i.e. at about 10 m in height, the impact of the presence of the chimney should be felt up to an elevation angle of:

$$\alpha = \tan^{-1} \frac{(80-10)}{90} = 33.7^\circ, \quad (2)$$

which matches the indications of the azimuth-elevation maps.

Figure 3.1.6 illustrates the dependence of the first Fresnel zone radius on distance. The antenna to chimney distance of about 90 m corresponds to a Fresnel radius of about 2.1 m. Considering that the radius of the chimney varies between 3 and 2.5 m from bottom to top, it mimics an “irregularity” of the same dimension of the Fresnel radius, resulting in both amplitude and phase scintillation caused by scattering of the wave encountering the chimney, the occurrence of which is roughly the same order of

magnitude. This indicates that, from a statistical point of view, the chimney is almost the sole cause of the ‘perceived’ scintillation effects along that path.

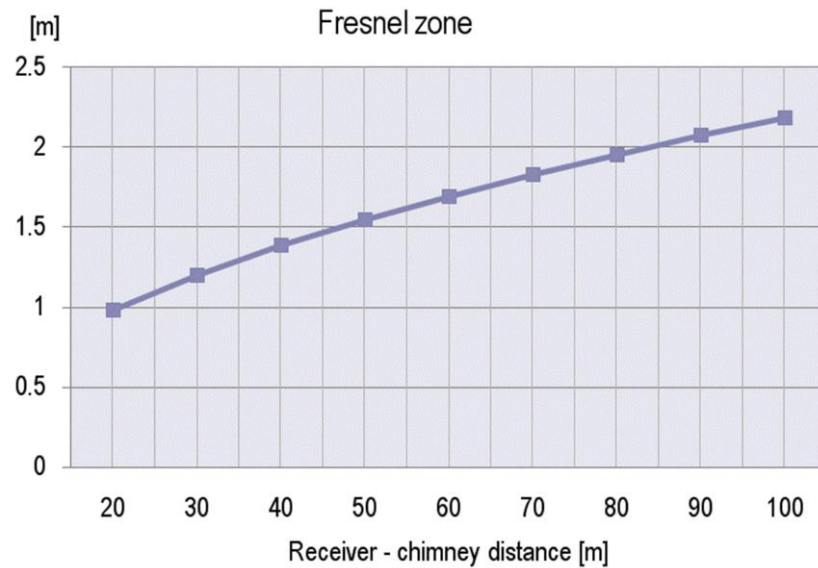


Figure 3.1.6. First Fresnel zone radius as a function of distance.

### 3.1.3 Antenna survey

The different features of the maps described in paragraph 3.1.2 are discussed and re-interpreted by analysing the surroundings of the former building of the IESSG, where the NSF06 receiver was located in 2008. The survey was conducted in February 2011 and geo referencing was carried out using the “DATA Live Ordnance Survey” vector data of the University of Nottingham Campus. Figure 3.1.7 shows the area of the Nottingham campus, together with some pictures taken along the various azimuths from the receiver position. At 171° is the chimney, the effect of which has already been discussed to explain the pattern of the data acquired by the NSF06 receiver during 2008 (Figures 3.1.2, 3.1.4, and 3.1.5). Other possible sources of multipath are the trees in the azimuth range between 230° and 273°, which were pruned and significantly reduced in height after 2008. They acted as a source of multipath, as shown by the enhancement in percentages of both CCSTDDEV and S4 in Figures 3.1.1 and 3.1.3. Similar sources of multipath, visible in the abovementioned maps and indicated in the pictures of Figure 3.1.7, include the building at an azimuth of about 50° spanning elevation angles between 5° and 20°, and the GPS antenna on the roof of the building at an azimuth of about 145°, visible in the same picture as the chimney (the crane tower seen in the photo was not present in 2008).

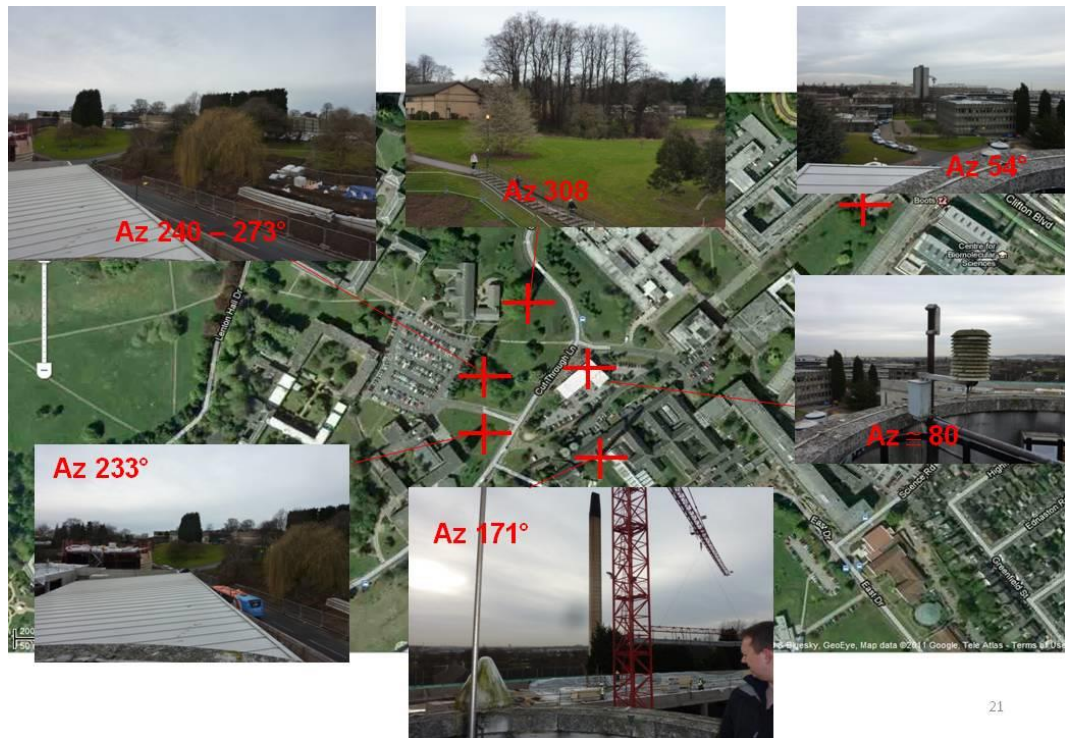


Figure 3.1.7 Map of the campus.

### 3.1.4 Trondheim data analysis

The analysis of the Trondheim station (receiver ID: NSF01) was done comparing the data acquired in 2008 with those of summer 2009, aiming to investigate a significant data quality degradation occurred since May 2009, probably due to interference phenomena with a radio bridge installed in 2009. The days of data acquisition in 2008 cover 80.6% of the whole year, with some gaps of several days in February, June, September, November and December, while the 2009 data covers the period between Jun 1<sup>st</sup> to Aug 31<sup>st</sup> with some data gaps in August. The analysed data, the period of investigation and the corresponding percentage of available days of data are summarized in Table 3.1.1.

	2008	2009
Period	1 Jan to 31 Dec	1 Jun to 31 Aug
Days of data (%)	295 (80.6)	67 (72.8)

Table 3.1.1 Summary of the data analysed from 2008 and 2009.

The field of view of the stations ranges between 50° and 77°N in latitude and -25° and 25°E in longitude, covering part of the sub-auroral regions of the ionosphere. Similarly to the procedure conducted for the Nottingham station, the signal quality was characterized with the L1 C/N, the standard deviation values of which are shown in Figure 3.1.8 with the top and bottom plots referring to the periods considered in 2008 and 2009, respectively. A part from the difference in statistics between the two samples, resulting in a less populated map for 2009, it is evident a general anisotropic degradation of the signal, appearing as higher values of the L1C/N standard deviation without identification of privileged areas of the ionosphere. Moreover, there is no meaningful degradation potentially due to multipath. This is quite evident in the two

maps of Figure 3.1.9, showing the mean values of the Code Carrier divergence standard deviation in geographic coordinates for 2008 (top) and 2009 (bottom), which are seen to be very similar. No meaningful variation in CCSTDDEV emerges, even if slightly larger values are present in the region (60; 70) $^{\circ}$ N in latitude and (-10; 0) $^{\circ}$ E in longitude, as confirmed by the corresponding standard deviation of CCSTDDEV maps in Figure 3.1.10.

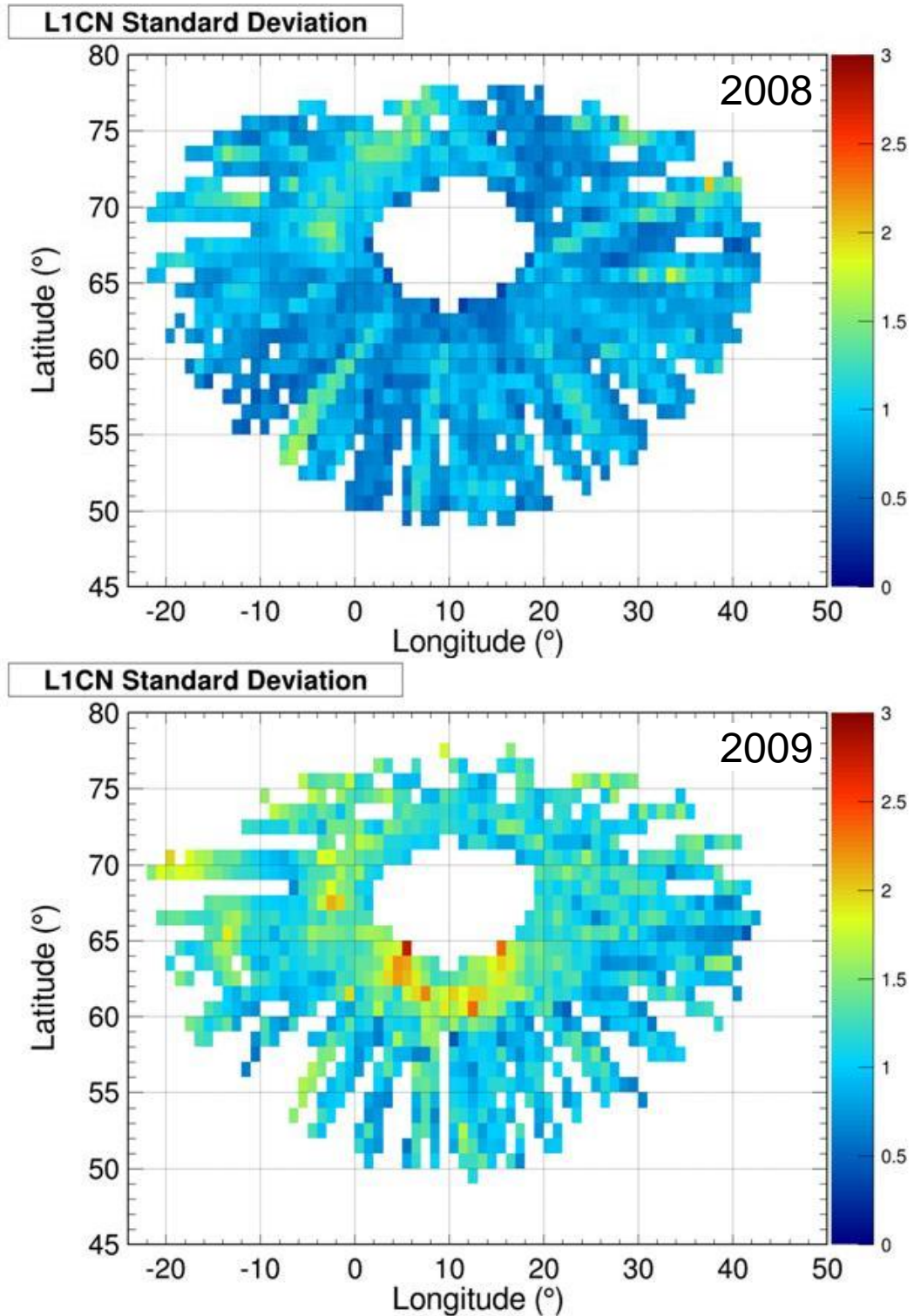


Figure 3.1.8. Maps of the standard deviation of L1C/N in geographic coordinates for the considered period of 2008 (top) and 2009 (bottom).

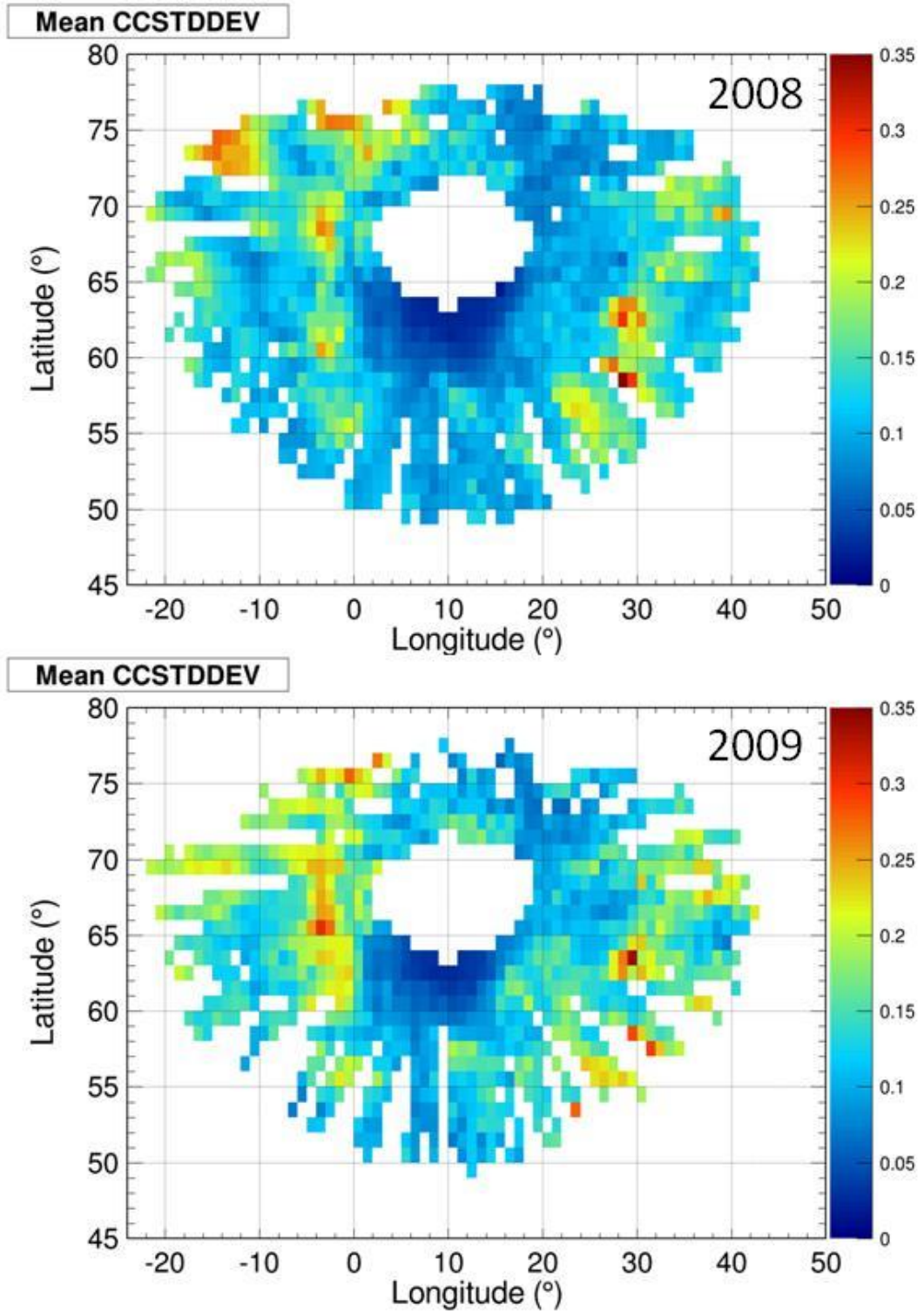


Figure 3.1.9. Maps of Code Carrier Divergence Standard Deviation in geographic coordinates for the periods considered in 2008 (top) and 2009 (bottom).

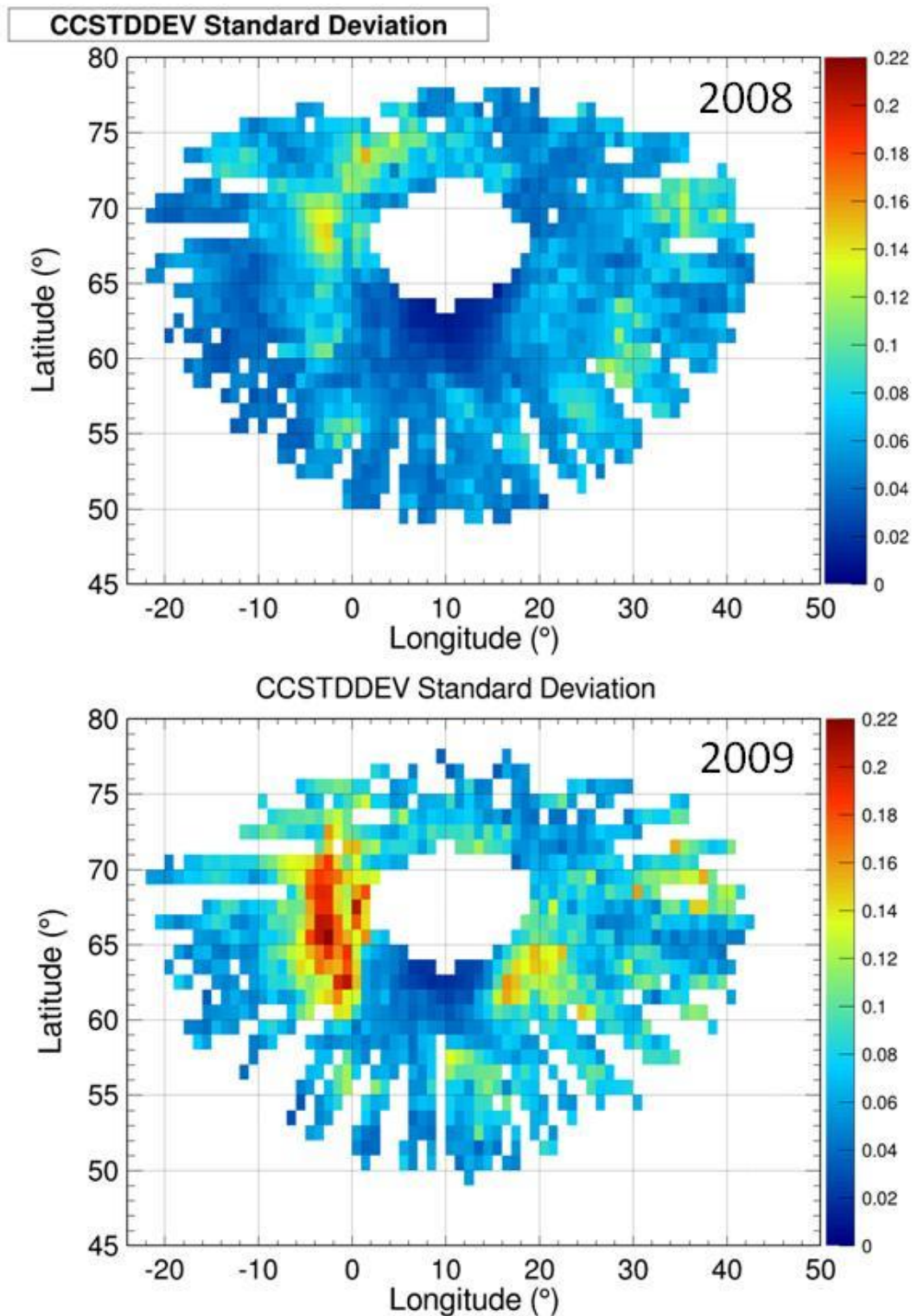


Figure 3.1.10. Maps of the standard deviation of the Code Carrier Divergence Standard Deviation in geographic coordinates for the periods considered in 2008 (top) and 2009 (bottom).

### 3.1.5 Nottingham station behaviour during the “Halloween Storm”

This paragraph provides some analyses of the NSF06 receiver data acquired during the so-called Halloween Storm, which occurred between 30 and 31 October 2003 and was the strongest of the last solar cycle. The analyses are illustrated and the results discussed in the light of the station characterisation conducted previously. Over these two days, severe solar events caused highly disturbed conditions in the ambient

ionosphere. In particular, a very fast full halo coronal mass ejection (CME) originating from an X10 flare reached the Earth at about 16:00 UT on 30 October (Weaver et al., 2004). The geomagnetic storm induced by this CME lasted for about 24 hours and reached extreme levels. As a consequence, episodes of severe scintillation were registered on 30 October by the GISTM receiver at Nottingham, NSF06 (see e.g. De Franceschi et al., 2008, and Spogli et al., 2009). Figure 3.1.11 and Figure 3.1.12 show the time profiles of  $S_4$  (top plot) and  $\sigma_\phi$  (bottom plot), as measured by the NSF06 receiver on 30 to 31 October 2003: each colour represents a different satellite.

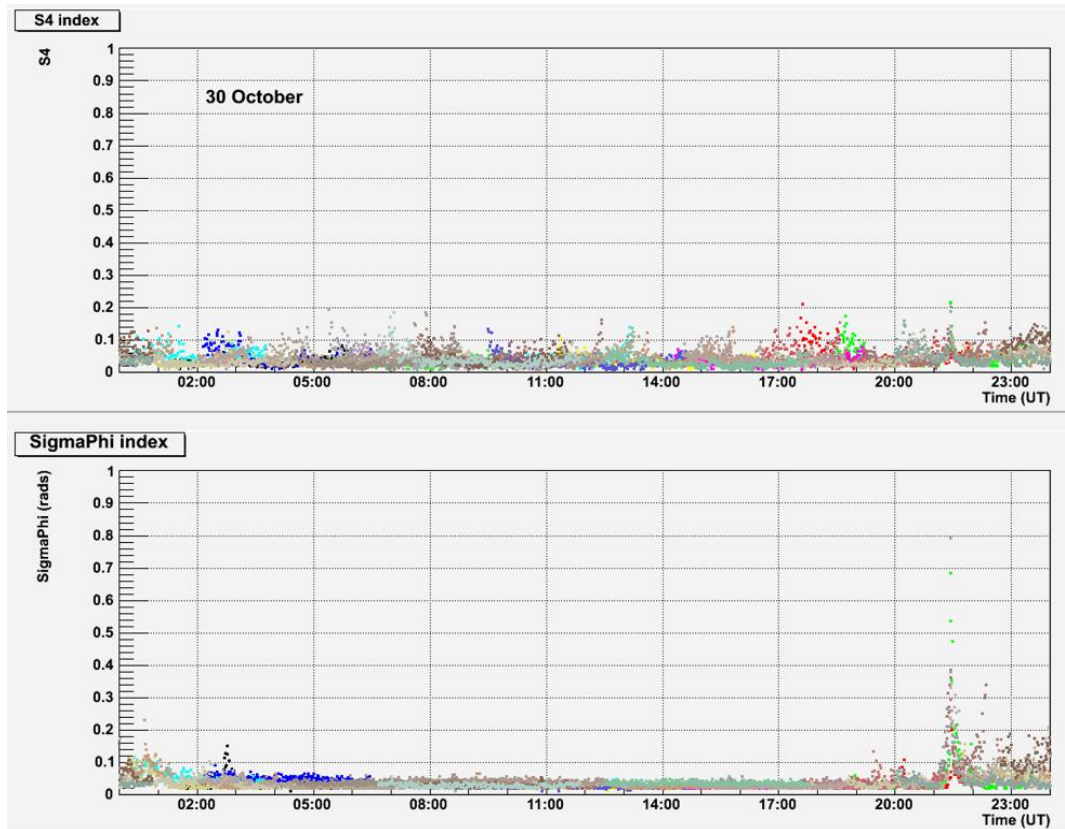


Figure 3.1.11. Time profiles of  $S_4$  (top) and  $\sigma_\phi$  (bottom) for all satellites in view as measured by NSF06 on 30 October 2003.

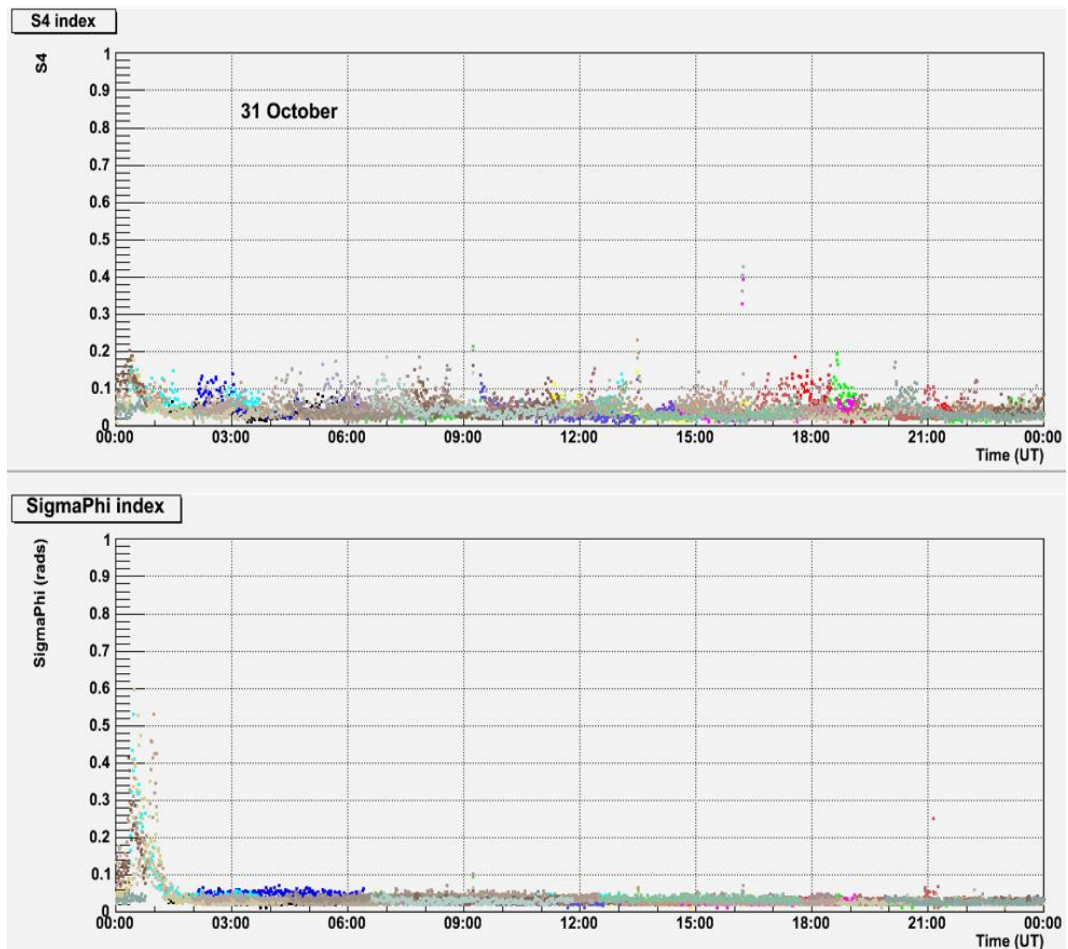


Figure 3.1.12. Time profiles of  $S4$  (top) and  $\sigma_{\phi}$  (bottom) for all satellites in view as measured by NSF06 on 31 October 2003.

Figures 3.1.13 and 3.1.14 show the corresponding time profiles of the vertical TEC ( $\nu\text{TEC}$ ) and the Rate of TEC change (ROT). All these plots show that, when the storm effects arrived in the field of view of NSF06 at around 20:00 UT on 30 October, the electron density perturbations increased, with steep gradients appearing as large ROT values for most of the satellites, up to 8 TECu/min. The signal phase was significantly influenced, with  $\sigma_{\phi}$  peaking at about 0.9 radians, while  $S4$  was not significantly influenced. This can be interpreted as the presence of irregularities of scale sizes above the Fresnel distance which, assuming an ionospheric piercing point at 350 km in height, is about 250 m for the L1 frequency. This is typical of the high latitude ionosphere, which is characterized by irregularities of scale sizes up to hundreds of kilometres, but not typical of the mid-latitude ionosphere, indicating a severe degree of turbulence induced in the ionosphere by this solar storm (see, e.g. Mitchell et al., 2005; Foster and Rideout, 2005; De Franceschi et al., 2008). The scintillation effects ended at about 3:00 UT on 31 October.

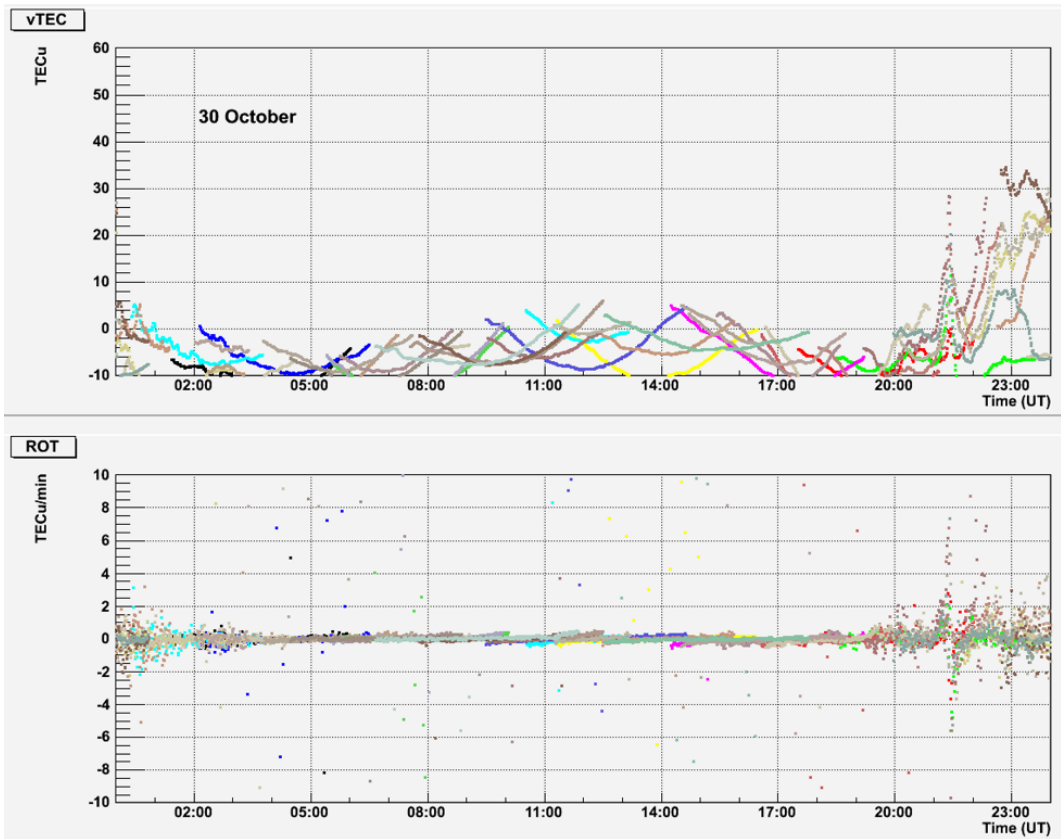


Figure 3.1.13. Time profiles of vTEC (top) and ROT (bottom) for all satellites in view as measured by NSF06 on 30 October 2003.

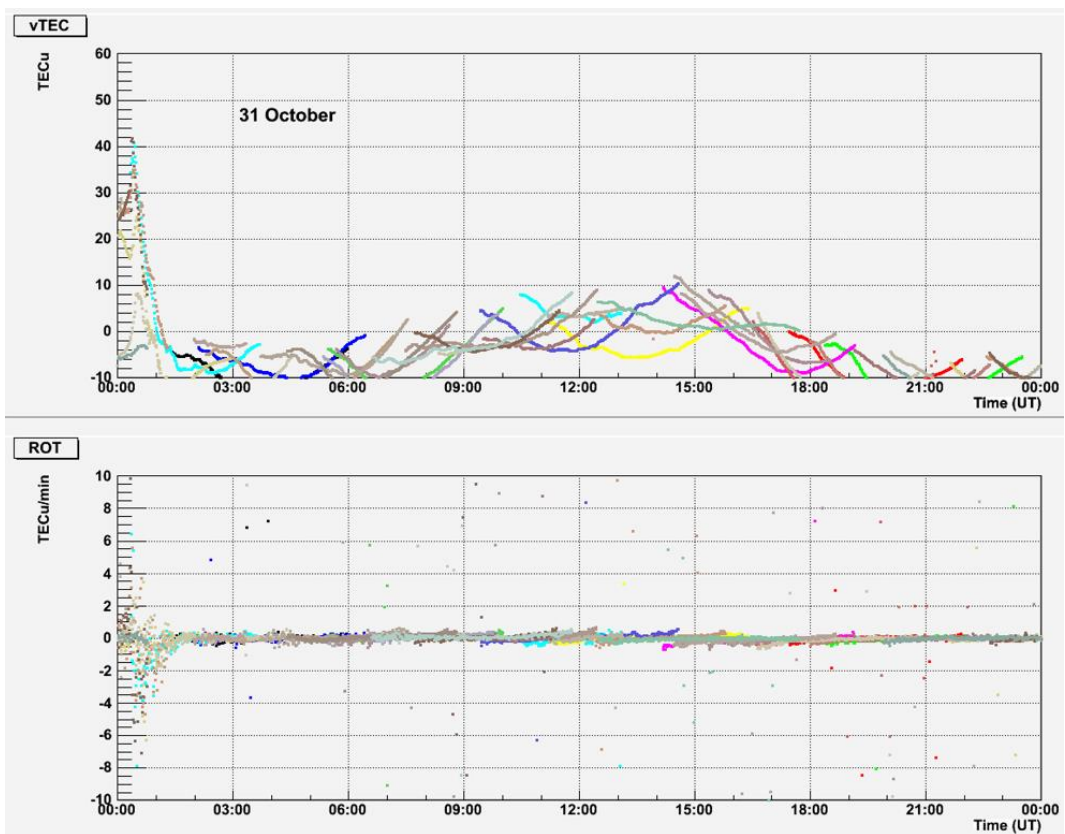


Figure 3.1.14. Time profiles of vTEC (top) and ROT (bottom) time profiles for all satellites in view as measured by NSF06 on 30 October 2003.

Figure 3.1.15 shows the azimuth-elevation map of the standard deviation of L1 C/N for the period 27 October to 3 November, i.e. from 3 days before the storm to 3 days after the storm. Figure 3.1.16 shows the azimuth-elevation map of code carrier divergence standard deviation for the same period. These maps show that signal degradation due to multipath sources and the chimney were already present in 2003. Figure 3.1.17 shows the azimuth-elevation maps of the  $\sigma_\phi$  standard deviation (left plot) and percentage of occurrence above 0.1 radians (right plot) for the same period as Figures 3.1.15 and 3.1.16. These two figures are provided firstly to show that standard deviation and occurrence are strictly related, and secondly to show how the enhancement of scintillation activity due to the presence of the chimney, clearly visible during the quiet year 2008, appears in the "Halloween Storm" occurrence plot at a lower value (about 1 to 2%) than seen in Figure 3.1.5 (about 10%). This is probably due to the fact that 1 week provided insufficient data for the chimney signature to be evident in the statistics under such marked scintillation conditions.

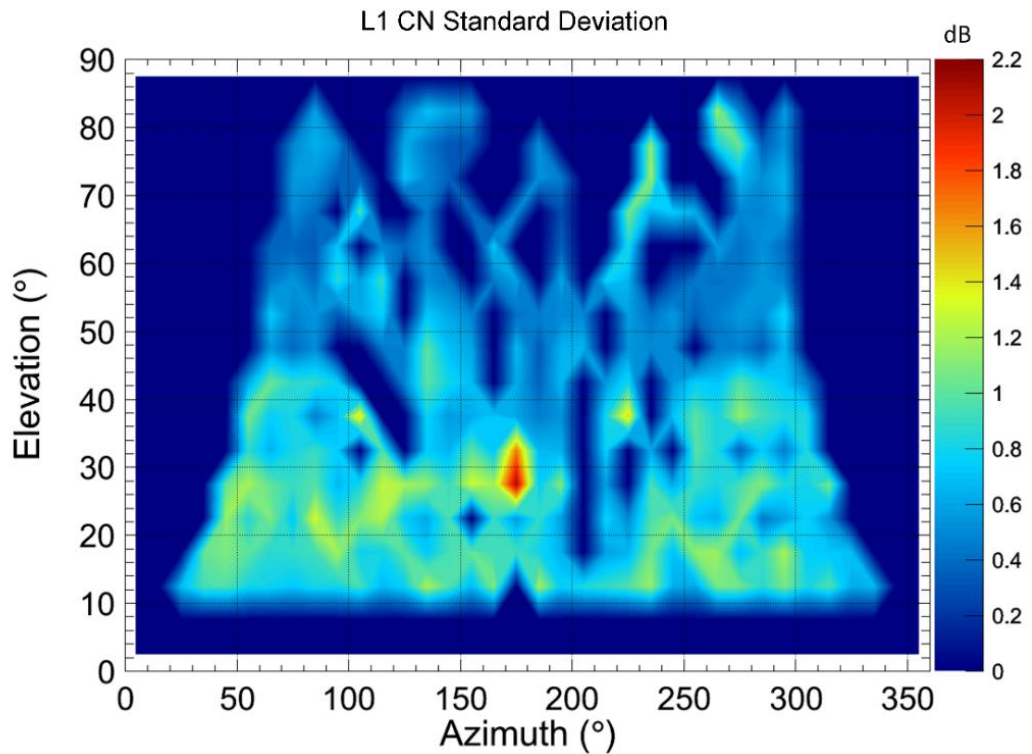


Figure 3.1.15. Azimuth–elevation map of the standard deviation of L1 C/N for the period 27 October to 3 November 2003.

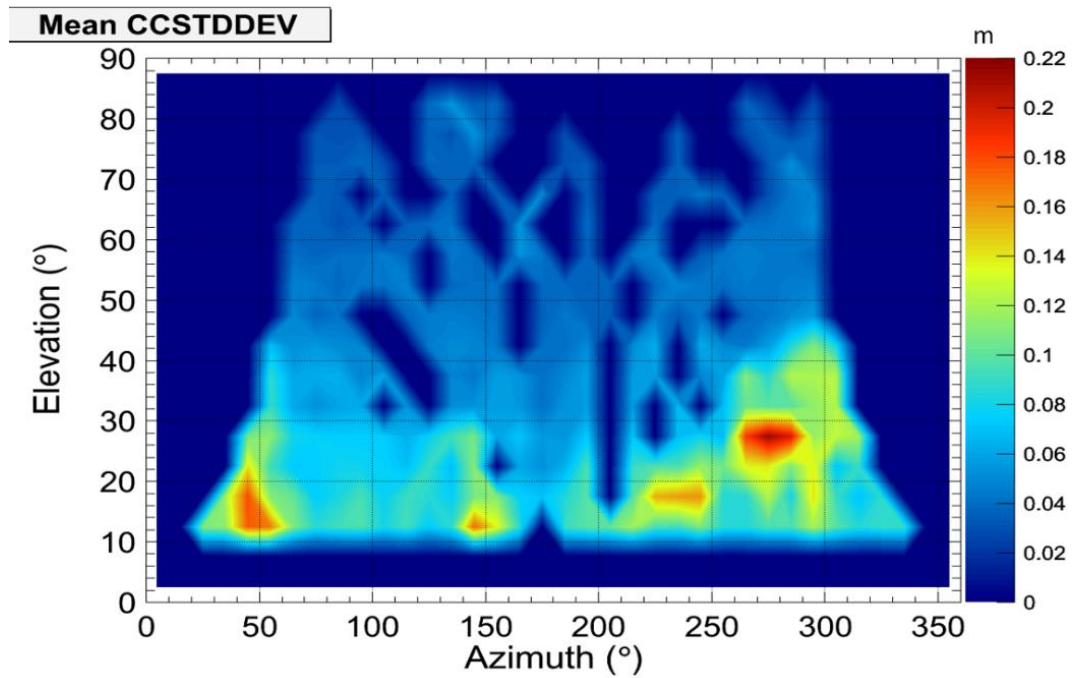


Figure 3.1.16 Azimuth–elevation map of the Code Carrier Divergence Standard Deviation for the period 27 October to 3 November 2003.

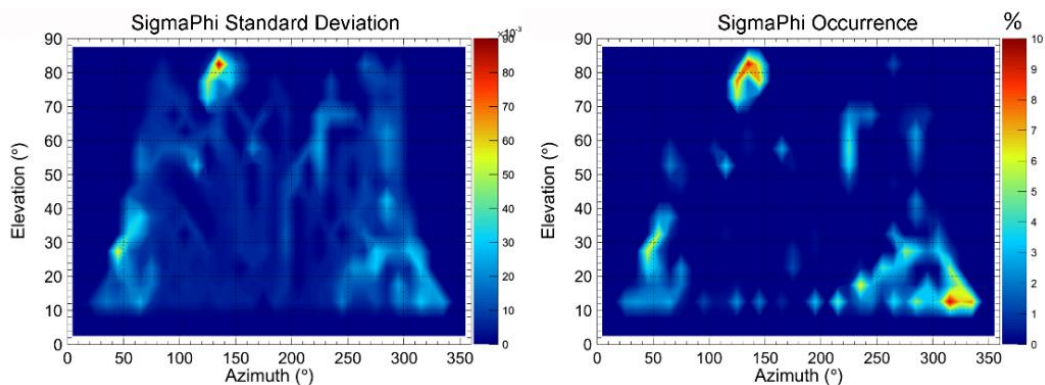


Figure 3.1.17. Azimuth–elevation maps of the  $\sigma_\phi$  standard deviation (left) and percentage of occurrence above 0.1 radians (right) for the period 27 October to 3 November 2003.

### 3.2 FILTERING TECHNIQUE

As discussed in previous sections, to study ionospheric scintillation on L-band radio signals it is nowadays typical to acquire data with receivers working at high frequency sampling rate (50-100 Hz) (Kintner et al., 2009). When dealing with such data, it is common to consider the contribution coming solely from observations at elevation angles, calculated from the receiver to the selected satellite, above an arbitrary threshold, typically 15-30°. Filtering out measurements made at low elevation angles helps keeping a high SNR (Signal to Noise Ratio) and eliminating non-ionospheric related effects, such as multipath (Skone and Jong, 2000).

The downside of that well consolidated method is a reduction of the field of view spanned by the GNSS receiver antenna, and, if it is the case, of the whole network. This is not crucial for dense networks or well covered areas, but it is in case of not well

covered regions, for logistics (e.g. forests, deserts, etc.) and/or environmental reasons (e.g. oceans). The loss of information in many applications could be crucial.

This PhD work has introduced a method to filter out spurious data based on an “outliers analysis” able to efficiently remove multipath affected measurements, reducing the data loss with respect to applying a fixed elevation angle cut-off threshold. It is based upon the Ground Based Scintillation Climatology (GBSC) technique (Spogli et al., 2009, Alfonsi et al., 2011) and the station characterization described in the previous section 3.1 and in Romano et al. (2013). In paragraph 3.2.1 the filtering method is presented, in paragraph 3.2.2 it is tested for the GISTM data of the Rome station. In Chapter 4, then, the method is applied to climatological studies and to the CIGALA<sup>17</sup>/CALIBRA<sup>18</sup> network in Brazil, enlarging the field of view and, then, improving the capability of investigating the dynamics of the ionosphere.

### 3.2.1 Method

Bearing in mind that a fool-proof standard procedure able to remove short and long term effects due to environmental multipath has not yet been implemented, the filtering method is based upon the identification of the outliers in the  $\sigma_{CCSTDDEV}$  histogram. Ray paths characterised by a large variability of CCSTDDEV can be tagged as affected by multipath and then removed for any further data analysis.

As stated in the general data analysis theory (Barnett et Lewis, 1995), most values of a distribution are expected to fall in the inter-quartile range (IQR) that is the distance between the 1<sup>st</sup> and the 3<sup>rd</sup> quartile. For single right tail distribution, that is the case of CCSTDDEV, the outliers are identified by the values lying above  $Q3+k \cdot IQR$ , where  $Q3$  is the 3<sup>rd</sup> quartile. Different definitions of outliers follow different values of the  $k$  parameter:  $k=1.5$  identifies the "mild outliers",  $k=3$  identifies the extreme outliers”.

Figure 3.2.1 describes step by step the filtering method:

- 1) The original data set of “S60” files coming from a GISTM station is arranged.
- 2) Data are converted into ROOT native format to be ingested by the GBSC, according to the block diagram in figure 2.3.5.
- 3) The related GBSC maps in azimuth vs. elevation of the Mean and Standard Deviation of the CCSTDDEV are created.
- 4) Each value of  $\sigma_{CCSTDDEV}$  is then used to create the corresponding histogram distribution.
- 5) The outlier identification method is applied: values lying outside  $k$  times the IQR are identified as outliers.
- 6) The bins corresponding to values of  $\sigma_{CCSTDDEV}$  greater than  $Q3+k \cdot IQR$  are filtered out.
- 7) The “datafilt.dat” table is created where indication of filtered bins is reported.
- 8) Datafilt.dat is read by a suitably modified version of the Data\_root routine (last stage in the block diagram of figure 2.3.5), that is called Data\_root\_filt (Appendix 7.10).
- 9) Data set is ready to be used for applications.

---

<sup>17</sup> CIGALA stands for Concept for Ionospheric-Scintillation Mitigation for Professional GNSS in Latin America.

<sup>18</sup> <http://www.calibra-ionosphere.net>

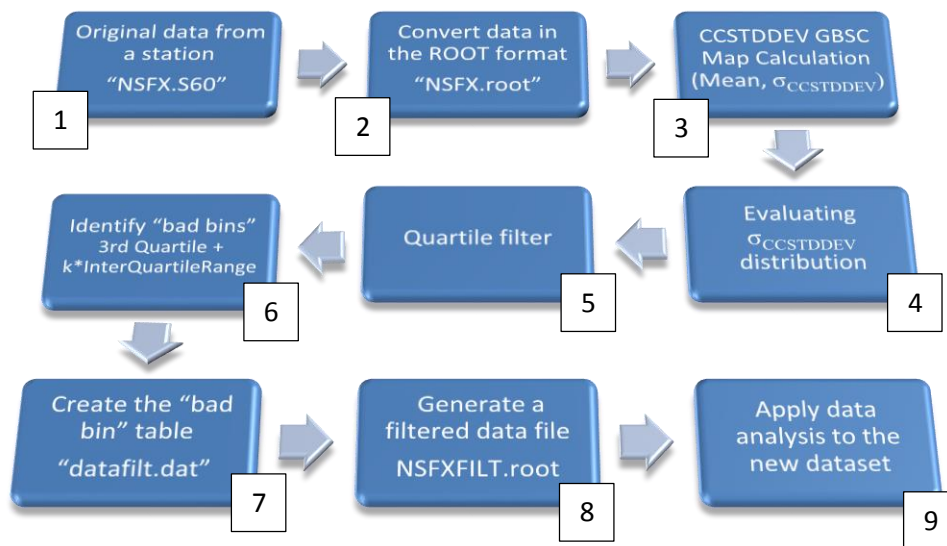


Figure 3.2.1 Logic diagram of the Filtering method

### 3.2.2 Test of the filtering technique

As a first test of the filtering capabilities of the technique, data acquired by the GISTM station of Rome have been filtered. Rome GISTM has been installed in March 2012 in the frame of the PhD project. Similarly to Nottingham, the Rome GISTM is located in an urban site, surrounded by many multipath sources. Rome is also weakly affected by ionospheric disturbances (on average quiet at mid-latitudes), allowing the disentanglement between ionospheric and non-ionospheric effects on the signal received at ground.

Applications of the method are then presented in Chapter 4 for validation and consolidation of the scientific results of the project. Figure 3.2.2 shows the map of  $\sigma_{CCSTDDEV}$  obtained for the Rome GISTM station in 2012 (in particular from 15 March to 8 December). The bin size adopted is  $10^{\circ} \times 5^{\circ}$  and observations on GPS L1 frequency have been considered.

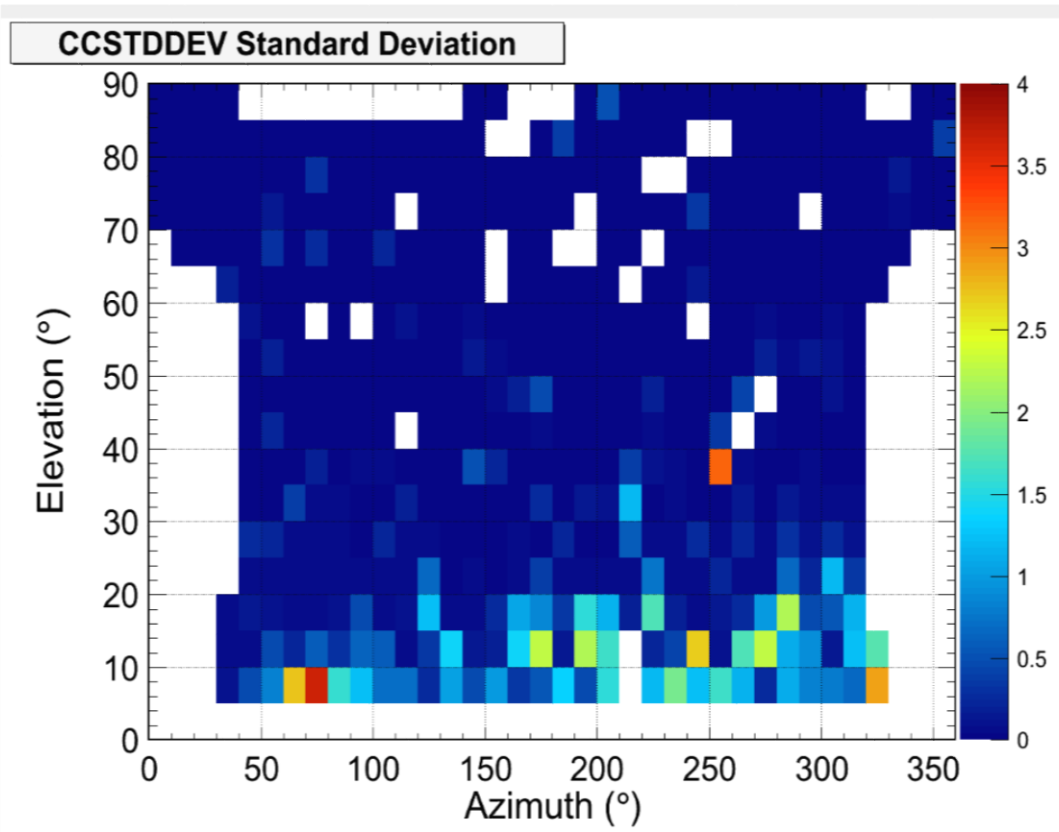


Figure 3.2.2. Map of the  $\sigma_{CCSTDDEV}$  in azimuth vs. elevation for Rome GISTM station on L1 frequency for 2012.

Each value of  $\sigma_{CCSTDDEV}$  is then used to create the corresponding histogram, shown in Figure 3.2.3. The red lines correspond to the cut-off thresholds evaluated for different values of  $k$ , from 1 to 5, by using the outliers formula from Barret and Lewis (1995):

$$Cutoff = Q3 + k * (IQR)$$

Table 3.2.1 shows the cut-off values for the different values of  $k$ . For each value, the corresponding number of bins filtered out is also reported.

The red lines in Figure 3.2.2 indicate the cut-off for different  $k$  values. The mild outliers are for  $k=1.5$ .

$k$	cut-off	# of bins filtered out
1	0.228	113
2	0.334	96
3	0.440	84
4	0.546	74
5	0.651	69

Table 3.2.1. Cut-off values for different  $k$  values and the corresponding number of bins filtered out

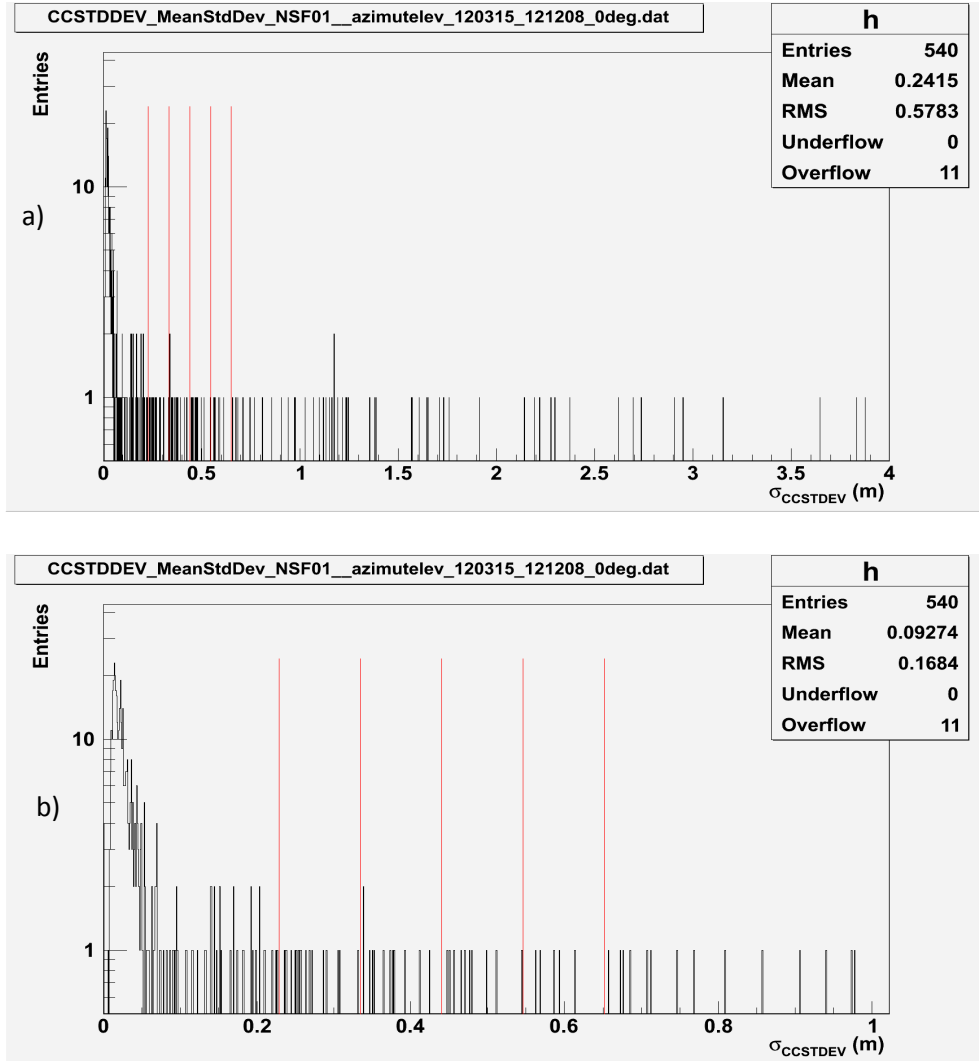


Figure 3.2.3. Distribution of the  $\sigma_{CCSTDDEV}$  corresponding to Rome GISTM data in 2012. The red lines indicate 5 different values of  $k$  to determine the cut-off thresholds ( $k=1, k=2, k=3, k=4$  and  $k=5$ ). The two histograms (top and bottom) report same quantities but with two different x-axis scales.

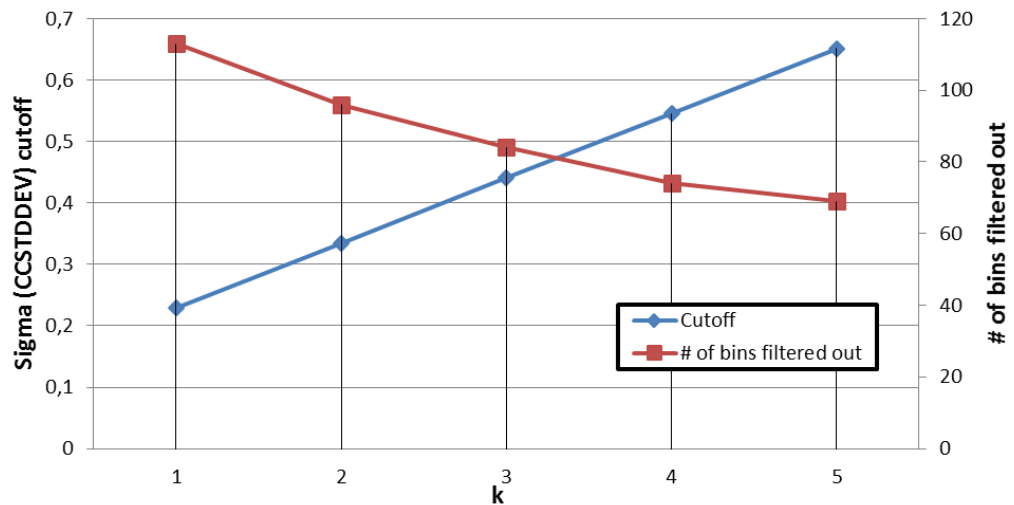


Figure 3.2.4.  $\sigma_{CCSTDDEV}$  cut-off values (blue line) and number of filtered out bins (red line) for different values of  $k$  from 1 to 5.

To test the filtering capabilities as a function of the  $k$  parameter, figures 3.2.5, 3.2.6, 3.2.7, 3.2.8 and 3.2.9 show Azimuth vs. Elevation maps of Mean (top-left) and Standard Deviation of CCSTDDEV (bottom-left). The corresponding maps filtered with  $k=1$  (Figure 3.2.5), 2 (Figure 3.2.6), 3 (Figure 3.2.7), 4 (Figure 3.2.8) and 5 (Figure 3.2.9) are at the right hand side of each figure. As expected, most of the bins filtered out are in correspondence to small elevation angles that are the most affected by multipath. The sectors in azimuth are not homogeneously distributed. In fact, most of the filtered out bins are in correspondence to azimuths greater than  $180^\circ$ . The choice of considering  $k=1.5$ , i.e. the commonly adopted definition of “mild outliers”, is satisfactory in identifying the ray paths most affected by multipath and, thus, can be used for the extensive filtering described and discussed in chapter 4.

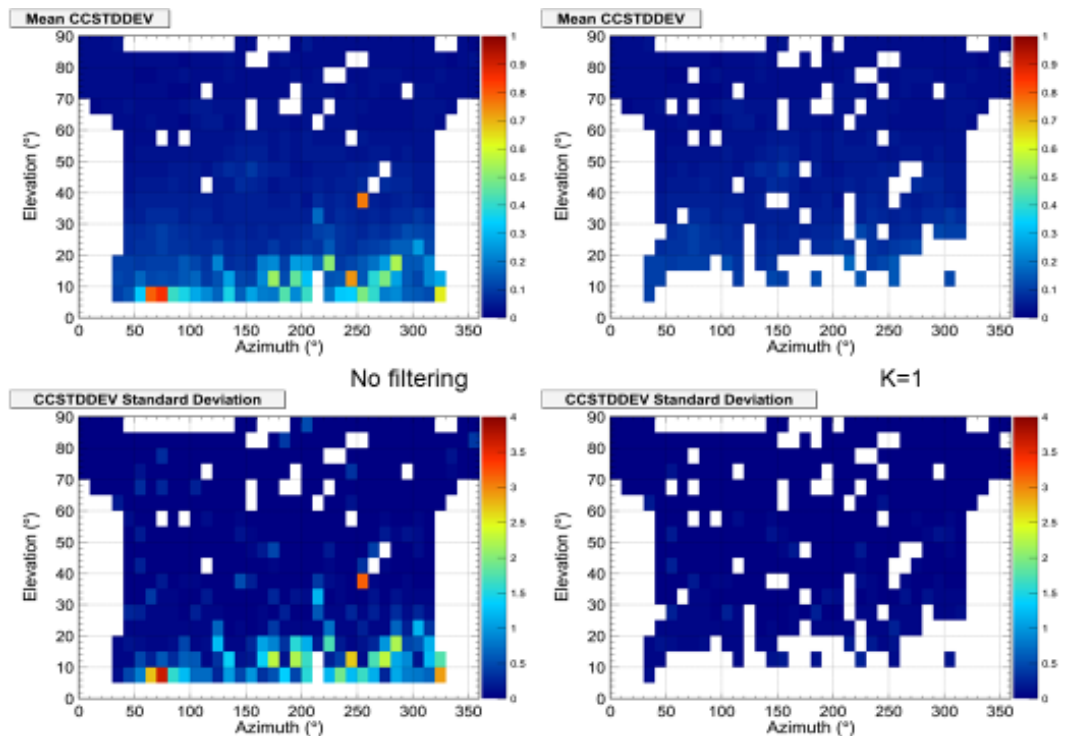


Figure 3.2.5 On the left the Azimuth vs. Elevation maps of Mean (top) and Standard Deviation of CCSTDDEV (bottom) and on the right the corresponding maps filtered with  $k=1$ . Data processing is related to the data acquired by the GISTM station of Rome in 2012.

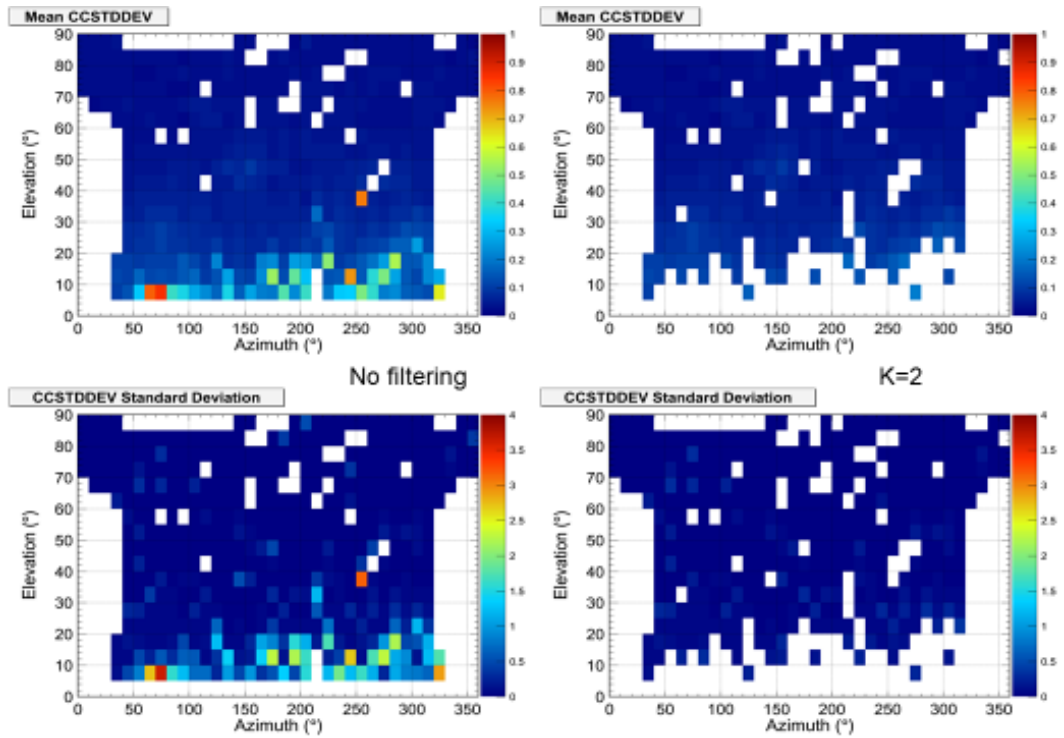


Figure 3.2.6. On the left the Azimuth vs. Elevation maps of Mean (top) and Standard Deviation of CCSTDDEV (bottom) and on the right the corresponding maps filtered with  $k=2$ . Data processing is related to the data acquired by the GISTM station of Rome in 2012.

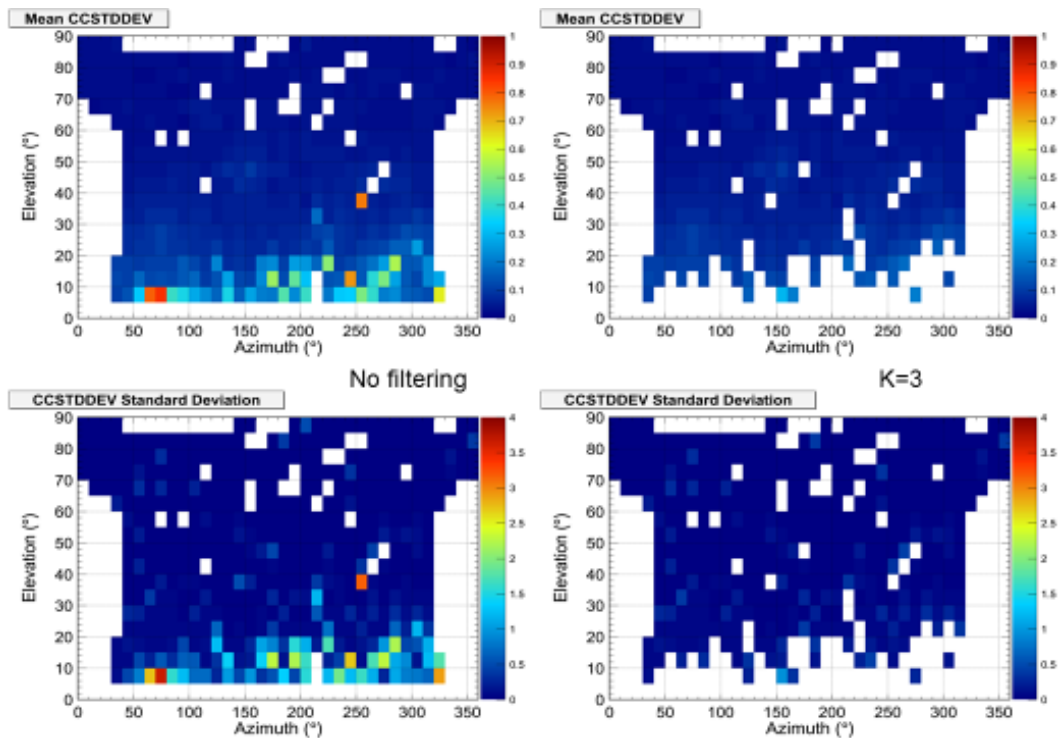


Figure 3.2.7. On the left the Azimuth vs. Elevation maps of Mean (top) and Standard Deviation of CCSTDDEV (bottom) and on the right the corresponding maps filtered with  $k=3$ . Data processing is related to the data acquired by the GISTM station of Rome in 2012.

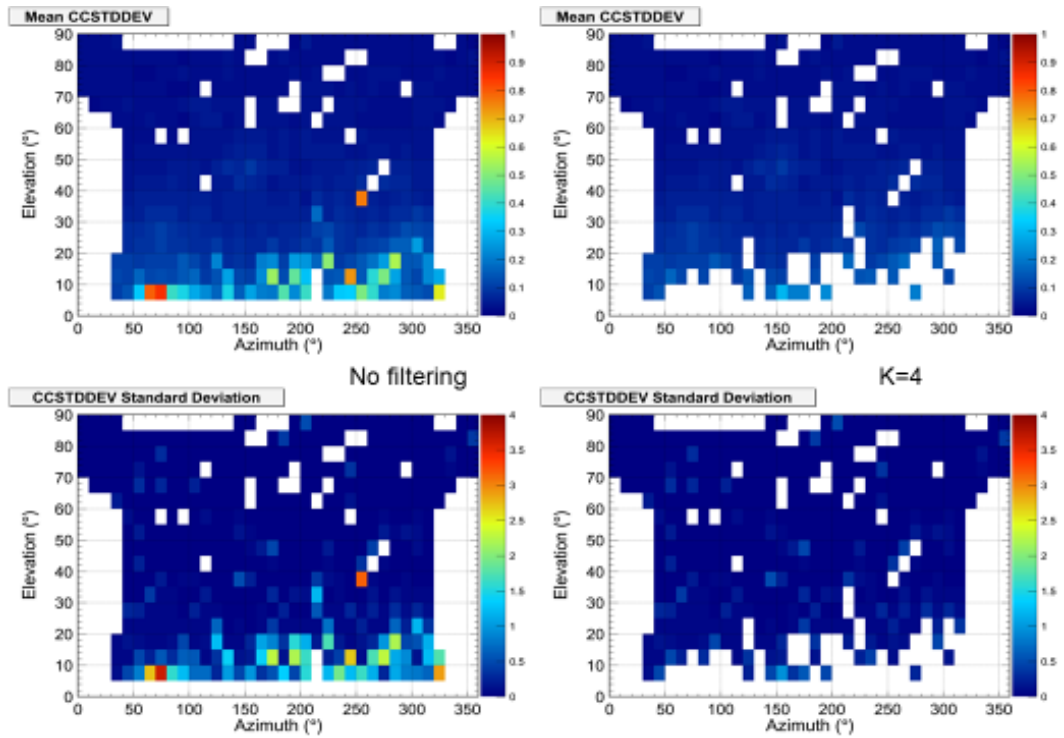


Figure 3.2.8 On the left the Azimuth vs. Elevation maps of Mean (top) and Standard Deviation of CCSTDDEV (bottom) and on the right the corresponding maps filtered with  $k=4$ . Data processing is related to the data acquired by the GISTM station of Rome in 2012.

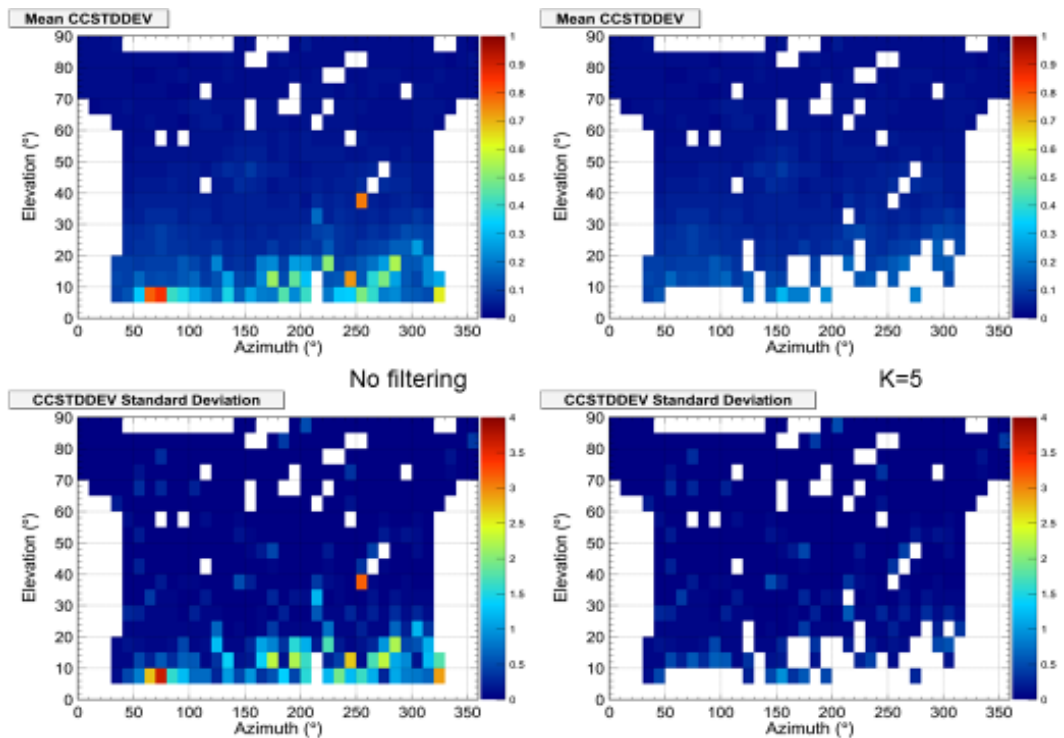


Figure 3.2.9 On the left the Azimuth vs. Elevation maps of Mean (top) and Standard Deviation of CCSTDDEV (bottom) and on the right the corresponding maps filtered with  $k=5$ . Data processing is related to the data acquired by the GISTM station of Rome in 2012.

## 4 CHAPTER 4 - APPLICATIONS USING REAL AND SIMULATED DATA

### 4.1 APPLICATION IN SCINTILLATION CLIMATOLOGY

As discussed in paragraph 2.3, the large volume of data stored at eSWua, the robustness and continuity of the acquisitions, and the effective data management and handling tools have enabled publication of a series of interesting papers focused on the climatological study of ionospheric scintillations. Figure 4.1.1 (extracted from Alfonsi et al., 2011) shows percentage occurrence maps of the phase scintillation index  $\sigma_\phi$  above 0.25 radians for the Northern (a) and Southern (b) hemispheres generated by applying the GBSC to 2008 scintillation data. The maps were defined using the INGV-NGI high-latitude network, as summarized in table 4.1.1

ID	Location	Latitude	Longitude
NYA0	Ny-Ålesund	78.9°N	11.9°E
NYA1	Ny-Ålesund	78.9°N	11.9°E
LYB0	Longyearbyen	78.2°N	16.0°E
NSF1	Trondheim	63.4°N	10.4°E
DMC0	Concordia Station	75.1°S	123.2°E
BTN0	Mario Zucchelli Station	74.7°S	164.1°E

Table 4.1.1. Receiver ID, location and geographic coordinates of the network (adapted from Alfonsi et al., 2011).

The position of the Feldstein auroral oval (Feldstein, 1963; Holzworth and Meng, 1975) has been superimposed over the scintillation occurrence maps for low level of magnetic activity (IQ=1), as 2008 was a year of quiet conditions of the near-Earth environment. The left-hand side of Figure 4.1.1 was generated by merging the NYA0, NYA1, and LYB0 Arctic stations data, while the right-hand side of Figure 4.1.1 shows merged data from the BTN0 and DMC0 Antarctic stations. In the example, scintillation occurrence is enhanced mainly around the boundaries of the auroral oval. A more thorough discussion of the scientific results is provided in the original paper. The methods for characterizing the stations and filtering the data were applied in the climatological studies and the upgraded results are presented here.

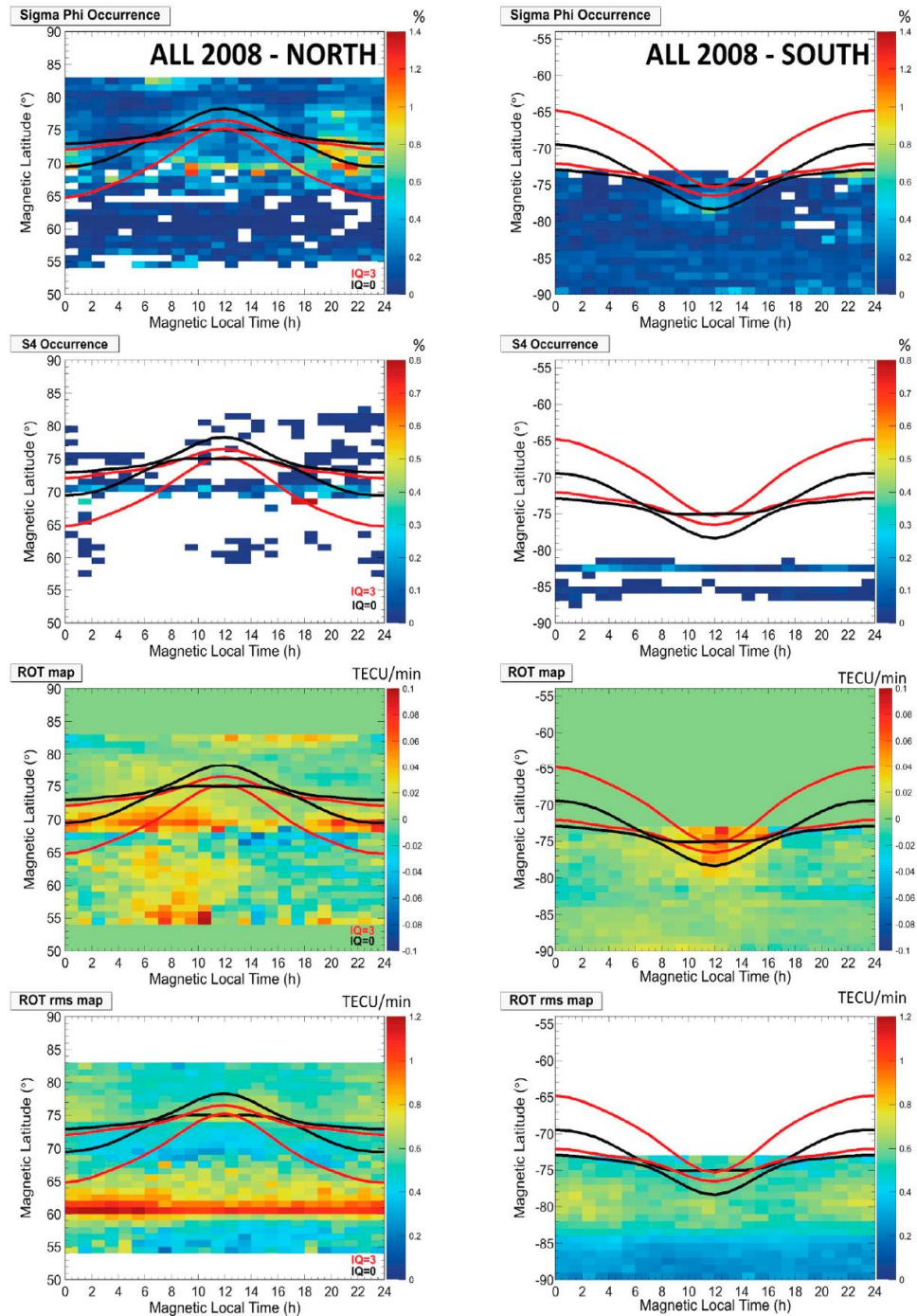


Figure 4.1.1. (top to bottom) Maps of: percentage occurrence of  $\sigma_\phi$ , percentage occurrence of the S4 (greater than 0.1), ROT and ROT RMS, in geomagnetic coordinates. Northern Hemisphere (left) and Southern Hemisphere (right). Black and red curves reproduce the Feldstein auroral ovals for IQ=0 and IQ=3, respectively. Figure extracted from Alfonsi et al. (2011).

First, each station was characterized using the method presented in 3.1, and then the data were filtered using the method presented in 3.2. Finally, the new climatological maps were generated and the differences, in comparison to the original ones, are discussed.

Figures 4.1.2 to 4.1.7 show the results of the application of the filtering technique to the network, applying an outlier definition of  $k=1.5$  ("mild outliers"). The same 2008 data set was considered for the same GISTM stations: BTNO (Figure 4.1.2), DMC0

(Figure 4.1.3), LYB0 (Figure 4.1.4), NSF01 (Figure 4.1.5), NYA1 (Figure 4.1.6), and NYA0 (Figure 4.1.7). In each figure, plot a) is the  $\sigma_{CCSTDDEV}$  input map for filtering, plot c) is the distribution of the  $\sigma_{CCSTDDEV}$  values extracted from the map with the cut-off at  $k=1.5$  indicated with a red line, and plot b) is the map of  $\sigma_{CCSTDDEV}$  after filtering.

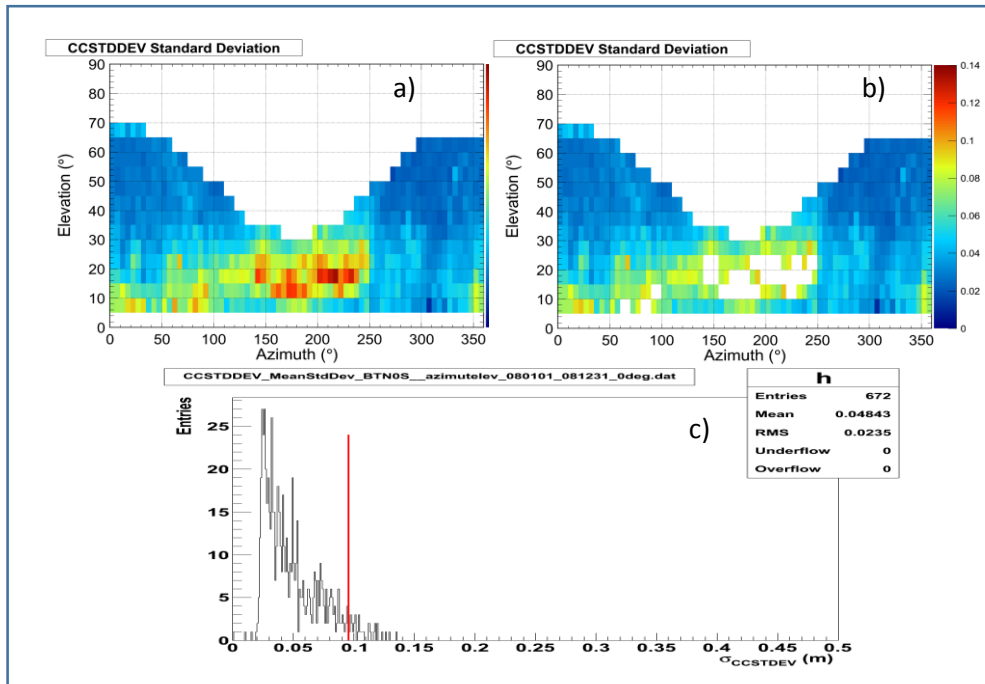


Figure 4.1.2. a) Map of the  $\sigma_{CCSTDDEV}$  in azimuth vs. elevation for the BTNO GISTM station on L1 frequency for 2008; b) corresponding map of the  $\sigma_{CCSTDDEV}$  filtered with  $k=1.5$ ; c) Distribution of the  $\sigma_{CCSTDDEV}$  of BTNO GISTM data for 2008, the red line indicates the value of the cut-off threshold for  $k=1.5$ .

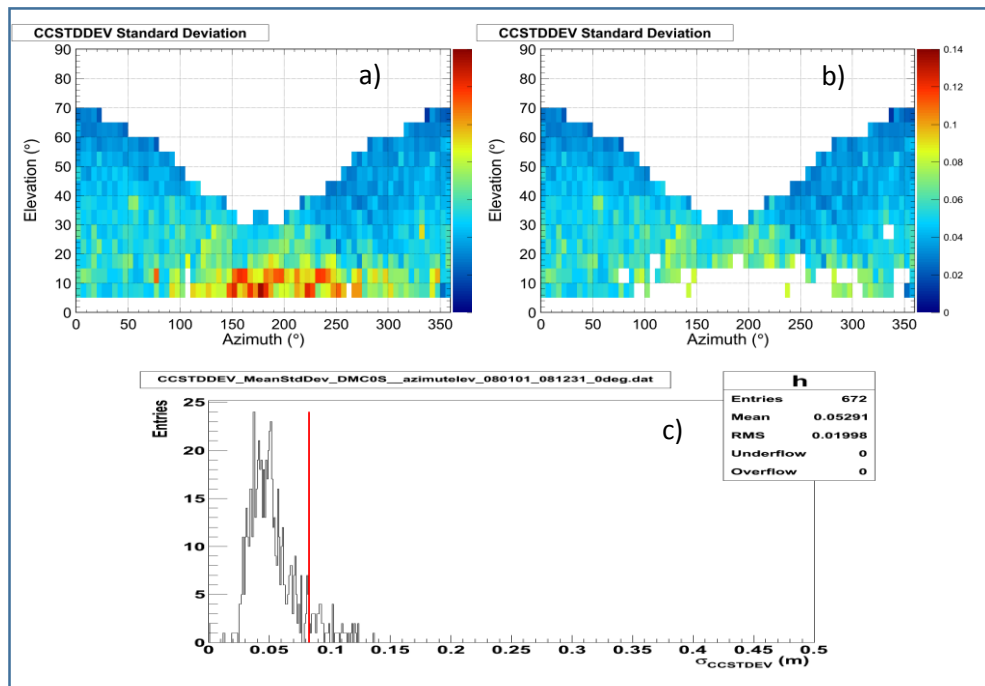


Figure 4.1.3. a) Map of the  $\sigma_{CCSTDDEV}$  in azimuth vs. elevation for the DMC0 GISTM station on L1 frequency for 2008; b) corresponding map of the  $\sigma_{CCSTDDEV}$  filtered with  $k=1.5$ ; c) Distribution of the  $\sigma_{CCSTDDEV}$  of DMC0 GISTM data for 2008, the red line indicates the value of the cut-off threshold for  $k=1.5$ .

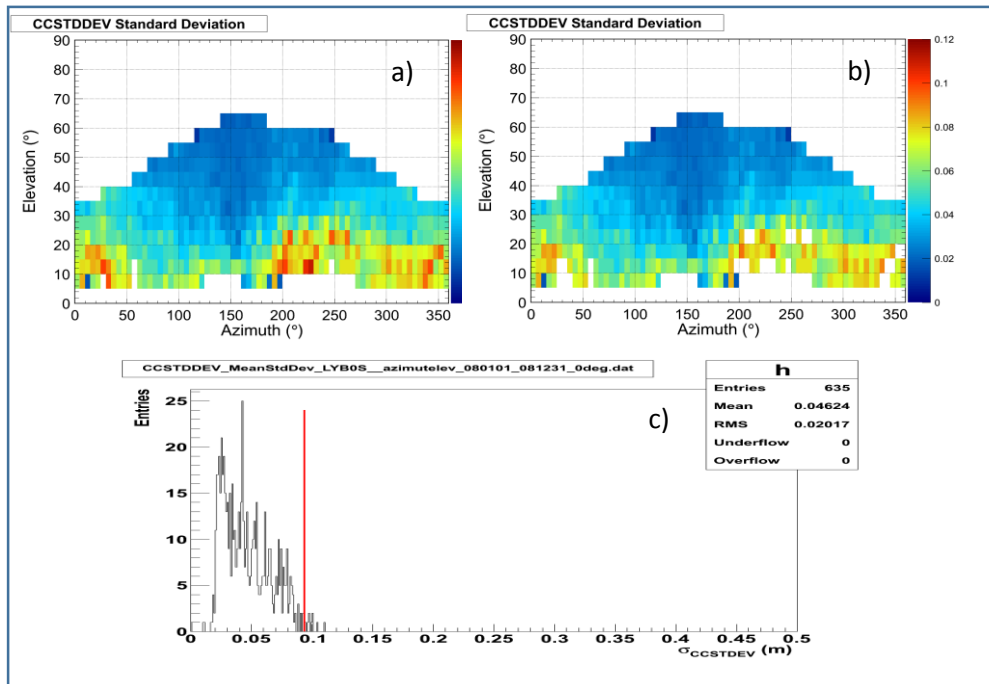


Figure 4.1.4. a) Map of the  $\sigma_{CCSTDDEV}$  in azimuth vs. elevation for the LYBO GISTM station on L1 frequency for 2008; b) corresponding map of the  $\sigma_{CCSTDDEV}$  filtered with  $k=1.5$ ; c) Distribution of the  $\sigma_{CCSTDDEV}$  of LYBO GISTM data for 2008, the red line indicates the value of the cut-off threshold for  $k=1.5$ .

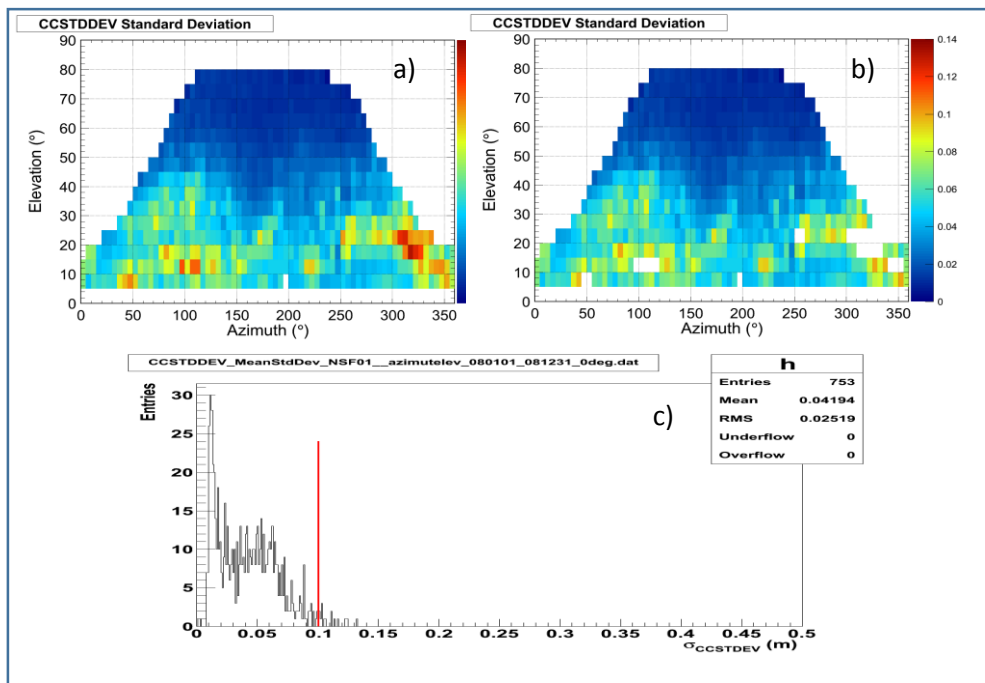


Figure 4.1.5. a) Map of the  $\sigma_{CCSTDDEV}$  in azimuth vs. elevation for the NSF01 GISTM station on L1 frequency for 2008; b) corresponding map of the  $\sigma_{CCSTDDEV}$  filtered with  $k=1.5$ ; c) Distribution of the  $\sigma_{CCSTDDEV}$  of NSF01 GISTM data for 2008, the red line indicates the value of the cut-off threshold for  $k=1.5$ .

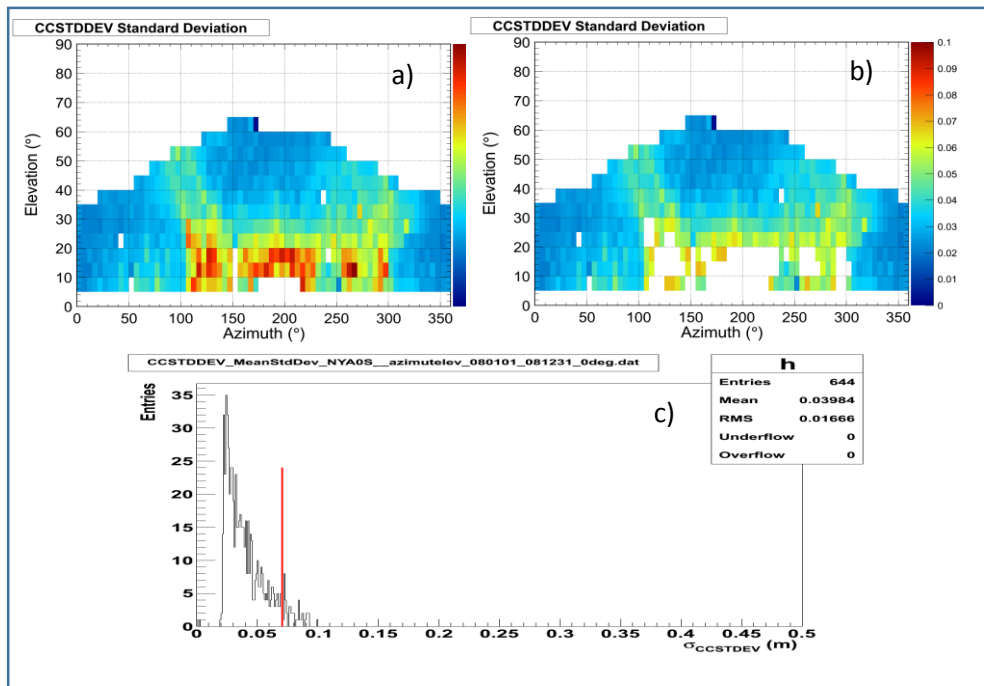


Figure 4.1.6. a) Map of the  $\sigma_{CCSTDDEV}$  in azimuth vs. elevation for the NYA0 GISTM station on L1 frequency for 2008; b) corresponding map of the  $\sigma_{CCSTDDEV}$  filtered with  $k=1.5$ ; c) Distribution of the  $\sigma_{CCSTDDEV}$  of NYA0 GISTM data for 2008, the red line indicates the value of the cut-off threshold for  $k=1.5$ .

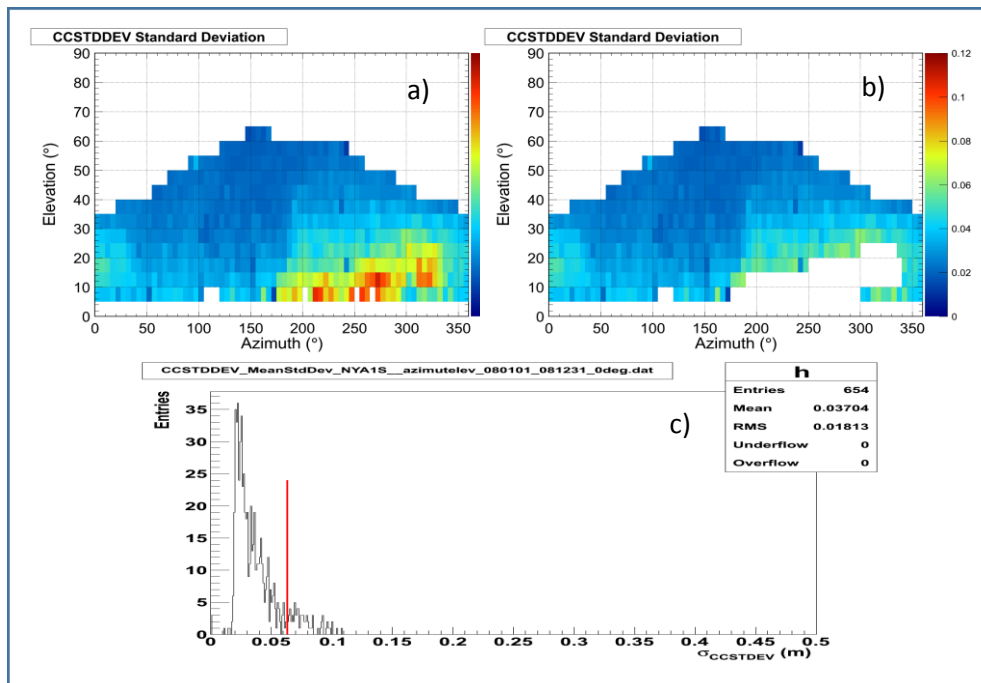


Figure 4.1.7. a) Map of the  $\sigma_{CCSTDDEV}$  in azimuth vs. elevation for the NYA1 GISTM station on L1 frequency for 2008; b) corresponding map of the  $\sigma_{CCSTDDEV}$  filtered with  $k=1.5$ ; c) Distribution of the  $\sigma_{CCSTDDEV}$  of NYA1 GISTM data for 2008, the red line indicates the value of the cut-off threshold for  $k=1.5$ .

Figure 4.1.8 shows the  $\sigma_{CCSTDEV}$  cut-off values (blue line), for each station in the network, with  $k=1.5$  and the percentage of filtered out bins (red line) relative to the total number of filled bins for each station.

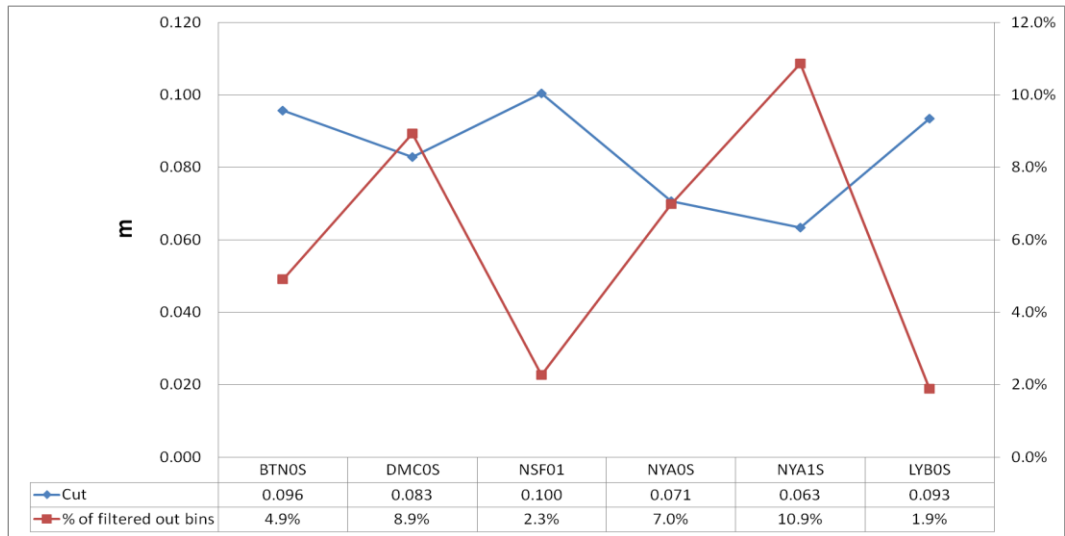


Figure 4.1.8.  $\sigma_{CCSTDEV}$  cut-off values (blue line) for  $k=1.5$ ; the percentage of filtered out bins (red line) relative to the total number of filled bins for each station.

Figure 4.1.9 shows the percentage of filtered out data obtained applying, respectively, the standard threshold of  $20^\circ$  on the elevation angle (red line) and the filtering technique (blue line) for each station. The percentage of discarded data is significantly reduced using the filtering technique, ranging from 1.9% to 7.7%.

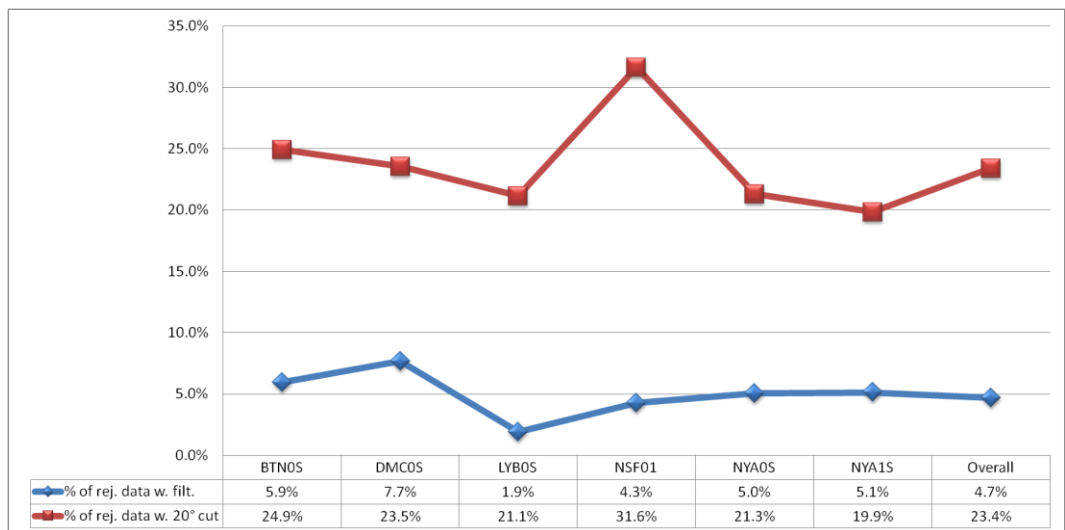


Figure 4.1.9. Percentage of discarded data applying the standard threshold of  $20^\circ$  on the elevation angle (red line); percentage of discarded data applying the filtering technique (blue line) for each station.

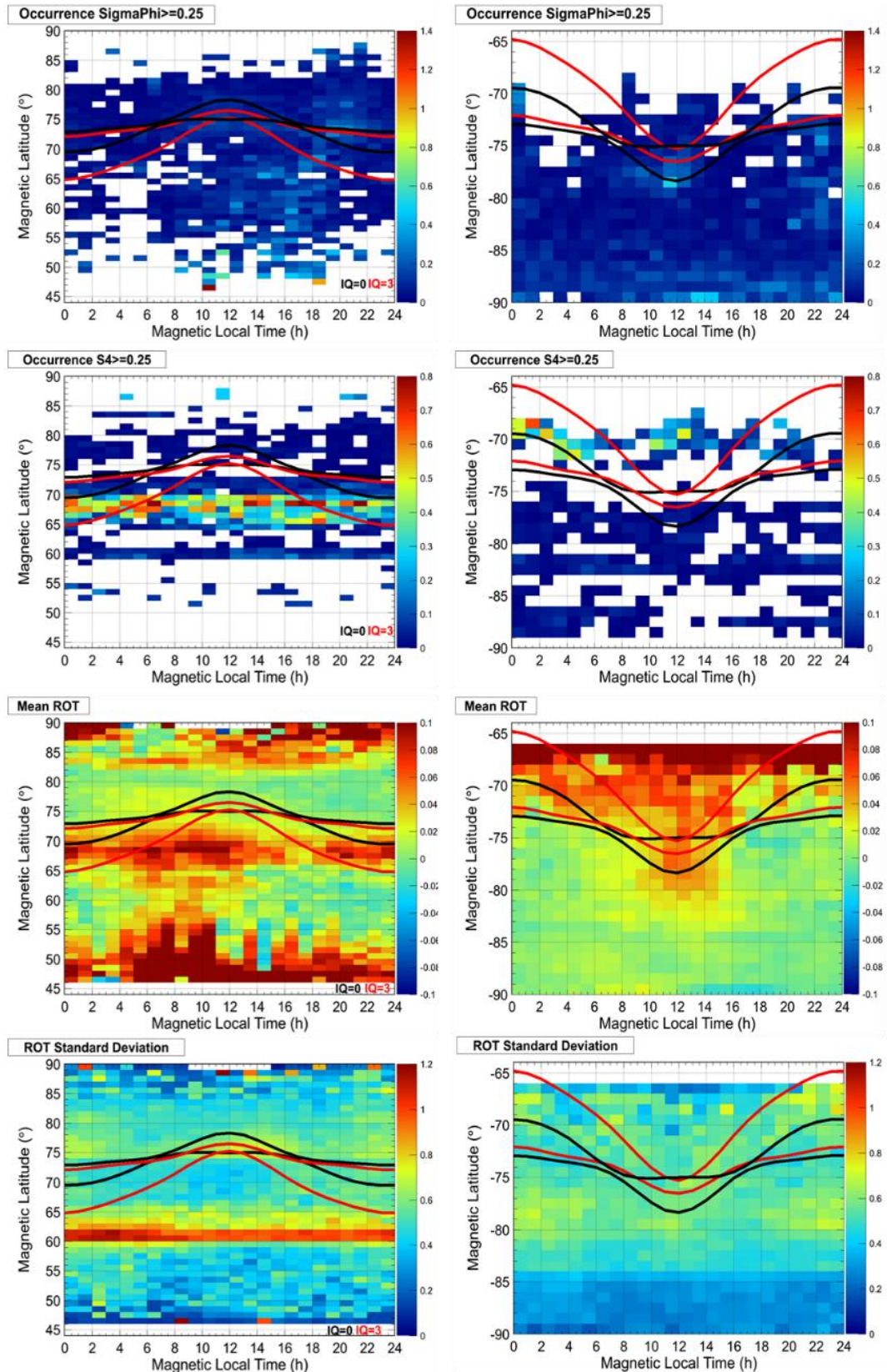


Figure 4.1.10. (top to bottom) Filtered maps of: percentage occurrence of  $\sigma_{\phi}$ , percentage occurrence of the S4, ROT and ROT standard deviation, in geomagnetic coordinates. Northern Hemisphere (left) and Southern Hemisphere (right). Black and red curves reproduce the Feldstein auroral ovals for IQ=0 and IQ=3, respectively.

Figure 4.1.10 shows the same maps as figure 4.1.1 obtained after the filtering technique was applied to each station. Filtering extends the field of view of the network and confirms the conclusions highlighted in Alfonsi et al (2011), in particular:

- In the cusp sector phase scintillation occurrence is more evident than amplitude scintillation.
- The occurrence of amplitude scintillation is generally lower than phase scintillation.
- Enhanced standard deviation of the ROT often corresponds with enhancements in both phase and amplitude scintillation, showing that a high variability of TEC is a good indicator of the presence of TEC gradients causing scintillation.

#### **4.2 APPLICATION ON THE CIGALA/CALIBRA NETWORK**

The CALIBRA project<sup>19</sup> built on the previous CIGALA project<sup>20</sup>, exploiting a combined network of specialized receivers installed for the two projects, the so-called CIGALA/CALIBRA network, which is equipped with Septentrio PolaRxS<sup>21</sup> receivers. The PolaRxS is a multi-frequency, multi-constellation receiver capable of simultaneously tracking GPS L1CA, L1P, L2C, L2P, L5; GLONASS L1CA, L2CA; GALILEO E1, E5a, E5b, E5AltBoc; and COMPASS B1, B2; SBAS L1 (Bougard et al., 2011). Sampling at 50 Hz, the receiver gives the following main output parameters:

- $\sigma_{\phi}$  phase scintillation index calculated over different time intervals (1, 3, 10, 30, 60 seconds);
- S4 amplitude scintillation index calculated over 60 seconds;
- TEC (Total Electron Content) and ROT (Rate of TEC change) every 15 seconds,
- Spectral parameters: spectral slope of the phase Power Spectral Density ( $p$ ) in the 0.1 to 25Hz range and the spectral strength of the phase Power Spectral Density ( $T$ ) at 1 Hz (60 seconds);
- Standard Deviation of the Code Carrier (CCSTDDEV - 60 seconds);
- SNR (60 seconds);
- Locktime (60 seconds).

All these quantities (except TEC and ROT) are calculated for all available signal frequencies transmitted by the satellites and along the slant path connecting receiver and satellite. TEC values are obtained by pseudorange measurements only. GPS-TEC measurement is based on the L2-P and L1-P pseudoranges; GLONASS-TEC is based on the L1-C/A and L2-C/A pseudoranges, and Galileo-TEC is based on the L1BC and E5a. ROT is computed from the carrier phase measurements only, and hence is much more accurate than TEC.

The data used in this analysis was acquired by the CIGALA/CALIBRA network of PolaRxS receivers during the whole year of 2012 (Spogli et al., 2014). Table 4.2.1 summarizes all the CIGALA/CALIBRA stations available during the period considered, with their corresponding identifiers, location and geographic coordinates.

---

<sup>19</sup> <http://www.calibra-ionsphere.net/>

<sup>20</sup> <http://www.gsa.europa.eu/concept-ionspheric-scintillation-mitigation-professional-gnss-latin-america>

<sup>21</sup> <http://www.septentrio.com/products/receivers/polarxs>

Name	Location	Lat (°N)	Lon (°E)
MANA	Manaus	-3.12	-60.01
PALM	Palmas	-10.20	-48.31
POAL	Porto Alegre	-30.07	-51.12
PRU1	Presidente Prudente	-22.12	-51.41
PRU2	Presidente Prudente	-22.12	-51.41
SJCI	Sao Jose dos Campos	-23.21	-45.86
SJCU	Sao Jose dos Campos	-23.21	-45.96

Table 4.2.1. List of the CIGALA/CALIBRA network receivers used in the analysis.

Figure 4.2.1 shows the impact of applying a standard 20° elevation cut-off in terms of percentage of data coverage of the network, normalized to the total number of data points (GPS and GLONASS) available in 2012. Figure 4.2.1(a) shows the coverage obtained by applying no threshold on the elevation angle, while Figure 4.2.1(b) shows the coverage obtained with a threshold of 20°. Both maps and the geomagnetic equator (red line) are projected to a height of 350 km, this being representative of the ionospheric F2-layer peak height.

The cut-off significantly reduces the capability of the network to depict the ionosphere northward of the geomagnetic equator and above the Atlantic Ocean, east of Brazil. The filtering method based on outliers is as follows. For each station in the network, a map of azimuth vs. elevation of the standard deviation of the CCSTDDEV ( $\sigma_{CCSTDDEV}$ ) is produced using the GBSC technique. The bin size adopted is 5°x5° and both GPS and GLONASS L1 frequency observations were considered in order to maximize the number of data points in each bin. The CCSTDDEV was chosen since it is a good indicator of the multipath activity experienced by the receiver antenna (Van Dierendonck et al., 1993, Romano et al., 2013) and its standard deviation ( $\sigma_{CCSTDDEV}$ ) identifies the bin in which it exhibits high variability.

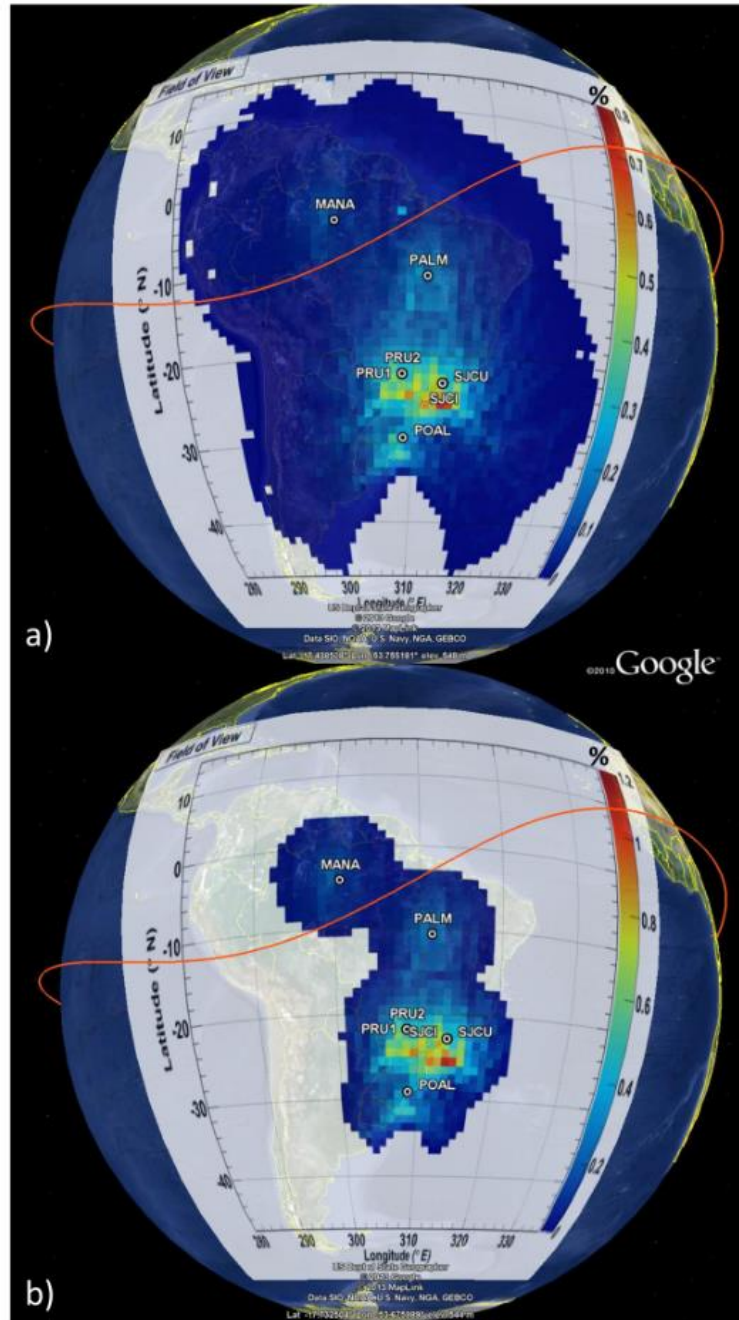


Figure 4.2.1. Percentage of data coverage of the CIGALA/CALIBRA network considering the full dataset for 2012, obtained respectively applying no threshold on the elevation angle (a) and with a threshold of  $20^\circ$  (b). Both maps and the geomagnetic equator (red line) are projected to a height of 350 km.

As an example, Figure 4.2.2(a) shows the map of  $\sigma_{CCSTDDEV}$  obtained for the MANA station in 2012. As introduced and described in section 3.2 the filtering method is applied to the MANA data by using the value  $k=1.5$ .

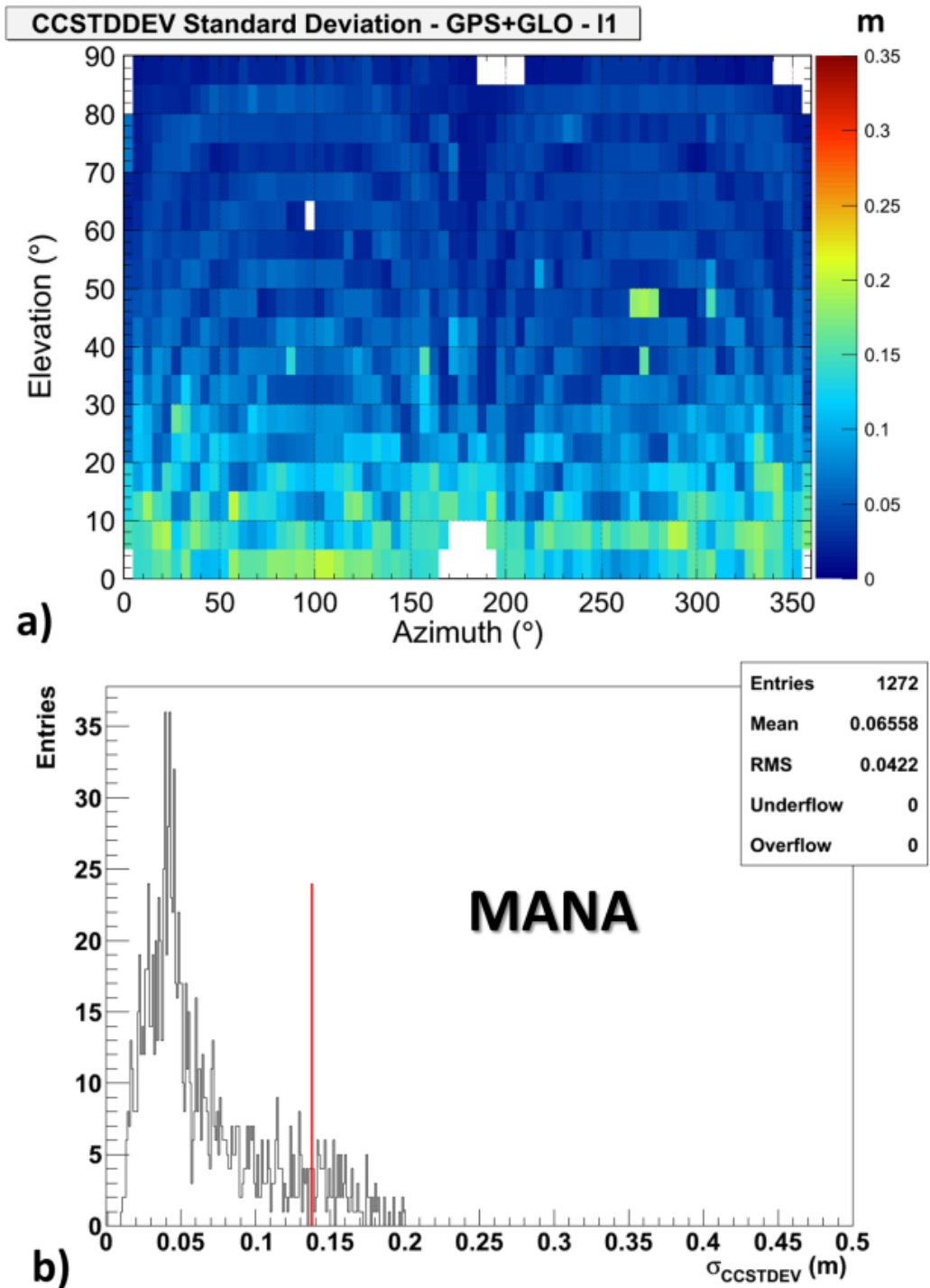
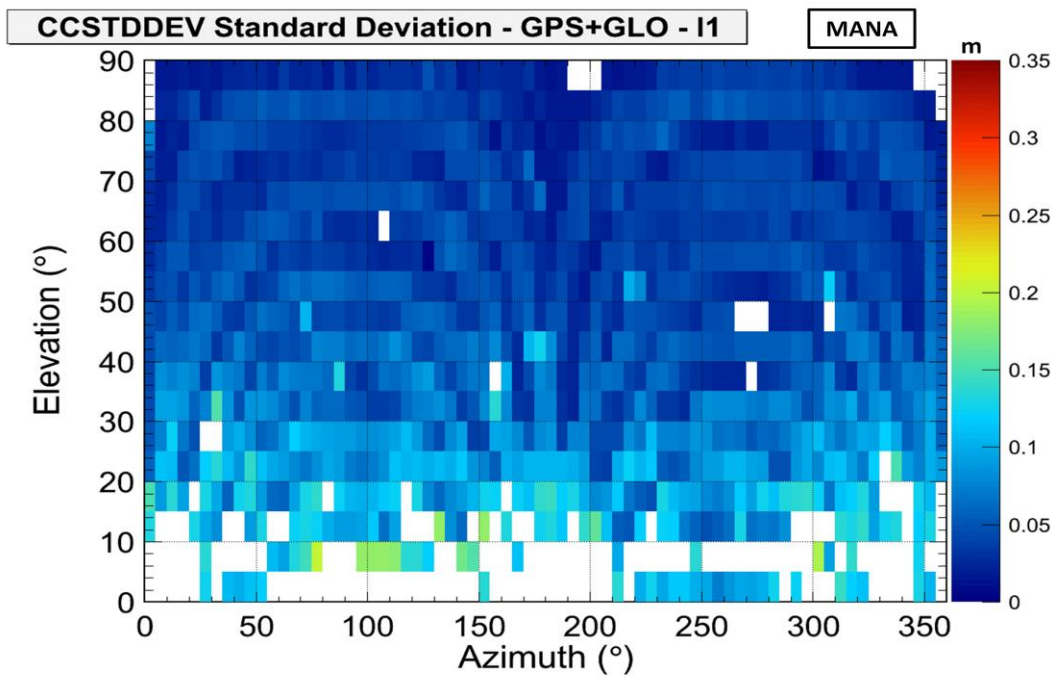


Figure 4.2.2. (a) Map of the  $\sigma_{CCSTDDEV}$  in azimuth vs. elevation for MANA (GPS+GLONASS data on L1 frequency) for 2012. (b) Corresponding distribution of the  $\sigma_{CCSTDDEV}$ . The red line indicates the cut-off for mild outliers.

The red line in Figure 4.2.2(b) indicates the cut-off for the mild outliers (1.5 IQR). The bins corresponding to values of  $\sigma_{CCSTDDEV}$  greater than  $Q_3+1.5$  IQR, i.e. the mild outliers, are filtered out and new analyses can be performed. As expected the method is able to remove the contribution deriving mostly from low elevation angles, but it also



maintains some “not noisy” bins. The results of the filtering method on the 2012 MANA data are shown in Figure 4.2.3

Figure 4.2.3. Filtered data map of the  $\sigma_{CCSTDDEV}$  in azimuth vs. elevation for MANA (GPS+GLONASS data on L1 frequency) for 2012.

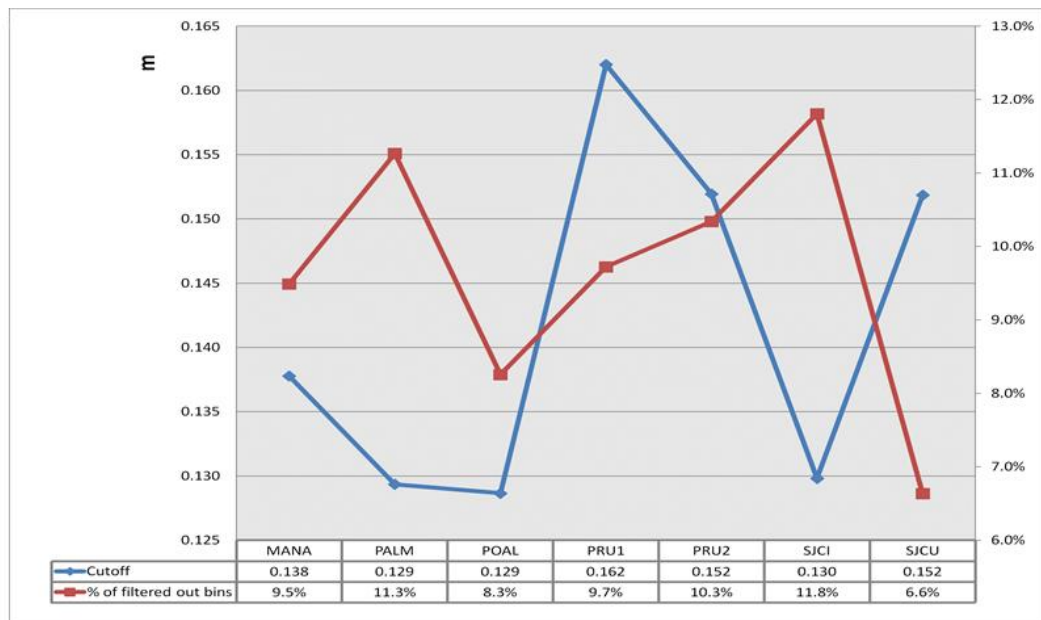


Figure 4.2.4.  $\sigma_{CCSTDDEV}$  cut-off values (blue line) for  $k=1.5$ ; the percentage of filtered out bins (red line) relative to the total number of filled bins for each station in the CIGALA/CALIBRA network.

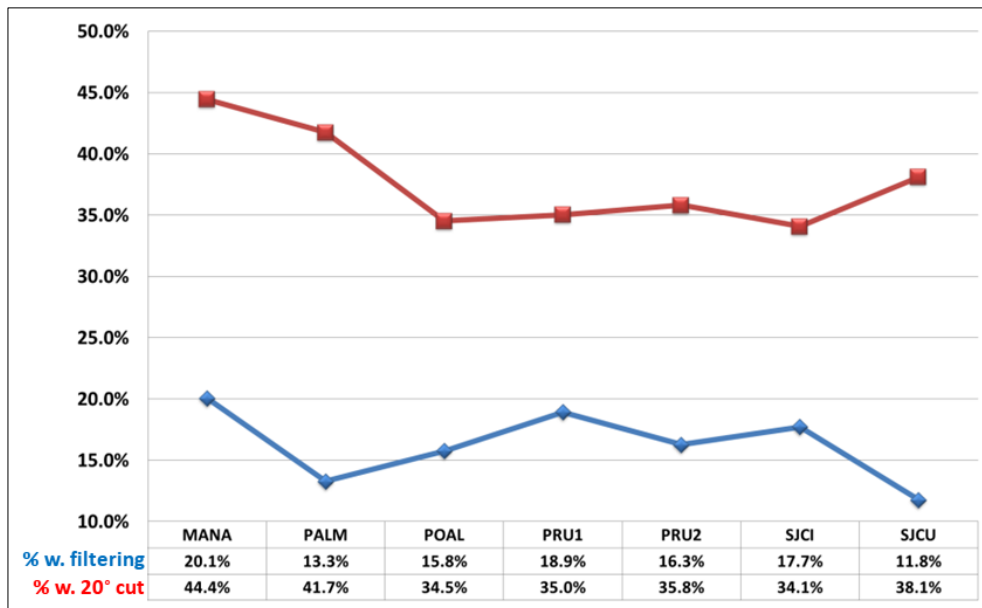


Figure 4.2.5. Percentage of filtered out data applying a cut-off elevation angle of 20° (red line) and percentage of filtered out data applying the filtering technique (blue line) for each station in the CIGALA/CALIBRA network.

When the filtering technique is applied to the entire CIGALA/CALIBRA network, the number of rejected bins ranges between 6.6% and 11.8% (figure 4.2.4), reducing the bins filtered out compared to the application of the standard elevation angle cut-off of 20°. This approach limits the data loss, the number of rejected observations ranges between 11.8% and 20.1%, reducing data loss compared to the application of the standard elevation angle cut-off of 20°, which ranges from 34.1% to 44.4%, as shown in figure 4.2.5. The reduction in data loss, averaged among all the stations, is of a factor of about 2.4.

Similarly to Figure 4.2.1, the percentage of data coverage of the CIGALA/CALIBRA network after the filtering procedure is shown in Figure 4.2.6, which together with Figure 4.2.1(b) reveal how this filtering provides cover of additional ionospheric sectors of interest, where it enables to characterize the pattern of ionospheric variability.

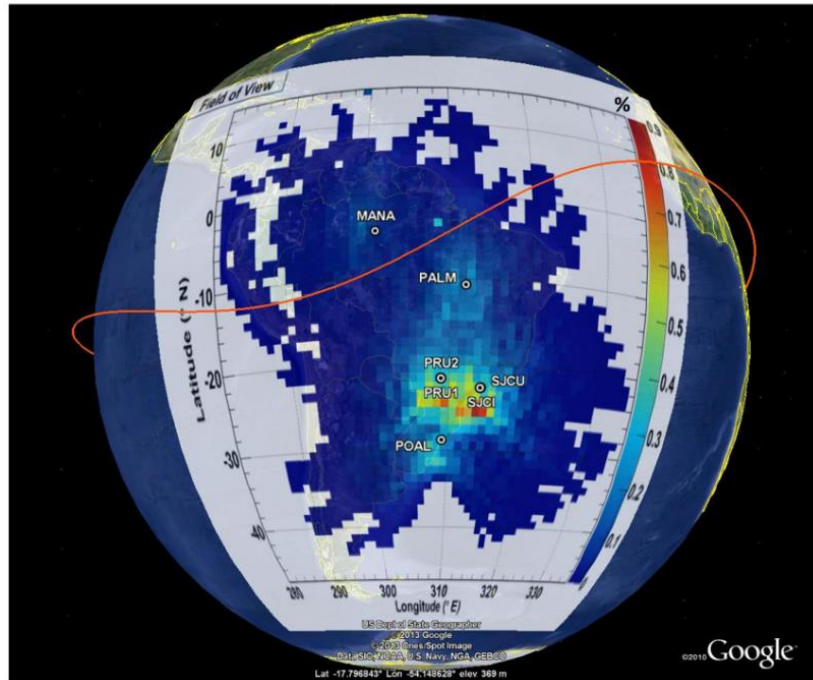


Figure 4.2.6. Percentage of data coverage of the CIGALA network receivers considering the full dataset for 2012 after the filtering procedure. The map and the geomagnetic equator (red line) are projected to a height of 350 km.

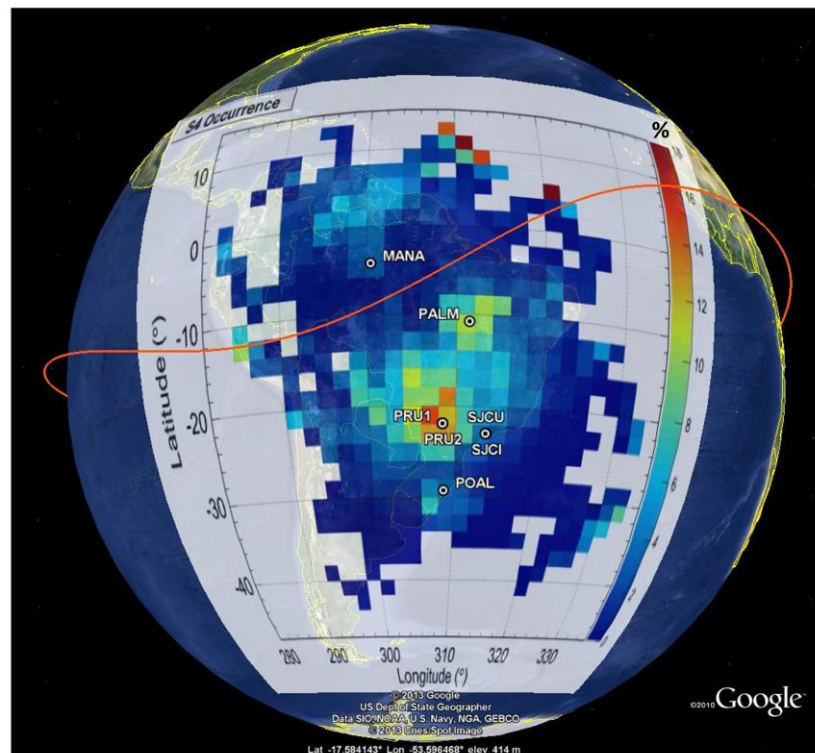


Figure 4.2.7. Map of percentage of occurrence of S4 above 0.25, in geographic coordinates (GPS + GLONASS, L1 frequency) in the UT range 22-04 UT.

Figure 4.2.7 shows the map of the percentage of occurrence of the amplitude scintillation index S4 values above 0.25, in geographic coordinates. The threshold of 0.25 allows characterization of the areas of the ionosphere in which scintillation affects GNSS signals from moderately to strongly. Only data acquired in the UT range between

22 and 04 UT were considered, in order to focus on the post sunset hours, in which most of the scintillation events occurs (see for e.g. Alfonsi et al., 2010). As seen in the map of Figure 4.2.7, the enlarged field of view covered by the CIGALA/CALIBRA network introduced by the filtering algorithm makes it possible to identify the increased occurrence along the northern crest of the Equatorial Ionospheric Anomaly (EIA) (Kelley et al., 1989), covered mainly by the observations from the station MANA. This enhancement affects geographic latitudes greater than 0°N and along a band nearly parallel to the geomagnetic equator (red line), where an occurrence peak of about 6% is reached. Conversely, the southern crest of the EIA is well covered by data and the effect of filtering in terms of amplitude scintillation occurrence is visible along the band of enhanced scintillation, nearly parallel to the geomagnetic equator (red line), reaching a peak value of about 16%. These observations reveal that the regions most affected are in the latitudinal range between 30°S and 10°N, and along longitudes between 300°E and 330°E, in particular over São Paulo and Tocantins States (due to the presence of the EIA southern crest), and northward of MANA (due to the presence of the EIA northern crest). The enhancement over POAL is also meaningful and possibly due to the presence of particle precipitation along the borders of the South Atlantic Magnetic Anomaly (SAMA) (Spogli et al., 2013). The SAMA is another source of ionospheric turbulence leading to scintillation, since it disturbs thermospheric circulation in the atmosphere and alters the rates of production and recombination of ionized species, mainly during geomagnetic storms (Abdu et al., 2005).

### **4.3 TECHNIQUE VALIDATION THROUGH APPLICATION WITH SIMULATED DATA**

In this section a simulated scenario was used in order to validate and eventually refine the newly developed filtering technique. In the framework of the PhD several simulated data have been produced in order to build a consistent GNSS data set of observations affected by known sources of multipath and scintillation. The Spirent GSS8000 GNSS signal simulator, which is able to provide RF outputs for GPS and Galileo signals, is available at the NGI GNSS laboratory. By connecting a GISTM receiver to the antenna output of the simulator, it is possible to acquire GNSS data absolutely similar to the real stations but with well-known user-defined multipath/scintillation scenarios. Such kind of simulated data make easy the application of the station characterization and filtering methods, specifically developed for data having the same format. Moreover specific tools included in the simulator seemed to give the opportunity to create ad hoc multipath and scintillation scenarios.

Figure 4.3.1 shows the logical flow of the simulation process performed during the PhD. Based on this logical diagram 4 steps can be identified.

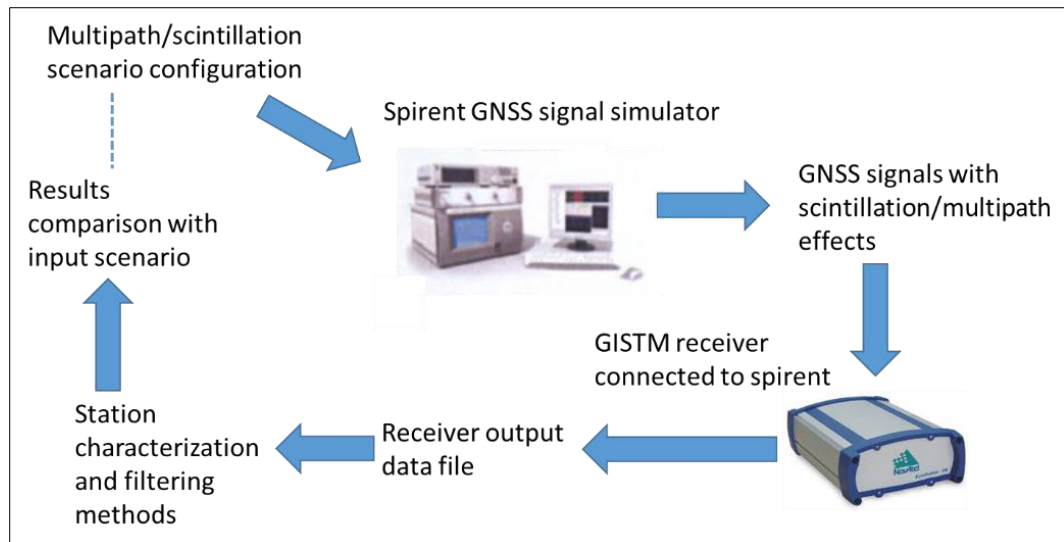


Figure 4.3.1. Logic flow diagram followed in simulation to apply the station characterization and filtering methods to simulated data.

- **Step 1** is about creating a scenario of multipath and ionospheric scintillation. Three or four different configurations for the same scenario are typically set up: a) multipath and scintillation together, b) multipath without scintillation, c) scintillation without multipath and d) neither scintillation nor multipath. A configuration at a time is set up in the simulator tools including the choice of the site of the receiving station and the data acquisition period of interest, typically one full day. When the first configuration is ready then it runs in step 2. The next configuration is set up after the previous acquisition is concluded in step 2. Scintillation time series can be also generated externally, either from a model or from open sky data.
- **Step 2** concerns the connection of the GISTM receiver to the simulator and running the GISTM data acquisition for one configuration for the time of the selected scenario. Acquisition is performed in real time. Data files are then archived and a new run with a new configuration is performed. Step1 and Step 2 are performed in loop till all the configurations of a single scenario are concluded and all the data files are stored.
- **Step 3** is related to the application of the station characterization and filtering method to the data obtained with the simulation. Methods are applied as described in paragraphs 3.1 and 3.2 for all the configurations of a single scenario. A series of scintillation and CCSTDDEV maps for the different configurations simulated data are the output of this step.
- **Step 4** focuses on the analysis of the results obtained in step 3, comparing them with the input scenario set up at step 1. This step is focalised on the validation of the technique and on the tuning of new configuration scenario.

Among a number of experiments, one specific case of application of the filtering technique to a simulated scenario was used in an attempt to validate the method (Scenario A).

### Scenario A

For use with the Spirent simulator, scintillation time series can be generated externally, either from a model or from open sky data (see e.g. the simulation procedure



difficult to track the signal. As presented in Elmas (2013)  $S4=0.3$  and  $\text{Tau}0=1.9\text{s}$  refers to weak scintillation and  $S4=0.9$  and  $\text{Tau}0=0.1\text{s}$  to strong scintillation. The choice made in our scenario deals a moderate scintillation case, which is the best practice in our case as the simulated station is located at mid-latitude.

Table 4.3.1 shows the features of the simulation of Scenario A. In this case, the scenario has been configured using the Spirent's tool for what concerns the multipath effects, while for the scintillation environment the external source given by the .ucd file has been implemented, as previously discussed.

<b>Station</b>	NSF6 (Nottingham)
<b>Coordinates</b>	52°N; 1°E
<b>Date of acquisition</b>	16 March 2008
<b>Multipath</b> (Az: 0°, 360°; Elev: 0°, 90°)	Az 220° – 250°, Elev 0° – 50° (building) Az 175° – 185°, Elev 0° – 40° (pillar)
<b>Scintillation</b>	$S4= 0.4$ , $\text{Tau}0=0,5$ , on the PRN 17 for the entire day.
<b>Configurations</b>	First day: Neither scintillation nor multipath Second day: Multipath without scintillation Third day: Scintillation without multipath Fourth day: Multipath and scintillation
<b>Tropospheric delay</b>	Disabled
<b>Ionospheric delay</b>	Disabled

Table 4.3.1. Simulation features of Scenario A.

This proposed configuration has been set up in the simulator. Figure 4.3.3 shows the screenshot of the multipath simulator tool in the Spirent GSS8000, where the proposed scenario has been set up.

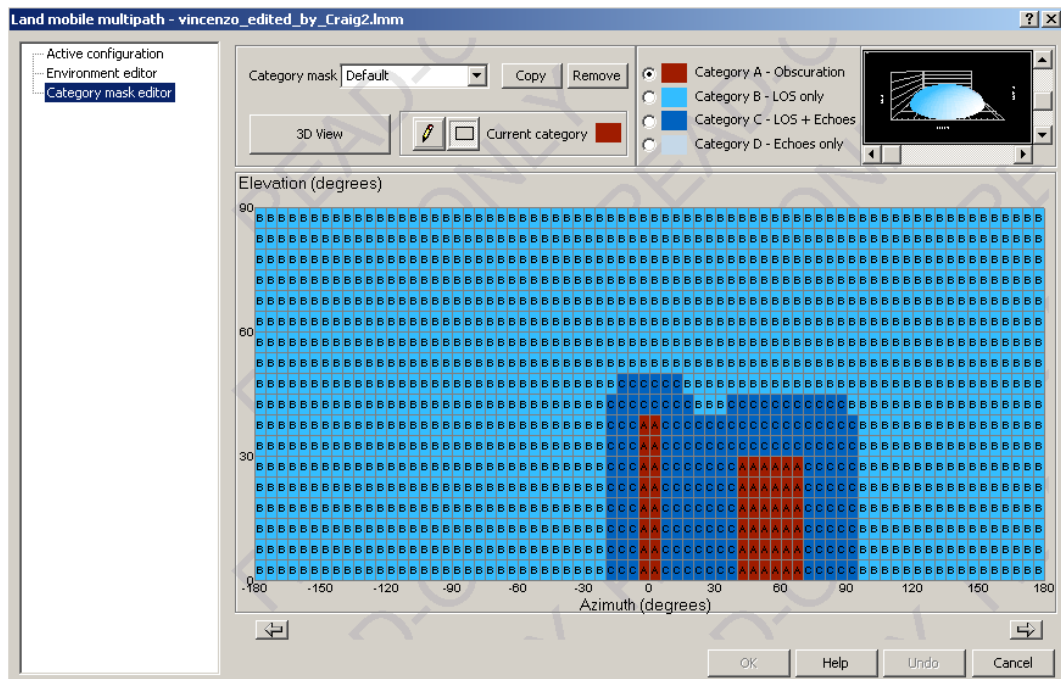


Figure 4.3.3. Spirent multipath tool user interface set up for the simulation of the Scenario A.

The Simulator uses four categories of signal, determined by signal arrival angles as described in the SimGEN software user manual (2009).

- *Category A - Obscuration: Simulator does not simulate satellites arriving at these segments, so this category represents a visibility mask.*
- *Category B – LOS only: Simulator simulates satellites arriving at these segments with a line-of-sight (LOS) signal only. The LOS signals represent generally unobstructed signals, not subject to reflections.*
- *Category C – LOS + Echoes: Simulator simulates satellites arriving at these segments as LOS plus multipaths, depending on the number of available channels. These signals represent unobstructed signals, subject to reflections. Satellites within category C suffer Rician fading on the LOS channel and modified Rayleigh fading on the multipaths.*
- *Category D – Echoes Only: Simulator simulates satellites arriving at these segments as multipaths only, depending upon the number of available channels. These signals represent obstructed LOS signals, present as reflections only. Satellites within category D suffer modified Rayleigh fading on the echoes.*

Figure 4.3.3 shows the Spirent’s multipath tool user interface where in an Azimuth vs. Elevation map the configuration of multipath for the Scenario A has been set up with 3 different categories: red bins represent Category A, dark blue corresponds to Category C and blue bins are the Category B ones.

The first configuration, where there is neither scintillation nor multipath effects, was run for the first day of the simulation. The result of the corresponding data analysis confirms that all the satellites in view from Nottingham have been acquired and there is no evidence of disturbances. Figure 4.3.4 shows the time profiles of S4 for all satellites during the day of acquisition, each colour corresponds to a satellite.

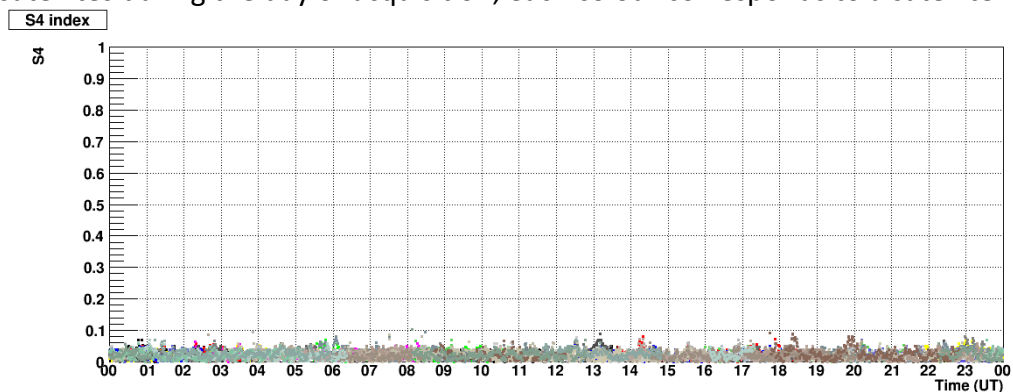


Figure 4.3.4. Time profiles of S4 for all satellites during the first day of acquisition. The simulated configuration is set up without scintillation and multipath effects. Each colour corresponds to a different satellite.

The configuration including the multipath effects and no scintillation has been set up in the simulator for the second day of acquisition. The acquisition of the GISTM receiver, connected with the Spirent simulator, worked during the full day with this configuration. Figure 4.3.5 shows the S4 time profile for all satellites in view from the site of Nottingham, each colour corresponds to a different PRN.

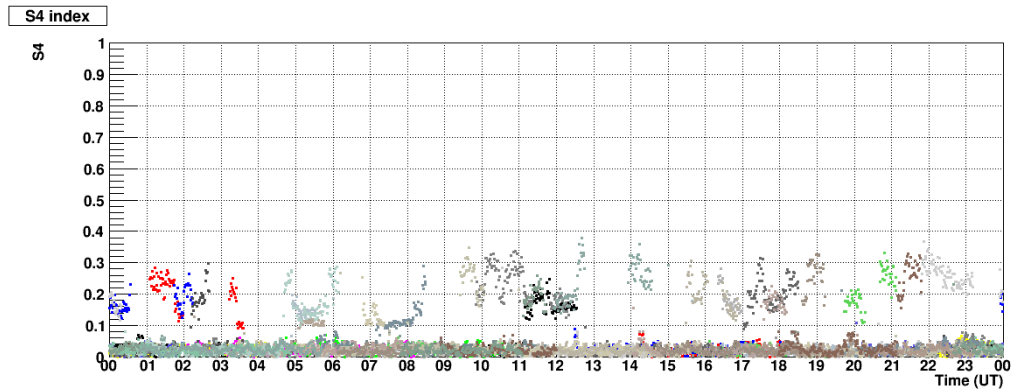


Figure 4.3.5. Time profile of  $S_4$  for all satellites during the second day of acquisition. The simulated configuration comprises multipath effects.

For the third day of simulation, the Spirent simulator was set up to include the scintillation effects only on PRN 17, modelled using the Cornell Scintillation Model external tool. The result of this day of acquisition is shown in Figure 4.3.6. The Figure shows the time profiles of  $S_4$  for all satellites during the third day of acquisition, the  $S_4$  pattern of PRN 17 is evident (light grey trace).

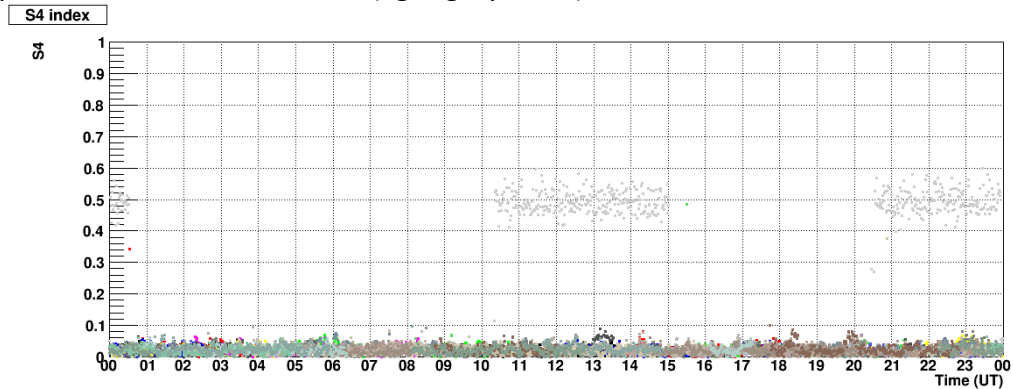


Figure 4.3.6. Time profile of  $S_4$  for all satellites during the third day of acquisition. The simulated configuration comprises the scintillation effects on PRN 17 (light grey trace).

Figure 4.3.7 shows, for the data set with scintillation only as input, the occurrence of  $S_4$  larger than 0.1 in Azimuth vs. Elevation. The scintillation effect on PRN 17 is clear and properly captured. The adopted bin size is  $10^\circ$  azimuth x  $5^\circ$  elevation, as it is a good compromise between a meaningful fragmentation of the map and the need to have a reasonable statistics in each bin.

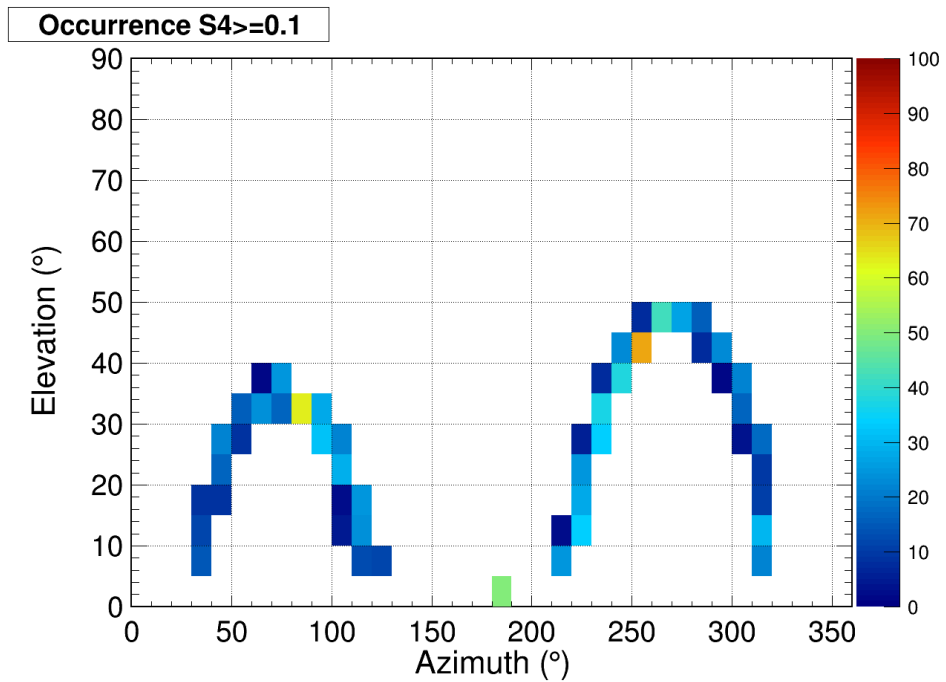


Figure 4.3.7. Azimuth–elevation map of the percentage of occurrence of amplitude scintillation index  $S_4$  above 0.1 for the third day of acquisition of simulated data.

The configuration including the scintillation and multipath effects has been set up in the simulator for the fourth day of acquisition. Figure 4.3.8 shows the time profiles of  $S_4$  for all satellites during the fourth day of acquisition. The figure clearly shows the superposition of multipath and scintillation effects, as a mixture of the patterns shown in figures 4.3.5 and 4.3.6.

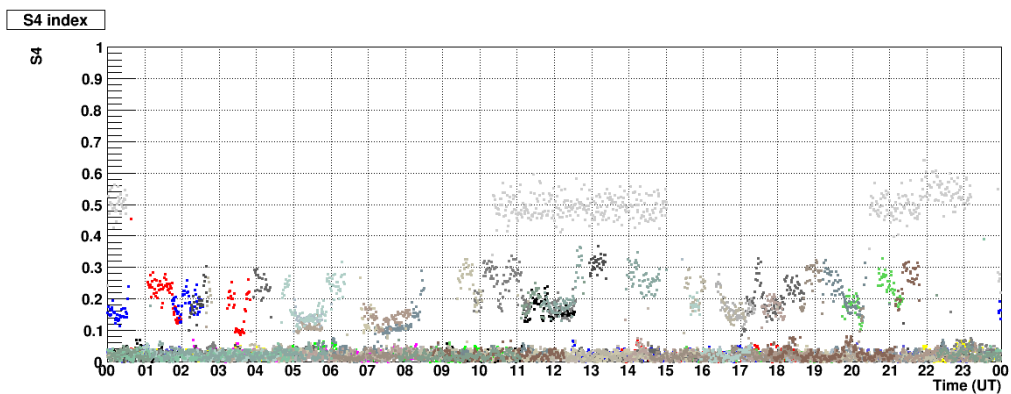


Figure 4.3.8 Time profiles of  $S_4$  for all satellites during the fourth day of acquisition. The simulated configuration comprises scintillation and multipath effects.

Figure 4.3.9 shows, for the scintillation plus multipath scenario, the occurrence of the  $S_4$  greater than 0.1 in Azimuth vs. Elevation. The adopted bin size is again  $10^\circ \times 5^\circ$ . Similarly to figure 4.3.8, also in the amplitude occurrence map the overlapping between the scintillation on PRN 17 and the multipath effects is evident. The multipath effect is located exactly in the azimuth range where the multipath environment has been set in the simulator (see Figure 4.3.3 and Table 4.3.1).

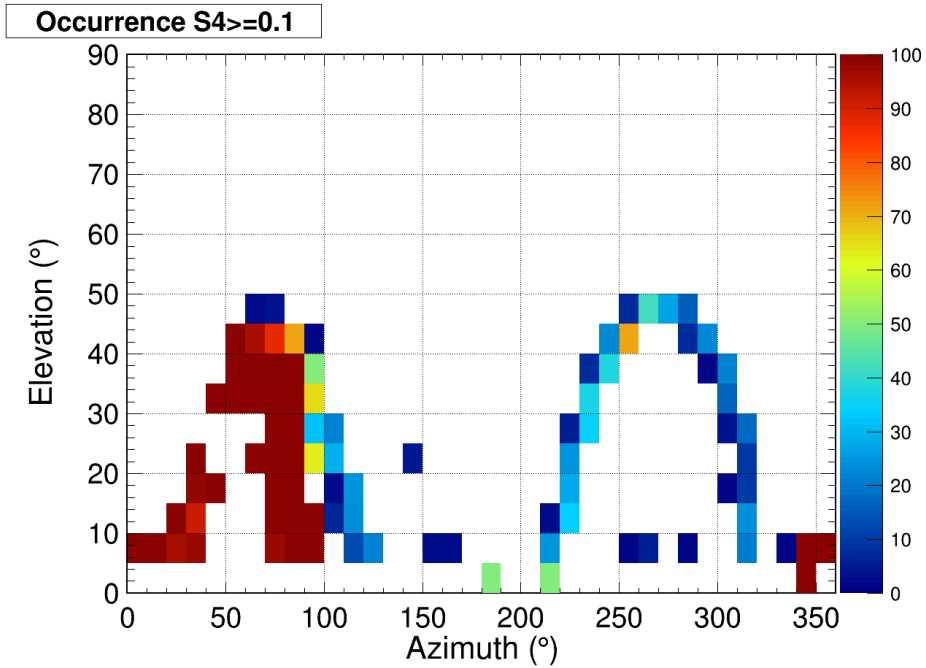


Figure 4.3.9. Azimuth–elevation map of the percentage of occurrence of amplitude scintillation index  $S_4$  above 0.1 for the fourth day of acquisition. Simulation comprises scintillation on PRN 17 and multipath effects.

Finally, the data set acquired during the fourth simulation day was filtered using the method presented in paragraph 3.2. Remembering that the filtering method is based upon the identification of the outliers in the  $\sigma_{CCSTDDEV}$  map, Figure 4.3.10 shows the map of  $\sigma_{CCSTDDEV}$  obtained for the last simulation configuration on 16 March 2008. The bin size adopted is again  $10^\circ \times 5^\circ$  and only observations on GPS L1 frequency have been considered.

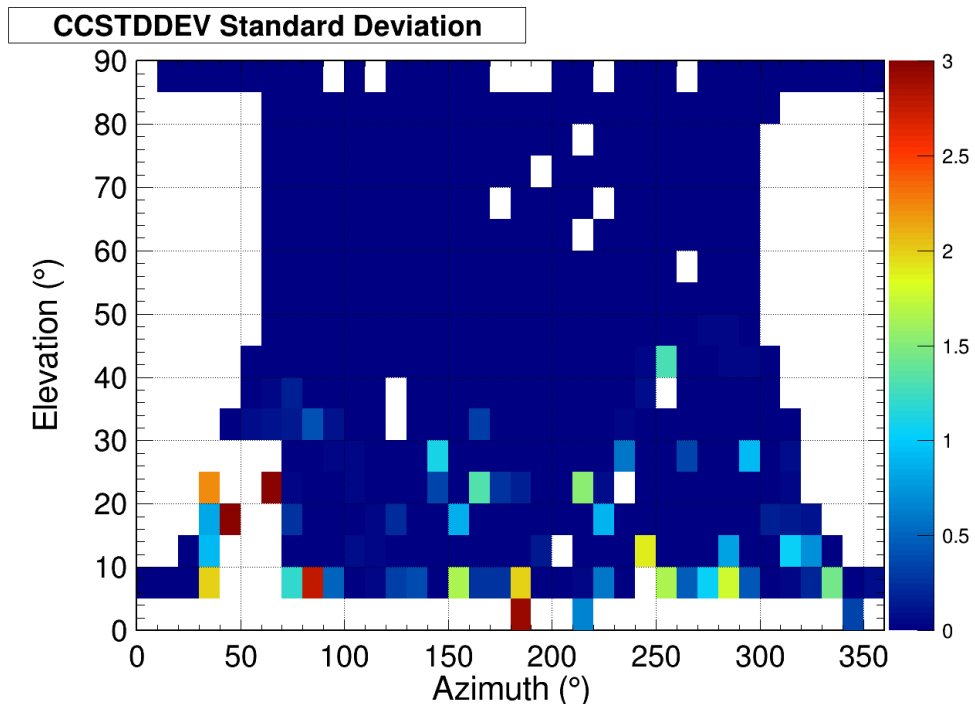


Figure 4.3.10. Map of the  $\sigma_{CCSTDDEV}$  in azimuth vs. elevation for the simulation of Scenario A for the Nottingham station on L1 frequency for the fourth day of simulation. Simulation comprises scintillation on PRN 17 and multipath effects.

Each value of  $\sigma_{CCSTDDEV}$  is then used to create the corresponding histogram, shown in Figure 4.3.11. The red line corresponds to the cut-off threshold evaluated for  $k=1.5$ , mild outliers. The bins corresponding to values of  $\sigma_{CCSTDDEV}$  greater than  $Q_3+1.5$  IQR, i.e. the mild outliers, are filtered out. In this case the number of bins filtered out is 86, which corresponds to 28% of the total available data.

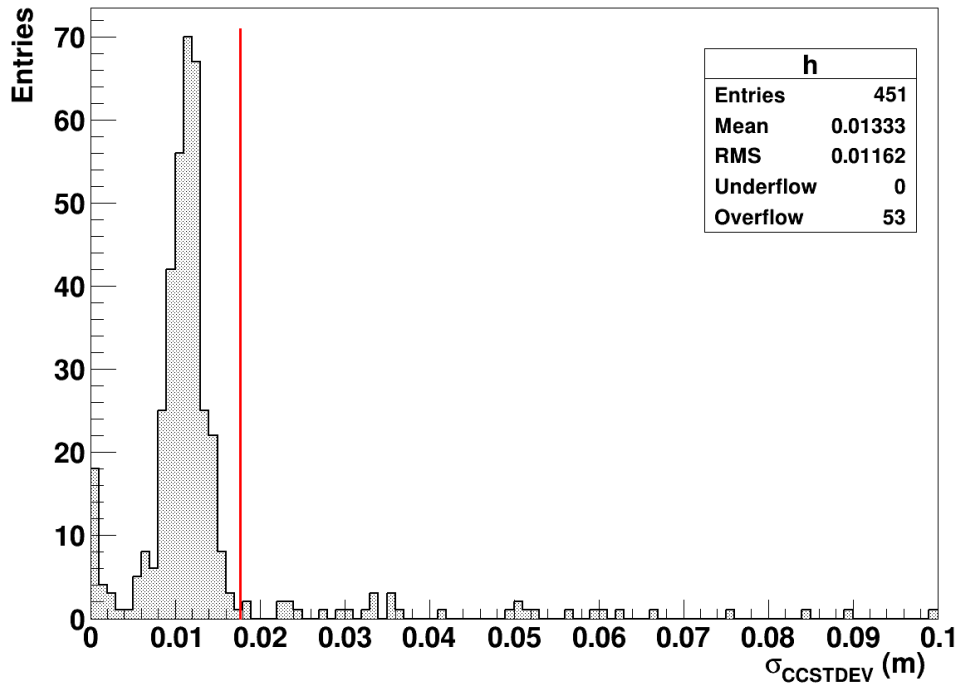


Figure 4.3.11. Distribution of the  $\sigma_{CCSTDDEV}$  corresponding to the fourth day of data acquisition simulation. The red line indicates the cut-off threshold for  $k=1.5$ .

The results of the filtering method on the data of the fourth day are shown in figures 4.3.12 and 4.3.13. In particular, Figure 4.3.12 shows the filtered data map of  $\sigma_{CCSTDDEV}$  in azimuth vs. elevation, while Figure 4.3.13 shows the filtered time profiles of S4 for all satellites.

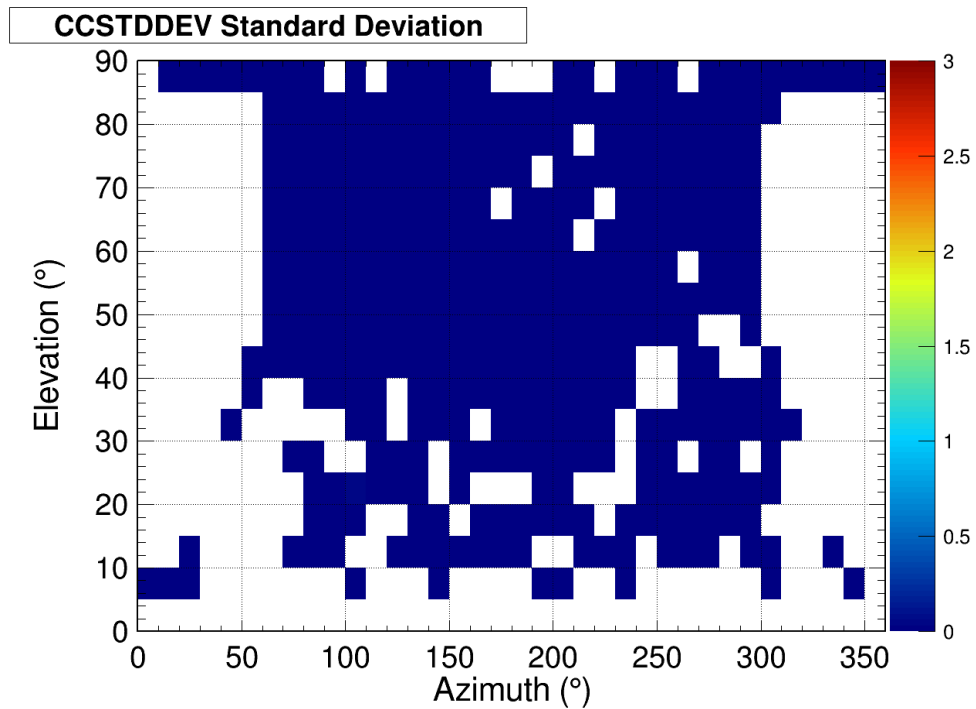


Figure 4.3.12. Filtered data map of the  $\sigma_{CCSTDDEV}$  in azimuth vs. elevation for the simulation of Scenario A.

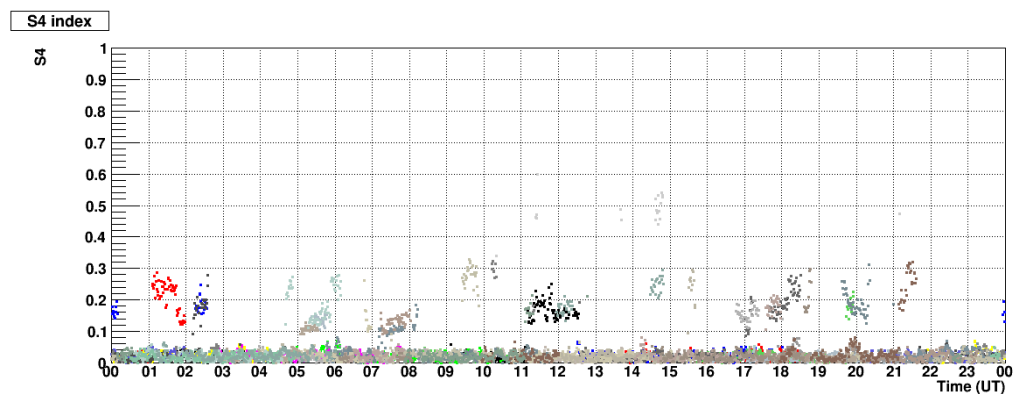


Figure 4.3.13. Filtered time profiles of S4 for all satellites during the fourth day of acquisition of Scenario A.

Results of the filtering technique show a limited selectivity on the effects of multipath and, on the contrary, an excessive selectivity of the map bins affected by scintillation. Such result is mostly expected. In fact, the filtering technique has been developed as a method able to identify long-term multipath effects, i.e. it needs a large statistics to be efficient. Thus, when tested against a much larger dataset than that of a single day of acquisition, the filtering technique could be tuned and refined to efficiently separate long-term multipath effects from scintillation. Unfortunately three different logistics aspects limited the possibility to perform a longer simulation test:

- Considering the method of obtaining the simulated data, it was necessary to use the GISTM for real time acquisition, as if the receiver were physically installed in continuous acquisition. This increases the need to control the acquisition runs, which must be continuous. It requires the availability of the simulator for a number of consecutive days, which was not always possible.

- Due to the part-time nature of this research and the distance between the student's location (Rome) and that of NGI (Nottingham), where the simulator sits, the simulation work could only be carried out during the periods of stay at NGI, which in turn were not long enough to accomplish more extensive data collection.
- It was very difficult to have the simulator available for long periods, due to the fact that it is shared with other groups and activities at NGI.

### Scenario B

In order to overcome the limitation in application of the filtering technique due to the scarce statistics of simulated data, and to progress further with the validation of the technique, a 10 days long artificial dataset has been obtained merging:

- 10 days like the second day of the Scenario A (multipath without scintillation);
- 1 day like the fourth day of the Scenario A (multipath and scintillation on PRN 17)

Such dataset would emulate a situation as close as possible to the real conditions, as the multipath sources are normally stable in time (i.e., long-term multipath) and scintillation appears only in one day and superimposed to the multipath. A limitation of such dataset is due to have reproduced exactly the same orbits of satellites for 10 days. Considering the bin resolution of the maps produced by the filtering technique (10° azimuth x 5° elevation) and the daily orbits variation, this scenario could be considered close to the one obtained with 11 days of continuous acquisition, not affecting significantly the results of our analysis.

After the application of the filtering, the time profile of S4 is shown in Figure 4.3.14, where it can be seen that the multipath effects are slightly more efficiently removed from the time profile and the scintillation is much more efficiently preserved in comparison to what is shown in Figure 4.3.13.

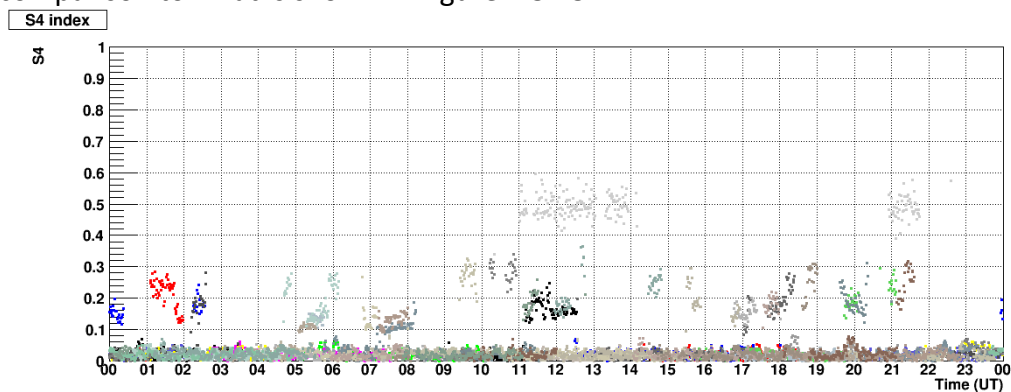


Figure 4.3.14 Filtered time profiles of S4 for all satellites.

The aim of this analysis, as highlighted in the above discussion, is to demonstrate that, when applied to a larger dataset, the filtering is more effective in cutting out multipath effects mimicking ionospheric scintillation. The potentiality of the filtering technique is confirmed by this result. As a recommended future work, a further simulation both, longer and of many scintillation and multipath scenarios, will enable further refinements of the technique and a better assessment of its capability in discarding ray paths affected by environmental noise in a larger range of cases.

To confirm the positive results of this approach data have been also analysed to show the filtering effects on phase scintillation index on the same data set of Scenario B (10 days with multipath and 1 day with scintillation on PRN 17).

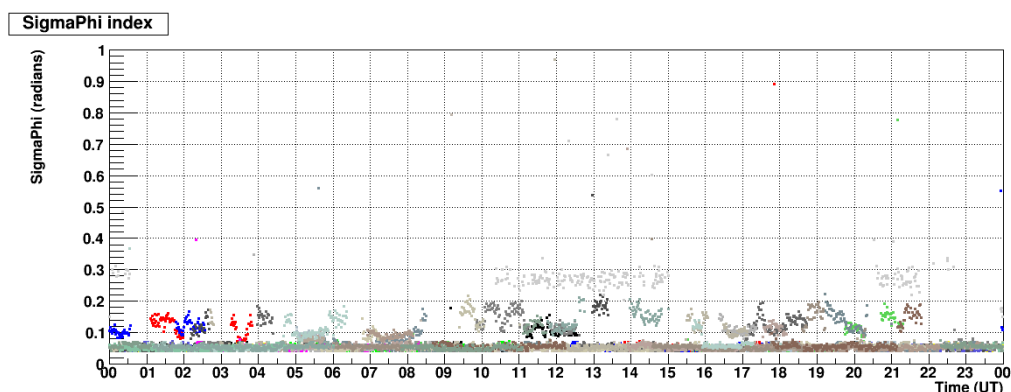


Figure 4.3.15. Time profiles of  $\sigma_\phi$  for all satellites during the fourth day of acquisition of Scenario A. The simulated configuration comprises scintillation and multipath effects.

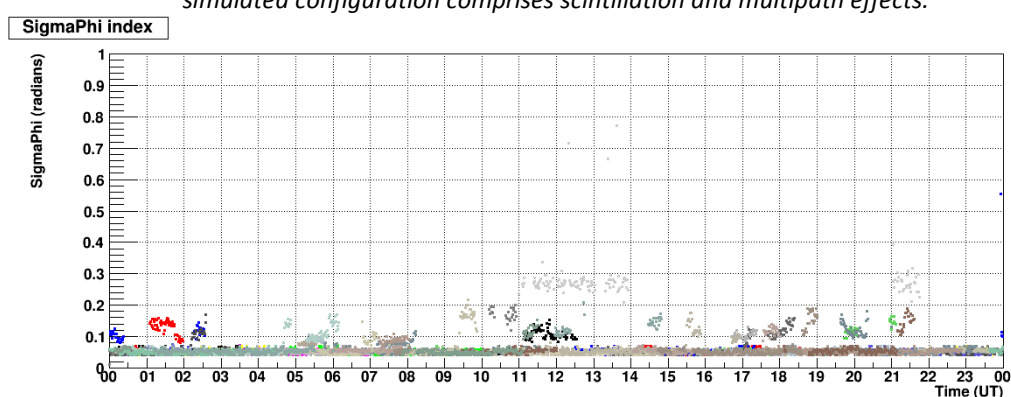


Figure 4.3.16. Filtered time profiles of  $\sigma_\phi$  for all satellites of Scenario B.

Figure 4.3.15 shows the time series of  $\sigma_\phi$  for all satellites during the fourth day of acquisition of Scenario A. The day of acquisition comprises scintillation on the PRN 17 and multipath effects configured as in figure 4.3.3 and described in Table 4.3.1. Figure 4.3.16 shows the filtered time profiles of  $\sigma_\phi$  for all satellites obtained using the dataset of Scenario B (dataset is obtained merging 10 days with multipath, corresponding to the second day of acquisition of Scenario A, and 1 day with multipath and scintillation on PRN 17, corresponding to the fourth day of acquisition of Scenario A).

As for the S4 discussion, it can be seen (Figure 4.3.16) that the multipath effects are partially removed from the time profile of  $\sigma_\phi$  and the phase scintillation is mostly preserved. Also the phase scintillation analysis show the good results of the technique in the application with acquired simulated data.

Some considerations can be underlined:

- The techniques for the characterization of the station and filtering are based on statistical methodologies which must be supported by an adequate amount of data.
- The simulations carried out, for the technical and logistical difficulties highlighted before, did not allow the availability of long series of simulated data. This definitely affects the final results of the application of the method to the data set obtained and a full validation for a large series of scenarios.
- The method for outlier identification has the limitation to filter an amount of data in any case, not considering the characteristics of the distribution itself. In the context of the simulated data, it poses a problem due to the limited presence of outliers, especially if the acquisition is made for a short period of time (i.e. one or few days).

- The analysis of simulated data presents unknown differences between the characteristics of real experimental data influenced by multipath and scintillation on the GISTM and the simulated ones. Surely the use of open sky data, in combination with the Spirent simulator, could help in the understanding of these differences and improve the results of the application of the technique.
- At the moment (June 2015) the simulator is under a procedure of firmware upgrading to solve some issues on the internal scintillation tool. The full availability of the Spirent simulator's internal tool will make possible in the future to realise various configurations of scintillation scenarios in an easy way to be applied during the GISTM acquisition of simulated data.

## 5 CHAPTER 5 – CONCLUSIONS AND RECOMMENDATIONS FOR FUTURE WORKS

---

The PhD work aimed to achieve the improvement of monitoring and data management and the development of novel data processing in the field of ionospheric scintillations. Specific aims of the research were:

- Development of software procedures and hardware configuration designs to optimize the station configurations of the existing measurement network of GISTM (GPS Ionospheric Scintillation and TEC Monitor).
- Development of techniques for remote, automatic instrument control and setting.
- Development of data management tools to achieve quasi real-time data accessibility.
- Development of data analysis methods to assess station characterization.
- Development of techniques to perform data quality filtering.
- Perform acquisition of experimental and simulation data.
- Support scientific investigations through the high quality of the NGI-INGV network data.

Hereafter is reported a summary of the conclusions of this research as well as most relevant recommendations for future works.

### **Conclusions:**

#### [1] Upgrading and reinforcement of monitoring capability.

The research project actively contributed to the reinforcement of the NGI-INGV GISTM network. This network was improved and enlarged in view of the recent solar maximum when knowledge and expertise on scintillation effects on GNSS applications were greatly in demand by a large number of bodies, in both the government and private sectors. High solar activity poses a serious threat to satellite based navigation and telecommunications systems because the artificial satellite signals propagate through the Earth's ionosphere, which is very strongly influenced by magnetic and solar activity. The research contributed in upgrading the international upper atmosphere network in Europe, enhancing the understanding of the physical processes causing the ionospheric effects that are potentially disruptive for positioning and navigation systems. This knowledge is crucial for Space Weather applications aiming to forecast and now-cast possible effects on technological systems, and is of particular interest for the design of receivers for the forthcoming Galileo system. In particular the research contributed through the specific results listed below.

- a) The Nottingham and Trondheim receivers were configured and set up using two specifically customised scripts. The scripts developed are able to simultaneously produce two different kinds of files. The first, known as "S60", is used for acquiring the parameters: one minute information related to navigational and observational data with files generated every 15 minutes, stored locally, and sent via ftp to the eSWua system. The second type, called "RWD", contains the 50 Hz L1 signal sampling amplitude and phase data, generated every hour and stored locally. The data acquisition and transfer problems identified for the Nottingham and Trondheim stations were resolved during the research period.
- b) Two external programs were developed to automatically guarantee data transmission to the eSWua system and to restart the acquisition procedure in case

of interruptions due to TCP/IP issues. These programs are currently running successfully and have improved the continuity of acquisitions.

- c) In March 2012 the monitoring activity of the PhD Course has included the installation of a GISTM station in Rome Italy, the development of the related acquisition script and the data management tools. The station owner is NGI and it is hosted at the headquarters of INGV.
- d) The experience gathered during the development of the acquisition programs enabled the realization of a specific script to acquire RINEX format data at a 1s sampling rate. RINEX files are typically produced every hour, but this time interval can be adjusted by the user according to specific needs. This acquisition procedure uses the second serial communication port of the receiver and can operate without affecting the regular acquisition of raw and processed scintillation data. This script has not yet been put into operation. However, it has been fully tested and is ready for easy implementation in response to specific needs. It was used, for example, within the CIGALA project, to produce a data set of 1s RINEX to support the development of a scintillation receiver, which was one of the aims of that project.

#### [2] Development of the eSWua data management system.

Within the framework of the research project, some of the data from the NGI GISTM stations were integrated into the eSWua data management system in order to develop specific tools for these stations. eSWua is installed at INGV, the host organization of the PhD student. Specific tools have been realised:

- a) Data transmission and database population. Data are sent automatically to eSWua, and then an extraction procedure runs automatically and converts the binary file into ASCII format. A PHP batch procedure reads this file and populates the database. Data are structured in tables containing all the observational and navigational parameters.
- b) eSWua tools. Linear plot and polar plot visualization tools, statistics page, and users' management system are fully implemented. Web access to data and tools is established for hosting the data from the Nottingham, Trondheim, and Dourbes sites. The initial web page shows a panorama of the three stations with a display of the last data processed by the system.
- c) eSWua state of the art. eSWua was designed to provide access to data and other outputs, like the plots and maps mentioned above, not only for scintillation indices but also for the main output parameters of the receivers and TEC related data. A comparison has been presented of the technical solutions adopted to develop eSWua and four of the other best known databases devoted to GNSS ionospheric data in the world. This comparison demonstrates that eSWua can be considered as the state-of-the-art system for GNSS ionospheric data.

#### [3] Development of data preparation tools.

The PhD course developed data preparation tools to support GISTM data analysis. The work focused on harmonizing and merging data acquired by different receivers owned by INGV and NGI to support the first statistical and climatological studies. The “converter” tool was programmed in FORTRAN and rewrites a data file for a given day and station into a proper standard format output file. Later the data preparation chain

changed and the PhD contributed to the data preparation needs realizing the “Data\_prep” algorithm. Such tool gets as input the receiver output in ISMR or ASCII format, producing daily files in ASCII format by merging the input data. This data preparation algorithm was further developed and tuned to also include data acquired by the PolarXs, Javad, and SCINTMON (Cornell Scintillation Monitor) receivers into the preparation chain. The data preparation chain guaranteed a robust procedure to feed ad hoc analysis tools developed to study the ionospheric impact on GNSS. In addition, the data harmonisation achieved by the preparation chain is vital when applying climatological and statistical techniques, which utilize data not only from single stations, but also entire networks of receivers. Data preparation has formed the basis for various climatological studies published in peer reviewed journals.

[4] Contribution of developed data management and monitoring tools to scientific results.

The tools developed to reinforce the data management and monitoring supported original investigations into the formation of the ionospheric irregularities that cause scintillations, the dynamics of high latitude plasma under disturbed conditions, and the development of countermeasures, i.e. mitigation techniques. The quality and volume of data collected by INGV and NGI has encouraged International collaborations with groups that manage similar experimental observations, and experts in irregularity and scintillation modelling, gave rise to several opportunities to exchange expertise and data and to collaborate in the frame of international projects. Below is listed a synthetic description of some results published on JCR papers in which data monitoring and/or management work contributed.

- a) Data monitoring supported attempts to apply new techniques for mitigating scintillation effects on the GNSS signal data acquired at Ny-Ålesund and Longyearbyen. Results showed the improvement in height error from the DGPS solution when applying the mitigation technique compared to the non-mitigated solution in a scintillating environment.
- b) Observations from GISTM receivers in Northern Europe were used to investigate the dynamics of ionospheric plasma during the storm events of October 30 and November 20, 2003. The total electron content (TEC) and scintillation data combined with ionospheric tomography revealed strong enhancements and steep gradients in TEC during night-time under a prevailing negative Bz component of the Interplanetary Magnetic Field (IMF). Amplitude and phase scintillation maxima were often co-located with the TEC gradients at the edge of plasma patches, revealing the presence of small scale irregularities and suggesting association with the Tongue of Ionization (TOI) convecting in an anti-sunward direction from the American sector across the polar cap.
- c) Rigorous and methodological data preparation has formed the basis for various climatological studies published in peer reviewed journals. The network considered includes 4 receivers in the Northern Hemisphere and two in the Southern. The northern array allows the observation of subauroral, auroral, cusp, and cap sectors, while the southern array essentially covers the cusp and cap regions. The study discussed how the IMF orientation influences scintillation distribution in magnetic local time, highlighting the important role of plasma inflow and outflow from and to the magnetosphere at noon and midnight.

- d) The decision to tune the data preparation algorithms to ingest data from other receivers was motivated by an interest in characterizing the low latitude ionosphere within the framework of the CIGALA and CALIBRA projects, in which INGV and NGI were consortium members. Some of the work completed within the framework of CIGALA led to the publication of a paper in which the ionosphere over Brazil, and in particular over São Paulo state, was characterized using the PolaRxS and SCINTMON receivers.

[5] Development of the station characterization tool.

The use of data for scientific and applicative purposes such as climatologic analysis, scintillation case studies and mitigation techniques depends on well established data quality. The quality of data available is in part determined by the environment surrounding the antenna. Thus, techniques to characterize this environment are of great importance. The station characterization technique has been introduced, developed and discussed in this thesis. The results indicated that this is a promising method for improving the quality of data for scientific studies such as in scintillation climatology and case events. The results obtained so far motivated the development of the data filtering procedures.

To realise the technique, modification of the GBSC has been done to include signal parameters measured by the GISTM receiver, such as:

- The standard deviation of the Code-Carrier Divergence (CCSTDDEV), calculated on the L1 over 60 seconds.
- Carrier to noise ratio (C/N) on L1 and L2, every 60 seconds.

GBSC code has been made more general, by extending the possibility to output the occurrence, mean values and standard deviation maps of the CCSTDDEV and the C/N. Such implementation is then used to develop the station characterization and data filtering techniques.

The method to characterize the environmental effects on a station based on a large statistical study of historical data was applied to several cases:

- a) Nottingham GISTM station. The characterisation of the environment of the Nottingham GISTM station was carried out using the data acquired during 2008, which was a very quiet year from a geomagnetic and solar point of view, allowing the impact of ionospheric turbulence to be ignored. As discussed in paragraph 3.1.2, the analysis performed showed several patterns indicating significant signal quality degradation. In particular:
- One case of multipath source generates in the map levels of scintillation with percentage of occurrence almost 100%, indicating an almost omnipresent degradation of the GPS signal amplitude.
  - The presence of the chimney mimics an “irregularity” of the same dimension of the Fresnel radius, resulting in both amplitude and phase scintillation caused by scattering of the wave encountering the chimney, the occurrence of which is roughly the same order of magnitude.

The considerations were also supported by a photographic and telemetric survey of the Nottingham campus site, where the antenna was installed. The survey of the surroundings of the antenna demonstrated to be a very useful method to relate degraded patterns resulting from the map with real sources of multipath mimicking scintillation.

- b) Trondheim GISTM station. The characterization of the Trondheim station was done comparing the data acquired in 2008 with those of summer 2009, aiming to investigate a significant data quality degradation occurred since May 2009. A general anisotropic degradation of the signal is observed, appearing as higher values of the L1C/N standard deviation without identification of privileged areas of the ionosphere. Moreover, there was no meaningful degradation potentially due to multipath. This was quite evident in the maps showing the mean values of the Code Carrier divergence standard deviation in geographic coordinates for 2008 and 2009, which are seen to be very similar. The effect was probably due to interference phenomena with a radio bridge installed in 2009.
- c) Nottingham station behaviour during the “Halloween Storm”. The station characterization method was applied to the Nottingham data acquired by the GISTM receiver during the so-called Halloween Storm, which occurred between 30 and 31 October 2003 and was the strongest of the last solar cycle. Over these two days, severe solar events caused highly disturbed conditions in the ambient ionosphere. In particular, a very fast full halo coronal mass ejection (CME) originating from an X10 flare reached the Earth at about 16:00 UT on 30 October. As a consequence, episodes of severe scintillation were registered on 30 and 31 October. The analysis showed that signal degradation due to multipath sources and the chimney were already present in 2003. Moreover the enhancement of scintillation activity due to the presence of the chimney, clearly visible during the quiet year of 2008, appeared in the "Halloween Storm" occurrence plot at a lower value. This was due to the fact that a limited number of days of acquisition did not provided sufficient data for the chimney signature to be evident in the statistics under such marked scintillation conditions.

[6] Development of data filtering technique.

Based on the station characterization method, a filtering technique has been developed. This technique was aimed to filter out spurious data based on an “outlier analysis”, thus efficiently removing multipath affected measurements and reducing the data loss with respect to applying a fixed elevation angle cut-off threshold. This cut-off is not crucial for dense networks or well covered areas, but it is important in case of not well covered regions (e.g. forests, deserts, oceans, etc.). The loss of information in many applications could be crucial. Bearing in mind that a fool-proof standard procedure able to remove short and long term effects due to environmental multipath had not yet been implemented, the filtering method was based upon the identification of the outliers in the  $\sigma_{CCSTDDEV}$  histogram. Ray paths characterised by a large variability of CCSTDDEV can be tagged as affected by multipath and then removed for any further data analysis.

[7] Testing of the data filtering technique.

Filtering capabilities of the technique were tested using data acquired by the GISTM station of Rome, installed in March 2012, during the PhD project. Similarly to Nottingham, the Rome GISTM is located in an urban site, surrounded by many multipath sources. The Rome station is also weakly affected by ionospheric disturbances (on average quiet at mid-latitudes), allowing the disentanglement between ionospheric and non-ionospheric effects on the signal received at ground.

Test has been performed as a function of the  $k$  parameter. Different definitions of outliers follow different values of the  $k$  parameter. The choice of considering  $k=1.5$ , i.e. the commonly adopted definition of “mild outliers”, is satisfactory in identifying the ray paths most affected by multipath and, thus, can be used for the extensive filtering applications described and discussed in Chapter 4.

[8] Data Filtering application in scintillation climatology and on the CIGALA/CALIBRA network.

To show how the development of a filtering method to remove spurious data, based on an analysis of outliers, was able to efficiently clean multipath and signal degradation from GNSS data; this method was applied in two different cases.

- a) The methods for characterizing the stations and filtering the data were applied in a published climatological study carried out using the INGV-NGI GISTM network at high-latitudes. First, each station was characterized using the station characterization method, and then the data were filtered using the filtering method. Finally, the new climatological maps were generated and compared to the original ones. The percentage of filtered out data obtained applying, respectively, the standard threshold of  $20^\circ$  on the elevation angle and the filtering technique for each station, significantly reduced using the latter. Filtering extended the field of view of the network and highlighted how:
  - In the cusp sector phase scintillation occurrence is more evident than amplitude scintillation.
  - The occurrence of amplitude scintillation is generally lower than phase scintillation.
  - Enhanced standard deviation of the ROT often corresponds with enhancements in both phase and amplitude scintillation, showing that a high variability of TEC is a good indicator of the presence of TEC gradients causing scintillation.
- b) The data used in the second application were acquired by the CIGALA/CALIBRA network of PolarXs receivers during the whole year of 2012. The elevation angle cut-off significantly reduced the capability of the network to depict the ionosphere northward of the geomagnetic equator and above the Atlantic Ocean, east of Brazil. This approach limited the data loss to 10-20%, while the traditional cut off of  $15^\circ$ - $30^\circ$  on the elevation angle led to losses of 35-45%. The reduction in data loss, averaged among all the stations, was of a factor of about 2.4. This method optimized the capability of GNSS networks and helped in planning the installation of additional new receivers aiming to enlarge network coverage in the framework of the CALIBRA project. The enlarged field of view made it possible to identify the increased occurrence of scintillation along the northern crest of the Equatorial Ionospheric Anomaly (EIA). This enhancement affected geographic latitudes greater than  $0^\circ$ N and along a band nearly parallel to the geomagnetic equator. Conversely, the southern crest of the EIA is well covered by data and the effect of filtering in terms of amplitude scintillation occurrence is visible along the band of enhanced scintillation, nearly parallel to the geomagnetic equator. These observations revealed that the regions most affected were in the latitudinal range between  $30^\circ$ S and  $10^\circ$ N, and along longitudes between  $300^\circ$ E and  $330^\circ$ E, in particular over São Paulo and Tocantins States (due to the presence of the EIA southern crest), and northward of MANA (due to the presence of the EIA northern

crest). The enhancement over POAL was also meaningful and possibly due to the presence of particle precipitation along the borders of the South Atlantic Magnetic Anomaly (SAMA). SAMA was another source of ionospheric turbulence leading to scintillation, since it disturbs thermospheric circulation in the atmosphere and alters the rates of production and recombination of ionized species, mainly during geomagnetic storms.

[9] Application to simulated data to validate the filtering technique.

As a final application of the filtering technique, the goal was to validate the developed method applying it to a simulated scenario. By connecting a GISTM receiver to the antenna output of the simulator, it was possible to acquire GNSS data similar to the real situation but with well-known user-defined multipath/scintillation scenarios. Such kind of simulated data made easy the application of the station characterization and filtering methods, specifically developed for data having the same format. The analysis demonstrated that, when applied to a large dataset, the filtering is more effective in cutting out multipath effects mimicking ionospheric scintillation. In particular, good results were obtained when the simulated dataset represented a situation as close as possible to the real conditions, as the multipath sources were normally stable in time (i.e., long-term multipath) and scintillation appeared only on one day and superimposed to the multipath. The potentiality of the filtering technique was confirmed by the simulation, recommendations for further analysis are suggested below.

**Recommendations for future works:**

[1] The first recommendation for future work is related to underlining the importance to continue the maintenance and the upgrading of the NGI-INGV GISTM network. This longstanding collaboration could be the base for supporting the IPDM idea of the realization of a European service to detect and monitor ionospheric perturbations and related scintillation occurrence. The knowledge and experience gathered during the development of acquisition programs and data analysis techniques could make easier the upgrading of the GISTM stations of the network. Currently most of the stations are equipped with the GSV4004B receivers that are only dual frequency and capable to evaluate scintillation only on L1. As shown in this thesis, during the CALIBRA/CIGALA PolarxS data analysis, the availability of multi-frequency and multi-constellation receivers enhanced the capability to monitor and study the variability and characteristics of the ionosphere.

[2] Development of a data management system like eSWua is well motivated by the awareness that geosciences need structured digital data and appropriate scientific procedures developed ad hoc by experts, unrestricted and shared among the international community. Complete sharing of algorithms and tools, not only data, should be one of the main drivers when developing such kind of systems with the final goal to create common interoperable ICT platforms able to support scientific and user needs. The TRANSMIT project supported the development of a prototype of an interoperable platform for GNSS services, this approach should be pursued in similar collaborative initiatives.

[3] Filtering techniques could be used to support other scientific and applicative cases where the improvement of the GISTM data quality is an important requirement. Examples of applications could be: development of mitigation techniques and calculation of estimation of signal tracking errors.

[4] The station characterization technique, which has started to raise interest in the scientific community (at the date of thesis submission, Romano et al. 2013 has been cited 2 times in international journals and downloaded about 50 times in the researchgate website), could be further developed for use in support of other applications where the knowledge of the multipath scenario is an important requirement. An example of application could be the evaluation of the best site to install GNSS permanent stations in particularly noisy environments (railway station, airport, city, etc.). The technique can be also developed in order to support the evaluation of the multipath impact on existing GNSS permanent stations, acquiring data with a GISTM connected to the same antenna of the station to characterize

[5] The filtering technique, could be further refined and consolidated performing long series of acquisitions of simulated data. The full availability of the Spirent simulator's internal tool will make possible to realise various configurations of scintillation scenarios to be applied during the simulation. Simulations of many scintillation and multipath scenarios will enable further refinements of the technique and a better assessment of its capability in discarding ray paths affected by environmental noise in a larger range of cases. Moreover, the analysis of simulated data highlights unknown differences between the characteristics of real experimental data influenced by multipath and scintillation on the GISTM and the simulated ones. Surely, the use of open sky data, in combination with the Spirent simulator, could help in the understanding of these differences and improve the results of the application of the technique.

## 6 REFERENCES

---

- Aarons J., Global morphology of ionospheric scintillations, *Proceedings of IEEE* 70(4), 360-378, 1982.
- Aarons J., The longitudinal morphology of equatorial F-layer irregularities relevant to their occurrence, *Space Sci. Rev.*, 63, 209-243, 1993.
- Abdu, M.A., Batista, I.S., Carrasco, A.J., Brum, C.G.M., 2005. South Atlantic magnetic anomaly ionization: a review and a new focus on electrodynamic effects in the equatorial ionosphere. *J. Atmos. Sol. Terr. Phys* 67, 1643–1657.
- Alfonsi L, Spogli L, Tong JR, De Franceschi G, Romano V, Bourdillon A, Huy ML, Mitchell CN (2010). GPS scintillation and TEC gradients at equatorial latitudes in April 2006. *ADVANCES IN SPACE RESEARCH*, vol. 47, p. 1750-1757, ISSN: 0273-1177, doi: 10.1016/j.asr.2010.04.020.
- Alfonsi, L., L. Spogli, G. De Franceschi, V. Romano, M. Aquino, A. Dodson, and C. N. Mitchell (2011). Bipolar climatology of GPS ionospheric scintillation at solar minimum, *Radio Sci.*, 46, RS0D05, doi:10.1029/2010RS004571.
- Aquino M, Rodrigues F S, Souter J, Moore T, Dodson A and Waugh S (2005a) Ionospheric scintillation and impact on GNSS users in Northern Europe: Results of a 3 year study. *Space Communications*, 20(1/2), pp 17-30
- Aquino M, Moore T, Dodson A, Waugh S, Souter J and Rodrigues FS (2005b) Implications of ionospheric scintillation for GNSS users in Northern Europe. *Journal of Navigation*, 58(2), pp 241-256
- Aquino M., JFG Monico, A.H. Dodson, H. Marques, G. De Franceschi, L. Alfonsi, V. Romano and M. Andreotti, Improving the GNSS Positioning Stochastic Model in the Presence of Ionospheric Scintillation, *Journal of Geodesy*, 10.1007/s00190-009-0313-6, 2009.
- Baker, K. B., and S. Wing (1989), A new coordinate system for conjugate studies at high latitudes, *J. Geophys. Res.*, 94 (A7), 9139, doi:10.1029/JA094iA07p09139.
- Barnett, V., Lewis, T., *Outliers in Statistical Data*. Wiley, 3rd Edition, 1995.
- Basu Su., and Sa. Basu, Equatorial scintillations: Advances since ISEA-6, *J. Atmos. Terr. Phys.*, 47, 753-768, 1985.
- Basu S., E. Mackenzie and S. Basu, Ionospheric Constraints on VHF/UHF Communication Links During Solar Maximum and Minimum Periods, *Radio Science*, 23(3), pp 363 – 378, 1988.
- Basu Sa., and Su. Basu, Ionospheric structures and scintillation spectra, in *Wave Propagation in Random Media (Scintillation)*, eds. V. I. Tatarski, A. Ishimaru, and V. U. Zavorotny, pp. 139- 153, The International Society for Optical Engineering, Bellingham, WA, USA , 1993.
- Beach, T.L., and P.M. Kintner, Development and use of a GPS ionospheric scintillation monitor, *IEEE Trans. Geosci. Remote Sens. (USA)*, 39, 918–928, 2001.
- Béniguel, Y., Romano, V., Alfonsi, L., Aquino, M., Bourdillon, A., Cannon, P., De Franceschi, G., Dubey, S., Forte, B., Gherm, V., Jakowski, N., Materassi, M., Noack, T., Pozoga, M., Rogers, N., Spalla, P., Strangeways, H., Warrington, E., Wernik, A., Wilken, V., & Zernov, N. (2009). Ionospheric scintillation monitoring and modelling. *Annals Of Geophysics*, 52(3-4), 391-416. doi:10.4401/ag-4595
- Benton, C. J., and C. N. Mitchell (2011), Isolating the multipath component in GNSS signal-to-noise data and locating reflecting objects, *Radio Sci.*, 46, RS6002, doi:10.1029/2011RS004767.

- Bhattacharyya A., K. C. Yeh, and S. J. Franke, Deducing turbulence parameters form transionospheric scintillation measurements, *Space Sci. Rev.*, 61, 335-386, 1992.
- Bourdillon, A., Cander, Lj.R., Zolesi, B. (Eds.), COST 296 MIERS Mitigation of Ionospheric Effects on Radio Systems, *Annals of Geophysics*, Special issue, vol. 52, pp. 3-4, 2009.
- Bougard, B., Sleewaegen, J.-M., Spogli, L., Sreeja, V.V., Galera Monico, J.F., 2011. CIGALA: challenging the solar maximum in Brazil with PolaRxS. In: *Proceeding of the ION GNSS 2011*. Portland, Oregon.
- Cannon M.E., S. Skone and C. Varner, LINCSS Mission Data Segment System Definition Studies, Report submitted to Loral Integrated Navigation and Communication Satellite Services (LINCSS), Department of Geomatics Engineering, The University of Calgary, 1997.
- Conker R. S., M. B. El Arini, C. J. Hegarty, and T. Hsiao, Modeling the effects of ionospheric scintillation on GPS/SBAS availability, *Radio Sci.*, Vol. 38, 2003.
- De Franceschi G., Alfonsi L. and Romano V., ISACCO: an Italian project to monitor the high latitudes ionosphere by means of GPS receivers, *GPS Solutions*, DOI 10.1007/s10291-006-0036-6, 2006.
- De Franceschi, G., Alfonsi, L., Romano, V., Aquino, M. H. O., Dodson, A., Mitchell, C. N., and Wernik, A. W.: Dynamics of high latitude patches and associated small scale irregularities, *J. Atmos. Sol.-Terr. Phys.*, 70, 879-888, doi:10.1016/j.jastp.2007.05.018, 2008.
- El-Arini, M. B., J. Secan, J. A. Klobuchar, P. H. Doherty, G. Bishop, and K. Groves (2009), Ionospheric effects on GPS signals in the Arctic region using early GPS data from Thule, Greenland, *Radio Sci.*, 44, RS0A05, doi:10.1029/2008RS004031.
- Elmas, Z.G. (2013) Exploiting New GNSS Signals to Monitor, Model and Mitigate the Ionospheric Effects in GNSS. Ph.D. dissertation, Nottingham Geospatial Institute, The University of Nottingham, Nottingham, UK.
- Fejer B. G., Natural ionospheric plasma waves, in *Modern Ionospheric Science*, eds. H. Kohl, R. Rüster and K. Schlegel, pp. 216-273, European Geophysical Society, Katlenburg-Lindau, FRG, 1996.
- Feldstein, Y. I. (1963), On morphology and auroral and magnetic disturbances at high latitudes, *Geomagn. Aeron.*, 3, 138.
- Foster, J. C. and Rideout, W.: Mid latitude TEC enhancements during the October 2003 supestorm, *Geophys. Res. Lett.*, 32, L12S04, doi:10.1029/2004GL021719, 2005.
- Hargreaves, J.K., *The Solar-Terrestrial Environment*, Cambridge University Press, Cambridge, 1992.
- Heppner, J. P., M. C. Liebrecht, N. C. Maynard, and R. F. Pfaff, High-latitude distributions of plasma waves and spatial irregularities from DE 2 alternating current electric field observations, *J. Geophys. Res.*, 98, 1629-1652, 1993.
- Holzworth, R.H. and Meng, C.-I. (1975). Mathematical representation of the auroral oval. *Geophysical Research Letters* 2: doi: 10.1029/GL002i009p00377. issn: 0094-8276.
- Humphreys, T. E., Psiaki, M. L., & Kintner, P. M. (2009a), Modeling the effects of ionospheric scintillation on GPS carrier phase tracking, *Aerospace and Electronic Systems*, *IEEE Transactions on*, Vol. 46(4), pp.1624-1637.

- Humphreys, T. E., Psiaki, M. L., Hinks, J. C., O'Hanlon, B., & Kintner, P. M. (2009b), Simulating ionosphere-induced scintillation for testing GPS receiver phase tracking loops, *Selected Topics in Signal Processing, IEEE Journal of*, Vol. 3(4), pp. 707-715.
- Holzworth, R. H., and C.-I. Meng (1975), Mathematical representation of the auroral oval, *Geophys. Res. Lett.*, 2, 377–380, doi:10.1029/GL002i009p00377.
- Huba, J. D., Theoretical and simulation methods applied to high latitude, F region turbulence, in *World Ionosphere/Thermosphere Study, WITS Handbook vol. 2*, ed. C. H. Liu, pp. 399-428, SCOSTEP Secretariat, Boulder, CO, 1989.
- Kelley M.C., *The Earth's Ionosphere*, International Geophysics Series, 43, Academic Press, London, 1989.
- Keskinen M. J., and S. L. Ossakow, Theories of high-latitude irregularities: A review, *Radio Sci.*, 18, 1077-1092, 1983.
- Kintner P. M., and C. E. Seyler, The status of observations and theory of high latitude ionospheric and magnetospheric plasma turbulence, *Space Sci. Rev.*, 41, 91-129, 1985.
- Kintner, P.M., T. Humphreys and J. Hinks (2009). GNSS and Ionospheric Scintillation - How to survive to the next solar maximum, *InsideGNSS*, July/August 2009, 22-30.
- Klobuchar J. A., *Ionospheric Effects on GPS*, *Global Positioning Systems: Theory and Applications*, Vol I, ed. B.W. Parkinson and J.J. Spilker Jr., American Institute of Aeronautics and Astronautics, Washington DC, pp. 485-516, 1996.
- Jin, S.G., O. Luo, P. Park (2008). GPS observations of the ionospheric F2-layer behavior during the 20<sup>th</sup> November 2003 geomagnetic storm over South Korea. *J. Geod.* 82, 883-892; doi:10.1007/s00190-008-0217-x.
- Leick A., *GPS Satellite Surveying*. John Wiley & Sons, Inc., New York , 1995.
- Mannucci, A. J., B. D. Wilson, and C. D. Edwards (1993), A new method for monitoring the Earth ionosphere total electron content using the GPS global network, paper presented at ION GPS-93, Inst. of Navig., Salt Lake City, Utah.
- Mitchell N., Alfonsi, L.; De Franceschi, G.; Lester, M.; Romano, V.; Wernik, A. W., GPS TEC and scintillation measurements from the polar ionosphere during the October 2003 storm, *Geophys. Res. Lett.*, 32 (12), L12S03 10.1029/2004GL021644, 2005.
- Rino, C. L. (1979), A power law phase screen model for ionospheric scintillation: 1. Weak scatter, *Radio Sci.*, 14(6), 1135–1145.
- Rodrigues F S, Aquino M, Dodson A, Moore T and Waugh S (2004) Statistical analysis of GPS ionospheric scintillation and short-time TEC variations over Northern Europe. *Journal of the Institute of Navigation*, Vol. 51, No. 1, pp 59-75
- Romano V., S. Pau, M. Pezzopane, E. Zuccheretti, B. Zolesi, G. De Franceschi, and S. Locatelli, The electronic Space Weather upper atmosphere (eSWua) project at INGV: advancements and state of the art, *Ann. Geophys.*, 26, 345–351, 2008.
- Romano V. (2009), Ionospheric scintillation effects on GNSS: monitoring and data treatment development, First Year Assessment PhD report, University of Nottingham.
- Romano V. (2011), Ionospheric scintillation effects on GNSS: monitoring and data treatment development, Second Year Assessment PhD report, University of Nottingham.
- Romano V, S. Pau, M. Pezzopane, L. Spogli, E. Zuccheretti, M. Aquino, C. M. Hancock, eSWua: a tool to manage and access GNSS ionospheric data from mid-to-high latitudes, *ANNALS OF GEOPHYSICS*, 56, 2 , R0223, doi: 10.4401/ag-6244, 2013.

- Romano, V., Spogli, L., Aquino, M., Dodson, A., Hancock, C., Forte, B., GNSS station characterisation for ionospheric scintillation applications, *Advances in Space Research* (2013), doi: <http://dx.doi.org/10.1016/j.asr.2013.06.028>.
- Rostoker G., Some observational constraints for substorm models. In Kan JR, Potemra TA, Kokubun S Iijima T (ed) *Magnetospheric Substorms*. Geophysical Monograph 64, AGU, Washington, D.C., 1991.
- Sato H., N. Hlubek and M. Aquino (2014). The Concept of the TRANSMIT Prototype-Network Based Service for Mitigation of Ionospheric Threats to GNSS, *Mitigation of Ionospheric Threats to GNSS: an Appraisal of the Scientific and Technological Outputs of the TRANSMIT Project*, Dr. Riccardo Notarpietro (Ed.), ISBN: 978-953-51-1642-4, InTech, DOI: 10.5772/58770.
- Skone S. and M.E. Cannon, Auroral zone considerations for WADGPS, *NAVIGATION: Journal of the Institute of Navigation*, 45, no. 2,117,1998.
- Skone S., and M. de Jong, The impact of geomagnetic substorms on GPS receiver performance. *Earth, Planets and Space*, 52, 1067-1071, 2000.
- SimGEN software user manual, SPIRENT COMMUNICATIONS PLC, DGP00686AAA Issue 1-36 December 2009.
- Spogli L., L. Alfonsi, G. De Franceschi, V. Romano, M. H. O. Aquino and A. Dodson (2009), Climatology of GPS ionospheric scintillations over high and mid-latitude European regions, *Ann. Geophys.*, 27, 3429-3437.
- Spogli L., Alfonsi Lu., G. De Franceschi, V. Romano, M. H. O. Aquino, A. Dodson, Climatology of GNSS ionospheric scintillation at high and mid-latitudes under different solar activity conditions, *Nuovo Cimento della Società Italiana di Fisica B-General Physics Relativity Astronomy And Mathematical Physics And Methods*, 125 B, N. 5-6, ISSN: 1826-9877, DOI 10.1393/ncb/i2010-10857-7, 2010.
- Spogli, L., Alfonsi, L., Cilliers, P. J., Correia, E., De Franceschi, G., Mitchell, C. N., Romano, V., Kinrade, J. and Cabrera, M. A., GPS scintillations and total electron content climatology in the southern low, middle and high latitude regions, *Annals of Geophysics*, 56 (2), 2013.
- Spogli L., L. Alfonsi, V. Romano, G. De Franceschi, Galera Monico Joao Francisco, Milton Hirokazu Shimabukuro, Bruno Bougard, Marcio Aquino, Assessing the GNSS scintillation climate over Brazil under increasing solar activity, *Journal of Atmospheric and Solar-Terrestrial Physics*, Volumes 105–106 (2013), Pages 199-206, ISSN 1364-6826, <http://dx.doi.org/10.1016/j.jastp.2013.10.003>.
- Spogli L., V. Romano, G. De Franceschi, L. Alfonsi, E. Plakidis, C. Cesaroni, M. Aquino, A. Dodson, J. F. Galera Monico and B. Vani (2014). A Filtering Method Developed to Improve GNSS Receiver Data Quality in the CALIBRA Project, *Mitigation of Ionospheric Threats to GNSS: an Appraisal of the Scientific and Technological Outputs of the TRANSMIT Project*, Dr. Riccardo Notarpietro (Ed.), ISBN: 978-953-51-1642-4, InTech, DOI: 10.5772/58778.
- Strangeways, H. J. (2009), Determining scintillation effects on GPS receivers, *Radio Sci.*, 44, RS0A36, doi:10.1029/2008RS004076.
- Strangeways, H. J., Y.-H. Ho, M. H. O. Aquino, Z. G. Elmas, H. A. Marques, J. F. G. Monico, and H. A. Silva (2011), On determining spectral parameters, tracking jitter, and GPS positioning improvement by scintillation mitigation, *Radio Sci.*, 46, RS0D15, doi:10.1029/2010RS004575.

- Strangeways, Hal J., Nikolay N. Zernov, and Vadim E. Gherm. "Comparison of four methods for transionospheric scintillation evaluation." *Radio Science* 49.10 (2014): 899-909.
- Tsunoda R. T., High latitude F region irregularities: A review and synthesis, *Rev.Geophys. Space Phys.*, 26, 719-760, 1988.
- Van Dierendonck A J, Klobuchar J and Hua Q (1993) Ionospheric scintillation monitoring using commercial single frequency C/A code receivers. In: Proceedings ION GPS-93: Sixth International Technical Meeting of the Satellite Division of the Institute of Navigation, Salt Lake City, Utah. pp 1333–1342.
- Van Dierendonck A. J. (2001), Measuring ionospheric scintillation effects from GPS signals. In: Proceedings of 57th Annual Meeting of the Institute of Navigation, Albuquerque, pp 391-396.
- Van Dierendonck, A J (2005), GSV4004B - GPS IONOSPHERIC SCINTILLATION & TEC MONITOR USER'S MANUAL (8 August 2005).
- Van Dierendonck A. J., GSV4004B GPS Ionospheric Scintillation & TEC Monitor (GISTM) User's Manual, 2007
- Weaver M., W. Murtagh, C. Balch, D. Biesecker, L. Combs, M. Crown, K. Doggett, J. Kunches, H. Singer, D. Zezula (2004), Halloween space weather storms of 2003, NOAA Technical Memorandum OAR SEC-88, available at [http://www.swpc.noaa.gov/Services/HalloweenStorms\\_assessment.pdf](http://www.swpc.noaa.gov/Services/HalloweenStorms_assessment.pdf).
- Yeh, K. C., and C. H. Liu, Radio wave scintillations in the ionosphere, *Proc. IEEE*, 70, 324-360,1982.

## 7 APPENDICES

### 7.1 ACQUISITION SCRIPT FOR NOTTINGHAM STATION

```
-----
;
; Script for parameters and raw data logging
;
-----
;
; User parameters
;
; Length of time to log in one indices file, must be evenly divisible into 60 or a multiple of 60.
; Files are reopened 0.8 seconds before the file interval. A new raw data file is opened on the hour.
global double dFileInterval = 15.0*60.0

; Internet address of the receiver, IP TX RX
global string sIpPort = "193.69.44.115 3001 3001"

; Drive, directory and file name prefix
global string sDirectory = "D:\new_slog"
global string sFilePrefix = "nsf6"

; Debug mode can be "none", "light" or "heavy" indicating the amount of data recorded
global string sDebug = "light"

;*****
;
; Global variables
;

global int iGpsWeek ; GPS week number
global double dGpsWeekSecs ; Seconds into the week
global double iStopWeek ; GPS week number of when we want to stop logging to this file
global double dStopWeekSecs ; GPS week seconds of when we want to stop logging to this file

global int iRaw, iNoRaw ; Copyfile handles
global string IndicesFile ; Name of the file with processed data
global string RawDataFile ; Raw data file

;*****
;
; Creates the pathed directory and file name
;
sub BuildFileNames

; Break down the week seconds into the classical units
double dHourOfWeek = Floor(dGpsWeekSecs/3600.0) ; Hour of week
double dDayOfWeek = Floor(dHourOfWeek/24.0) ; Day of week
double dHourOfDay = dHourOfWeek - dDayOfWeek*24.0 ; Hour of day

; Get the ISO string version of time
string sGpsTime = GpsToIsotime(iGpsWeek, dGpsWeekSecs)

; Break down the ISO time into its parts
string aaaa = midstr ( sGpsTime, 0, 4 ) ; Year
string danna = midstr ( sGpsTime, 2, 2 ) ; Month
string dmese = midstr ( sGpsTime, 5, 2 ) ; Day
string dgiorno = midstr ( sGpsTime, 8, 2 ) ; Hour
string dminuto = midstr ( sGpsTime, 14, 2 ) ; Minute
```

```

; File names
IndicesFile =
"%sDirectory%\indices\%aaaa%_%dmese%_%dgiorno%\%sFilePrefix%S_%danno% %dmese% %dgior
no%%02.0dHourOfDay% %dminuto%.S60"
RawDataFile =
"%sDirectory%\raw_data\%aaaa%_%dmese%_%dgiorno%\%sFilePrefixR_%danno% %dmese% %dg
iorno%%02.0dHourOfDay%.RWD"

; Tell the operator what time it is
print "dHourOfWeek = %dHourOfWeek%"
print "dDayOfWeek = %dDayOfWeek%"
print "dHourOfDay = %dHourOfDay%"

return

;*****
;
; Creates the pathed directory and advances to the next time
;
sub SetupNextFile bool bFirstTime

; Is this the first time in?
if bFirstTime == TRUE
; Create the filenames from the GPS week and weekseconds
gosub BuildFileNames

; Start the logging
opencopyfile rcvr "%IndicesFile%" append iNoRaw \
"%RawDataFile%" append iRaw

; Copy to the indices file
copyfile rcvr iNoRaw versiona 0.0
copyfile rcvr iNoRaw rxconfiga 0.0
;copyfile rcvr iNoRaw gpsephemb 0.0
copyfile rcvr iNoRaw waas18B 0.0
copyfile rcvr iNoRaw waas26B 0.0
copyfile rcvr iNoRaw oem4ismrb 0.0
copyfile rcvr iNoRaw rxstatuseventa 0.0

; Copy to the raw file
copyfile rcvr iRaw rawsinb 0.0
else
; Immediately Open the new files without the potential of losing data in a closefile
newcopyfile rcvr iNoRaw "%IndicesFile%"

; We open a new raw on the hour
if (Floor(dGpsWeekSecs/3600.0))*3600.0 == dGpsWeekSecs
newcopyfile rcvr iRaw "%RawDataFile%"
endif
endif

; Put these logs at the beginning of the file
send rcvr "log versiona once\r"
pause 4 ; Pace the logging
send rcvr "log rxconfiga once\r"
pause 4 ; Pace the logging
send rcvr "log rxstatuseventa onchanged\r"
pause 4 ; Pace the logging

```

```

send rcvr "log ismrb onnew\r"
pause 4 ; Pace the logging

; WAAS Ionospheric Correction Data to use for TEC Calibration
send rcvr "log waas18B onchanged\r"
pause 4 ; Pace the logging
send rcvr "log waas26B onchanged\r"
pause 4 ; Pace the logging

; Debug?
run "copy %IndicesFile% D:\2send_INGV"
; spawn "sendS60file.bat"

; This is when we stop logging to this file. The TIMEB log will arrive 0.2 seconds after the second,
; putting the data written to the file first in line, and guaranteeing that the time has been exceeded
; to ensure the triggering of the GpsTime function.
iStopWeek = iGpsWeek
dStopWeekSecs = dGpsWeekSecs+dFileInterval
if dStopWeekSecs >= 7.0*24.0*3600.0
    iStopWeek = iStopWeek + 1
    dStopWeekSecs = dStopWeekSecs - 7.0*24.0*3600.0
endif

; Advance to the next log interval
dGpsWeekSecs = dGpsWeekSecs + dFileInterval
; Have we gone into the next week?
if dGpsWeekSecs >= 7.0*24.0*3600.0
    iGpsWeek = iGpsWeek + 1
    dGpsWeekSecs = dGpsWeekSecs - 7.0*24.0*3600.0
endif

; Create the filenames from the GPS week and weekseconds
; By doing this now we don't waste time in opening the next building it when the time expires
gsub BuildFileNames

return

,*****
;
; Mainline with no user parameters
;
main

testname "Scintillation Monitor Data Logging"

;-----

; Variables used to apply the desired level of debug data
string sAppendMode, sSliMode

; Check the level of debugging to be done if any
if sDebug == "none"
    sAppendMode = "none"
    sSliMode = ""
else
    if sDebug == "light"
        sAppendMode = "noappend"
        sSliMode = "slionly"
    else

```

```

    if sDebug == "heavy"
        sAppendMode = "noappend"
        sSliMode = ""
    else
        print "Invalid sDebug mode"
        exit -1
    endif
endif
endif

;-----

; Open the TCP/IP port of the receiver
find com1 115200 rcvr %sAppendMode% %sSliMode%

; Tcp/Ip can surge and lag, time cannot be set reliably all the time by it
ExitOnTimeShift(false)

;-----

; Configure the receiver
send * "ecutoff 5\r"
send * "SinBandWidth 0.1 0.0\r"
send * "assign 11 122 0 500\r"
send * "clockadjust disable\r"

; Debug?
; send * "SinTECCalibration -26.076\r" ; For SN NYM04370002
; send * "CPOFFSET -0.0159 0 -0.0033 0.435 -0.2832 0.1614 -0.3684 -0.0729 0.1203 -0.4746
0.1659 0 0.4863 0.1323 -0.2844 -0.123 -0.2505 0.0189 -0.6969 -0.3222 -0.1035 0.1815 -0.0675 0.0867
0.171 0.3831 0.0003 -0.0612 0.2907 0.6285 -0.1347 0\r"

pause 5 ; Give Tcp/Ip time to send the data

;-----

; Wait for time to be set
send * "log rangeb ontime 5.0\r"
label WaitForTime
    jump TimeIsSet GpsSet() == TRUE
    pause 1.0
    jump WaitForTime
label TimeIsSet

; Make sure the script doesn' start near the week rollover so that the GPS
; week number and weekseconds are from the same week
jump WaitForTime GpsWeekSecs() > 7.0*24.0*3600.0-60.0

;-----

; We now declare the start time that is aligned with the logging interval.
; The first file will be shorter than the rest.
iGpsWeek = GpsWeek()
dGpsWeekSecs = (Floor(GpsWeekSecs()/dFileInterval))*dFileInterval

; Start the logs that never stop
send rcvr "log rawsinb ontime 1.0\r"

; Used to synchronize file times, have it come out 0.2 seconds after the second.
; Not logged to disk.

```

```

send rcvr "log timeb ontime 1.0 0.2\r"

; For the first time, set up the pathed directory and wait for the next logging interval
gosub SetupNextFile TRUE

;-----

; Loop Forever
Label again

; Log until the end of the logging interval
gpstime %iStopWeek% %6.0dStopWeekSecs%

; Once again, set up the pathed directory and wait for the next logging interval
gosub SetupNextFile FALSE

; Set the PC clock with the GPS card time plus extra to compensate for transmit delay
; The value 1.6 was derived from TIMECHECK data found in RCVR_01jan08.SLI
; This script does not require PC time to be set accurately.
SetPcTime(EstGpsWeek(), EstGpsWeekSecs()+1.6)

; Do this until operator hits "Q"

jump again

;-----

End

```

## 7.2 PHP CODE FOR NOTTINGHAM STATION

### 1. *PHP code for Nottingham station: DB population*

```
<?

#### data to DB connection ####

include("conn/connect.php");

#### selection of nott0 station ####

$idstazione = 5;
$query_stazione = "SELECT nome, latitudine, longitudine, path_src,
path_raw, path_dest FROM ingv_isacco_stazioni WHERE
idstazione='$idstazione'";
$result_stazione = mysql_query($query_stazione, $db2);
$row_stazione = mysql_fetch_array($result_stazione);
$nomestazione = $row_stazione['nome'];
// deg2rad - Convertè il numero in gradi
$lat = deg2rad($row_stazione['latitudine']);
$long = deg2rad($row_stazione['longitudine']);
$path_src = $row_stazione['path_src'];
$path_raw = $row_stazione['path_raw'];
$path_dest = $row_stazione['path_dest'];

#### file selection ####

$query3 = "SELECT qid, dir, filetoscan FROM
ingv_isacco_". $nomestazione. "_queue ORDER BY filetoscan LIMIT 0,1";
$result3 = mysql_query($query3, $db2);
$num3 = mysql_num_rows($result3);

if ($num3 >= 1) {

    while ($row3 = mysql_fetch_array($result3)) {
        $qid = intval($row3['qid']);
        $dir = $row3['dir'];
        $filetoscan = $row3['filetoscan'];
        #echo "coda numero $qid\n\r";
        #### inizio scansione

        $srcfilename = "$dir/$filetoscan";
        $destfilenametemp = "$dir/ext.tmp";

        #### Poco Elegante ma efficace. :( ####
        $win_cmd_temp = "C:\\Inetpub\\ParseIsmr.exe all $srcfilename
$destfilenametemp";
        exec($win_cmd_temp); // Esegue un programma esterno
        #$handle2 = file($destfilenametemp) or die("non indicizzato!");

        if (!file($destfilenametemp)) {
            $query4 = "DELETE FROM ingv_isacco_". $nomestazione. "_queue
WHERE qid = '$qid'";
            mysql_query($query4, $db2);
            $noindex_srcfilename = "$dir/no_index/$filetoscan";
            copy($srcfilename, $noindex_srcfilename);
            unlink($srcfilename);
            die($query4);
        }
    }
}

```

```

    } else {
    $handle2 = file($destfilenametemp);
    $riga1 = $handle2[1];
    $arg1 = explode(",", $riga1);
    $week1 = $arg1[0];
    $gpstow1 = $arg1[1];
    $ts_gps1 = $week1 *7*24*60*60 + $gpstow1;
    $ts_sat1 = 315964800+$ts_gps1;
    $year = strftime("%Y", $ts_sat1);
    $month = strftime("%m", $ts_sat1);
    $day = strftime("%d", $ts_sat1);
    $hour = strftime("%H", $ts_sat1);
    $min = strftime("%M", $ts_sat1);
    unset($riga1);
    unset($arg1);
    unlink($destfilenametemp);
    }
    #echo $year."\n";
    #####

    $totallen = strlen($filetoscan);
    $lennoext = $totallen -4;
    $filenoext = substr($filetoscan,0,$lennoext);

    $tsfile = mktime($hour,$min,0,$month,$day,$year);

##### Deve essere sostituito con i timestamp dei momenti in cui i
formati son cambiati #####
#if ($year == '2003') {
#   $filenameest = "$filenoext.EST";
#   $filenameraw = eregi_replace("sec60", "rwd", $filetoscan);
#} else {
# if ($tsfile < '1097334000') {
#   $filenameest = "$filenoext.EST";
#   $filenameraw = eregi_replace("sec60", "rwd", $filetoscan);
# } elseif ($tsfile <= '1162249200') {
#   $filenameest = "$filenoext.EST";
#   $yearsmall = substr($year,2,2);
#   $filenameraw = "$yearsmall".".$month".".$day".".$hour".".SRD";
# } else {
#   $filenameest = "$filenoext.EST";
#   $filenameraw = "$filenoext.SRD";
# }

    $jday = strftime("%j", $tsfile);
    $destfilename = "$path_dest/$year/$jday/$filenameest";
    $srcfileraw = "$dir/$filenameraw";
    $destrawfile = "$path_raw/$year/$jday/$filenameraw";

    $tabletocreate =
"ingv_isacco_"$nomestazione."_".$year."_".$month."";

    $query5 = "CREATE TABLE IF NOT EXISTS $tabletocreate (
    `scintid` int( 100 ) NOT NULL AUTO_INCREMENT ,
    `idstazione` int( 3 ) NOT NULL default '0',
    `destfilename` varchar( 255 ) NOT NULL default '',
    `rawfilename` varchar( 255 ) NOT NULL default '',
    `srcfilename` varchar( 255 ) NOT NULL default '',
    `week` int( 4 ) NOT NULL default '0',
    `gpstow` double( 8, 2 ) NOT NULL default '0.00',
    `prn` int( 2 ) NOT NULL default '0',

```

```

`rxstatus` varchar( 8 ) NOT NULL default '0',
`az` double( 5, 2 ) NOT NULL default '0.00',
`elv` double( 4, 2 ) NOT NULL default '0.00',
`l1cno` double( 4, 2 ) NOT NULL default '0.00',
`s4raw` double( 14, 6 ) NOT NULL default '0.000000',
`s4cor` double( 14, 6 ) NOT NULL default '0.000000',
`s4` double( 14, 6 ) NOT NULL default '0.000000',
`sec1sigma` double( 14, 6 ) NOT NULL default '0.000000',
`sec3sigma` double( 14, 6 ) NOT NULL default '0.000000',
`sec10sigma` double( 14, 6 ) NOT NULL default '0.000000',
`sec30sigma` double( 14, 6 ) NOT NULL default '0.000000',
`sec60sigma` double( 14, 6 ) NOT NULL default '0.000000',
`codecarrier` double( 14, 6 ) NOT NULL default '0.000000',
`ccstdev` double( 5, 3 ) NOT NULL default '0.000',
`tec45` double( 14, 6 ) NOT NULL default '0.000000',
`tecrate45` double( 14, 6 ) NOT NULL default '0.000000',
`tec30` double( 14, 6 ) NOT NULL default '0.000000',
`tecrate30` double( 14, 6 ) NOT NULL default '0.000000',
`tec15` double( 14, 6 ) NOT NULL default '0.000000',
`tecrate15` double( 14, 6 ) NOT NULL default '0.000000',
`tec0` double( 14, 6 ) NOT NULL default '0.000000',
`tecrate0` double( 14, 6 ) NOT NULL default '0.000000',
`l1locktime` double( 14, 6 ) NOT NULL default '0.000000',
`chanstatus` varchar( 12 ) NOT NULL default '',
`l2locktime` double( 14, 6 ) NOT NULL default '0.000000',
`l2cno` double( 14, 6 ) NOT NULL default '0.000000',
`vtec` double( 14, 6 ) NOT NULL default '0.000000',
`YPP` double( 14, 6 ) NOT NULL default '0.000000',
`IPP350LAT1` double( 4, 3 ) NOT NULL default '0.000',
`IPP350LONG1` double( 4, 3 ) NOT NULL default '0.000',
`IPP350LAT2` double( 5, 2 ) NOT NULL default '0.00',
`IPP350LONG2` double( 5, 2 ) NOT NULL default '0.00',
`ts_sat` int( 10 ) NOT NULL default '0',
`ts_gps` int( 10 ) NOT NULL default '0',
PRIMARY KEY ( `scintid` ) ,
KEY `prn` ( `prn` ) ,
KEY `ts_sat` ( `ts_sat` ) ) ENGINE = InnoDB DEFAULT CHARSET =
latin1 AUTO_INCREMENT =0";
mysql_query($query5, $db2);

```

```

#echo "$query5\n\n$srcfilename ($totalen $lennoext $filenoext)
$filenameest - $filenameraw ($jday) $destfilename\n";

```

```

#### controllo se i files sono stati scansionati ####
$query2 = "SELECT destfilename FROM $tabletocreate WHERE
destfilename='$destfilename' limit 0,1";
$result2 = mysql_query($query2, $db2);
@$num2 = mysql_num_rows($result2);

```

```

$path_destyear = "$path_dest/$year";
if (!file_exists($path_destyear)) {
mkdir($path_destyear);
}

```

```

$path_destjday = "$path_destyear/$jday";
if (!file_exists($path_destjday)) {
mkdir($path_destjday);
}

```

```

$path_srcyear = "$path_src/$year";
if (!file_exists($path_srcyear)) {

```

```

mkdir($path_srcyear);
}

$path_srcjday = "$path_srcyear/$jday";
if (!file_exists($path_srcjday)) {
mkdir($path_srcjday);
}

$path_rawyear = "$path_raw/$year";
if (!file_exists($path_rawyear)) {
mkdir($path_rawyear);
}

$path_rawjday = "$path_rawyear/$jday";
if (!file_exists($path_rawjday)) {
mkdir($path_rawjday);
}

$sourcefilename = "$path_srcjday/$filetoscan";

if (!file_exists($destfilename)) {
$win_cmd = "C:\\Inetpub\\ParseIsmr.exe all $srcfilename
$destfilename";
exec($win_cmd);
}
if (!file_exists($sourcefilename)) {
copy($srcfilename, $sourcefilename);
}
if (file_exists($srcfileraw)) {
copy($srcfileraw, $destrawfile);
unlink($srcfileraw);
} else {

### Nel caso i raw file siano zippati .Z ###

$zsrcfileraw = ".$srcfileraw.Z";
if (file_exists($zsrcfileraw)) {
$destrawfile = ".$destrawfile.Z";
copy($zsrcfileraw, $destrawfile);
unlink($zsrcfileraw);

} else {

### Nel caso i raw file mancano inserisco il dato nella tabella
raw_mancanti

$sql = "INSERT INTO ingv_raw_mancanti VALUES (NULL,
'$nomestazione', ".$day.". ".$month.". ".$year." ".$hour." : ".$min."',
'$srcfileraw')";
mysql_query($sql, $db2);
}
}
unlink($srcfilename);

$i = 0;

$handle1 = file($destfilename) or die("non indicizzato!");

foreach ($handle1 as $riga) {

    $i++;

```

```

if ($i != '1') {
$arg = explode(",", $riga);
$week = trim($arg[0]);
$gpstow = trim($arg[1]);

$sts_gps = $week *7*24*60*60 + $gpstow;
$sts_sat = 315964800+$sts_gps;
$prn = trim($arg[2]);
$rxstatus = trim($arg[3]);
$az = trim($arg[4]);
$elv = trim($arg[5]);
$l1cno = round(trim($arg[6]),6);
$s4raw = round(trim($arg[7]),6);
$s4cor = round(trim($arg[8]),6);
$secsigma1 = round(trim($arg[9]),6);
$secsigma3 = round(trim($arg[10]),6);
$secsigma10 = round(trim($arg[11]),6);
$secsigma30 = round(trim($arg[12]),6);
$secsigma60 = round(trim($arg[13]),6);
$codecarrier = round(trim($arg[14]),6);
$ccstdev = round(trim($arg[15]),6);
$tec45 = round(trim($arg[16]),6);
$tecrate45 = round(trim($arg[17]),6);
$tec30 = round(trim($arg[18]),6);
$tecrate30 = round(trim($arg[19]),6);
$tec15 = round(trim($arg[20]),6);
$tecrate15 = round(trim($arg[21]),6);
$tec0 = round(trim($arg[22]),6);
$tecrate0 = round(trim($arg[23]),6);
$l1locktime = round(trim($arg[24]),6);
$chanstatus = trim($arg[25]);
$l2locktime = round(trim($arg[26]),6);
$l2cno = round(trim($arg[27]),6);

    if ($s4raw > $s4cor) {
        $s4 = sqrt($s4raw*$s4raw-$s4cor*$s4cor);
        $s4 = round($s4,6);
    } else {
        $s4 = 0;
    }

$az1 = deg2rad($az);
$elv1 = deg2rad($elv);
$vttec = $tec0*(cos(M_PI/2 - $elv1));
#### radianti ####
$YPP = M_PI/2 - $elv1 - (asin(0.948*(cos($elv1))));
$YPP = round($YPP,6);
$IIPP350LAT1 =
asin(sin($lat)*cos($YPP)+cos($lat)*sin($YPP)*cos($az1));
$IIPP350LAT1 = round($IIPP350LAT1,3);
$IIPP350LONG1 =
$long+asin(sin($YPP)*sin($az1)/cos($IIPP350LAT1));
$IIPP350LONG1 = round($IIPP350LONG1,3);
#### gradi ####
$IIPP350LAT2 = rad2deg($IIPP350LAT1);
$IIPP350LAT2 = round($IIPP350LAT2,2);
$IIPP350LONG2 = rad2deg($IIPP350LONG1);
$IIPP350LONG2 = round($IIPP350LONG2,2);
#### Inserimento nel database ####
if ($num2 != '0') {
    #### Gestione file già inseriti ####

```

```

        if ($i == 2) {
            ##### Alla prima riga del file, prima dell'inserimento,
            cancello tutti i record già inseriti in passato #####
            $query5 = "DELETE FROM $tabletocreate WHERE
            destfilename='$destfilename'";
            mysql_query($query5, $db2);
            #echo "Sovrascrittura file\n\r";
        }
        } else {
            #echo "Nuovo inserimento\n\r";
        }
        ##### Inserimento #####
        $query = "INSERT INTO $tabletocreate VALUES (NULL,
        $idstazione, '$destfilename', '$destrawfile', '$sourcefilename',
        '$week', '$gpstow', '$prn', '$rxstatus', '$az', '$elv', '$l1cno',
        '$s4raw', '$s4cor', '$s4', '$secsigma1', '$secsigma3', '$secsigma10',
        '$secsigma30', '$secsigma60', '$codecarrier', '$ccstdev', '$tec45',
        '$tecrate45', '$tec30', '$tecrate30', '$tec15', '$tecrate15',
        '$tec0', '$tecrate0', '$l1locktime', '$chanstatus', '$l2locktime',
        '$l2cno', '$vtec', '$YPP', '$IPP350LAT1', '$IPP350LONG1',
        '$IPP350LAT2', '$IPP350LONG2', '$ts_sat', '$ts_gps')";
        mysql_query($query, $db2);

        ##### debug tool!
        #####
        #####
        #echo "$query<br>";
        #echo "$week $gpstow $prn $az $elv $tec0 $deg $vtec $YPP
        $IPP350LAT1 $IPP350LONG1 $IPP350LAT2 $IPP350LONG2 $ts_sat\n\n$query";

        #####
        #####
        }
    }
    $query4 = "DELETE FROM ingv_isacco_". $nomestazione. "_queue WHERE qid
    = '$qid'";
    mysql_query($query4, $db2);
    #echo "Rimozione file in coda: $query4 \n\n\n";
}
##### fine scansione
}
include("conn/disconnect.php");
?>

```

## 2. PHP code for Nottingham station: linear plot tool

```
<?
include("includes/session.php");
if (($_SESSION['level'] >= 2) AND ($_SESSION['status'] == 1)) {

include("includes/header_int_1024.php");

#### Evaluation of the year ####

$timestamp_now = strtotime("now");
$yearnow = date('Y', $timestamp_now);
$monthnow = date('n', $timestamp_now);
$daynow = date('j', $timestamp_now);
$hournow = date('H', $timestamp_now);
$minnow = date('i', $timestamp_now);
#if ($minnow >= 20) { $last = "newhour"; } else { $last = "prehour";
}

#### database connection ####

#### array caratteristiche ####

include("includes/arraytipoval.php");

#### Controllo sull'inserimento dei dati per la ricerca ####

#### Selection of the station ####

    if (isset($_POST['idstazione'])) { $idstazione =
intval($_POST['idstazione']); } else {
    if (isset($_GET['idstazione'])) { $idstazione =
intval($_GET['idstazione']); } else { $idstazione = 1; }
}
$query_stazione = "SELECT min_elv, min_lllocktime, nome FROM
ingv_isacco_stazioni WHERE idstazione='$idstazione'";
$result_stazione = mysql_query($query_stazione, $db2);
$row_stazione = mysql_fetch_array($result_stazione);
$nomestazione = $row_stazione['nome'];
#if ($_POST['minelv'] != '') { $minelv = intval($_POST['minelv']);
} else { $minelv = $row_stazione['min_elv']; }
#if ($_POST['minlllocktime'] != '') { $minlllocktime =
intval($_POST['minlllocktime']); } else { $minlllocktime =
$row_stazione['min_lllocktime']; }

    if ($_POST['minelv'] != '') {
        if (preg_match("/^[0-9]{1,2}$/i", $_POST['minelv'])) {
            $minelv = intval($_POST['minelv']);
        } else {
            $minelv = $row_stazione['min_elv'];
        }
    } else {
        $minelv = $row_stazione['min_elv'];
    }

    if ($_POST['minlllocktime'] != '') {
        if (preg_match("/^[0-9]{1,3}$/i", $_POST['minlllocktime'])) {
            $minlllocktime = intval($_POST['minlllocktime']);
        } else {
            $minlllocktime = $row_stazione['min_lllocktime'];
        }
    }
}
```

```

    } else {
        $minl1locktime = $row_stazione['min_l1locktime'];
    }

if (($_POST['sday'] != '') AND ($_POST['smmonth'] != '') AND
($_POST['syear'] != '') AND ($_POST['shour'] != '')) {

#### Dati Inseriti: Valore richiesto di default: Track ####

$yday = $_POST['sday'];
$smmonth = $_POST['smmonth'];
$syear = $_POST['syear'];
$shour = $_POST['shour'];

} else {

#### Dati non inseriti: apertura della pagina per la prima volta,
Valore richiesto di default: Track ####

#### Dati non inseriti: apertura della pagina per la prima volta,
Valore richiesto di default: Track ####

#$yday = $daynow;
#$smmonth = $monthnow;
#$syear = $yearnow;
#$shour = $hournow-1;

#### Calcolo ultimo intervallo orario disponibile ####

    $risultatol = mysql_list_tables('ingv');

    while ($rigal = mysql_fetch_array($risultatol)) {
        if (eregi($nomestazione, $rigal[0])) {
            if(!eregi("queue", $rigal[0])) {
                $tabscint[] = $rigal[0];
            }
        }
    }
    $last = (count($tabscint))-1;
    $table_lastdata = $tabscint[$last];

$querylast = "SELECT ts_sat FROM $table_lastdata ORDER by ts_sat DESC
LIMIT 0,1";
$reslast = mysql_query($querylast, $db2);
$rowlast = mysql_fetch_array($reslast);
$timestamp_last = $rowlast['ts_sat'];
$syear = date('Y', $timestamp_last);
$smmonth = date('n', $timestamp_last);
$syday = date('j', $timestamp_last);
$shour = date('G', $timestamp_last);
$smin = date('i', $timestamp_last);

if ($smin == '00') { $shour = $shour-1; }

$prn[0] = 0;

}

        if (!isset($_POST['typeview'])) { $sel[4] = "checked"; $sel[5]
= "checked"; } else {
            foreach ($_POST['typeview'] as $tv) {

```

```

        $sel[$tv] = "checked";
    }
}
echo "<center>\n";

echo "<table width=\"760\" border=\"0\" cellspacing=\"0\"
cellpadding=\"1\">"
."<form
action=\"view_scint_linear.php?idstazione=$idstazione\"
method=\"post\">\n"
." <tr>\n"
." <td align=\"right\" class=\"sometd\">
$arraynamenu[4]</td>\n"
." <td><input type=\"checkbox\" name=\"typeview[]\"
value=\"4\" $sel[4]></td>\n"
." <td align=\"right\" class=\"sometd\">
$arraynamenu[5]</td>\n"
." <td><input type=\"checkbox\" name=\"typeview[]\"
value=\"5\" $sel[5]></td>\n"
." <td align=\"right\" class=\"sometd\">
$arraynamenu[6]</td>\n"
." <td><input type=\"checkbox\" name=\"typeview[]\"
value=\"6\" $sel[6]></td>\n"
." <td align=\"right\" class=\"sometd\">
$arraynamenu[7]</td>\n"
." <td><input type=\"checkbox\" name=\"typeview[]\"
value=\"7\" $sel[7]></td>\n"
." <td align=\"right\" class=\"sometd\">
$arraynamenu[8]</td>\n"
." <td><input type=\"checkbox\" name=\"typeview[]\"
value=\"8\" $sel[8]></td>\n"
." <td align=\"right\" class=\"sometd\">
$arraynamenu[9]</td>\n"
." <td><input type=\"checkbox\" name=\"typeview[]\"
value=\"9\" $sel[9]></td>\n"
." <td align=\"right\" class=\"sometd\">
$arraynamenu[10]</td>\n"
." <td><input type=\"checkbox\" name=\"typeview[]\"
value=\"10\" $sel[10]></td>\n"
." </tr>\n"
." <tr>\n"
." <td align=\"right\" class=\"sometd\">
$arraynamenu[11]</td>\n"
." <td><input type=\"checkbox\" name=\"typeview[]\"
value=\"11\" $sel[11]></td>\n"
." <td align=\"right\" class=\"sometd\">
$arraynamenu[12]</td>\n"
." <td><input type=\"checkbox\" name=\"typeview[]\"
value=\"12\" $sel[12]></td>\n"
." <td align=\"right\" class=\"sometd\">
$arraynamenu[13]</td>\n"
." <td><input type=\"checkbox\" name=\"typeview[]\"
value=\"13\" $sel[13]></td>\n"
." <td align=\"right\" class=\"sometd\">
$arraynamenu[14]</td>\n"
." <td><input type=\"checkbox\" name=\"typeview[]\"
value=\"14\" $sel[14]></td>\n"
." <td align=\"right\" class=\"sometd\">
$arraynamenu[15]</td>\n"
." <td><input type=\"checkbox\" name=\"typeview[]\"
value=\"15\" $sel[15]></td>\n"

```

```

        ."      <td align=\"right\" class=\"sometd\">
$arraynamenu[16]</td>\n"
        ."      <td><input type=\"checkbox\" name=\"typeview[]\"
value=\"16\" $sel[16]></td>\n"
        ."      <td align=\"right\" class=\"sometd\">
$arraynamenu[17]</td>\n"
        ."      <td><input type=\"checkbox\" name=\"typeview[]\"
value=\"17\" $sel[17]></td>\n"
        ."    </tr>\n"
        ."    <tr>\n"
        ."      <td align=\"right\" class=\"sometd\">&nbsp;</td>\n"
        ."      <td>&nbsp;</td>\n"
        ."      <td align=\"right\" class=\"sometd\">&nbsp;</td>\n"
        ."      <td>&nbsp;</td>\n"
        ."      <td align=\"right\" class=\"sometd\">
$arraynamenu[3]</td>\n"
        ."      <td><input type=\"checkbox\" name=\"typeview[]\"
value=\"3\" $sel[3]></td>\n"
        ."      <td align=\"right\" class=\"sometd\">
$arraynamenu[18]</td>\n"
        ."      <td><input type=\"checkbox\" name=\"typeview[]\"
value=\"18\" $sel[18]></td>\n"
        ."      <td align=\"right\" class=\"sometd\">
$arraynamenu[19]</td>\n"
        ."      <td><input type=\"checkbox\" name=\"typeview[]\"
value=\"19\" $sel[19]></td>\n"
        ."      <td align=\"right\" class=\"sometd\">&nbsp;</td>\n"
        ."      <td>&nbsp;</td>\n"
        ."      <td align=\"right\" class=\"sometd\">&nbsp;</td>\n"
        ."      <td>&nbsp;</td>\n"
        ."    </tr>\n"
        ."  </table>\n";

```

```

echo "<div id=\"form\"><table cellpadding=\"3\"
cellspacing=\"0\"><tr>\n"
        ."<td align=\"right\" class=\"sometd\">Station
</td><td><select name=\"idstazione\">\n";

```

```

$query9 = "SELECT idstazione, nome FROM ingv_isacco_stazioni";
$result9 = mysql_query($query9, $db2);
while ($row9 = mysql_fetch_array($result9)) {
    $selidstazione = $row9['idstazione'];
    $sel[$idstazione] = "SELECTED";
    echo "<option value=\"".$selidstazione\"
\".$sel[$selidstazione].\">".$row9['nome'].\"</option>\n";
}

```

```

echo "</select></td>\n"
        ."<td align=\"right\" class=\"sometd\">from </td>\n"
        ."<td><select name=\"syear\">\n"
        ."<option value=\"".$syear.\">$syear</option>\n";
$resultato1 = mysql_list_tables('ingv');
if($_GET['idstazione'] == "2"){
    $tipotabella = "btn0";
}
else
if($_GET['idstazione'] == "3"){
    $tipotabella = "lyb0";
}
else
if($_GET['idstazione'] == "4"){
    $tipotabella = "nyal";
}
else

```

```

if($_GET['idstazione'] == "5"){
    $tipotabella = "not0";
}else{
    $tipotabella = "nya0";
}

$oldy = "";
while ($riga1 = mysql_fetch_array($risultatol)) {
    if (eregi($tipotabella, $riga1[0])) {
        if(!eregi("queue", $riga1[0])) {
            $explode = explode("_", $riga1[0]);
            if($oldy != $explode[3]){
                $array[] = $explode[3];
                $oldy = $explode[3];}
        }
    }
}
rsort($array);
foreach($array as $anno){
    echo "<option value=\"".$anno."\">".$anno."</option>\n";
}
#for ($y = $yearnow; $y >= 1970; $y--) {
#echo "<option value=\"$y\">$y</option>\n";
#}
echo "</select></td>\n"
    ."<td><select name=\"smonth\">\n"
    ."<option value=\"$smonth\">$smonth</option>\n";
for ($m = 1; $m <= 12; $m++) {
    echo "<option value=\"$m\">$m</option>\n";
}
echo "</select></td>\n"
    ."<td><select name=\"sday\">\n"
    ."<option value=\"$sday\">$sday</option>\n";
for ($d = 1; $d <= 31; $d++) {
    echo "<option value=\"$d\">$d</option>\n";
}
if ($shour != '') {
    $fhour = $shour+1;
    if ((strlen($shour)) == '1') { $shour = "0$shour"; }
    if ((strlen($fhour)) == '1') { $fhour = "0$fhour"; }
    if ($fhour == 24) { $fhour = "00"; }
    $setfhour = "-$fhour";
}
echo "</select></td>\n"
    ."<td align=\"right\" class=\"sometd\">hour [UT]</td>\n"
    ."<td><select name=\"shour\">\n"
    ."<option value=\"$shour\">".$shour.":00</option>\n";
for ($h = 0; $h <= 23; $h++) {
    $f = $h+1;
    if ((strlen($h)) == '1') { $h = "0$h"; }
    if ((strlen($f)) == '1') { $f = "0$f"; }
    if ($f == 24) { $f = "00"; }
    echo "<option value=\"$h\">".$h.":00</option>\n";
}

foreach ($_POST['prn'] as $prnlist) {
    $sele[$prnlist] = "selected";
}
if ((count($sele)) == 0) { $sele[0] = "selected"; }
if ($_POST['daily'] == '1') { $chkdaily = "checked"; } else {
$chkhourly = "checked"; }

```



### 7.3 FORTRAN CODE FOR THE CONVERTER

format.f

```

      program format
      character*80 ad
      character*80 station,month
      integer iweek,iprn,imonth,iday,iyear,iy
      real*8 tow,s4,s4corr,sigmaphi,vtec,l1cn,l2cn,azimut,elev
      real*8 phi0r,alf,lamr,finals4
      real*8 lam0r,radzenit,zenit,radazimut
c     Reading Station and Date info from filelist.txt
      open(10,file='filelist.txt',status='old')
      read(10,100) station,iy,month,iday
100   format(a5,1x,i2,a3,i2)
101   format (i4,1x,i2,1x,i2,1x,i2,1x,i2,1x,i4,1x,i2,1x,f8.6,1x,
+       f8.6,1x,f10.6,1x,f5.2,1x,f5.2,1x,f5.2,1x,f6.2,1x,f5.2)

c     Conversion to 200X format
      iyear=iy+2000

c     Date string to integer conversion
      if (month.eq.'jan') imonth = 1
      if (month.eq.'feb') imonth = 2
      if (month.eq.'mar') imonth = 3
      if (month.eq.'apr') imonth = 4
      if (month.eq.'may') imonth = 5
      if (month.eq.'jun') imonth = 6
      if (month.eq.'jul') imonth = 7
      if (month.eq.'aug') imonth = 8
      if (month.eq.'sep') imonth = 9
      if (month.eq.'oct') imonth = 10
      if (month.eq.'nov') imonth = 11
      if (month.eq.'dec') imonth = 12

c     Opening input data file
      open(8,file='tempfile.dat',status='old')
c     Reading header
      read(8,'(a)') ad
c     Opening output data file
      open(9,file='data.dat',status='new')

c     Setting right latitude and longitude
      if (station.eq.'nsf01') then
        phi0r=70.691878 * 3.14 /180
        lam0r=23.723089 * 3.14 /180
        write(*,*) 'Hammerfest station data conversion'
      else if (station.eq.'nsf03') then
        phi0r=65.462089 * 3.14 /180
        lam0r=12.216433 * 3.14 /180
        write(*,*) 'Bronnysund station data conversion'
      else if (station.eq.'nsf05') then
        phi0r=60.393533 * 3.14 /180
        lam0r=5.270753 * 3.14 /180
        write(*,*) 'Bergen station data conversion'
      else if (station.eq.'nsf06') then
        phi0r=52.940728 * 3.14 /180
        lam0r=1.192325 * 3.14 /180
        write(*,*) 'Nottingham station data conversion'
      else
        write(*,*) 'Unrecognized station: exiting'
```

```

        goto 999
    endif

c     Earth radius in km
    rz = 6370

c     Loop on data and UT determination
    do j=1,100000
        read(8,*,err=999,end=999) tow,iweek,iprn,s4,s4corr,
+     sigmaphi,vtec,l1cn,l2cn,azimut,elev

c     UT
        time=(((tow/86400.)-int(tow/86400.))*24)
        ih=int(((tow/86400.)-int(tow/86400.))*24)
        im=int((((tow/86400.)-int(tow/86400.))*24-ih)*60)

c     Zenit determination
        zenit=90-elev
        radzenit=zenit*3.14/180
c     write(*,*) 'radzenit =',radzenit

c     Azimut
        radazimut=azimut*3.14/180
c     write(*,*) 'radazimut=',radazimut

c     Angle between geocentre and observing station
c     from the satellite
        sbet=rz*sin(radzenit)/(rz+350)
        bet=asin(sbet)
c     write(*,*) sbet,bet

c     Angle from the geocenter between observer and satellite
        alf=radzenit-bet
c     write(6,*) alf

c     Geographic latitude of subsatellite point
        phir=asin(sin(phi0r)*cos(alf)+cos(phi0r)*sin(alf)*
+cos(radazimut))
c     write(*,*) phir

c     Geographic longitude of subsatellite point
        slam=sin(alf)*sin(radazimut)/cos(phir)
        clam=(cos(alf)-sin(phi0r)*sin(phir))/cos(phi0r)/cos(phir)
        lamr=lam0r+atan2(slam,clam)
c     write(*,*) lamr,slam,clam,atan2(slam,clam)

        finals4=sqrt(s4*s4-s4corr*s4corr) !s4 definition
c     Write on output file
        if (vtec.lt.300..and finals4.lt.2..and sigmaphi.lt.2.
+and.vtec.gt.-100..and finals4.gt.0..and sigmaphi.gt.0.
+ .and.l1cn.lt.100..and.l1cn.gt.0..and.l2cn.lt.100.
+ .and.l2cn.gt.0..and.elev.gt.15.) then

            write(9,101) iyear,imonth,iday,ih,im,iweek,iprn,finals4,
+             sigmaphi,vtec,l1cn,l2cn,phir*180/3.14,lamr*180/3.14,elev
        endif
    enddo
999  continue
    stop
end

```

#### 7.4 WATCHDOG SCRIPT IMPLEMENTED ON THE NOTTINGHAM GISTM STATION.

Watchdog.bat is a batch file that starts every 15 minutes just after the data file is closed.

```
@ECHO OFF
REM Watch Dog
REM 5 s waited
PING 1.1.1.2 -n 1 -w 15000 >NUL

REM PING 1.1.1.1 -n 5 >NUL
REM TYPE NUL | CHOICE.COM /N /CY,5 >NUL

REM Year, month and day from date command
for /f "tokens=1,2,3 delims=/" %%a in ("%date%") do set day=%%a&set month=%%b&set year=%%c
REM ECHO. day=%day%, month=%month%, year=%year%
REM Hour and minute from time command
for /f "tokens=1,2 delims=:" %%a in ("%time%") do set hh=%%a&set mm=%%b
REM ECHO. hh=%hh%, mm=%mm%

IF %hh% LSS 10 set h=%hh: =%

REM check the minutes
FOR /L %%i IN (0,1,9) DO IF %mm%==0%%i SET quarto=00
FOR /L %%i IN (10,1,14) DO IF %mm%==%%i SET quarto=00
FOR /L %%i IN (15,1,29) DO IF %mm%==%%i SET quarto=15
FOR /L %%i IN (30,1,44) DO IF %mm%==%%i SET quarto=30
FOR /L %%i IN (45,1,59) DO IF %mm%==%%i SET quarto=45

SET percorso=indices\%year%_%month%_%day%
SET nomefile=NSF6S_%year:~2,2%%month%%day%%hh%%quarto%.S60
IF %hh% LSS 10 SET nomefile=NSF6S_%year:~2,2%%month%%day%0%h%%quarto%.S60

ECHO.The file is: %percorso%\%nomefile%
ECHO. %time% %month% %day% %hh% %mm% >> craig.txt
REM ECHO. quarto=%quarto%, mm= %mm%, hh=%hh%
IF EXIST %percorso%\%nomefile% ECHO. The file %percorso%\%nomefile% EXISTS!!! >> craig.txt
IF NOT EXIST %percorso%\%nomefile% ECHO.The file %percorso%\%nomefile% DOESN'T EXIST!!! >>
craig.txt
REM IF NOT EXIST %percorso%\%nomefile% ECHO. %date%, %time%
IF NOT EXIST %percorso%\%nomefile% restart.bat

REM Command line to schedule the task:
REM SHTASKS /create /RU iszma /RP iszmarcio /SC MINUTE /MO 15 /TN DIK /TR
D:\New_Slog_NSF01\watchdog.bat /ST 10:15:20
```

## 7.5 SCRIPT TO SEND THE DATA IN REAL TIME TO ESWUA SYSTEM. IT IS IMPLEMENTED ON THE NOTTINGHAM GISTM STATION.

Every 15 minutes this python script (copy\_last\_15\_minutes.py) copies the last data file to the folder D:\New\_Slog\2Send\_eswua in the Nottingham station PC

```
#!/usr/bin/env python
# Script to copy files logged in the previous hour to raw-scint-1

import datetime
import os

# rcvr = ['NSF1', 'NSF6']

# for r in rcvr:
#   if r == 'NSF1':
#     baseraw = r'D:\New_Slog_NSF01\raw_data'
#     baseind = r'D:\New_Slog_NSF01\indices'
#   if r == 'NSF5':
#     baseraw = r'D:\New_Slog_NSF05\raw_data'
#     baseind = r'D:\New_Slog_NSF05\indices'
#   if r == 'NSF6':
#     baseraw = r'D:\New_Slog\raw_data'
#     baseind = r'D:\New_Slog\indices'

r = 'nsf6'
baseind = r'D:\New_Slog\indices'
print baseind

# last_hour = datetime.datetime.utcnow() - datetime.timedelta(hours = 1)

last_quarter = datetime.datetime.utcnow() - datetime.timedelta(minutes = 16)

# YYYY, MM, DD, HH = last_hour.timetuple()[0:4]

YYYY, MM, DD, HH, MN = last_quarter.timetuple()[0:5]

datedir = r'\%04d_%02d_%02d' % (YYYY, MM, DD)

# rawdir = baseraw + datedir
inndir = baseind + datedir

YY = str(YYYY)[2:4]

# rawfile = r'%s\%sR_%s%02i%02i%02i.RWD' % (rawdir, r, YY, MM, DD, HH)
# indfile = r'%s\%sS_%s%02i%02i%02i*.S60' % (inndir, r, YY, MM, DD, HH)
indfile = r'%s\%sS_%s%02i%02i%02i.S60' % (inndir, r, YY, MM, DD, HH, MN)
# dest = r'\128.243.138.50\in'
dest = r'D:\New_Slog\2Send_eswua'

# print last_hour
print last_quarter
print indfile
print dest
# if os.path.isfile(rawfile) and os.path.isdir(dest):
```

```
if os.path.isfile(indfile)and os.path.isdir(dest):
#   os.system('copy %s %s' % (rawfile, dest))
  os.system('copy %s %s' % (indfile, dest))
  os.system('sendS60file.bat')
else:
  print 'No files to copy for receiver ' + r
```

*SendS60file.bat* is called in the *copy\_last\_15\_minutes.py*, it is here reported. This batch file send by ftp the data to eswua by means of the wput.exe open source program (<http://wput.sourceforge.net/>)

```
@ECHO OFF
```

```
REM procedure to send the nottingham station data to eswua
```

```
cd D:\New_Slog\2Send_eswua
D:\Scripts_IESSG\wput.exe -R -t 0 -T 50 -o D:\New_Slog\outsend.txt
ftp://nottingham:iessg11@93.63.40.58/
cd D:\Scripts_IESSG
```

## 7.6 SCRIPT TO ACQUIRE 1 S RINEX DATA TO BE IMPLEMENTED IF NEED BE.

This slog acquisition script is ready to be used for the receiver acquisition of RINEX data with a sampling rate of 1s

```
; Script for rinex data logging at 1s sampling

;-----
define double dLogInterval
; Length of time to log in one file
dLogInterval = 3600
;-----

testname "Rinex Data Logging"
;Initiate communication with Novatel via COMx on PC
find com1 38400 rcvr none
pause 60 ; Give the enough time for the find to do its job
; Wait for time to be set
send rcvr "log rangeb ontime 1.0\r"
label WaitForTime
jump TimelsSet gpsset() == TRUE
pause 2.0
jump WaitForTime
label TimelsSet
; Make sure the script doesn't start near the rollover so that the GPS
; week number and weekseconds are from the same week
jump WaitForTime GPSWEEKSECS() > 604800.0-10.0

;-----

; Start logging (hourly) data files

define double dGpsWeek ; GPS week number
define double dGpsWeekSecs ; Seconds into the week
define double dHourOfWeek ; Hour into the week
define double dDayOfWeek ; Day into the week
define double dHourOfDay ; Hour into the day

define string danno
define string dmese
define string dgiorno
define string dminuto
define string aaaa

define string gpsfile ; Name of the file

define double dStopWeekSecs ; Seconds into the week at end of file
int iRinex

let dGpsWeek = GPSWEEK()
; GpsWeekSecs aligned with interval
let dGpsWeekSecs = (floor(GPSWEEKSECS()/dLogInterval))*dLogInterval

; Loop Forever

label again

; Clear the time set so that we can check the time offset
```

```

ResetTimeSet
; Give enough time for a new log to come out to see the new PC/GPS time offset
pause 1

; GPS file name

let dHourOfWeek = FLOOR(dGpsWeekSecs/3600.0) ; Hour of week
let dDayOfWeek = FLOOR(dHourOfWeek/24.0) ; Day of week
let dHourOfDay = dHourOfWeek - dDayOfWeek*24.0 ; Hour of day

let aaaa = midstr ( PCTIME(), 0, 4 )
let danna = midstr ( PCTIME(), 2, 2 )
let dmese = midstr ( PCTIME(), 5, 2 )
let dgiorno = midstr ( PCTIME(), 8, 2 )
let dminuto = midstr ( PCTIME(), 14, 2 )
let
                                gpsfile
                                =
"C:\data\rinex\%aaaa%_%dmese%_%dgiorno%\TESTX_%danna%_%dmese%_%dgiorno%02.0dHourOf
Day%.GPS"

print "dHourOfWeek = %dHourOfWeek%"
print "dDayOfWeek = %dDayOfWeek%"
print "dHourOfDay = %dHourOfDay%"

;let gpsfile = "%4.0dGpsWeek%_%1.0dDayOfWeek%_%02.0dHourOfDay%_%dminuto%"
;let gpsfiler = "%4.0dGpsWeek%_%1.0dDayOfWeek%_%02.0dHourOfDay%"

; Start the logging until the next hour
opencopyfile rcvr "%gpsfile%" append iRinex \
copyfile rcvr iRinex versiona 0.0
copyfile rcvr iRinex rxconfiga 0.0
copyfile rcvr iRinex rawephemb 0.0
copyfile rcvr iRinex bestposb 0.0
copyfile rcvr iRinex almanacb 0.0
copyfile rcvr iRinex rangeb 0.0
copyfile rcvr iRinex rxstatureventa 0.0
copyfile rcvr iRinex ionutca 0.0

send rcvr "log versiona once\r"
send rcvr "log rxconfiga once\r"
send rcvr "log rawephemb onnew\r"
send rcvr "log bestposb ontime 60.0\r"
send rcvr "log almanacb onnew\r"
send rcvr "log rangeb ontime 1.0\r"
send rcvr "log rxstatureventa onchanged\r"
send rcvr "log ionutca onchanged\r"

; Following commands set up logs -- last two are for collecting WAAS
; Ionospheric Correction Data to use for TEC Calibration
; send rcvr "log waas18B onchanged\r"
; send rcvr "log waas26B onchanged\r"

let dStopWeekSecs = dGpsWeekSecs+dLogInterval

; Log until the end of the logging interval

gpstime %0dGpsWeek% %6.0dStopWeekSecs%

```

```

; Increase GPS week seconds

let dGpsWeekSecs = dGpsWeekSecs + dLogInterval
if dGpsWeekSecs >= 604800.0
  let dGpsWeek = dGpsWeek + 1
  let dGpsWeekSecs = dGpsWeekSecs - 604800.0
endif

run "convert4 %gpsfile% -r -batch"
;pause 3.0
run      "rename          C:\data\rinex\%aaaa_%dmese_%dgiorno%\TEST???0.??N
TEST%dmese%%dgiorno%%02.0dHourOfDay%.??N"
run      "rename          C:\data\rinex\%aaaa_%dmese_%dgiorno%\TEST???0.??O
TEST%dmese%%dgiorno%%02.0dHourOfDay%.??O"

; run "copy %gpsfile% C:\send"

; spawn "sendS60.bat"

;pause 1.0

closecopyfile com1 iRinex

jump again

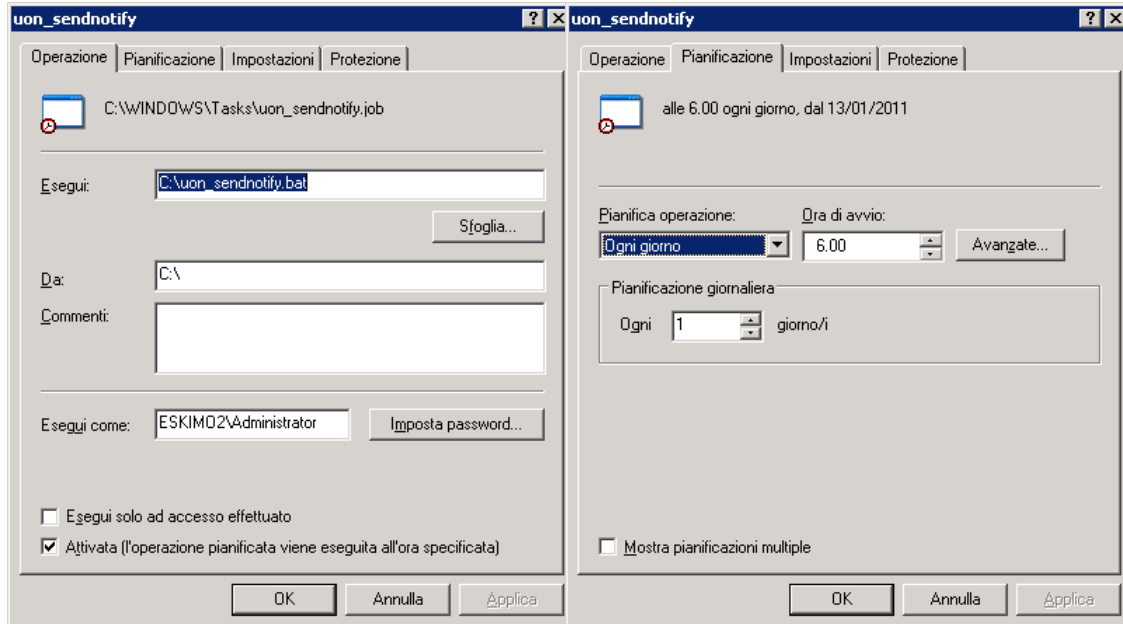
; Do this until operator hits "Q"

End

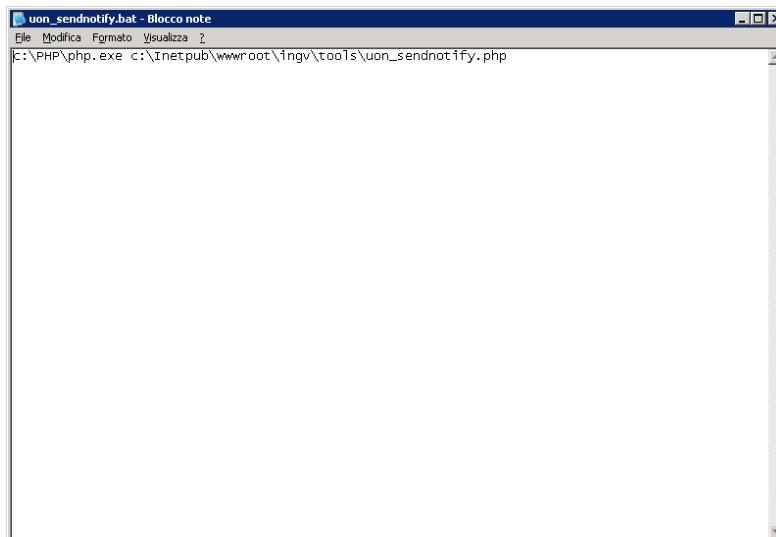
```

## 7.7 PHP PROGRAM TO SEND A DAILY EMAIL REPORTING THE STRUCTURED DATA FOR EACH STATION. IT IS IMPLEMENTED AT ESWUA SYSTEM.

*Email Report starts every day at 6.00 AM (UT). The scheduled task executes a batch script: uon\_sendnotify.bat*



*Batch Script executes a php script through the php interpreter.*



### PHP Script

```
<?  
# Extend Execution Time  
set_time_limit(270);
```

```

# Database connection Parametrs
include("../conn/connect_db_isacco.php");

# Start script timestamp
$timestamp_now = strtotime("now");

# Database tables list
$result = mysql_query('SHOW TABLES');
$totalrecords = 0;

while($row = mysql_fetch_row($result)) {

    # Select University of Nottingham Tables
    if ((preg_match("/ingv_uon/", $row[0])) AND (!preg_match("/_queue/", $row[0])) AND
        (!preg_match("/_summary/", $row[0]))) {
        $tt++;

        # Count records in tables and Compare with history summary
        $sql1 = "SELECT * FROM ingv_uon_summary WHERE tablename = ".$row[0]."";
        $res1 = mysql_query($sql1, $db);
        $num1 = mysql_num_rows($res1);

        $sql3 = "SELECT count(scintid) FROM ".$row[0]."";
        $res3 = mysql_query($sql3, $db);
        $row3 = mysql_fetch_array($res3);

        if ($num1 > 0) {
            $row1 = mysql_fetch_array($res1);

            # Update of history summary
            $sql2 = "UPDATE ingv_uon_summary SET numrecords=".$row3[0].",
lastindexing='$timestamp_now', lastnumrecords=".$row1['numrecords']."' WHERE tableid =
".$row1['tableid']."";
            mysql_query($sql2, $db);
            $tablerecords = $row3[0] - $row1['numrecords'];
        } else {
            # Insert in history summary
            $sql4 = "INSERT INTO ingv_uon_summary (tablename, lastindexing, numrecords) VALUES
('".$row[0]."', '$timestamp_now', ".$row3[0].")";
            mysql_query($sql4, $db);
            $tablerecords = $row3[0];
        }

        # Create text and html mail messages
        $msg .= "Sono stati indicizzati <b>$tablerecords</b> di <b>".$row3[0]."</b> records nella tabella
<b>".$row[0]."</b><br>";
        $msgtxt .= "Sono stati indicizzati $tablerecords di ".$row3[0]." records nella tabella
".$row[0]."\r\n";

        # Total records
        $totalrecords = $totalrecords + $tablerecords;
    }
}

# Update text and html messages with records information
if ($totalrecords == 0) {

```

```

        $msg = "Non è stato inserito alcun Record";
        $msgtxt = "Non è stato inserito alcun Record";
    } else {
        $msg .= "<br>Per un totale di <b>$totalrecords</b> records";
        $msgtxt .= "\r\nPer un totale di $totalrecords records";
    }

    # Using phpmailer to send email
    require("../conn/class.phpmailer.php");
    $msg_from = "eswua@ingv.it";
    $msg_from_name = "eSWua Project";
    $msg_subject = "Indexing Notify";
    $msg_to = "nottingham@volanet.it";
    $msg_to_name = "University of Nottingham Staff";

    $mail = new phpmailer();
    $mail->From = $msg_from;
    $mail->FromName = $msg_from_name;
    $mail->Host = "ultra.ingv.it";
    $mail->Mailer = "smtp";
    $mail->Subject = $msg_subject;
    $mail->Body = $msg;
    $mail->AltBody = $msgtxt;
    $mail->AddAddress($msg_to, $msg_to_name);
    $mail->Send();

    # Close database connection
    mysql_close($db);

?>

```

## 7.8 SUBROUTINE READMEANDATA.C OF THE GBSC TO INCLUDE CCSTDDEV AND C/N INTO THE MAPS.

```
void readmeandata(TH2 *hmean, TH2 *hsigma) {

    Bool_t fgStatOverflows = kFALSE;

    selegut=Form("%d",cutelev);
    cout << "readmeandata(...) << endl;
    if (Ycoordinates=="lat" || Ycoordinates=="mlat") {
        if (hemisphere == "North") {
            if (ymin < 0 && ymax < 0) {
                a=-ymax;
                b=-ymin;
                action="reverse";
                ymin=a;
                ymax=b;
            } else {
                action="normal";
            }
        }
        if (hemisphere == "South") {
            if (ymin > 0 && ymax > 0) {
                a=-ymax;
                b=-ymin;
                action="reverse";
                ymin=a;
                ymax=b;
            } else {
                action="normal";
            }
        }
    }

    if (Xcoordinates=="lat" || Xcoordinates=="mlat") {
        if (hemisphere == "North") {
            if (xmin < 0 && xmax < 0) {
                a=-xmax;
                b=-xmin;
                action="reverse";
                xmin=a;
                xmax=b;
            } else {
                action="normal";
            }
        }
        if (hemisphere == "South") {
            if (xmin > 0 && xmax > 0) {
                a=-xmax;
                b=-xmin;
                action="reverse";
                xmin=a;
                xmax=b;
            } else {
                action="normal";
            }
        }
    }
}
```

```

}

//loop on x and y
startx=xmin;
starty=ymin;
endy=ymax;
endx=xmax;

if ( (Ycoordinates=="lon" || Ycoordinates=="mlon") && ymin<=0 ) {
    endy = 360;
    starty = 0;
}
if ( (Xcoordinates=="lon" || Xcoordinates=="mlon") && xmin<=0 ) {
    endx = 360;
    startx = 0;
}

for (Float_t ix=startx; ix<endx; ix=ix+xstep) {
    for (Float_t iy=starty; iy<endy; iy=iy+ystep) {

        Float_t inx, iny;
        if (action == "reverse") {
            if ((Ycoordinates=="lat" && Xcoordinates=="mlat") || (Xcoordinates=="lat" &&
Ycoordinates=="mlat")) {
                inx=-ix-xstep;
                iny=-iy-ystep;
            } else {
                if (Ycoordinates=="lat" || Ycoordinates=="mlat") {
                    inx=ix;
                    iny=-iy-ystep;
                } else if (Xcoordinates=="lat" || Xcoordinates=="mlat") {
                    inx=-ix-xstep;
                    iny=iy;
                }
            }
        } else {
            inx=ix;
            iny=iy;
        }

        if ((Ycoordinates=="lon" || Ycoordinates=="mlon") && ymin<0 && iny>180) iny=iny-360;
        if ((Xcoordinates=="lon" || Xcoordinates=="mlon") && xmin<0 && inx>180) inx=inx-360;

        if ( (Xcoordinates=="lon" || Xcoordinates=="mlon") && ix>xmax && ix<360+xmin && xmin<0 ) {
            if (quantity=="ROT" || quantity=="ROT") { //This to avoid non-white bins in ROT map
                hmean->Fill(inx,iny,-9999);
                hsigma->Fill(inx,iny,0);
                // cout << "Filling map: x=" << inx << " - y=" << iny << " - Mean=" << -9999 << " - Sigma=" <<
0 << " - Acc=" << accuracy << endl;
                if (asciisel=="yes") out << inx << " " << iny << " " << -9999 << " " << 0 << " " << accuracy <<
endl;
            }
            goto skip;
        }
        if ( (Ycoordinates=="lon" || Ycoordinates=="mlon") && iy>ymax && iy<360+ymin && ymin<0 ) {
            if (quantity=="ROT" || quantity=="ROT") { //This to avoid non-white bins in ROT map
                hmean->Fill(inx,iny,-9999);
            }
        }
    }
}

```

```

        hsigma->Fill(inx,iny,0);
        // cout << "Filling map: x=" << inx << " - y=" << iny << " - Mean=" << -9999 << " - Sigma=" <<
0 << " - Acc=" << accuracy << endl;
        if (asciisel=="yes") out << inx << " " << iny << " " << -9999 << " " << 0 << " " << accuracy <<
endl;
    }
    goto skip;
}

//Defining cut to select the bin
upy=Form("%f",iy+ystep);
lowy=Form("%f",iy);
upx=Form("%f",ix+xstep);
lowx=Form("%f",ix);

if (Xcoordinates!="ut" && Ycoordinates!="ut" ) {
    cut = Ycoordinates + "<" + upy +
        " && " + Ycoordinates + ">=" + lowy +
        " && " + Xcoordinates + "<" + upx +
        " && " + Xcoordinates + ">=" + lowx;
} else {
    if (Xcoordinates=="ut") {
        cut = Ycoordinates + "<" + upy +
            " && " + Ycoordinates + ">=" + lowy +
            " && h+min/60<" + upx +
            " && h+min/60>=" + lowx;
    } else if (Xcoordinates=="ut") {
        cut = Xcoordinates + "<" + upx +
            " && " + Xcoordinates + ">=" + lowx +
            " && h+min/60<" + upy +
            " && h+min/60>=" + lowy;
    }
}

// Cut on elevation, locktime and prn
cut = cut + " && prn >=1 && prn <= 32 && elev >= " +selecut + " && l1locktime >= "+lockcut ;

sum=Form("%f",Re+IPP);
sRe=Form("%f",Re);
sPl=Form("%f",Pl);
obl=sum+"/sqrt(pow("+sum+",2)-pow("+sRe+"*cos(elev*" +sPl+"/180),2))";
if (quantity=="vTEC" ) {
    qmin=-10;
    qmax=100;
    proquant="((tec15+tec30+tec45+tec0)/4)/("+obl+"))";
} else if (quantity=="sTEC") {
    qmin=-10;
    qmax=100;
    proquant="(tec15+tec30+tec45+tec0)/4";
} else if (quantity=="ROT") {
    qmin=-50;
    qmax=50;
    proquant="(tec_rate15+tec_rate30+tec_rate45+tec_rate0)";
} else if (quantity=="ROT") {
    qmin=-50;
    qmax=50;
    proquant="(4/3)*(tec_rate0-tec_rate45)";
}

```

```

} else if (quantity=="SigmaPhi") {
    qmin=0;
    qmax=5;
    if (type=="Vertical")    proquant="sigma60/pow("+obl+",.5)";
    if (type=="Slant")      proquant="sigma60";
} else if (quantity=="S4") {
    qmin=0;
    qmax=5;
    if ( type=="Vertical")  proquant="(sqrt(s4raw*s4raw-s4corr*s4corr))/pow("+obl+",.9)";
    if ( type=="Slant")    proquant="sqrt(s4raw*s4raw-s4corr*s4corr)";
} else if (quantity=="L1CN") {
    qmin=0;
    qmax=100;
    proquant="l1cn";
} else if (quantity=="L2CN") {
    qmin=0;
    qmax=100;
    proquant="l2cn";
} else if (quantity=="CCSTDDEV") {
    qmin=0;
    qmax=100;
    proquant="ccstdev";
} else if (quantity=="Multipath") {
    qmin=0;
    qmax=20000;
    proquant="ccstdev/s4raw";
}

qstep=(qmax-qmin)*10;
TH1F *hdist = new TH1F("hdist","hdist",qstep,qmin,qmax);
hdist->StatOverflows(fgStatOverflows);

if (imfcomp!="No") {
    appo->Project("hdist",proquant,cut);
} else if (imfcomp=="No") {
    chdata->Project("hdist",proquant,cut);
}
entries=hdist->GetEntries();

if (entries !=0) {
    accuracy=100/sqrt(entries);//accuracy calculation

    //Calculating mean and sigma
    mean=hdist->GetMean();
    sigma=hdist->GetRMS();

    if (asciisel=="yes") out << inx << " " << iny << " " << mean << " " << sigma << " " << accuracy <<
endl;

    if (accuracy < stacut) {

        cout << "Filling map: x=" << inx << " - y=" << iny << " - Mean=" << mean << " - Sigma=" <<
sigma << endl;
        hmean->Fill(inx,iny,mean);
        hsigma->Fill(inx,iny,sigma);

```

```

    } else {
        if (quantity=="ROT") { //This to avoid non-white bins in ROT map
            hmean->Fill(inx,iny,-9999);
            hsigma->Fill(inx,iny,0);
            if (asciisel=="yes") out << inx << " " << iny << " " << -9999 << " " << 0 << " " << accuracy <<
endl;
        }
    }
} else {
    if (quantity=="ROT") { //This to avoid non-white bins in ROT map
        hmean->Fill(inx,iny,-9999);
        hsigma->Fill(inx,iny,0);
        // cout << "Filling map: x=" << inx << " - y=" << iny << " - Mean=" << -9999 << " - Sigma=" <<
0 << " -Acc=" << 9999 << endl;
    }
    if (asciisel=="yes") out << inx << " " << iny << " nan nan nan " << endl;
}

    hdist->Delete();
    skip: continue;
} // End loop on y
} // End loop on x
}

```

## 7.9 EXAMPLES OF GBSC INPUT DATACARDS: MEANMAP.DATACARD AND OCCUMAP.DATACARD

### MEANMAP.DATACARD

```
#Meanmap.datacard  
#leave one and only one line between different sections  
  
#Start date (YYMMDD)  
031001  
  
#End date (YYMMDD)  
031231  
  
#Number of stations  
1  
  
#RECEIVER ID(s):  
NSF01  
  
#Quantity (vTEC - sTEC - ROT - SigmaPhi - S4 - L1CN - L2CN - CCSTDDEV)  
CCSTDDEV  
  
#Slant or Vertical quantities (only for SigmaPhi and S4)  
Vertical  
  
#Elevation angle threshold (degrees)  
20  
  
#Accuracy cut (0->100)  
10  
  
#Locktime (l1 and l2) cut in seconds  
240  
  
#Selection of data upon geomagnetic activity (All/Quiet/Dist)  
All  
  
#Geomagnetic behavior selection criterion (Kp/Dst)  
Dst  
  
#IMF component No - Bgsm_x - Bgsm_y - Bgsm_z (>0 or <0)  
No  
  
#Maps dimension (2D/3D)  
2D  
  
#Which type of hemisphere (North/South)  
North  
  
#X-axis Coordinates: (lat lon mlt mlat mlon ut azimuth elev)  
azimut  
  
#X-axis Range (Min Max Step)  
0 360 5
```

*#Y-axis Coordinates: (lat lon mlt mlat mlon ut azimuth elev)*  
elev

*#Y-axis Range (Min Max Step)*  
0 90 5

*#Rootfile location*  
/home/vincenzo/Data\_root

*#Write the maps also in ASCII (yes/no)*  
Yes

## **OCCUMAP.DATACARD**

*#occumap.datacard*  
*#leave only one line between different sections*

*#Start date (YYMMDD)*  
080101

*#End date (YYMMDD)*  
081231

*#Number of stations*  
4

*#RECEIVER ID(s):*  
NYA05 NSF01 NSF03 NSF05

*#Quantity (vTEC - sTEC - ROT - SigmaPhi - S4 - L1CN - L2CN - CCSTDDEV)*  
S4

*#Threshold to calculate occurrence (ROT is in absolute value)*  
>=0.25

*#Slant or Vertical quantities (only for SigmaPhi and S4)*  
Vertical

*#Elevation angle threshold (degrees)*  
20

*#Accuracy cut (0->100)*  
10

*#Locktime (l1 and l2) cut in seconds*  
240

*#Selection of data upon geomagnetic activity (All/Quiet/Dist)*  
All

*#Geomagnetic behavior selection criterion (Kp/Dst)*  
Dst

*#IMF component No - Bgsm\_x - Bgsm\_y - Bgsm\_z (>0 or <0)*  
No

*#Maps dimension (2D/3D)*

2D

*#Which type of hemisphere (North/South) - where the receiver(s) is(are)*

North

*#X-axis Coordinates: (lat lon mlt mlat mlon ut azimuth elev)*

lon

*#X-axis Range (Min Max Step)*

-50 50 2

*#Y-axis Coordinates: (lat lon mlt mlat mlon ut azimuth elev)*

lat

*#Y-axis Range (Min Max Step)*

50 90 5

*#Rootfile location*

/home/vincenzo/Data\_root

*#Write the maps also in ASCII (yes/no)*

Yes

## 7.10 DATA\_ROOT\_FILT.C ROUTINE TO PREPARE ROOT FILES WITH FILTERED DATA

*//This is a ROOT macro generating a root file from a data filtering table*

*//Global variables*

```
Double_t y;
Double_t m;
Double_t d;
Double_t h;
Double_t min;
Double_t gpsweek;
Double_t gpstow;
Int_t prn;
TString azimuth;
TString elev;
TString l1cn;
TString s4raw;
TString s4corr;
TString sigma1;
TString sigma3;
TString sigma10;
TString sigma30;
TString sigma60;
TString cc;
TString ccstdev;
TString tec45;
TString tec_rate45;
TString tec30;
TString tec_rate30;
TString tec15;
TString tec_rate15;
TString tec0;
TString tec_rate0;
TString l1locktime;
TString l2locktime;
TString l2cn;
TString lat;
TString lon;
TString mlat;
TString mlon;
TString str_mlth;
TString str_mlts;
Int_t mlth;
Int_t mlts;
TString mlt;
Int_t station;
Int_t month;
TString smonth;
Int_t day;
TString sday;
TString stat;
Int_t endday;
Float_t filler[36];
```

```
void Data_root_prep() {
```

```

gROOT->Reset();
TString year;
TString indir = "/home/vincenzo/Data_magcoord/";
TString outdir = "/home/vincenzo/Data_root_filt";
TString s_k="1.5";

cout << "Insert station ID (format=XXXXX)" << endl;
cin >> stat;

//filename of the filter data
TString asciifilter="/home/Vincenzo/datafilt.dat";

cout << "Insert year (format=XX)" << endl;
cin >> year;

for (month=1;month<=12;month++) { //Start loop on months

    //Block for the determination of the number of day in the given month
    endday = 0;
    if (month == 11 || month == 4 || month == 6 || month == 9) endday = 30;
    if (month == 1 || month == 3 || month == 5 || month == 7 || month == 8 || month == 10 || month
    == 12) endday = 31;
    if (month == 2 && (year == "04" || year == "08" || year == "12" || year == "16" || year == "20" )) endday
    = 29;
    if (month == 2 && (year != "04" || year != "08" || year != "12" || year != "16" || year != "20" )) endday
    = 28;
    if (endday == 0) {
        cout << "Wrong day determination - please check code!" << endl;
        exit();
    }

    for (day=1;day<=endday;day++){ //Start loop on day

        //Setting format XX for days and months
        smonth=Form("%d", month);
        if (smonth.Length()==1) smonth="0"+smonth;
        sday=Form("%d", day);
        if (sday.Length()==1) sday="0"+sday;
        cout << stat << " - year " << year << " - month " << smonth << " - day " << sday << endl;

        //Ascii File opening
        ifstream in;
        TString asciifile = indir+stat+"/"+stat+"_"+year+"_"+smonth+"_"+sday+".dat";
        in.open(asciifile);

        //Checking for ascii file existence
        if(!in) {
            cout << "File not found - " << stat << " - year " << year << " - month " << smonth << " - day " <<
            sday << endl;
            goto skip;
        }

        //Rootfile creation and opening
        TString rootfile = outdir+stat+"/"+stat+"_"+year+"_"+smonth+"_"+sday+".root";
        TFile *f = new TFile(rootfile,"RECREATE");

```

```

    TNtuple          *data          =          new
TNtuple("data","data","y:m:d:h:min:gpsweek:gpstow:prn:azimut:elev:lat:lon:mLAT:mLON:mlt:l1cn:s4raw
w:s4corr:sigma1:sigma3:sigma10:sigma30:sigma60:cc:ccstdev:l1locktime:l2locktime:l2cn:tec45:tec_ra
te45:tec30:tec_rate30:tec15:tec_rate15:tec0:tec_rate0",64000);

    Int_t nlines=0;
    //Ntuple filling
    while (1) {
        if (!in.good()) break;
        //reading 36 colums
        in >> y >> m >> d >> h >> min >> gpsweek >> gpstow >> prn >> azimuth >> elev >> l1cn >> s4raw
>> s4corr >> sigma1 >> sigma3 >> sigma10 >> sigma30 >> sigma60 >> cc >> ccstdev >> tec45 >>
tec_rate45 >> tec30 >> tec_rate30 >> tec15 >> tec_rate15 >> tec0 >> tec_rate0 >> l1locktime >>
l2locktime >> l2cn >> lat >> lon >> mlat >> mlon >> mlt ;

        Float_t filaz, filelev, fils4, filsphi;

        ifstream infil;
        infil.open(asciifilter);

        Int_t filflag=0;
        while (infil.good()) {

            infil >> filaz >> filelev >> fils4 >> filsphi;
            if (azimut.Atof()>=filaz && azimuth.Atof()<(filaz+10) && elev.Atof()>=filelev &&
elev.Atof()<(filelev+5)) {
                filflag=1;
                break;
            }
            if (filflag==1) break;
        }
        infil.close();

        //      cout << filflag << endl;
        if (filflag == 0) {

            str_mlth = mlt(0,2);
            str_mltS = mlt(3,2);
            Float_t sec=str_mltS.Atoi();
            Float_t den=sec/60;
            Float_t mltnew=str_mlth.Atoi()+den;

            Float_t val= gpstow/86400;
            Int_t fval=floor(gpstow/86400);
            Int_t ora=floor((val-fval)*24);
            Int_t minuti=floor((((val-fval)*24)-ora)*60);
            Int_t secondi=gpstow-(fval*24*60*60+ora*60*60+minuti*60);
            if (secondi == 60) min=min+1;

            //Root-ple Filling
            filler[0]=y;
            filler[1]=m;
            filler[2]=d;
            filler[3]=h;
            filler[4]=min;
            filler[5]=gpsweek;

```

```

        filler[6]=gpstow;
        filler[7]=prn;
        filler[8]=azimut.Atof();
        filler[9]=elev.Atof();
        filler[10]=lat.Atof();
        filler[11]=lon.Atof();
        filler[12]=mlat.Atof();
        filler[13]=mlon.Atof();
        filler[14]=mltnew;
        filler[15]=l1cn.Atof();
        filler[16]=s4raw.Atof();
        filler[17]=s4corr.Atof();
        filler[18]=sigma1.Atof();
        filler[19]=sigma3.Atof();
        filler[20]=sigma10.Atof();
        filler[21]=sigma30.Atof();
        filler[22]=sigma60.Atof();
        filler[23]=cc.Atof();
        filler[24]=ccstdev.Atof();
        filler[25]=l1locktime.Atof();
        filler[26]=l2locktime.Atof();
        filler[27]=l2cn.Atof();
        filler[28]=tec45.Atof();
        filler[29]=tec_rate45.Atof();
        filler[30]=tec30.Atof();
        filler[31]=tec_rate30.Atof();
        filler[32]=tec15.Atof();
        filler[33]=tec_rate15.Atof();
        filler[34]=tec0.Atof();
        filler[35]=tec_rate0.Atof();
        data->Fill(filler);
        nlines++;
    }

}

//write out Root-ple
cout << " found " << nlines << " data" << endl;
cout << "~~~~~" << endl;
f->Write();
f->Close();
skip: cout << " " << endl;

//closing ASCII file
in.close();
}
}
}

```

## 7.11 DATA\_PREP ROUTINE TO PREPARE GISTM OUTPUT FILES

### Routine

```
#!/bin/bash

clear
echo ~~~~~
echo "Reading Datacard (datacard_parseismr.data)"

#reading datacard
. datacard_parseismr.data

#exporting paths
export RUNDIR="$Rundir"
export WORKDIR="$Workdir"
export INDIR="$InputDirectory"
export OUTDIR="$OutputDirectory"
export STAID="$StationID"

echo 'Run directory = ' $RUNDIR
echo 'Working directory = ' $WORKDIR
echo 'Input directory = ' $INDIR
echo 'Output disrectory = ' $OUTDIR
echo 'Station ID = ' $STAID

echo ~~~~~
echo 'Processing data...'

#checking the existence of the output directory
if [ -d $OUTDIR ] ; then
    echo 'Writing in ' $OUTDIR
else
    mkdir $OUTDIR
fi

#Entering run directory
cd $RUNDIR

if [ -e list.tmp ] ; then
    /bin/rm -f list.tmp
    touch list.tmp
else
    touch list.tmp
fi

/bin/ls $INDIR/ > list.tmp

echo $FILENAME
if [ -e parse.dat ] ; then
    /bin/rm -f parse.dat
    touch parse.dat
else
    touch parse.dat
fi

echo $FILENAME
```

```

cd $INDIR

find * -name "*.S60" > $RUNDIR/parse.dat
cd -

while read INSEC
do
    ID=$STAID
    export YEAR=${INSEC:10:2};
    export MONTH=${INSEC:12:2};
    export DAY=${INSEC:14:2};

    $OUTDIR/$STAID_"$YEAR"_"$MONTH"_"$DAY".out"
    echo Parsing $INDIR/"$INSEC " --> "$OUTDIR/$STAID_"$YEAR"_"$MONTH"_"$DAY".out"

    ./ParseismrLinux.exe all $INDIR/"$INSEC $OUTDIR/parsetemp.dat

    #This line remove also the header of the files. To keep it change it into
    #cat $OUTDIR/parsetemp.dat >> $OUTDIR/$STAID_"$YEAR"_"$MONTH"_"$DAY".out"
        sed "/Week/d" $OUTDIR/parsetemp.dat >>
    $OUTDIR/$STAID_"$YEAR"_"$MONTH"_"$DAY".out"

    done < parse.dat

    echo ~~~~~
cd $WORKDIR
echo 'Files are in ' $OUTDIR

```

### **Datacard**

```

#Datacard for data_prep

#Directory where parseismr executable is
Rundir=/home/vincenzo/AJutils

#Directory where parseismr.sh
Workdir=/home/vincenzo/Scripts/GISTM

#Input sec60 directory
InputDirectory=/home/vincenzo/Data/Data_Nottingham

#Output for ASCII Files
OutputDirectory=/home/vincenzo/Data_ASCII/

#Station Identifier
StationID=NSF06

```